

University of Naples “Federico II”
Department of Structures for Engineering and Architecture



Candidate:
RAFFAELE GAGLIARDO

**PERFORMANCE – BASED DAMAGE ASSESSMENT OF
MASONRY STRUCTURES SUBJECTED TO SETTLEMENT
USING RIGID BLOCK MODELS**

Doctorate of Philosophy in
Structural, Geotechnical Engineering and Seismic Risk

PhD Thesis
XXXIII Cycle

Tutor:
Prof. Raffaele Landolfo

Co-Tutor:
Prof. Francesco Portioli

Coordinator:
Prof. Luciano Rosati

*A te,
luce che illumini
ogni mio passo*

Acknowledgments/Ringraziamenti

(Only in the printed version)

TABLE OF CONTENTS

Acknowledgments/Ringraziamenti	v
TABLE OF CONTENTS	vi
List of Figures	xi
List of Tables	xxvi
Abstract	xxix
About the author.....	xxx

Chapter 1 – Introduction

1.1 Background and Framework.....	1
1.2 Motivation of research	8
1.3 Thesis outline and organization	9
References.....	12

Chapter 2 – Settlement-induced damages, monitoring and movement profiles

2.1 Introduction.....	13
2.2 Settlement induced by natural and man-made hazards.....	15
2.2.1 Subsidence	17
2.2.2 Landslides	23
2.2.2.1 Classification based on type of movement and material.....	24
2.2.2.2 Classification based on state of activity	33
2.2.2.3 Classification according to intensity	35
2.3 Subsidence-induced damage	38
2.4 Landslide-induced damage	44

2.5	From subsidence and landslide phenomena to field of settlement displacements	62
2.5.1	In-situ monitoring displacements	62
2.5.2	Satellite monitoring displacements	64
2.5.3	Experimental monitoring displacements	71
	Conclusions	73
	References	75

Chapter 3 – Overview on masonry structures and modelling approaches

3.1	Introduction	83
3.2	Masonry structures: a thousand-year history	86
3.3	Material	91
3.3.1	Uniaxial compressive behaviour	93
3.3.2	Uniaxial tensile behaviour	96
3.3.3	Biaxial behaviour	97
3.4	Preliminary observation to modelling approaches	101
3.5	Modelling approaches for masonry structures	106
3.5.1	Classification according to masonry model	106
3.5.2	Classification according to modelling strategy	108
3.5.2.1	Numerical approaches	110
3.5.2.1.1	Block-based models	110
3.5.2.1.2	Continuum models	112
3.5.2.1.3	Macro-element models	116
3.5.2.1.4	Geometry-based models	119
3.5.2.2	Analytical approaches	120
3.5.2.2.1	The Limiting Tensile Strain Method (LTSM)	121

3.5.2.2.2 The Load Path Method (LPM).....	124
3.6 Rigid block models based on limit analysis.....	130
3.6.1 State of art.....	131
3.6.2 Other proposed rigid block models.....	136
Conclusions.....	141
References.....	144

Chapter 4 – Proposed rigid block models for linear and non-linear kinematic analysis

4.1 Introduction.....	176
4.2 Rigid block model with rigid contacts for linear kinematic analysis....	179
4.2.1 Formulation of limit equilibrium problem.....	182
4.3 Rigid block model with no-tension elastic contacts for non-linear kinematic analysis.....	188
4.3.1 Formulation of incremental static contacts problem	190
4.3.2 Input data for the model.....	194
4.4 Conclusions.....	197
References.....	198

Chapter 5 – Numerical applications using linear kinematic analysis

5.1 Introduction.....	204
5.2 Applications of rigid block model for linear kinematic analysis.....	205
5.2.1 Lateral and vertical live loads.....	206
5.2.1.1 Circular arches and vault subjected to vertical live loads.....	206
5.2.1.2 A skew arch subjected to point live load	210
5.2.1.3 Masonry dome subjected to horizontal live loads.....	213

5.2.1.4 Small scale wall components	215
5.2.1.4.1 Single-leaf masonry walls	215
5.2.1.4.2 Three-leaf masonry walls	221
5.2.1.5 Application to monumental historical masonry buildings	225
5.2.1.5.1 Ponti della Valle di Maddaloni	225
5.2.1.5.2 Church of San Nicolò di Campodimonte	230
5.2.2 Spreading supports and settlements	237
5.2.2.1 Circular arch subjected to spreading support	237
5.2.2.2 Cross vault subjected to support movement	239
5.2.2.3 Two-story masonry façade	240
5.2.2.3.1 The façade without openings	242
5.2.2.3.2 The façade with openings	246
5.2.3 Applications to case studies subjected to both lateral loads and settlement	253
5.2.3.1 Two-story masonry building	253
5.2.3.2 Palazzo d'Avalos	258
Conclusions	272
References	274

Chapter 6 – Comparisons with experimental tests using non-linear kinematic analysis

6.1 Introduction	277
6.2 Comparisons of rigid block model for non-linear kinematic analysis with experimental tests	278
6.2.1 Small scale single-leaf wall panel	279
6.2.2 Small scale portal frame	282
6.2.3 T-panels with and without interlocking	285
6.2.4 Small-scale masonry façade	290

Conclusions.....	294
References.....	295

Chapter 7 – Damage assessment by a performance-based approach

7.1 Introduction.....	297
7.2 Damage classification: state of art on empirical methods.....	299
7.3 Assessment by push-down curves.....	303
7.3.1 Application to a full-scale monumental building façade.....	306
7.3.2 Application to a full-scale historic masonry church façade.....	312
Conclusions.....	321
References.....	323

Chapter 8 – Conclusions

8.1 Conclusive remarks.....	326
8.2 Further developments.....	331
References.....	336

List of Figures

Figure 1.1 – Typical damage patterns for masonry structures subjected to settlements: (a) Façade with and without openings; (b) buildings corner connections; (c) T-connections; (d) arches, vaults and domes.	2
Figure 1.2 - PERICLES project field of application: (a) assets subjected to prevailing in-plane damage; (b) assets subjected to prevailing out-plane damage; (c) blocky structures subjected to overturning; (d) arched structures in-plane; (e) building aggregates.	4
Figure 1.3 - PERICLES project: (a) main task flowchart and (b) proposed methodological approach.	5
Figure 1.4 - PERICLES project: multi-scale top-down approach.	6
Figure 1.5 – Flowchart of thesis organization.....	11
Figure 2.1 - Examples of crack patterns and collapse mechanism induced by settlements in existing masonry and confined masonry structures: A clay brick masonry building in Bovino, Italy, 2019 (a) (b); Building in Riviera di Chiaia, Naples, Italy, 2013 (c); Building of the Faculty of Veterinary Medicine, Naples, Italy, 2015 (d).....	14
Figure 2.2 - Fall according to (Varnes, 1978): schematic diagram (a); example of rockfall in Valtopina, Umbria (Italy), unknown date. Photographer: Fausto Guzzetti. Source: EGU Blogs, https://blogs.egu.eu/ (b).	25
Figure 2.3 - Topples according to (Varnes, 1978): schematic diagram (a); example of topple in Utah, Canyonlands (USA), unknown date. Photographer: J. Novotny (b).....	26
Figure 2.4 - Rotational, translational and block slide according to (Varnes, 1978): schematic diagrams in the case of rotational (a), translational (c) and block (e) slide. Example of rotational slide in Fort St. John area, B.C. (USA), 2001. Photographer: Réjean Couture. Source: Canadian Landscapes (b). Example of translational slide in Tully Valley. (USA), 1993. Photographer: Gerard Wieczorek. Source: U.S. Geological Survey (d). Example of block slide in Forest Road 19, Oregon (USA), 2001. Photographer: U.S. Forest Service photo (f).....	27

Figure 2.5 - Lateral spread according to (Varnes, 1978): schematic diagram (a); example of lateral spread in Papu Valley, Sulawesi (Indonesia), 2018. Source: Gilles Brocard, University of Sydney (b).	28
Figure 2.6 - Earth flow according to (Varnes, 1978): schematic diagram (a); example of earth flow in Slungullion, Highway 149, Lake City (Utah), from seven hundred years ago until today. Source: https://www.uncovercolorado.com/ (b).	29
Figure 2.7 - Creep according to (Varnes, 1978): schematic diagram (a); example of creep in Haymond Formation, (Texas). Photo Credit: B. Bradley, University of Colorado. Source: National Geophysical Data Center (NGDC) (b).....	30
Figure 2.8 - Complex landslide according to (Varnes, 1978): schematic diagram of a complex landslide made by combination of rotational slide and flow (a); example of complex Muskwa-Chisca in British Columbia (Canada), 2001. Source: Marten Geertsema, BC Ministry of Forest, 2002 (b).....	31
Figure 2.9 - Landslide classification according to (Hutchinson, 1988).....	31
Figure 2.10 - Geotechnical landslide classification according to (Leroueil et al., 1996): (a) schematic diagram, (b) various landslide stage and (c) involved material.....	33
Figure 2.11 - Method proposed by (Cruden and Varnes, 1996): (a) state of activity of landslides over time; (b) toppling landslide in different states of activity: 1. Active, erosion at toe of slope causes block to topple; 2. Suspended, local cracking/fracturing in crown area; 3. reactivated, toppling of a new block; 4. dormant, the body of the landslide is colonised by vegetation, the slopes are remodelled by the weather; 5. Naturally stabilised, fluvial deposits have protected the base of the slope; 6. relict, a uniform vegetation cover has been re-established.	35
Figure 2.12 - Landslide velocity scale and probable destructive significance proposed by (Cruden and Varnes, 1996).	37
Figure 2.13 - Sled model proposed by (Sassa, 1988).....	38
Figure 2.14 - Schematic illustration of building damage associated with various types of subsidence movement, some of which may occur together (Cooper, 2008): (a) hogging, (b) sagging, (c) extension and (d) support loss.	39
Figure 2.15 - Maps of Italian municipalities affected by subsidence elaborated by the Italian Environmental Data Yearbook. Comparison between data related to (a) 2003 and (b) 2018.....	40

Figure 2.16 - Italian municipalities per each region affected by subsidence according to the Italian Environmental Data Yearbook 2018.....	42
Figure 2.17 - Ancona (Italy) landslide in 1982 as reported in (Cotecchia, 2006). Damage to man-made structures caused by the landslide: (a) University Medical Faculty, (b)(d)(f) Flaminia road and (c)(e) Adriatic railway.	45
Figure 2.18 - San Pietro in Guarano (Italy) landslide in 1981 as reported in (Antronico et al., 2003). Damage suffered by (a) a primary school, (b) a secondary school and (c) a private building subjected to the landslide.	47
Figure 2.19 - Some photographs of the March 7 th 2005 landslide at Cavallerizzo: (a) a panoramic view of the village (in foreground, the main earth flow); (b) view of buildings damaged along the crown; (c) view of damage to the provincial road; (d) view of the main scarp (in foreground, the landslide lake); (e)(f)(g) view of damage to the urbanized area, along the main scarp (Iovine et al., 2006).	48
Figure 2.20 - Population exposed to landslide risk in Italy (Trigila et al., 2018).	53
Figure 2.21 - Data collected in (Trigila et al., 2018): population at risk living in high and very high landslide hazard zones (no. of inhabitants) on (a) regional and (b) municipal basis.	53
Figure 2.22 - Families exposed to landslide risk in Italy (Trigila et al., 2018)..	54
Figure 2.23 - Data collected in (Trigila et al., 2018): number of families at risk living in high and very high landslide hazard zones on (a) regional and (b) municipal basis.....	55
Figure 2.24 - Buildings exposed to landslide risk in Italy (Trigila et al., 2018).	56
Figure 2.25 - Data collected in (Trigila et al., 2018): number of buildings at risk located in high and very high landslide hazard zones on (a) regional and (b) municipal basis.....	57
Figure 2.26 - Industry and services local units exposed to landslide risk in Italy (Trigila et al., 2018).	58
Figure 2.27 - Data collected in (Trigila et al., 2018): number of industry and services local units at risk located in high and very high landslide hazard zones on (a) regional and (b) municipal basis.....	58
Figure 2.28 - Cultural Heritage exposed to landslide risk in Italy (Trigila et al., 2018).	59

- Figure 2.29 - Data collected in (Trigila et al., 2018): number of Cultural Heritage at risk located in high and very high landslide hazard zones on (a) regional and (b) municipal basis.60
- Figure 2.30 - Settlement profile derived by in-situ monitoring. The case study of Lisbon's downtown developed in (Couto, Bento and Gomes, 2020): (a) settlements isoline map of Lisbon's downtown; (b) normalized settlement profiles; (c) time evolution of settlements; (d) displacement configurations. ...63
- Figure 2.31 -Application at detailed scale for subsidence. The case study of a reinforced concrete building described in (Cascini et al., 2013): (a) view of the Castel Volturno area with an indication of the grid of satellite covered cells and the analysed buildings; (b) example of cumulative vertical settlement obtained with three dataset time series; (c) vertical cumulative settlements to be applied along the longitudinal cross section of the building.67
- Figure 2.32 - Application at detailed scale for subsidence. The case study of two buildings in Sarno and described in (Cascini et al., 2011a, 2011b): (a) map of the cumulative settlements; (b)(c) investigated buildings.68
- Figure 2.33 - Application at detailed scale for subsidence. The case study of a infrastructural system close to Naples described in (Cascini et al., 2013): (a) zoom over the railway lines with the indication of the covered satellite cells; (b) one-year cumulative settlements computed along the vertical direction; the trend of cumulative vertical settlements for the (c) railway and (d) viaduct..... 69
- Figure 2.34 – Settlement profile derived by satellite monitoring. The case study of Agrigento Cathedral developed in (Reale et al., 2019): (a) Landslide inventory map of the area of Agrigento; (b) estimated deformation mean velocity over the area of interest; (c) crack pattern; (d) settlement profile under the assumed macro-elements of the main façade..... 70
- Figure 2.35 – Settlement profile derived by centrifuge test as described in (Dejong, 2016): (a) comparison of the vertical displacements at the soil surface for greenfield and building tests (volume loss=0.5%, 1%, 2%, 4%); (b) comparison of the vertical greenfield soil surface displacements to the vertical displacement of the base of the structure (volume loss=2%); (c) comparison with results obtained with a FEM computational model.72
- Figure 3.1 – Timeline of the thousand-year history of structural masonry.....90
- Figure 3.2 - Uniaxial compressive behaviour of masonry prism compared with those of mortar and brick.93

Figure 3.3 - Stacked bond prism model: stress state due to uniaxial compression.	94
Figure 3.4 - Tension in the direction parallel to the bed joints: (a) failure occurs with a stepped crack through head and bed joints; (b) failure occurs vertically through head joints and units.	97
Figure 3.5 - Biaxial behaviour stress states: principal stress and rotation angle (a) and full stress vector (b).	97
Figure 3.6 - Failure modes of solid clay units masonry under biaxial loading, (Dhanasekar, Page and Kleeman, 1985).	98
Figure 3.7 - Failure domain for a masonry panel subjected to shear (Dhanasekar, Page and Kleeman, 1985).	100
Figure 3.8 - Modelling approaches for masonry structures: a) detailed micro-modelling; b) simplified micro-modelling; c) macro-modelling. (Gagliardo et al., 2019).	108
Figure 3.9 - Modelling strategies for masonry structures according to (D’Altri et al., 2020).	109
Figure 3.10 - Examples of block-based model: (a) (Lourenço and Rots, 1997); (b) (Sandoval and Arnau, 2017); (c) (Minga, Macorini and Izzuddin, 2018); (d) (Foti, Vacca and Facchini, 2018); (e) (Lengyel, 2017); (f) (Beatini, Royer-Carfagni and Tasora, 2017); (g) (Petrasca, Pelà, Rossi, Zaghi, et al., 2017); (h) (Serpieri, Albarella and Sacco, 2017); (i) (Abdulla, Cunningham and Gillie, 2017).	113
Figure 3.11 - Examples of continuum model: (a) (D’Altri, Castellazzi and de Miranda, 2018); (b) (Valente and Milani, 2016); (c) (Pelà, Cervera and Roca, 2013); (d) (Milani, P. B. Lourenço and Tralli, 2006a); (e) (Godio et al., 2017); (f) (Addressi and Sacco, 2012); (g) (Petrasca, Pelà, Rossi, Oller, et al., 2017); (h) (Leonetti et al., 2018); (i) (Brasile, Casciaro and Formica, 2007b).	114
Figure 3.12 - Examples of macro-element model: (a) (Belmouden and Lestuzzi, 2009); (b) (Addressi, Mastrandrea and Sacco, 2014); (c) (Cattari et al., 2018); (d) (Chen, Moon and Yi, 2008); (e) (Caliò, Marletta and Pantò, 2012); (f) (Rinaldin, Amadio and Macorini, 2016).	118
Figure 3.13 - Examples of geometry-based model: (a) (Angelillo, Babilio and Fortunato, 2013); (b) (Marmo, Masi and Rosati, 2018); (c) (Block and Lachauer, 2014a); (d) (Milani, 2015); (e) (Chiozzi, Milani and Tralli, 2017).	120

Figure 3.14 - Limit Tensile Strain Methods scheme, according to (Giardina, 2013).	122
Figure 3.15 - Load Path Method in the case of (a) zero deviation and (b) only one deviation, according to (Palmisano and Elia, 2015). The representation of the stress regime in the case of (c) compressive and (d) tensile stress regime.	127
Figure 3.16 - Load Path Method in the case of a settlement located at one end of the masonry wall. Static equilibrium condition located at (a) state 1 and (b)(c)(d) state 2.	129
Figure 3.17 - Rigid block limit analysis proposed models: (a) (Livesley, 1978); (b) (Baggio and Trovalusci, 1998); (c) (Ferris and Tin-Loi, 2001); (d) (Tran-Cao, 2009).	134
Figure 3.18 - Examples of proposed limit analysis approaches: (a) (Orduña and Lourenço, 2005a); (c) (Portioli et al., 2014); (c) (Milani, 2008); (d) (Baraldi and Cecchi, 2017).	135
Figure 3.19 - Rigid block model proposed in (Zampieri, Amoroso and Pellegrino, 2019): (a) diagrams for the analytical proposal and (b)(c)(d) examples of predicted collapse mechanisms and corresponding thrust line.	137
Figure 3.20 - Rigid block model proposed in (Galassi et al., 2018): (a) interfaces model and involved forces; (b)(c) applications to arches subjected to movable support.....	139
Figure 3.21 - Application of the rigid block model proposed in (Maurizio Angelillo, 2014; Iannuzzo et al., 2018): (a) façade of a XVIII century building in Torre Annunziata (Naples); (b) cross section of XVII centuries church (Naples).	140
Figure 4.1 - Application examples of LiABlock_3D to historic masonry structures under (a) lateral loads and (b) settlement (Cascini, Gagliardo and Portioli, 2020).	180
Figure 4.2 – (a) CAD model of a simple portal arch made of polyhedral blocks and (b) block types with contact interfaces and attributes (Cascini, Gagliardo and Portioli, 2020).	181
Figure 4.3 – (a) CAD model of a simple portal arch made of polyhedral blocks and (b) block types with contact interfaces and attributes (Cascini, Gagliardo and Portioli, 2020).	182

Figure 4.4 - Example of settlement analysis on a portal arch: (a) geometrical model and (b) failure mode (Cascini, Gagliardo and Portioli, 2020).	184
Figure 4.5 - (a) Associative (dilatant) and (b) non-associative (non-dilatant) collapse mechanisms of a masonry block arch subjected to sliding failure at the right end support; (c) Coulomb failure surface used for the associative solution; and (d) fictitious failure surface adopted in the iterative solution procedure for the non-associative behaviour (Cascini, Gagliardo and Portioli, 2020).	187
Figure 4.6 - Rigid block model with elastic contact interfaces: (a) block assemblage; (b) rigid block ‘i’, interface ‘j’, contact point ‘k’ and no-tension elastic normal stiffness ‘kn’ (Gagliardo et al., 2021).....	190
Figure 4.7 - Contact laws for normal reaction force (a) and shear force (b) at point <i>k</i>	192
Figure 4.8 – (a) External and contact forces; (b) Initial gap at contact point <i>k</i> and kinematic variables at block centroid <i>i</i> and contact point <i>k</i> ; (c) Elastic contact interpenetration (Gagliardo et al., 2021).....	193
Figure 4.9 - Non-linear kinematic analysis formulation: (a) block assemblage in the case of a wall sample and (b) definition of a block by a simple CAD polyline.	196
Figure 4.10 - Settlement protocol in the case of a linear settlement law: (a) definition of the support blocks at the foundation layer and (b) vectors of settlement displacements for the support blocks.....	196
Figure 5.1 - (a) Circular arch dimensions; (b) circular arch collapse mechanism; (c) two-ring arch dimensions; (d) two-ring arch collapse mechanism; (e) barrel vault dimensions; and (f) barrel vault collapse mechanism (Cascini, Gagliardo and Portioli, 2020).....	207
Figure 5.2 – Sketches of the analytical solutions in the case of (a) circular arch and (b) two-ring arch.....	208
Figure 5.3 - Four block arch subjected to eccentric live load: (a) configuration and (b) sensitivity analysis to friction coefficient (Cascini, Gagliardo and Portioli, 2020).	209
Figure 5.4 - Skew arch first type: geometrical model in AutoCAD (a) and rigid block model (b).	211
Figure 5.5 - Skew arch first type: numerical vs experimental comparison in terms of load-displacement curve (a) and RBM failure mode (b).	211

Figure 5.6 - Skew arch second type: geometrical model in AutoCAD (a) and rigid block model (b).	212
Figure 5.7 - Skew arch second type: numerical vs experimental comparison in terms of load-displacement curve (a) and RBM failure mode (b).	213
Figure 5.8 - (a) Hemispherical dome dimensions and (b) hemispherical dome collapse mechanism (Cascini, Gagliardo and Portioli, 2020).	214
Figure 5.9 - Test S22 (Restrepo Vélez, Magenes and Griffith, 2014): (a) associative and (b) non-associative failure mechanisms using rigid block limit analysis (Malena, Portioli, Gagliardo et al., 2019).	216
Figure 5.10 - Test S5 (Restrepo Vélez, Magenes and Griffith, 2014): (a) associative and (b) non-associative failure mechanisms using rigid block limit analysis (Malena, Portioli, Gagliardo et al., 2019).	217
Figure 5.11 - Test S22: (a) sensitivity analyses to the friction coefficient and (b) to the block size ratio (Malena, Portioli, Gagliardo et al., 2019).	217
Figure 5.12 - Test S22: sensitivity analyses to the friction coefficient ($\mu = 0.4$ in the Figure). (a) associative and (b) non-associative failure modes predicted with the rigid block model (Malena, Portioli, Gagliardo et al., 2019).	218
Figure 5.13 - Test S22: sensitivity analyses to the size ratio ($b = 40$ mm in the Figure). (a) associative and (b) non-associative failure modes predicted with the rigid block model (Malena, Portioli, Gagliardo et al., 2019).	218
Figure 5.14 - Test S5: (a) sensitivity analyses to the friction coefficient and (b) to the block size ratio (Malena, Portioli, Gagliardo et al., 2019).	219
Figure 5.15 - Test S5: sensitivity analyses to the friction coefficient ($\mu = 0.4$ in the Figure). (a) associative and (b) non-associative failure modes predicted with the rigid block model (Malena, Portioli, Gagliardo et al., 2019).	219
Figure 5.16 - Test S5: sensitivity analyses to the size ratio ($b = 40$ mm in the Figure). (a) associative and (b) non-associative failure modes predicted with the rigid block model (Malena, Portioli, Gagliardo et al., 2019).	220
Figure 5.17 - Convergence plots and sensitivity analyses to starting conditions for (a) Test S22 and (b) Test S5 (Malena, Portioli, Gagliardo et al., 2019). ...	220
Figure 5.18 - Three-leaf masonry walls geometry and loading condition: a) simple wall; b) T-wall (Gagliardo, Cascini, et al., 2019).	222

Figure 5.19 - Collapse mechanism induced by live load applied along x-axis in both directions: (a)(c) simple wall; (b)(d) T-wall (Gagliardo, Cascini, et al., 2019).	223
Figure 5.20 - Collapse load factor vs iteration number for both simple wall (a)(c) and T-wall (b)(d) numerical simulation considering live loads applied along both negative (a)(b) and positive (c)(d) x-axis (Gagliardo, Cascini, et al., 2019). ..	224
Figure 5.21 - Aqueduct Carolino - “I Ponti della Valle di Maddaloni”.....	226
Figure 5.22 - In-plane collapse mechanism: a) Geometry and load; b) Associative plot; c) Non-Associative plot (Gagliardo, Terracciano, et al., 2019).....	227
Figure 5.23 - Out-of-plane collapse mechanism: a) Geometry and load; b) Associative plot; c) Non-Associative plot (Gagliardo, Terracciano, et al., 2019).	227
Figure 5.24 - In-plane loading condition. Comparison between the distribution of the equivalent plastic strain (PEEQ) in the FEM model and cracks position in the rigid block model (Gagliardo, Terracciano, et al., 2019).....	228
Figure 5.25 - Out-of-plane loading condition. Comparison between the distribution of the equivalent plastic strain (PEEQ) in the FEM model and cracks position in the rigid block model (Gagliardo, Terracciano, et al., 2019).....	229
Figure 5.26 - Dimensions of the numerical case study of an ancient masonry church building.	231
Figure 5.27 - Rigid block model of the church: non-associative failure modes for lateral load applied along the (a) x-axis and (b) along y-axis (Malena, Portioli, Gagliardo et al., 2019).....	232
Figure 5.28 - Rigid block model convergence plot and sensitivity analysis to starting conditions(Malena, Portioli, Gagliardo et al., 2019).....	233
Figure 5.29 - Lateral load applied only to the bell tower along the x-axis: (a) front and (b) back views of non-associative failure mode (Malena, Portioli, Gagliardo et al., 2019).....	234
Figure 5.30 - Lateral load applied only to the bell tower along the x-axis: failure mechanism at the triumphal arch between the nave and the transept (Malena, Portioli, Gagliardo et al., 2019).....	234
Figure 5.31 - Lateral load applied along the (a) x-axis and (b) y-axis. Non-associative rigid block failure mechanism for the reduced block size (Malena, Portioli, Gagliardo et al., 2019).....	235

Figure 5.32 - Comparison between the proposed rigid block model and a finite element model (Malena et al., 2019) in terms of load factor vs displacement: (a) x-axis; (b) y-axis (Malena, Portioli, Gagliardo et al., 2019).....	237
Figure 5.33 - (a) Voussoir circular arch on spreading support and (b) predicted failure mechanism (Cascini, Gagliardo and Portioli, 2020).....	238
Figure 5.34 - Cross vault (Rossi, Calderini and Lagomarsino, 2016) (a) size and (b) collapse mechanism (Cascini, Gagliardo and Portioli, 2020).	239
Figure 5.35 - Cross vault: comparison of numerical and experimental results (Rossi, Calderini and Lagomarsino, 2016).	240
Figure 5.36 - The case study of a masonry façade subject to settlement: (a) the front side of the building; (b)rigid block model (Landolfo, Gagliardo et al., 2020).	241
Figure 5.37 - The settlement configurations on the base of movable support block length: (a) short settlement, (b) medium settlement and (c) long settlement...	242
Figure 5.38 - Failure modes of the façade without openings subjected to short settlement and for the two block sizes (40x25 cm first row and 25x12 cm second row). (a), (c): non-associative solution with no friction on vertical contacts (Type A); (b), (d): associative solution with friction on vertical contacts (Type B) (Landolfo et al., 2020).....	243
Figure 5.39 - Failure modes of the façade without openings subjected to medium settlement and for the two block sizes (40x25 cm first row and 25x12 cm second row). (a), (c): non-associative solution with no friction on vertical contacts (Type A); (b), (d): associative solution with friction on vertical contacts (Type B) (Landolfo, Gagliardo et al., 2020).....	245
Figure 5.40 - Failure modes of the façade without openings subjected to long settlement and for the two block sizes (40x25 cm first row and 25x12 cm second row). (a), (c): non-associative solution with no friction on vertical contacts (Type A); (b), (d): associative solution with friction on vertical contacts (Type B) (Landolfo, Gagliardo et al., 2020).....	246
Figure 5.41 - Failure modes of the façade with openings subjected to short settlement and for the two block sizes (40x25 cm first row and 25x12 cm second row). (a), (c): non-associative solution with no friction on vertical contacts (Type A); (b), (d): associative solution with friction on vertical contacts (Type B) (Landolfo, Gagliardo et al., 2020).....	247

- Figure 5.42 - Failure modes of the façade with openings subjected to medium settlement and for the two block sizes (40x25 cm first row and 25x12 cm second row). (a), (c): non-associative solution with no friction on vertical contacts (Type A); (b), (d): associative solution with friction on vertical contacts (Type B) (Landolfo, Gagliardo et al., 2020).....249
- Figure 5.43 - Failure modes of the façade with openings subjected to long settlement and for the two block sizes (40x25 cm first row and 25x12 cm second row). (a), (c): non-associative solution with no friction on vertical contacts (Type A); (b), (d): associative solution with friction on vertical contacts (Type B) (Landolfo, Gagliardo et al., 2020).....250
- Figure 5.44 - Reactions at the moving support in the case of the façade without openings subjected to short (a), (b), medium (c), (d) and long (e), (f) settlement: 40x25 block size (a), (c), (e) and 25x12 block size (b), (d), (f) (Landolfo, Gagliardo et al., 2020).....251
- Figure 5.45 - Reactions at the moving support in the case of the façade with openings subjected to short (a), (b), medium (c), (d) and long (e), (f) settlement: 40x25 block size (a), (c), (e) and 25x12 block size (b), (d), (f) (Landolfo, Gagliardo et al., 2020).....252
- Figure 5.46 - (a) Size of two-story masonry building; (b) interior view with barrel vault dimensions. Failure modes under the assumption of: (c) no interlocking and tie forces equal to 3.0 kN; (d) no interlocking and tie forces equal to 25.0 kN; (e) with interlocking and without ties; and (f) with interlocking and tie forces equal to 25.0 kN (Cascini, Gagliardo and Portioli, 2020).254
- Figure 5.47 - Failure mechanisms predicted for horizontal live loads along y-axis: (a) $\mu = 0.6$ and (b) $\mu = 0.3$ (Cascini, Gagliardo and Portioli, 2020).....256
- Figure 5.48 - (a) Sensitivity analysis to friction coefficient μ ; and (b) collapse load factor vs. iteration for $\mu = 0.6$ (Cascini, Gagliardo and Portioli, 2020). ..256
- Figure 5.49 - Two-storey masonry building: Predicted failure mechanism under support vertical movement (Cascini, Gagliardo and Portioli, 2020).257
- Figure 5.50 – Palazzo d’Avalos in Procida, Italy. Picture by Giovanni De Simone, 2018.....258
- Figure 5.51 – The position of the Palazzo d’Avalos on Procida island, located in Terra Murata village (source: Google Earth).259
- Figure 5.52 – Palazzo d’Avalos historic evolution from the construction until the current days.260

Figure 5.53 – Palazzo d’Avalos historic evolution maps: (a) design by Eng. Agostino Caputo, 1738; (b) actual intervention realized in 1738; (c) design by Eng. Giovanni Campana; (d) current state of the building.	262
Figure 5.54 – Maps developed in (Regione Campania, 2017): (a) landslide risk and (b) landslide hazard.	263
Figure 5.55 – Foundation drilling surveys designed by Prof Eng. Mario Rosario Migliore and Prof. Giovanbattista de Medici, 1989.....	265
Figure 5.56 – Crack pattern representation in order to describe the settlement-induced collapse mechanism exhibited by Palazzo d’Avalos. (Source: Master Thesis by Giovanni de Simone, 2019).	267
Figure 5.57 – Rigid block model (generated in CAD environment) of the investigated portion of Palazzo d’Avalos.	268
Figure 5.58 – Collapse mechanisms predicted by the limit analysis rigid block proposed formulation in the case of lateral live loads applied in both (a)(b) longitudinal and (c)(d) transversal directions.	270
Figure 5.59 – Settlement-induced collapse mechanism capacity investigation: (a) identification of the selected masonry wall used for the 2D settlement analysis and (b) rigid block model (generated in Cad environment) of the selected bearing wall.....	271
Figure 5.60 – Comparison between (a) the current crack pattern observed in the investigated façade and (b) the crack pattern predicted by the limit analysis rigid block proposed formulation in the case of uniform settlement applied to the entire bearing walls.	272
Figure 6.1 - Wall sample 12C: experimental set-up (a) and geometrical properties (b).	279
Figure 6.2 - Wall sample 12C (Portioli and Cascini, 2016) comparison between experimental (a)(b) and non-linear kinematic numerical (c)(d) outcomes: deformed shape of the specimen and plot of the failure mode at vertical displacement equal to (a)(c) 20 mm and (b)(d) 50 mm.	280
Figure 6.3 - Wall sample 12C (Portioli and Cascini, 2016) comparison between experimental and non-linear kinematic numerical outcomes in terms of loss of base reaction against vertical imposed settlement.	281
Figure 6.4 - Portal frame 8B_FH: experimental set-up (Portioli and Cascini, 2017) (a) and geometrical properties (b).....	282

Figure 6.5 - Portal frame 8B_FH_2: comparison between experimental (a) and non-linear kinematic numerical (b) outcomes: deformed shape of the specimen and plot of the failure mode at vertical displacement equal to 100 mm.	284
Figure 6.6 - Portal frame 8B_FH (Portioli and Cascini, 2017) comparison between experimental and non-linear kinematic numerical outcomes in terms of loss of base reaction against vertical imposed settlement.	285
Figure 6.7 - T-panel: views (a)(c) and sketches (b)(d) of the experimental test set-up (Gagliardo et al., 2021).	286
Figure 6.8 - Failure mechanism at incipient collapse ($\delta = 110$ mm) of the T-panel without interlocking (S1 specimen): experimental (a) versus numerical (b) comparison (Gagliardo et al., 2021).	288
Figure 6.9 - Failure mechanism at incipient collapse ($\delta = 140$ mm) of the T-panel with interlocking (S2 specimen): experimental (a) versus numerical (b) comparison (Gagliardo et al., 2021).	288
Figure 6.10 - Base reaction against vertical settlement displacements for three test repetitions: S1 (a) and S2 (b) specimens (Gagliardo et al., 2021).	289
Figure 6.11 - Small-scale model of the Loggia Palace in Brescia (Italy): (a) dimensions in mm and location of dial gauges at points a, b and c; (b) location of the additional loads (Gagliardo et al., 2021).	291
Figure 6.12 - Test 1: crack pattern for both experimental (a) and numerical (b) case (Gagliardo et al., 2021).	292
Figure 6.13 - Test 2: crack pattern for both experimental (a) and numerical (b) case (Gagliardo et al., 2021).	292
Figure 6.14 - Experimental measured values versus numerical results, in terms of crack width and horizontal displacement against vertical settlement: (a) Test 1; (b) Test 2 (Gagliardo et al., 2021).	293
Figure 7.1 - Parameters involved in the damage classification proposed in (Burland and Wroth, 1974).	302
Figure 7.2 - Damage levels definition in the case of (seismic) push-over analysis (a), (b) and (settlements) push-down analysis (c), (d) (Gagliardo et al., 2021).	303
Figure 7.3 - Damage levels identification by using push-down capacity curve: (a) proposed criteria; (b) yielding displacement definition.	304

Figure 7.4 - Loggia Palace in Brescia (Italy) (a); geometrical properties (measures in m) and loading condition of the full-scale façade model (b).....	306
Figure 7.5 – Full-scale monumental building façade. Sensitivity analysis to the block size: large mesh (a)(b); reduced mesh with one-block-lintels (c); reduced mesh with flat arch lintels (d) (Gagliardo et al., 2021).	307
Figure 7.6 - Full-scale monumental building façade. Crack 1 openings development in terms of measure of the crack width against settlement: large mesh (a) and reduced mesh (b) (Gagliardo et al., 2021).....	308
Figure 7.7 - Criteria proposed for the definition of the damage limits in the case of a push-down curve obtained with the non-linear kinematic rigid block model with elastic contacts applied to a full-scale monumental building façade (Gagliardo et al., 2021).	309
Figure 7.8 - Full-scale monumental building façade. Comparison of the proposed approach with empirical methods: (Skempton and Mac Donald, 1956) (a); (Boscardin and Cording, 1989) (b).	311
Figure 7.9 – (a) Façade of the church of the Natività della Beata Vergine Maria in Bondeno; (b) numerical model and geometry.	312
Figure 7.10 – Predicted failure modes and crack patterns for the church façade. Comparison between (a) linear kinematic model outcomes, and non-linear kinematic model outcomes in the case of (b) $2e6 \text{ kN/m}^3$, (c) $4e6 \text{ kN/m}^3$ and (d) $8e6 \text{ kN/m}^3$ normal contact stiffness k_n	314
Figure 7.11 - Comparison between linear and non-linear kinematic outcomes in terms of loss of base reaction against applied settlement displacement at foundation of a masonry church façade.	315
Figure 7.12 - Damage propagation analysis of the full-scale masonry church façade. Predicted crack patterns at (a)(b) 0.05 m. (c)(d) 0.15 m and (e)(f) 0.25 m according to the (a)(c)(e) coarse and (b)(d)(f) refined mesh.	317
Figure 7.13 - Full-scale masonry church façade. Sensitivity analysis to the mesh size in terms of crack widths against foundation settlement: (a) crack A and (b) crack B.	318
Figure 7.14 - Criteria proposed for the definition of the damage limits in the case of a push-down curve obtained with the non-linear kinematic rigid block model with elastic contacts applied to a full-scale historic masonry church façade...	319

Figure 8.1 – Qualitative examples of (a) vulnerability curve and (b) fragility curves.	332
---	-----

List of Tables

Table 2.1 - Case studies of subsidence (modified after (Nelson, 2012)).	18
Table 2.2 - Slope movements types and processes (Varnes, 1978).	25
Table 2.3 - Landslide classification according to activity (Cruden and Varnes, 1996).	34
Table 2.4 - Landslide classification according to the description of first movement (Cruden and Varnes, 1996).	35
Table 2.5 - Landslide intensity classification according to the not stabilized mass (Fell, 1994).	37
Table 2.6 - Italian municipalities affected by subsidence according to the Italian Environmental Data Yearbook 2018.	43
Table 2.7 - National mosaic of landslide hazard zones according to (River Basin Plans PAI).	51
Table 2.8 - High and very high landslide hazard zones on regional basis according to (River Basin Plans PAI).	52
Table 2.9 - Landslide risk indicators related to population, families, buildings, industry and services, cultural heritage (Trigila et al., 2018).	61
Table 4.1 - The scheme of the Excel spreadsheet obtained using the AutoCAD data Extraction.	182
Table 5.1 - Masonry arches and vaults under vertical live loads: comparison of numerical results.	208
Table 5.2 - Masonry dome under horizontal live loads: comparison of numerical and experimental results.	214
Table 5.3 - The case study of the simple wall: numerical output using rigid block limit analysis.	223
Table 5.4 - The case study of the T-wall: numerical output using rigid block limit analysis.	224
Table 5.5 - Numerical outcomes for in-plane and out-of-plane collapse mechanisms analysis of Ponti della Valle di Maddaloni.	228

Table 5.6 - Numerical outcomes for lateral loads-induced collapse mechanisms analysis of a single-nave masonry church.....	232
Table 5.7 - Circular arch subjected to spreading support: comparison of numerical and analytical results.....	238
Table 5.8 - Base reaction and CPU Time in the case of the façade without openings subjected to short settlements.....	244
Table 5.9 - Base reaction and CPU Time in the case of the façade without openings subjected to medium settlements.....	244
Table 5.10 - Base reaction and CPU Time in the case of the façade without openings subjected to long settlements.....	244
Table 5.11 - Base reaction and CPU Time in the case of the façade with openings subjected to short settlements.....	248
Table 5.12 - Base reaction and CPU Time in the case of the façade with openings subjected to medium settlements.....	248
Table 5.13 - Base reaction and CPU Time in the case of the façade with openings subjected to long settlements.....	248
Table 5.14 - Two-story masonry building subjected to horizontal live loads along x-axis. Numerical results for the investigated configurations.....	255
Table 5.15 – Numerical outcomes of the collapse mechanisms analysis in the case of lateral live loads applied in both longitudinal and transversal directions....	270
Table 6.1 - Small scale wall panels: comparison of numerical and experimental (average of three tests is given) results.....	290
Table 7.1 - Comparison of settlement-induced damage classifications proposed in literature and in the present paper applied to a full-scale monumental building façade.....	310
Table 7.2 – The façade of the church of Natività della Beata Vergine Maria in Bondeno: comparison between linear and non-linear kinematic: numerical outcomes.....	316
Table 7.3 - Comparison of settlement-induced damage classifications proposed in literature and in the present paper applied to a full-scale historic masonry church façade.....	320

Abstract

The issue of built Cultural Heritage (CH) exposed to natural hazards is a challenging topic in both research and engineering practice. In the last decades, many efforts were addressed to the protection of CH against seismic hazard, which is the main threat for the integrity and stability of structures. On the other hand, settlements induced by hydrogeological phenomena such as subsidence and landslides also represent a severe risk for existing buildings. Nevertheless, the investigation of damage induced by settlements on structures is a still open challenge. Empirical approaches were proposed, commonly based on the assessment of damage in terms of local parameters, e.g. crack widths. However, the severity of crack width can be affected by different factors such as structural configuration, masonry texture and material properties. Thus, models for the quantitative assessment of damage in terms of global safety levels of structures subjected to foundation movements are demanded.

In this framework, this dissertation thesis aims at the development and application of a numerical approach based on rigid block modelling for the performance-based damage assessment of masonry structures subjected to settlement. Two in-house numerical models are proposed, namely a rigid block model with rigid contacts for the linear kinematic analysis and a rigid block model with no-tension elastic contacts for the non-linear kinematic analysis. The first tool aims at the prediction of the failure shape for settled structures as well as the value of the base reaction at the onset of mechanism. It is worth noting that masonry buildings usually exhibit a resilient safety behaviour with respect to settlements. Conversely, appropriate considerations of serviceability limit state are demanded to control damage on the structure and preserve the aesthetics. To this end, the non-linear kinematic model aims to predict the response of masonry structures under settlements also in the early damage states. The output is mainly represented by specific capacity curves, named “push-down curves”, where the loss of base reaction is plotted as a function of the displacement of a control point at the settling support. Thus, the numerical formulation allows the damage propagation monitoring, from crack opening until incipient collapse. The dissertation thesis explores the possibility to use such a capacity curve to propose criteria for the displacement-based damage assessment and quantification. A comparison of the proposed approach with empirical damage classification methods is performed.

About the author

Raffaele Gagliardo held a Master degree in Architecture at the University of Naples “Federico II” in 2015, discussing a thesis on a comparison between the European and North-American codes in the design criteria of Inverted-V concentrically braced frames, under the supervision of Prof. Raffaele Landolfo. He attended a PhD Course in Structural, Geotechnical Engineering and Seismic Risk, at the Department of Structures for Engineering and Architecture of the University of Naples “Federico II”. As for the research work, he is mainly focusing on the assessment of historical masonry structures subjected to seismic events, settlement and moving supports. He provided a contribution to the development and application of in house-made numerical tools for both linear and non-linear kinematic analysis of structures idealized into an assemblage of rigid blocks interacting at frictional contact interfaces. He is co-author of 4 articles and 4 conference papers. He participated as presenting author in both national and international conferences.

Chapter 1

Introduction

1.1 Background and Framework

Most of built Cultural Heritage is made by historic masonry structures which have been living for a long time. How to protect these pieces of art against natural hazards is a real mission for the human beings to avoid that something unique could be lost for ever.

Masonry structures can suffer severe damage due to both seismic loads and settlements. In the past decades, most of the research activity on vulnerability and damage assessment of historic masonry buildings was focused on seismic actions. Nevertheless, it is well known that settlements are further causes of damage, and even collapse for existing masonry structures. Settlements can be originated both from natural and man-made hazards such as landslides, floods, subsidence and tunneling. Such phenomena, whose effects have been even getting worse because of climate change and uncontrolled urbanization, represent a severe risk not only for the life-safety but also for the preservation and integrity of cultural heritage monuments and buildings. Thus, specific analysis methods and verification approaches play an important role in the Cultural Heritage risk

mitigation against natural hazards. The studies developed in the last decades on the issue of masonry structures subjected to foundation movements allowed to create a strong knowledge, with particular regard to the observation of typical damage patterns for specific masonry types, such as façades, corners, connection, arches and vaults (Mastrodicasa, 1943). It was observed that these types usually develop typical failure patterns when they are affected by ground movements at the base, also depending on the position of the settled area and on the portion of the structure involved in the movements. Figure 1.1 shows a series of typical damage patterns which can be observed in masonry types.

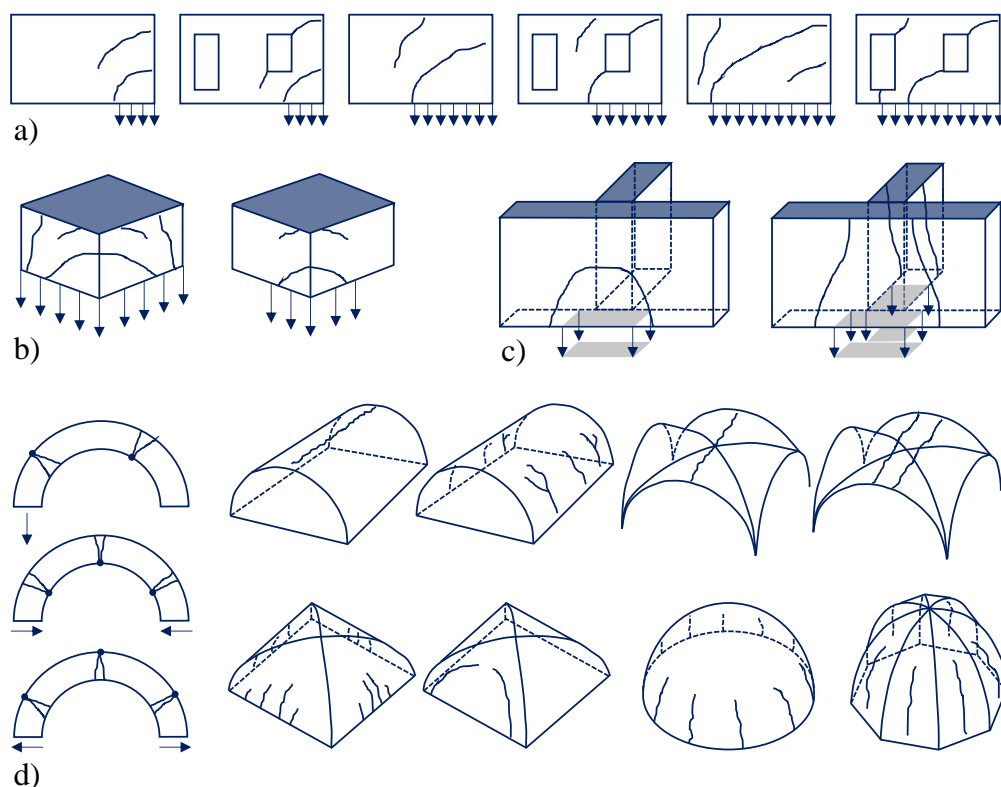


Figure 1.1 – Typical damage patterns for masonry structures subjected to settlements: (a) Façade with and without openings; (b) buildings corner connections; (c) T-connections; (d) arches, vaults and domes.

A challenging task in this field is represented by the ability to develop numerical formulations and software able to simulate the capacity behaviour of such a structure against natural threats in order to analyse the structural vulnerability and design effective solutions to protect its priceless value. The success of a numerical model lies in the capability to simplify a problem like the settlement hazard, that is highly complex in its nature. Several modelling approaches exist in literature, each one of them trying to better simulate the very hard structural behaviour of a material like masonry, which exists in a huge number of different mechanical and constructive solutions. This great heterogeneity of masonry-like material is mainly due to the over-centuries use of it compared to innovative materials like steel and reinforce concrete.

The present thesis is framed within the activities of the research project PERICLES “Protecting the Cultural Heritage from water-soil interaction related threats”, funded by the Italian Ministry of Education, Universities and Research (MIUR). The project aims to develop sustainable management strategy for Cultural Heritage (CH) exposed to landslides and subsidence, with a special focus on vulnerability assessment models for masonry structures. This project also developed a sustainable management strategy for CH at water-soil interaction risk that aims to identify priorities and innovative methodologies for risk assessment, monitoring and mitigation together with conservation and valorisation measures for CH sites and structures. The Consortium is composed by five Research Unit (RU): RU1 (Naples), coordinated by Prof. Landolfo focuses on vulnerability models; RU2 (Salerno) coordinated by Prof. Petti deals with geotechnical issues; RU3 (Genoa) coordinated by Prof. Calderini is working on damage abacus; RU4 (CNR) coordinated by Senior Researcher Fornaro deals with satellite measurements; RU5 (Palermo) is coordinated by Prof. Angelini deals with valorisation policies. A big group of end-users is also involved in the project.

PERICLES is a three-year project, started on 5th of February of 2017 and is now ending with the publication of the final deliverables. The reference environment is mainly represented by: assets subjected to prevailing in-plane damage (Figure 1.2a), assets subjected to prevailing out-plane damage (Figure 1.2b), blocky

structures subjected to overturning (Figure 1.2c), arched structures in-plane (Figure 1.2d), building aggregates (Figure 1.2e).

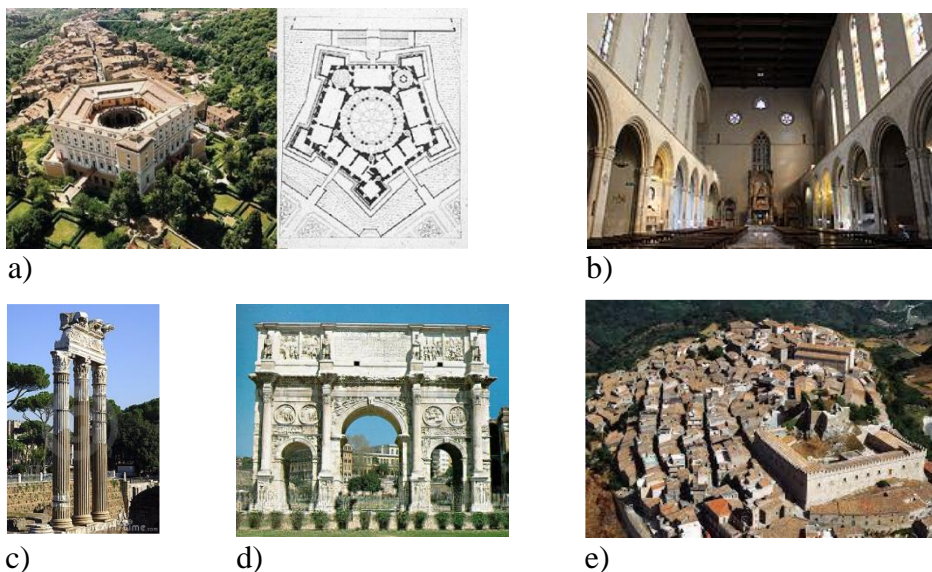


Figure 1.2 - PERICLES project field of application: (a) assets subjected to prevailing in-plane damage; (b) assets subjected to prevailing out-plane damage; (c) blocky structures subjected to overturning; (d) arched structures in-plane; (e) building aggregates.

In this framework, PERICLES project is mainly devoted to the risk analysis of two natural hazards, that are essentially landslides and subsidence, deeply investigated in Chapter 2. With reference to water-soil interaction threats, the main tasks of the project are essentially (Figure 1.3a):

- identify, localize and model which hazards could affect a CH structure and to which extent.
- model the response of CH structures to the hazard and quantify their vulnerability.
- plan appropriate, cost-effective mitigation, conservation and protection measures.
- develop a management approach that integrate methods and tools into an end-user management strategy for CH.

The methodological approach proposed within PERICLES project is based on three keywords, namely multi-disciplinary, multi-risk and multi-scale (Figure 1.3b).

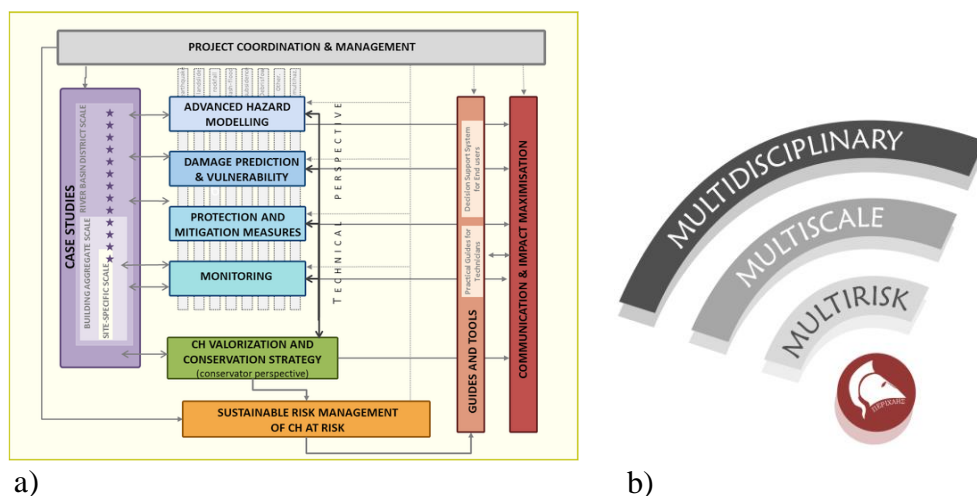


Figure 1.3 - PERICLES project: (a) main task flowchart and (b) proposed methodological approach.

Multi-disciplinary means that the project relies on the collaboration between workers from several scientific and professional fields: experts from geotechnical and structural engineering, conservation, sociology, ecology, telecommunication engineering signal and image processing, end-users.

Multi-risk means that the project aims to develop a sustainable strategy to protect built Cultural Heritage against several natural hazards such as fast (debris flow, flash flooding, etc.) and slow-moving landslides as well as subsidence.

Multi-scale means that the project has the scope to analyse the water-soil interaction related threats considering different scales, that are essentially:

- The small-medium scale (1:100000 – 1:25000) also named “River Basin District scale”. At the small-medium scale the project identifies the CH at risk-prone areas by combining the satellite data observation with current risk zoning maps and other available knowledge in the literature.

With respect to the vulnerability assessment, the structural response can be evaluated by means of vulnerability indexes based on the specific CH typology and the analysis of past damages.

- The large scale (1:25000 – 1:5000) also named “Building aggregate scale”. At large scale, heuristic and/or simple engineering methods are developed to assess the impact force caused by fast landslides on the CH. Moreover, new zoning criteria are developed, also by means of satellite data elaboration, to localize with the aid of gradient displacement maps the cultural heritage at risk interacting with slow-moving landslides or subsiding areas. The vulnerability of CH against such hazards is evaluated by means of fragility functions. Procedures for the definition of vulnerability curves using numerical, analytical and empirical approaches are developed and calibrated for the selected case studies.
- The detailed scale ($> 1:5000$) also named “site – specific scale”. At detailed scale, quantitative analysis of the actions induced by landslides and subsidence on the CH structures are provided (in terms of vertical and horizontal displacement, impact forces and so on) with the aid of advanced methods. The evaluation of structural vulnerability is carried out according to refined numerical models taking into account geotechnical and structural non-linearity in both static and dynamic field.

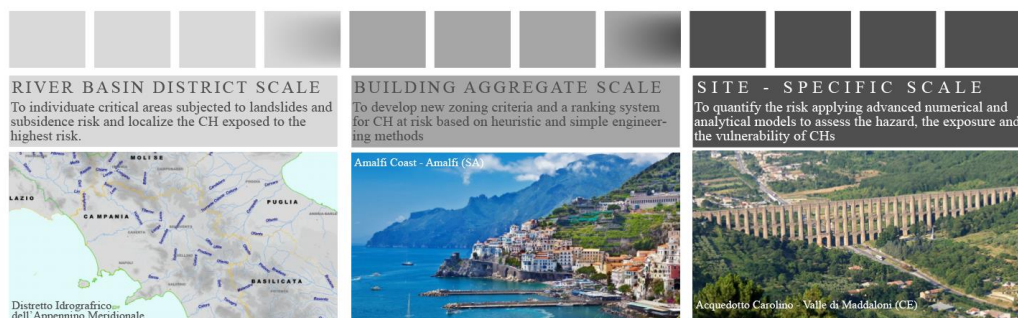


Figure 1.4 - PERICLES project: multi-scale top-down approach.

The project is based on a case studies approach pre-selected following a top-down approach. At the River Basin scale (small-medium scale), the Campania

Region has been pre-selected considering its high exposure to the water-soil related hazards. At this scale, the main aim of the research is to individuate critical areas subjected to landslides and subsidence risk and to localize the CH exposed to the highest risk. Going down to the building aggregate the main goals is to develop new zoning criteria, with the aid of the available databases and satellite data elaboration, and to provide a ranking system for exposed CH at risk using heuristic and/or simple engineering methods. At site specific scale detailed analysis by means of numerical and analytical refined models are performed (Figure 1.4).

In such a framework, the projects started with the following scopes:

- to better identify priorities for the Italian cultural heritage risk analysis and management.
- to develop a novel homogenised risk management strategy for CH at risk and reduce fragmentation.
- to advance modelling of natural hazards
- to better predict and assess damage at different scales.
- to provide reliable predictive and cost-effective mitigation measures.
- to adapt advanced monitoring technologies to CHs monitoring requirements.
- to assess and potentially prioritize policy options for the purpose of informing the decision process and promote improved practices.
- to inform and shape robust restoration and adaptation policies.

The project activities were managed according to three indicated phases:

- phase 1 focused on an in-depth implementation of specific technical topics, dealing with scientific open issues to be solved for the realization of the expected multi-risk and multi-scale strategy.
- phase 2 was devoted to case studies. The proposed models, methods and tools was tested and validated, corrective measures are defined, when appropriate.
- phase 3 focused on the transition from current practice to a novel strategy for risk management and firstly intends to harmonize the achieved results

and then propose a novel strategy taking into account scientific findings on both risk analysis and mitigation, CH conservation and End User's needs.

1.2 Motivation of research

Recent events highlighted the vulnerability of masonry-made Cultural Heritage against natural hazards. It is worth noting that seismic-induced damage is more in depth investigated compared with other natural hazards. In the seismic field, both European and North-American international codes (*EN 1998-2005. Eurocode 8: Design of structures for earthquake resistance*, 2005; American Society of Civil Engineers, 2017) adopt the Performance-Based Assessment (PBA) which assumes a set of Performance Levels (PLs) that a specific structure can exhibit against defined earthquake hazard levels. The PBA approach feasibility is far from easy especially in the case of existing building (e.g. built cultural heritage) because ancient historical buildings were constructed following the so-called “rule of thumb” (based on the experience from previous built structure) and they were not capacity designed and it is not possible to analyse them with linear procedures and behaviour factor approach. The idea of limit states is related to the possibility that the structure should accommodate different performance levels (PLs) which represent the attainment of specific damage states (DSs) and produce specific damage levels (DLs). Two different types of limit states are introduced in the seismic Italian Code (Ministero delle infrastrutture e dei trasporti., 2018, 2019): Ultimate Limit State (SLU) and Serviceability Limit State (SLE). The Ultimate Limit State includes both Near Collapse Limit State (SLC) and Life-Safety Limit State (SLV). The Serviceability Limit State includes both Damage Limit State (SLD) and Operativity Limit State (SLO). The Italian guidelines for the evaluation and reduction of seismic risk of cultural heritage (Consiglio superiore dei lavori pubblici, 2010) also introduce a new limit state for the assets of the Cultural Heritage, named Damage Limit State for Artistic Assets (SLA), in order to save the artistic and historical values of specific pieces of arts (such as frescoes and plasters).

In this framework, the dissertation thesis aims at the performance-based assessment (PBA) of masonry panels subjected to settlements. Contrary to the seismic analysis, in the field of hydrogeological risk and settlement analysis, serviceability limit state represents the higher challenging task whereas the incipient collapse is almost impossible to reach in terms of ultimate settlement displacement according to the high resilience of masonry structure to accommodate large foundation movements. In this framework, several methods were proposed in literature for the assessment of the structural behaviour of settled masonry buildings in the early damage states. It is worth noting that most of them evaluates the settlement-induced damage only in terms of severity of crack width. With this in mind, the development of methods for a quantitative assessment of damage for masonry structures subjected to foundation movements in terms of safety levels of the overall structure is a still open challenge.

1.3 Thesis outline and organization

The thesis organization is here reported and is showed in Figure 1.5.

Chapter 2. The dissertation starts with a full description of settlement-induced damages for masonry structures. An overview of various phenomena in the field of hydrogeological hazard (such as landslides and subsidence) is also pointed out in this chapter. The scope is to investigate the distribution of such a severe hazard at the national and international scales as well as to describe possible solutions to derive movement profiles induced by the analysed phenomena.

Chapter 3. A comprehensive description of the masonry-like material in terms of mechanical properties as well as various numerical approaches proposed in literature for the analysis of masonry structures is pointed out. Masonry is the first material human beings applied to construction and buildings, resulting in a very long history where various and different constructive solutions were proposed. As a matter of fact, historical masonry structures can be very sensitive to seismic action and ground movement, exhibiting various crack patterns based on load intensity and structural quality. In this framework, mechanical behaviour of masonry is described according to a macroscopic approach. The need for

numerical model able to simulate the complex behaviour of such a structure is crucial for the analysis and the assessment of monumental buildings belonged to the Cultural Heritage. A lot of modelling strategies were proposed in literature to face this challenging task.

Chapter 4. The modelling approach is part of a numerical project founded by Francesco Portioli and Lucrezia Cascini at the University of Naples “Federico II”. This project was originally devoted to the development of a fast and accurate software tool for three-dimensional limit analysis of historic masonry structures subjected to point live loads, seismic induced lateral loads and moving supports. In this thesis, a progress of the previous formulation (based on limit analysis) is developed. A 2-D rigid block model with unilateral elastic contacts and finite friction is developed for the evaluation of the displacement capacity in the large displacement regime by push-down analysis. In this Chapter the two above-mentioned numerical formulations, based on linear and non-linear kinematic analysis approaches respectively, are extensively described.

Chapter 5. This Chapter is dedicated to the description of the results obtained by numerical applications using the first proposed computational model, i.e. the rigid block model for linear kinematic analysis. A huge number of case studies are presented in this section to test the abilities of the limit analysis formulation against both seismic-induced lateral loads and foundation movements.

Chapter 6. The validation of the novel proposed rigid block model based on non-linear kinematic analysis is performed. To this scope, comparisons with experimental tests on small-scale masonry panels subjected to settling supports are described and discussed.

Chapter 7. A displacement-based assessment approach for the damage classification of masonry panels is considered to evaluate the possibility to extend consolidated procedures for the assessment of global behaviour in the field of seismic assessment to the case of settlements. Following classic force-displacement methods that are used in the case of seismic actions, capacity curves are proposed for the damage assessment induced by foundation movements. Those state the relation between the base reaction at the moving supports and the displacement of a control point, which is obtained from the push-down analysis.

The potentialities of the proposed performance-based assessment approach are discussed by comparisons with empirical methods for the damage assessment of masonry structures subjected to settlements.

Chapter 8. Conclusive remarks and further developments of the work carried out in this dissertation thesis are described. The next step of the on-going research project is essentially represented by the capacity investigation of masonry structures subjected to a combination of lateral loads and foundation settlements. The fragility and vulnerability analysis of historical masonry structures could also represent an important development to be faced. It is worth noting that major progress in the field of fragility analysis were developed in the field of seismic action, while the fragility against settlement is a still open challenge. In this framework, the first topic to be faced will be the possibility to numerically investigate the influence of settlement effects on the seismic capacity of masonry structures.

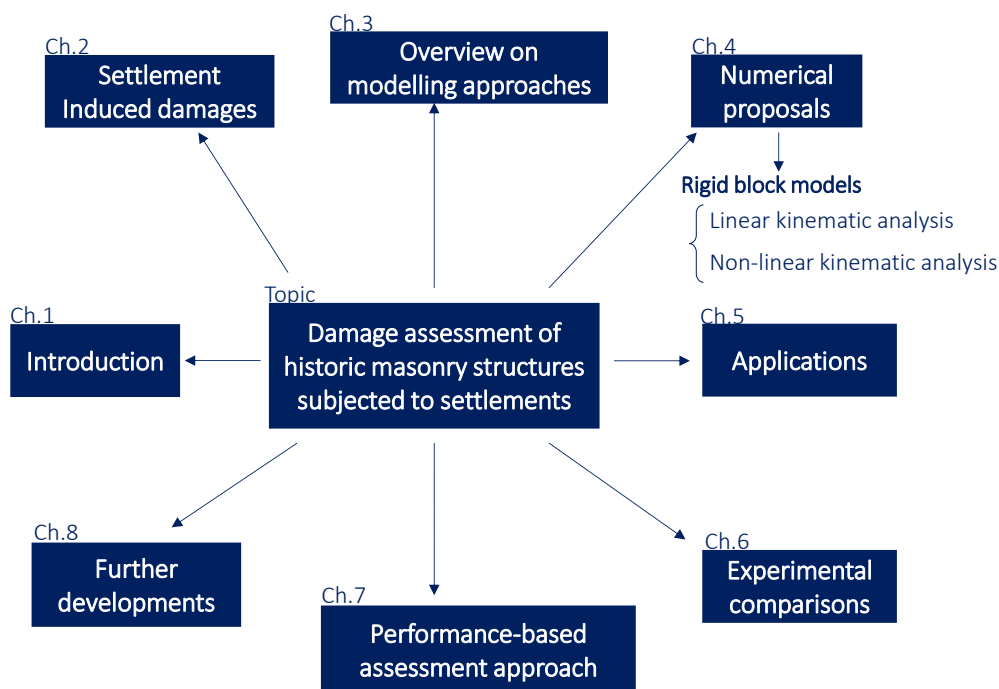


Figure 1.5 – Flowchart of thesis organization.

References

American Society of Civil Engineers (2017) *Minimum Design Loads and Associated Criteria for Buildings and Other Structures* (7-16).

Consiglio superiore dei lavori pubblici (2010) *Circolare n. 26/2010 - «Linee guida per la valutazione e la riduzione del rischio sismico del patrimonio culturale con riferimento alle Norme tecniche per le costruzioni di cui al decreto del Ministero delle Infrastrutture e dei trasporti del 14 gennaio 2010»*.

EN 1998-2005. *Eurocode 8: Design of structures for earthquake resistance* (2005).

Mastrodicasa, S. (1943) *Dissesti statici delle strutture edilizie. Diagnosi e Consolidamento*. Edited by Ulrico Hoepli Editore. Milano.

Ministero delle infrastrutture e dei trasporti. (2018) *Decreto ministeriale 17 gennaio 2018 - Aggiornamento delle «Norme tecniche per le costruzioni»*.

Ministero delle infrastrutture e dei trasporti. (2019) *CIRCOLARE 21 gennaio 2019, n. 7 C.S.LL.PP - Istruzioni per l'applicazione dell'«Aggiornamento delle «Norme tecniche per le costruzioni»»*.

Chapter 2

Settlement-induced damages, monitoring and movement profiles

2.1 Introduction

The main topic this research dissertation has been facing deals with the damage assessment of masonry structures subjected to foundation movements. This is a challenging issue in literature, where structural, geotechnical and geological expertise are demanded at the same time. The possibility to best focus this topic strictly depends on an adequate knowledge of the triggering phenomenon, i.e. the foundation settlement. In this spirit, the present Chapter aims to deeply investigate the settlement risk in terms of promoting causes and observed effects. The causes are mainly related to the man-made and natural categories. The various reported sections will describe the different natural phenomena able to provoke settlement movements at building foundation, in terms of intensity and distribution with regard to national and international scale.

As a matter of fact, the vulnerability assessment and investigation of built Cultural Heritage mainly focused on the safety of historic masonry structures against seismic-induced lateral loads. Nevertheless, the last decades showed to which extent settlements of the foundation system can represent a severe threat

for affected structures, in terms of both damage and collapse, especially in the case of existing monumental buildings (Dejong, 2016).



a)



b)



c)



d)

Figure 2.1 - Examples of crack patterns and collapse mechanism induced by settlements in existing masonry and confined masonry structures: A clay brick masonry building in Bovino, Italy, 2019 (a) (b); Building in Riviera di Chiaia, Naples, Italy, 2013 (c); Building of the Faculty of Veterinary Medicine, Naples, Italy, 2015 (d).

With the scope to highlight this point, Figure 2.1 shows some examples of crack patterns and collapse mechanisms induced by settlements in existing masonry

and confined masonry structures located in Italy due to ground movements occurred in the last few years.

In this framework, Chapter 2 aims at developing two main points. First of all, an overview on the various events (essentially subsidence and landslides) which can produce foundation settlements is reported, in terms of both morphological and geological properties. Then, a description of the damage-induced by each one of the mentioned events is investigated with reference to national and international database in order to show the weight of this fundamental hazard in everyone life, too often forgotten or neglected because of other crucial hazards such as seismic one. The final scope of this Chapter is represented by the solutions presented in literature to derive a field of settlement displacements by the investigated hazard phenomena such as subsidence and landslide. As for the motivations of the present dissertation, the possibility to correlate monitored natural events to the promoted effects in terms of induced displacements can be regarded as a fundamental point in order to open to the topics discussed in the next Chapters. In this spirit, the next Chapters will present numerical simulations of masonry panels subjected to base displacements where the settlement profile (or the assigned vector of foundation displacements) is already given. For sake of simplicity, most of the simulations deals with uniform settlement.

2.2 Settlement induced by natural and man-made hazards

The first part of this Chapter is devoted to the description of the settlement induced by natural and man-made hazards. This issue is shared among structural, geotechnical, and geological research fields, being involved factors and parameters related to the movements of the various soil layers, which can somehow affect the foundation systems and the building structural response in turn.

In the case of natural triggering causes, subsidence and both slow-moving and fast-moving landslide phenomena are among the most damaging geohazards in terms of both their worldwide distribution and their related effects on structure

and infrastructures. The number of events significantly grew in the last decades and they are expected to increase for many reasons, such as the increased demographic pressure and climate changes (Füssel *et al.*, 2012). With regard to the severity of the above-mentioned phenomena, it is worth noting that slow-moving landslides are widely spread in Italy, but they usually do not cause any loss of human life. However slow-moving landslides can induce severe effects on structures causing loss of functionality, or even collapse, for the involved buildings. On the other hand, fast-moving landslides often caused victims and big economic damages mainly due to the large distance that the moving soil masses is able to cover in a very short time as well as the unexpected nature of the first-failure stage (Cascini, 2005). Regarding the effects on buildings, it is commonly stated that the impact with fast-moving landslides results as the highest damage, most of the case corresponding to a full or partial collapse of the structure. As for land subsidence, it generally causes severe damages to build facilities due to the seawater intrusion and flood. In this case, the damage severity on affected building is a function of the structural typology and of the soil-to-foundation relative stiffness. In this framework, masonry buildings on high deformable shallow footings are very fragile against land subsidence.

As for the tools developed for the analysis of such a phenomenon, it is generally introduced a multi-scale approach for the investigation of landslides. In the case of medium scale vulnerability curves are required in order to correlate the intensity of the landslide event and the expected damage on affected buildings based on their locations with respect to the movable soil masses. At a detailed scale instead, the success of the adopted analysis tool is related to the ability to combine the results obtained with numerical formulation and those derived by applying empirical damage criteria. On the other hand, in the case of subsidence the analysis tools are mainly based on the measurement of the superficial strains, which are the most relevant effects associated to high-risk events. Different monitoring techniques were developed to this scope, aiming at modelling the natural event as a settlement profile, as showed later in this Chapter.

In the case of man-made hazard, tunneling represents one of the most relevant threats to the stability of building and infrastructures (Giardina, 2013; Dejong,

2016). These events are highly increasing in the last decades mainly due to the huge and worldwide distributed works for metro lines construction and propagation in most of the developed Countries. It is also very common a combination of different causes, e.g. the possibility of subsidence promoted by tunneling effect.

With this in mind, in the next sections the settlement causes will be deeply investigated in terms of morphological features and damage-induced on structures and buildings.

2.2.1 Subsidence

Subsidence deals with movements of ground surface, especially in the vertical direction, caused by natural or anthropogenic factors. Subsidence due to natural causes is highly slow, even developing during geological periods. Main causes of natural subsidence are essentially: tectonic movement, natural consolidation or modification of physical and chemical properties of the involved soils.

On the other hand, anthropogenic subsidence, generally very rapid, causes effects also in the short term. In this case, it can be originated by withdrawals of fluids, mining or removal of solids (e.g. tunneling). It was observed that the main cause is represented by fluids withdrawal from subsoil. Pumping fluids are generally water, oil or gas. The severity and the spatial distribution of settlements can be highly influence by soil stratigraphy, geotechnical soil properties; hydraulic conditions; withdrawal characteristics.

Mining is also a common cause of subsidence because of the possibility to produce sudden sinking. In this case, subsidence severity is mainly affected by : seam thickness, depth of working, mine geometry, total amount of mining, angle of draw, seam inclination, geological conditions, time, direction and rate of advance of the face and method of working, as reported in (Jones and Bellamy, 1973).

It is worth noting that tunnelling is another cause of subsidence due to anthropogenic factors. As described in (Peck, 1969), deformations caused by tunneling as well as the damage induced on structures and services is strictly

related to the following parameters: ground and groundwater conditions, the tunnel depth and diameter and the construction details, which is the most relevant.

City	Maximum settlement [m]	Area (km ²)	Cause	Some References
Los Angeles, U.S.A.	9	50	Petroleum withdrawal and tectonic activity	(Allen and Mayuga, 1970)
New Orleans, LA	2	175	Compaction of river sediments	(Törnqvist <i>et al.</i> , 2008)
Houston, USA	2.7	12100	Coastal sediments	(Gabrysch, 1984)
San Joaquin Valley, U.S.A.	8.8	13500	Groundwater withdrawal	(Prokopovich and Marriott, 1983; Ireland, Poland and Riley, 1984)
Mexico City	8.5	225	Filled lake	(Booker, Carter and Small, 1985; Bell, 1993; Ovando-Shelley <i>et al.</i> , 2003; López-Quiroz <i>et al.</i> , 2009)
Tokyo, Japan	4.5	3000	Groundwater withdrawal from unconsolidated coastal sediments and tectonic activity	(Konagai <i>et al.</i> , 2013)
Niigata, Japan	3	500	Groundwater withdrawal from unconsolidated coastal sediments	(Okumura, 1969)
Shanghai, China	2.63	121	Ground water withdrawal	(Shi <i>et al.</i> , 2008)
Bangkok, Thailand	1	800	Groundwater withdrawal from unconsolidated river sediments	(Phien-wej, Giao and Nutalaya, 2006)
Venice, Italy	0.22	150	Groundwater withdrawal from unconsolidated coastal sediments	(Ricceri, 2007)
Bologna	4	225	Groundwater withdrawal	(Modoni <i>et al.</i> , 2013)
Ripon, England	30	300	Dissolution of Gypsum	(Cooper, 2008)

Table 2.1 - Case studies of subsidence (modified after (Nelson, 2012)).

The main causes for subsidence events were described. Nevertheless, most of cases are characterized by a combination of causes for the development of the subsidence phenomenon. In such a case, it is not easy to exactly define the weight of the various causes and the promoted effects. In the majority of cases, subsidence events are induced by both natural and anthropogenic causes: one of the most common examples is represented by the construction of cities on

unconsolidated soils. As a matter of fact, unconsolidated clays (or silts, peats, sands) are highly sensitive against subsidence. On the other hand, building cities is one of the main causes of subsidence mainly due to the following factors: the compaction of sediments under the weight of structures; the loss of the water table as a consequence of drainage in the involved surface; the use of water for several needs, both at the industrial and human levels. Huge civil engineering work such as the construction of levees and dams can be also ascribed as cause of subsidence. The effect of these constructions is to suddenly stop the natural supply of new sediment to the area. The natural replenishment plays a fundamental role against the development of subsidence movements. In the case the sediment supply is cut off, the replenishment does not occur and the rate of subsidence tends to increase (Nelson, 2012).

Subsidence represents a worldwide threat. Table 2.1 aims to report various case studies, describing the main causes and the maximum settlement induced by the subsidence event. It can be observed that most of case studies reported in Table 2.1 are coastal cities (Houston and Venice) or are built on river flood plains and deltas (New Orleans, Baton Rouge, and the San Joaquin Valley of central California). Such an observation leads to the conclusion that subsidence can even produce an increase of the flood risk for specific areas. The example of Mexico City is a very specific one since the city was built in a former lake.

In the field of the research related to subsidence risk, a highly useful and important contribution is provided by the work carried out by the UNESCO Working Group on Land Subsidence (WGSL), which is one of the oldest working groups within the International Hydrological Programme (IHP), initiating activities during the 1965-1974 International Hydrological Decade (IHD). In the 1970s the WGLS started its activities to improve and disseminate knowledge on land subsidence, mainly in developed and newly developed countries and regions, e.g., Japan, The Netherlands, USA, Italy, Mexico, China, Taiwan that were strongly affected by LS following the economic boom after the World Wars. Since 2010 the members of the WGLS established new linkages and collaborations with other international and national hydrologic programs and projects concerned with the sustainable development of global land and

freshwater resources and the subsidence hazards accompanying their exploitation, mainly in developing countries such as Indonesia, Pakistan, Egypt, Vietnam, India, Iran, etc. Now, facing global changes, the need to disseminate this knowledge more broadly and to intensify applications of the accumulated knowledge is urgent. In the IHP-VIII Phase Strategic Plan (2014-2021) which addresses water security, land subsidence is considered as a major threat, mainly due to the strong anthropogenic component of the prevalent subsidence processes (UNESCO WGS�, 2021).

It is worth to note that land subsidence is still a critical societal issue. Society is facing many challenges related to the sustainable use of land and water resources that will increase in the next decades. The effects of climate change in terms of sea-level rise and variation in the distribution and timing of precipitation, runoff and recharge, are compounded by the increasing concentration of population in (mega-) cities and elsewhere along the coasts of the world. The consequences related to the expanding need of freshwater resources in even more concentrated, at-risk zones of the world will inevitably affect a growing number of people (UNESCO WGS�, 2021).

The reports produced by WGS� contain worldwide case studies in order to clarify the severe situation produced by aquifer over-exploitation. The first example deals with Jakarta, Indonesia, where the population grew from 8.2 million to more than 30 million from 1970 to 2016, groundwater extraction has caused the sinking of land surface at rates of 10-20 cm/year, with a dramatic increase of vulnerability to flooding from river and sea waters. Another described example is represented by many deltaic and coastal areas of the world (e.g., the Bengal, Mekong, Nile, and Mississippi river deltas) where land subsidence occurs as a result of compaction and oxidation increasing CO₂ emissions to the atmosphere, loosing valuable ecosystems, and enhancing the vulnerability to coastal and riverine flooding. The next case study describes the condition of numerous regions (e.g., China, Mexico, Arizona, Iran, Pakistan) in the world where large ground fractures occur as a result of land subsidence with damages to structures/infrastructures and increased aquifer contamination favoured by rapid infiltration of wastewaters and pollutants through the fissures. Finally, in Mexico

City many buildings and houses were severely damaged during the September 19th, 2017 earthquake in areas where the subsoil was strongly weakened by ground fractures that previously developed with the more than 10 m of subsidence accompanying groundwater exploitation (UNESCO WGSL, 2021).

Despite the facts that the scientific basis of aquifer-system compaction and LS due to groundwater pumping, and the means to mitigate its occurrence are well known, the process is increasingly affecting more and larger regions and with greater consequences throughout the world. Nevertheless, the attention afforded by LS in sustainable planning of water services and safe urban development is still undervalued. Although difficult to quantify, the direct and indirect costs associated to damages caused by LS are extremely large. Furthermore, the prediction reveals that the consequences are expected to increase in the next decades (UNESCO WGSL, 2021).

Until now, a still growing group of scientists from all over the world have – on a voluntary basis – joined in the WGLS. They are willing to share their knowledge, mainly collected through individual research projects, and enhance subsidence awareness. As a LaSII (Land Subsidence International Initiative) the group of experts and collaborators will seek stronger support from the UNESCO IHP and the governments of the 11 countries that are now participating, to consolidate the development of methodologies for characterization and modelling of subsidence phenomenon, monitoring networks, transfer of information to decision makers, advise creation of public policies and ideally, in the end contribute to an increase in the security and resilience of inhabitants of subsidence affected areas. Moreover, there is an urgent need to transfer the generated knowledge to developing countries with limited access to research studies and monitoring. The main scopes are to improve access to scientists and engineers from developing countries, enhance knowledge transfer and achieve a better planning for the sustainable use of the groundwater resources LS-affected regions in view of the expected climate changes (UNESCO WGSL, 2021).

With reference to the objectives and activities, Land Subsidence International Initiative focuses on four main aspects:

- land subsidence due to groundwater resources overexploitation

-
- land subsidence in coastal areas, related with sea-level rise
 - land subsidence related with earth fissures, ground fractures and fault reactivation
 - land subsidence related with water security in urban areas.

In this spirit, the main goals in the activities carried out by LaSII can be briefly summarized as follow:

- to propose effective methodologies for land subsidence identifying and establishing an inventory of subsiding areas in the world.
- to publish guidelines for the identification, investigation, development and management of subsidence-related phenomena to be used in emergencies.
- to support capacity building in member countries in order to gain and advocate better understanding and handling of hazards, vulnerabilities and benefits involving land subsidence and other groundwater-related disasters.
- to raise awareness of decision makers, implementers, users and the general public of the importance of groundwater as a store of freshwater in order to encourage improved protection and sustainable exploitation of groundwater – through leaflets, publications, the media, education and training.
- strengthen capacity building and educational capabilities in urban water management aimed at relevant target groups, including decision makers, planners and practitioners, with a special emphasis on developing countries.
- to facilitate participation of IHP Focal Points and National Committees in the development of case studies and the dissemination of land subsidence mitigation guidelines.
- strengthen linkages with other IHP Programs: ICHARM (International Centre for water Hazard And Risk Management), FRIEND (Flow Regimes from International Experimental and Network Data), HELP (Hydrology for the Environment, Life and Policy), and Urban Water Management (UWMP) together with international institutions (i.e.

International Association of Hydrogeologists, International Society of Soils Mechanics and Geotechnical Engineering, Eurogeosurveys, etc.).

- to facilitate financial support from external sources, such as World Bank, UNDP, EU, national founding agencies (UNESCO WGSF, 2021).

2.2.2 Landslides

According to (Cruden, 1991) the term landslide refers to any “movements of a mass of rock, debris or earth down a slope”. Landslides could be activated or triggered by different factors.

(Terzaghi, 1950) divides the causes triggering the landslides in: external and internal causes. The external ones produce an increase of shear stresses; they could be either human causes such as excavations at the toe or surcharging at the crest, or natural phenomena such as erosion at the toe or earthquake. Internal causes are related to a decrease in strength of materials in the absence of changes in total stresses. Very frequently, the internal causes are related to the increase in pore water pressure or progressive decrease in the cohesion of the slope materials. Intermediate causes are for example the phenomena of rapid emptying of rivers and dams or sub-surface erosion and liquefaction.

As reported in (Trigila and Iadanza, 2008a), Italian relief and lithological and structural features awarded a quite high landslide risk to the country. Landslide events are widespread all over the Italy and are the most frequently occurring natural disasters and are the second natural hazard for number of victims after earthquakes. According to (Trigila and Iadanza, 2008b), the main cause of this scenario is represented by the huge increase in the human pressure on the country since the Second World War when the urban areas and road and rail infrastructures expanded in unstable areas. In this framework, landslide is becoming a severe problem with regard to the safety of the population and damage to facilities. About the last thirty years the most disastrous events in Val Pola (1987), Piemonte (1994), Versilia (1996), Sarno and Quindici (1998), north-west Italy (2000) and in Val Canale – Friuli Venezia Giulia (2003).

2.2.2.1 Classification based on type of movement and material

Owing to the complexity and extreme variability of landslides, several landslide classifications have been proposed in the scientific literature, all based on the description of the mechanism of post-failure deformation and movement (Picarelli, 2018). Among them the most widely used are those proposed by (Skempton, 1953; Varnes, 1958, 1978; Hutchinson, 1968, 1988, 2004; Blong, 1973; Cruden and Varnes, 1996; Leroueil and Locat, 1998; Hungr *et al.*, 2001).

This variety is due to many reasons; for instance (Walker, Blong and MacGre, 1987) stress that “the basic problem, and the reasons that there are so many different classifications, is that landslides form a continuum and there are an infinite number of ways dividing a continuum”.

Among the landslide classification system that can be found in the international literature, the most widely accepted to describe both the type of movement and the involved material are the systems proposed by (Varnes, 1978) and by (Hutchinson, 1988).

In the classification proposed by (Varnes, 1978), the materials can belong to rock (a hard or firm mass that was intact and in its natural place before the movement started), earth (when a percentage equal or greater than 80% of the material particles is smaller than 2 mm) and debris (with a consistent percentage of coarse material; 20% to 80% of the particles are greater than 2 mm). With regard to the movements, the classification proposed five types, namely falls, topples, slides, spread and flows (Table 2.2).

Falls are sudden movements of masses generally involving rock materials, originating from steep slopes or cliffs. In such a case, the rock blocks separate through lines of discontinuity like fractures, joints and bedding planes and the mechanism is characterized by a combination of free-fall, bouncing and rolling. The factor which can have some influences on this type of phenomena are essentially gravity, mechanical weathering and interstitial water. Figure 2.2b shows an illustration of rockfall occurred in Valtopina, Umbria Region, in Italy.

Toppling mechanism occurs with the rotation of one or more units around a crucial point located under the unit centroid, due to the action of the gravity and

of the pressure worked by close units or by the presence of fluids in subvertical cracks. Figure 2.3b shows an example of a topple in the Canyonlands, Utah (USA).

Type of movement	Type of material		
	Bed Rock	Engineering soils	
		Predominantly coarse	Predominantly fine
Falls	Rock fall	Debris fall	Earth fall
Topples	Rock topple	Debris topple	Earth topple
Slides	Rock slide	Debris slide	Earth slide
		Rotational	
Translational		Debris spread	Earth spread
Lateral spreads	Rock spread	Debris spread	Earth spread
Flows	Rock flow (deep creep)	Debris flow (soil creep)	Earth flow (soil creep)
	Complex		
Combination of two or more principal types of movement			

Table 2.2 - Slope movements types and processes (Varnes, 1978).



a)



b)

Figure 2.2 - Fall according to (Varnes, 1978): schematic diagram (a); example of rockfall in Valtopina, Umbria (Italy), unknown date. Photographer: Fausto Guzzetti. Source: EGU Blogs, <https://blogs.egu.eu/> (b).

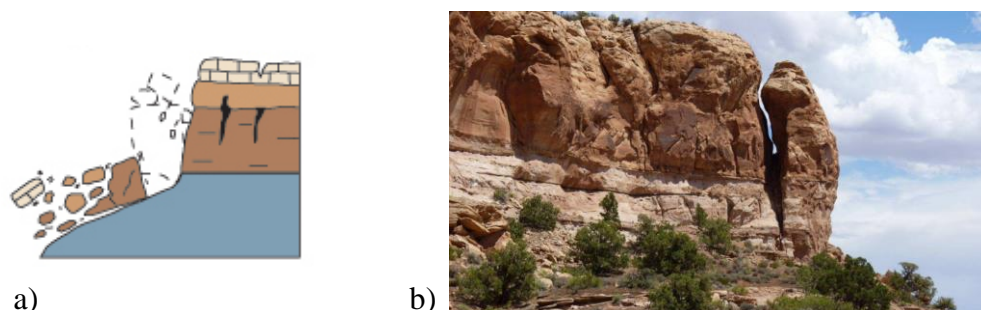


Figure 2.3 - Topples according to (Varnes, 1978): schematic diagram (a); example of topple in Utah, Canyonlands (USA), unknown date. Photographer: J. Novotny (b).

Nowadays the term “landslide” includes several type of mass movements but the proper use of this word deals with a specific type of mass movements named slides which is mainly identified by a known wake area separating the sliding material out from the stable part. Two different types of slides can occur, namely rotational slides and translational slides.

Rotational slide is featured by a concave sliding surface and the global movements consists of a rough rotation around an axis in the same direction of the ground surface. Cecil Lake Road landslide (Figure 2.4b), in British California (Canada), is an illustrative example of rotational slide. The event occurred in July 2001, in the Beaton River Valley, producing a full interruption of the highway traffic for 24 hours and a partial block for the next four weeks. The slide developed from clayey glacio-lacustrine sediments (from the lake) activated by weather conditions also combined with other factors. Translational slide moves along a roughly planar surface involving a light rotation or a backward tilting. In this failure mode, it is very common to observe surfaces of collapse which follow earlier discontinuities such as bedding planes, faults, joints or bedrock-regolith interface. The amount of fracture a moving mass can reach during a translational slide strictly depends on the fracture level of the surface departing from the planar and on the distance to be moved by the translating mass.

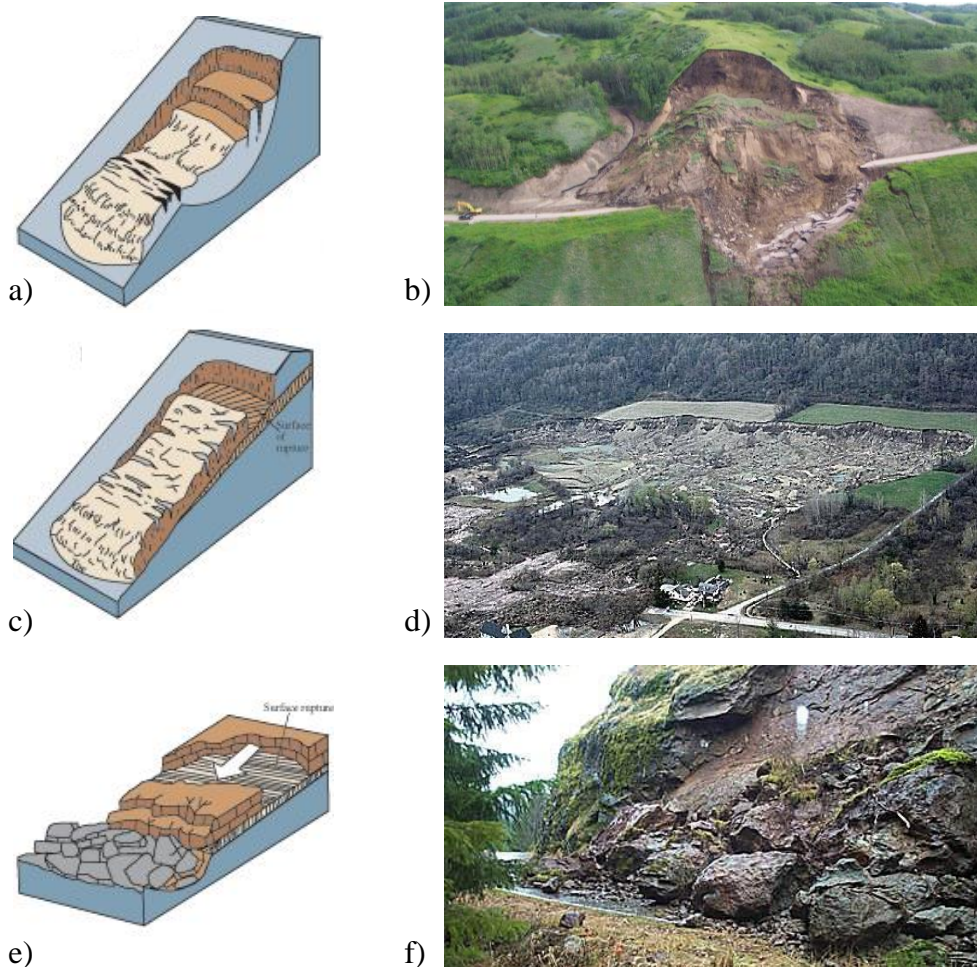


Figure 2.4 - Rotational, translational and block slide according to (Varnes, 1978): schematic diagrams in the case of rotational (a), translational (c) and block (e) slide. Example of rotational slide in Fort St. John area, B.C. (USA), 2001. Photographer: Réjean Couture. Source: Canadian Landscapes (b). Example of translational slide in Tully Valley. (USA), 1993. Photographer: Gerard Wiczoreck. Source: U.S. Geological Survey (d). Example of block slide in Forest Road 19, Oregon (USA), 2001. Photographer: U.S. Forest Service photo (f).

An exhaustive example of translational slide is represented by the event occurred in Tully Valley (USA) in 1993 (Figure 2.4d). That phenomenon was triggered by

a saturated superficial soil moving upon a glacial clay. A translational slide can be considered like a block side in the case the moving mass is made by a single unit or very few units which moves downslope like a relatively coherent mass. Such a movement was registered in January 2006 in Forest Road 19, Oregon (USA) as showed in Figure 2.4f. The road to Terwilliger Hot Springs was blocked due to the block slide. In that case, the movement involved mud and wood, but the main material was represented by rock blocks with few deformations.

Lateral spreads are typical in case of flat terrain or with a very low slope. This mechanism is essentially identified by lateral extension together with shear and tensile cracks. The main causes of the failure mode are the occurrence of liquefaction in saturated, loose, zero-cohesion sands and silts which pass from solid to liquid state. Lateral spreads can be provoked by naturally or artificially induced fast ground motion of the same intensity of motion experienced during a seismic event. This type of failure can occur in the case of a coherent material, bedrock or soil, located on liquefiable materials: in such a case, upper units may experience fractures and extension and finally collapse by subsidence, translation, rotation, rupture or liquefying and flowing. In the case of fine-grained materials located upon shallow slopes instead, lateral spreading failure uses to be progressive.

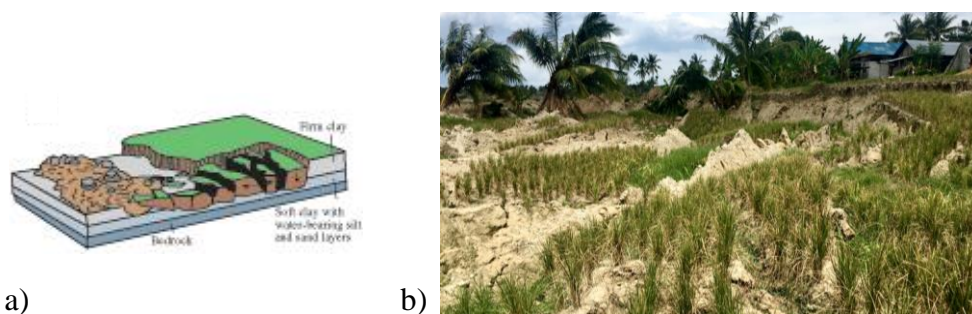


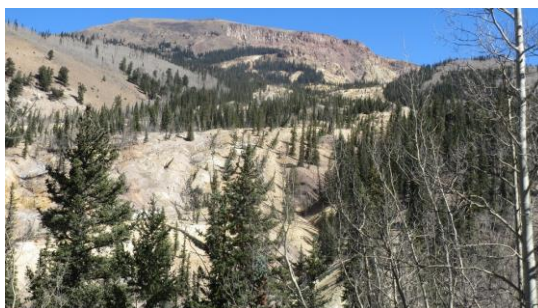
Figure 2.5 - Lateral spread according to (Varnes, 1978): schematic diagram (a); example of lateral spread in Papu Valley, Sulawesi (Indonesia), 2018. Source: Gilles Brocard, University of Sydney (b).

The failure moves in a sudden way starting from a small area and fast spreading around. The first failure movement is usually a slump. Figure 2.5b shows the Palu Valley lateral spreading area, generated by a magnitude-7.5 earthquake occurred during the early evening of 28 September 2018. Lateral spreading in the Palu Valley was surprising because it occurred on relatively steep slopes far away from the coast or a major river channel. The affected area had a slope of about 1° , which doesn't sound very steep but is actually much steeper than previously documented lateral spreads, which occurred on slopes between 0° and 0.5° .

Flows consist of moving masses with local differential movements spread throughout the mass. When the type of material is represented by earth or debris masses, the differential movements can be intergranular, with or without visible shear surfaces. Another possible scenario is characterized by differential movements taking place on closely spaced shear surfaces, which can be fully or partially short-lived and heal without visible track in the deposits. Movements in bedrock which can be attribute to flows are very slow and distributed between various closely spaced fractures. Slumgullion Earthflow in Lake City, Utah (Figure 2.6b) is an excellent example of the geologic process of mass wasting. Seven hundred years ago, a huge mass of volcanic rock slumped from the mountainside and flowed into the main valley where it spread laterally to form Lake San Cristobal. The older flow is presently being overridden by a new flow moving up to 20 feet per year.



a)



b)

Figure 2.6 - Earth flow according to (Varnes, 1978): schematic diagram (a); example of earth flow in Slumgullion, Highway 149, Lake City (Utah), from seven hundred years ago until today. Source: <https://www.uncovercolorado.com/> (b).

The creep refers to very slight slow, stable, downward movement of slope-forming soil or rock. This type of movement is triggered by shear stress able to create permanent strain but not enough large to shear collapse. Three different creep type exist, namely seasonal, continuous and progressive. The seasonal creeps deal with movement developed within the depth of soil affected by seasonal changes in soil wetness and temperature. Continuous creep is characterized by shear stress frequently over the material strength. Progressive creep is the case of slopes moving to the failure exhibiting other types of mass movements. Creep is easy to recognize through curved tree trunks, bent fences or retaining walls, tilted poles or fences and small soil ripples or ridges. An example of this type of movement is represented by the creep in Haymond Formation (made by sandstone and shale) in the neighbouring area with Marathon, in Texas (Figure 2.7b). The apparent bending of sandstone beds is produced when beds collapse creating small vertical sections. These sections are then moved down slope at various rates based on the deepness measured from the surface. The units located close to the surface suffer movements downslope to the greatest extent.

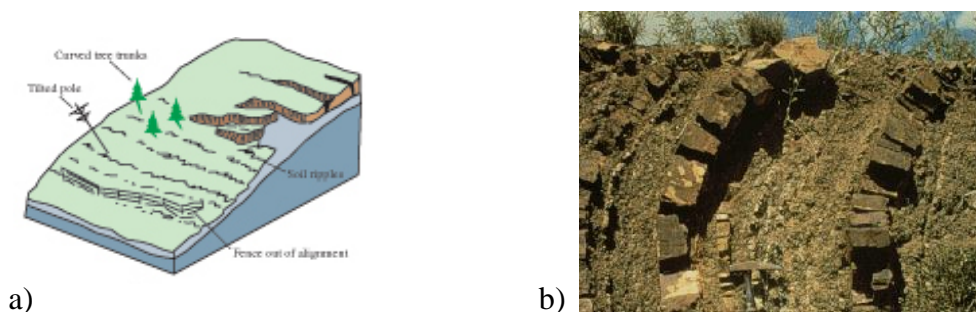


Figure 2.7 - Creep according to (Varnes, 1978): schematic diagram (a); example of creep in Haymond Formation, (Texas). Photo Credit: B. Bradley, University of Colorado. Source: National Geophysical Data Center (NGDC) (b).

Complex landslides are identified by a combination of two or more of the previously described landslide types. Figure 2.8b shows the complex slide that occurred in the summer of 2001 in the area where Muskwa and Chisca Rivers converge, in the northeast of British Columbia (Canada). The movement is a

combination of rotational slide in sandstone and shale in the first step, followed by a flow movement in cohesive sediment.

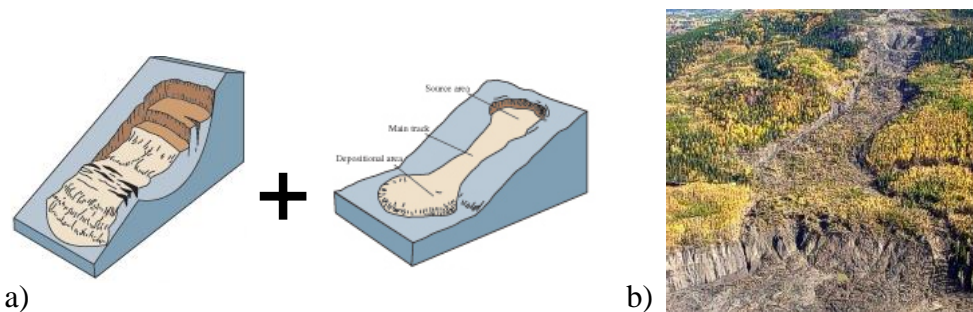


Figure 2.8 - Complex landslide according to (Varnes, 1978): schematic diagram of a complex landslide made by combination of rotational slide and flow (a); example of complex Muskwa-Chisca in British Columbia (Canada), 2001. Source: Marten Geertsema, BC Ministry of Forest, 2002 (b).

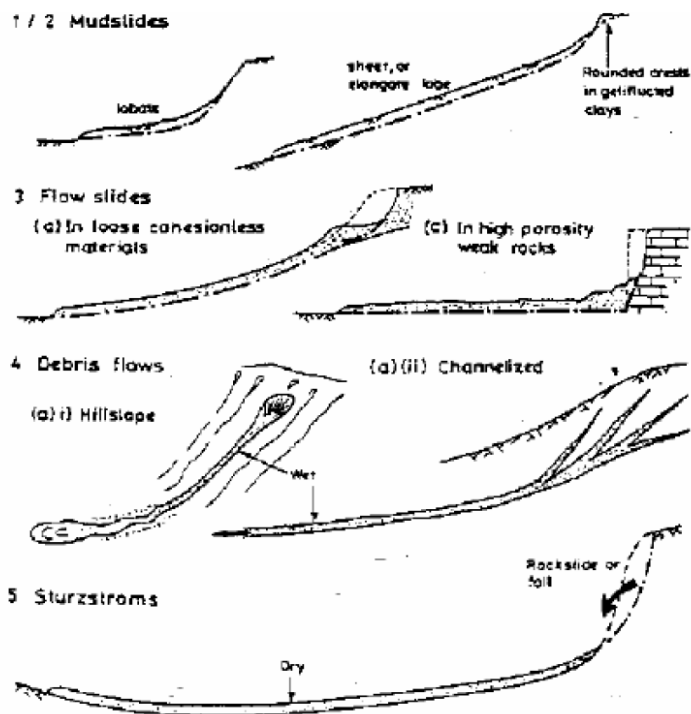


Figure 2.9 - Landslide classification according to (Hutchinson, 1988).

According to the classification proposed by (Hutchinson, 1988), the method is based on the morphology, involving various factors such as mechanisms, material and rate of movement. The idea suggested by the author is that landslides are characterized by a starting failure and a following run-out. In such a definition, the crucial point in order to define a classification lays in the relevance to be assigned to these two stages. First of all, the classification proposed by (Hutchinson, 1988) looks at sub-aerial mass movements on natural or man-made slopes, aiming to classify the moderate run-out landslides. As a matter of fact, this classification does not deal with large-scale movements involved in gravity tectonics, subsidence-involved mass movements and other types of sinking of ground surface. In a classification based on the concept of morphology, landslides characterized by a long run-out are considered flow-like form landslides. Based on this assumption, the authors introduced the following landslide types (Figure 2.9): “mudslide”, when the movement is mainly represented by slide rather than flow; “flowslides” and “debris flows”, when the morphological weight of slide and flow movement is equivalent; “sturzsstroms” in the case the movement is mainly addressed to flow.

The above-described landslides classifications are the most known and used in literature. Besides those, it is worth noting that another efficient method was proposed in (Leroueil *et al.*, 1996), where the authors investigated the relevance of a classification based on the geotechnical features of this type of movements (Figure 2.10). In such a proposal, the event is identified according to the type of soil involved in the mechanism and to the movement stage which can be essentially pre-failure, post-failure and reactivation. In this case, the movement style and soil mechanical parameters represents the main factors able to influence the classification. With this in mind, the approach proposed in (Leroueil *et al.*, 1996) can be ascribed as a powerful tool in the field of risk analysis because it moves from the idea of landslide modelling and slope movement geotechnical behaviour. It is an approved idea that hazard and vulnerability are highly influenced by landslides mechanism rate and stage.

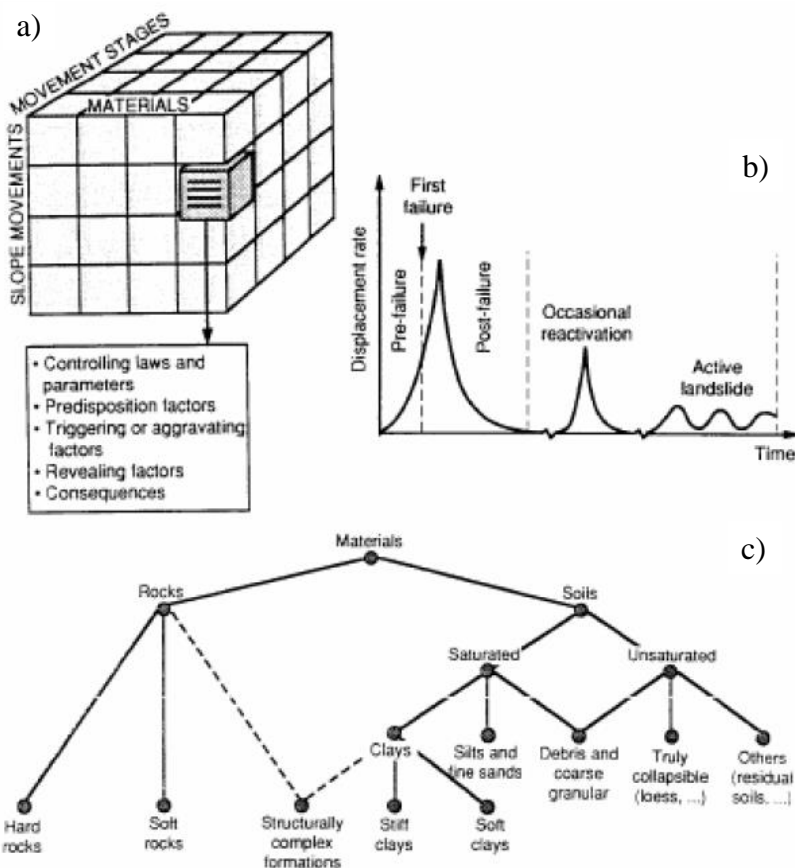


Figure 2.10 - Geotechnical landslide classification according to (Leroueil *et al.*, 1996): (a) schematic diagram, (b) various landslide stage and (c) involved material.

2.2.2.2 Classification based on state of activity

In this section, the landslide movements are classified according to the landslide activity. This point was deeply investigated in (Cruden and Varnes, 1996), where the authors also analysed the influence of other parameters such as landslide rate, water content, material and type. Moving from the definitions introduced in (Varnes, 1978), three headings were proposed according to movement sequence or repetition: state of activity, distribution of activity and style of activity. The first heading deals with the description of the movement timing. Distribution of

activity refers to the space features of the landslide movement. Style of activity heading allows to identify the number and types of movements involved in the event and their contribute to the global mechanism.

The classification according to the state of activity allows to distinguish the landslides among active, suspended and inactive. Active landslides are characterized by still-moving masses, including both first-time and reactivations movements. Suspended landslide is used to refer to a landslide which exhibited movements during the last annual cycle of season but is not moving more at present. Inactive is a term to describe landslide which last moved more than one annual cycle of seasons ago. Inactive landslides can be further subdivided into different types, that are essentially dormant, abandoned, stabilized and relict. Dormant landslides are characterized by movement causes still alive. In the case the river which was causing the erosion of the moving slope toe changes its natural course, the landslide can be ascribed as abandoned (Hutchinson, 1973; Hutchinson and Gostelow, 1976). Stabilized landslides are characterized by the fact the toe of the slope was not affected by the erosion thanks to the protection of bank armouring or the movement was stopped via artificial solutions. Finally, relicts are landslides which developed suffering different geomorphological or climatic conditions, probably thousands of years ago. When a landslide comes back to an active scenario after being inactive, it can be described as a reactivated landslide; in such a case, slides use to move on pre-existing shear surfaces characterized by strength parameters equal to residual or ultimate values (Skempton, 1970; Krahn and Morgenstern, 1979). Table 2.3 and Table 2.4 summarizes the approach proposed in (Cruden and Varnes, 1996).

State	ACTIVITY	
	Distribution	Style
Active	Advancing	Complex
Reactivated	Retrogressive	Composite
Suspended	Widening	Multiple
Inactive	Enlarging	Successive
Dormant	Confined	Single
Abandoned	Diminishing	
Stabilized	Moving	
Relict		

Table 2.3 - Landslide classification according to activity (Cruden and Varnes, 1996).

DESCRIPTION OF FIRST MOVEMENT			
Rate	Water content	Material	Type
Extremely rapid	Dry	Rock	Fall
Very rapid	Moist	Soil	Topple
Rapid	Wet	Earth	Slide
Moderate	Very wet	Debris	Spread
Slow			Flow
Very slow			
Extremely slow			

Table 2.4 - Landslide classification according to the description of first movement (Cruden and Varnes, 1996).

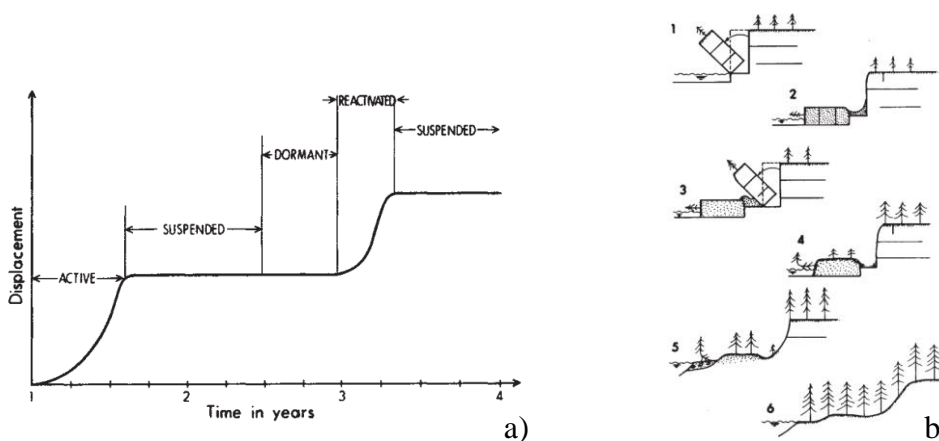


Figure 2.11 - Method proposed by (Cruden and Varnes, 1996): (a) state of activity of landslides over time; (b) toppling landslide in different states of activity: 1. Active, erosion at toe of slope causes block to topple; 2. Suspended, local cracking/fracturing in crown area; 3. reactivated, toppling of a new block; 4. dormant, the body of the landslide is colonised by vegetation, the slopes are remodelled by the weather; 5. Naturally stabilised, fluvial deposits have protected the base of the slope; 6. relict, a uniform vegetation cover has been re-established.

2.2.2.3 Classification according to intensity

Intensity is one of the most important parameters in order to better describe a natural hazard such as considered landslide. The intensity is essentially defined through a series of both quantitative and qualitative spatially distributed factors which contribute to the determination of a specific landslide event to trigger the

damage (Hungr, 1997). According to (Leone et al., 1996), intensity parameters can be grouped into three categories based on the type of landslide:

- dimensional or geometric parameters (surface, volume, shape, depth, amplitude, distance, height and thickness).
- kinetic parameters (velocity, flowrate, acceleration and deformation fields).
- additional parameters, such as viscosity, mass, sediment load and density.

It is worth noting that natural hazard intensity also owns probabilistic contents which play a fundamental role in a fragility sense when they are compared with the annual probability rates of occurrence of a specific type of landslide (Hungr, 1997).

A comparison with other natural hazards (first of all seismic hazard) reveals how the idea of intensity is still lowly defined in the field of landslide analysis and no methodological approach is currently available in literature in order to cover several events in an overall formulation. Despite this state of fact, the possibility to measure the intensity level of existing or potential mass movements represents a crucial and challenging point in the framework of the prediction of the effects an element (or a structure) exposed to such a phenomenon can suffer. The vulnerability of a structure subjected to landslide-induced ground movements is a function of the event intensity and of course of its own characteristics.

In this framework, how to evaluate landslide intensity is a still open and challenging task in literature, involving several parameters among which the history of an existing landslide and the entity of potentially unstable masses. The most used approach for the intensity estimation was proposed in (Cruden and Varnes, 1996), where the authors suggested to associate landslide intensity to the body mass velocity. On the example of Mercalli's scale for the seismic hazard, where the earthquake is described on the base of the local effects, Cruden and Varnes introduced the probable destructive significance of the landslide associated with seven velocity class. Figure 2.12 shows that a significant limit exists among very rapid and extremely rapid movement, something like the speed of a person running (5 m/sec). The figure also reveals that another crucial limit

exists between the slow and very slow class (1.6 m/year) which represents a limit damage threshold including undamaged structures.

Velocity Class	Description	Velocity (mm/sec)	Typical Velocity	Probable Destructive Significance
7	Extremely Rapid	5×10^3	5 m/sec	Catastrophe of major violence; buildings destroyed by impact of displaced material; many deaths; escape unlikely
6	Very Rapid	5×10^1	3 m/min	Some lives lost; velocity too great to permit all persons to escape
5	Rapid	5×10^{-1}	1.8 m/hr	Escape evacuation possible; structures; possessions, and equipment destroyed
4	Moderate	5×10^{-3}	13 m/month	Some temporary and insensitive structures can be temporarily maintained
3	Slow	5×10^{-5}	1.6 m/year	Remedial construction can be undertaken during movement; insensitive structures can be maintained with frequent maintenance work if total movement is not large during a particular acceleration phase
2	Very Slow	5×10^{-7}	15 mm/year	Some permanent structures undamaged by movement
	Extremely SLOW			Imperceptible without instruments; construction POSSIBLE WITH PRECAUTIONS

Figure 2.12 - Landslide velocity scale and probable destructive significance proposed by (Cruden and Varnes, 1996).

Magnitude	Description	Volume (m ³)
7	Extremely large	$> 5 \cdot 10^6$
6	Very large	$1 \cdot 10^6 \div 5 \cdot 10^6$
5	Medium large	$2.5 \cdot 10^5 \div 1 \cdot 10^6$
4	Medium	$5 \cdot 10^4 \div 2.5 \cdot 10^5$
3	Small	$5 \cdot 10^3 \div 5 \cdot 10^4$
2.5	Very small	$5 \cdot 10^2 \div 5 \cdot 10^3$
2	Extremely small	$< 5 \cdot 10^2$

Table 2.5 - Landslide intensity classification according to the not stabilized mass (Fell, 1994).

To be thorough, (Fell, 1994) also proposed an interesting approach aiming at landslide intensity quantification. This method was based on the idea that the intensity of a mass movement can be associated to the volume of the not

stabilized mass. Table 2.5 shows the contents of the classification approach proposed by (Fell, 1994): once again, seven classes of magnitude are identified to identify the landslide intensity, from extremely small to extremely large.

The last described classification approach is the one proposed by (Sassa, 1988), where the landslide intensity is estimated through the estimation of its kinetic energy using the so-called “sled model” showed in Figure 2.13.

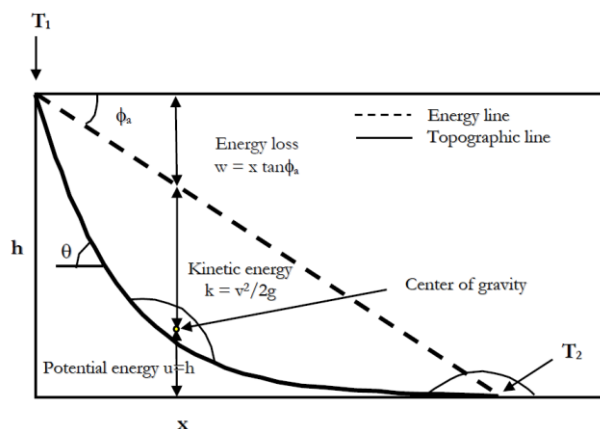


Figure 2.13 - Sled model proposed by (Sassa, 1988).

2.3 Subsidence-induced damage

In this section, a research on the subsidence-induced damage is developed in order to describe the weight this type of phenomenon has at national and international levels.

With regard to the structures and buildings, the structural typology and the soil-footing relative stiffness are the parameters which strongly influence the severity of damage induced by subsidence. For sake of clarity, a masonry building resting on high deformable shallow footings can be affected by ground movements more than a reinforced concrete building with very stiff shallow footings. It is worth noting that vertical components of the ground displacements may coexist with horizontal ones, thus inducing (Cooper, 2008) concave upward bending (hogging) or convex bending (sagging) mode of deformation (Figure 2.14).

According to movement type, also including footing extension or support loss (Figure 2.14), several combinations of stresses can be imposed to the structure, though damage is often concentrated upon corners or stress concentrators such as door or window areas.

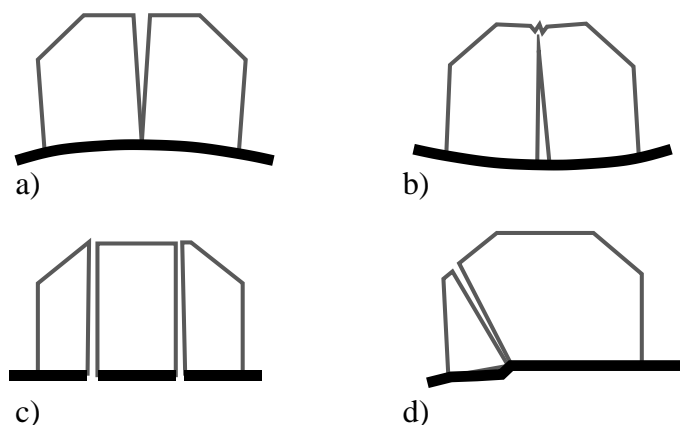




Figure 2.14 - Schematic illustration of building damage associated with various types of subsidence movement, some of which may occur together (Cooper, 2008): (a) hogging, (b) sagging, (c) extension and (d) support loss.

Recent years have been proving that subsidence and landslide may cause severe damages to facilities (pipelines, linear infrastructures, buildings), also involving huge economic losses all over the world. Asian, American and European countries discovered that landslide is a very challenging issues to face, with annual economic losses in the range between hundreds and thousands million dollars. It is common in European countries to find household insurance policies cover loss or damage caused by subsidence. But the issue is that these policies often do not cover the cost for subsidence prevention. In such a case, damage repairing costs (i.e. to repair cracks) to the building are covered but the policies do not cover the cost to save the building against future movements.

In Italy no economical evaluation of subsidence induced damage were formulated. One of the most important projects for knowledge and monitoring the subsidence risk in Italy is represented by the “Italian Environmental Data Yearbook” (Annuario dei dati ambientali), that is the result of the collaboration

between several components of the “Sistema Nazionale per la Protezione e l’Ambiente” (SNPA). The Italian Environmental Data Yearbook arrived at the 17th edition and represents the most exhaustive official publication on environmental data and information in Italy. The data indicator selected for the subsidence investigation is the number of Italian municipalities located in risk area, aiming to provide a national comprehensive framework of the subsidence phenomenon and of its environmental impact. The idea is also motivated by the fact the subsidence is becoming an important environmental hazard factor especially in the highly urbanized area or recently urbanized area and in the cost area, particularly when they are located under the sea level. The interaction between man-made and natural factors makes very hard subsidence analysis and mitigation. In this framework, subsidence quantification and time analysis are fundamental task to be achieved, by using several methodologies.

-  Municipalities affected by subsidence
-  Municipalities not affected by subsidence

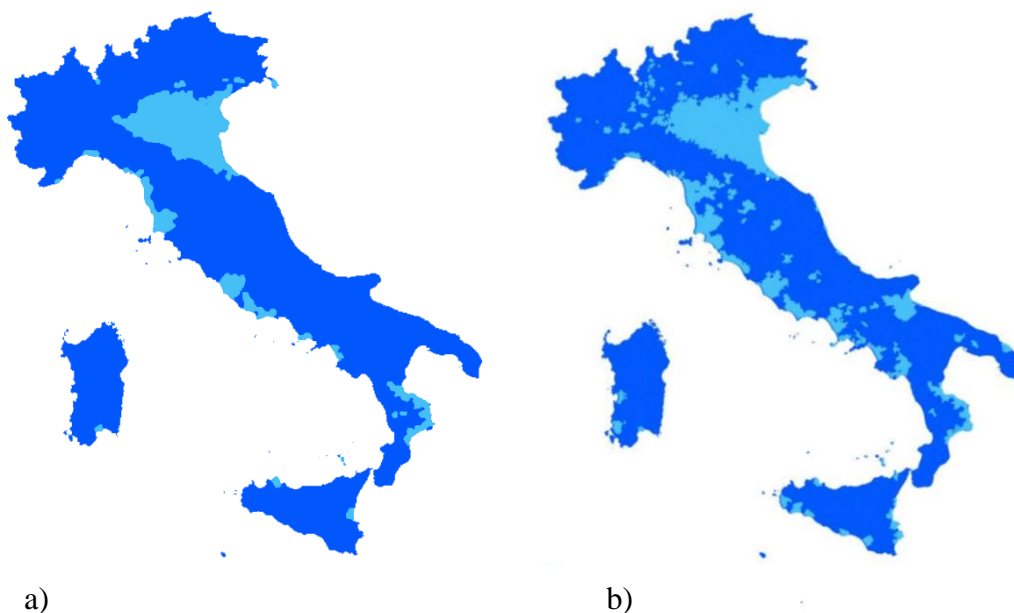


Figure 2.15 - Maps of Italian municipalities affected by subsidence elaborated by the Italian Environmental Data Yearbook. Comparison between data related to (a) 2003 and (b) 2018.

The project uses three main criteria for the selection of the data to be considered in order to analyse the subsidence risk: 1) relevance, 2) measurability and 3) robustness. According to relevance criterion, the indicator must be appropriate to be applied at national level or, at least, at regional environmental themes which can be significant in the national contest. The indicator must be easy to be interpreted and sensitive and flexible to the changes occurring in the environment and strictly related to the human activities. Finally, for the relevance criterion, the indicator must provide a general basis in order to allow for national comparisons. The measurability criterion asks for data used in the indicator definition which are characterized by an acceptable spatial coverage as much as time coverage (at least 5 years). In the case of robustness criterion, the selected indicator is required to be valid and supported by technical and scientific theories and assumptions, and reliable with regard to measure strategies and data collection. As a matter of fact, it should be admitted that the indicator described by the “Italian Environmental Data Yearbook” still presents some limitations. First of all, the indicator cannot completely show the real national extension and the real entity of subsidence in the various area because of the dis-homogeneity in monitoring data techniques and the complexity of the investigated phenomenon. To be honest, subsidence is regularly monitored only in some areas, by using different methodologies, but a full national catalogue still not exists at all. In recent years, some Italian Regions has been starting to study and monitor the subsidence activity by using high tech strategies such as radar-satellite observation techniques. One of the most dangerous threat is represented by the observation that subsidence often does not produce visible or relevant effects and this aspect means that the phenomenon is often ignored or underestimated so that the data collection on the event intensity represents a very hard task. Furthermore, a huge dis-homogeneity in the data collected by the various Region still exists, mainly due to the complexity and the expensive cost of the collection of data. In conclusion, available data at the present day do not allow to comprehensively describe land subsidence on a national base. The produced information is certainly substantial, but the data accuracy is medium level because the phenomenon is not regularly surveyed and update. Collected data are fully useful to make in-time and in-space comparisons only when

historical sequences are available, acquired with both classical and modern methodologies. So it can be observed that the coverage is generally enough but the same cannot be said for the comparability. Some areas, first of all Po Valley, can count on very high developed instrumental monitoring networks. On the other hand, some Italian areas such as Emilia-Romagna Region and Venezia are characterized by relevant fluids extraction from the subsoil, and the adopted codes and regulations for the environment protection reduced or even blocked the subsidence movements. Unfortunately, these measures were not adopted in every subsidence-affected area. For the future, “Programma Copernicus” project will aim to monitor the subsidence at national scale by using satellite data for studying soil movements.

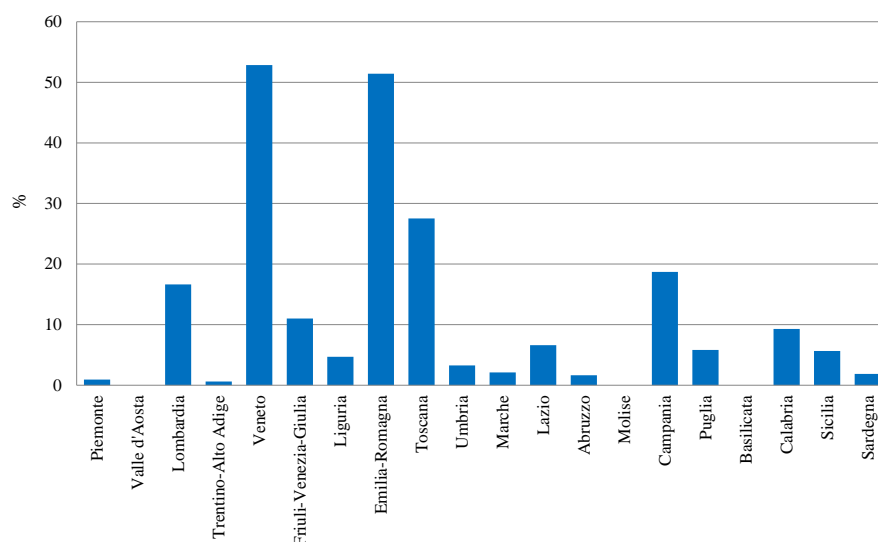


Figure 2.16 - Italian municipalities per each region affected by subsidence according to the Italian Environmental Data Yearbook 2018.

According to the last Data Yearbook (ISPRA, 2018), 14% of the Italian municipalities is affected by land subsidence (1093 out from 8092) as it possible to see in Figure 2.16 and Table 2.6. Most of affected municipalities are located in the North of Italy, especially in the Po Valley. From this point of view, subsidence in Italy is very risky for a lot of artistic cities and historic centres,

such as Venezia and Ravenna. With regard to Central and South of Italy, the subsidence risk is mainly concentrated along the coast valleys. The most affected Regions are represented by Veneto and Emilia-Romagna, with more than 50% of total municipalities located in involved area (307 and 179 municipalities respectively). Medium affected Region are represented by Toscana (79 involved municipalities, equal to 28%), Campania (103 involved municipalities, equal to 19%), Lombardia (257 involved municipalities, equal to 17%) and Friuli-Venezia Giulia (24 involved municipalities, equal to 11%).

Region	Total Municipalities	Municipalities affected by subsidence	Percentage of Municipalities affected by subsidence
	no.	no.	%
Piemonte	1206	11	1
Valle d' Aosta	74	0	0
Lombardia	1544	257	17
Trentino-Alto Adige	333	2	1
Veneto	581	307	53
Friuli Venezia Giulia	218	24	11
Liguria	235	11	5
Emilia Romagna	348	179	51
Toscana	287	79	28
Umbria	92	3	3
Marche	239	5	2
Lazio	378	25	7
Abruzzo	305	5	2
Molise	136	0	0
Campania	551	103	19
Puglia	258	15	0
Basilicata	131	0	0
Calabria	409	38	9
Sicilia	390	22	6
Sardegna	377	7	2
Total	8092	1093	14

Table 2.6 - Italian municipalities affected by subsidence according to the Italian Environmental Data Yearbook 2018.

In this framework, a virtuous Italian scenario is represented by Emilia-Romagna Region, where ARPAE project (“Agenzia regionale per la prevenzione, l’ambiente e l’energia dell’Emilia-Romagna”) is controlling the state of the environment and supporting the sustainability of human activities, aiming at the

protection of human health and territorial competitiveness. ARPAE carries out interventions to monitor the compliance to environmental law and to assess the status of all environmental components (air quality, water, energy, radioactivity, etc.). Emilia-Romagna valley is subjected to a natural subsidence characterized by an estimated velocity equal to some millimeters per year. The natural subsidence has been associating with a man-made subsidence since 1950s, which is due to excessive fluid extraction from subsoil. This second type of subsidence velocity is generally higher than the natural subsidence velocity. This phenomenon triggered monumental and artistical heritage with severe damages, producing a general loss of efficiency of the hydraulic infrastructures, a highly erosion speed of the coast and an increasing aptitude to overflow for both coast and internal areas. Once the causes were identified, different strategies were designed aiming to remove the causes and to check subsidence geometrical evolution. Several institutions worked to create subsidence monitoring networks in the areas where the phenomenon appeared with greater intensity and severity. Emilia-Romagna experience represents a valid example to understand both the Italian sensitivity and exposure to subsidence risk and above all the high potentialities of a well-designed monitoring system for the study and the prediction of severe natural events (<https://www.arpae.it/>).

In this framework, it seems to be clear that subsidence in Italy is a still risking hazard. This phenomenon is mainly due to geological factors but in the last decades man-made causes weight is highly increasing. In particular, the amount of the natural subsidence in Italy is estimated to be in the order of some millimetres per year, meaning very few consequences because the effects are expected in very long period. On the other hand, the subsidence induced and/or accelerated by man-made factors in Italy achieves values in the range between 1 and 10 centimetres per year, with consequences that can show also in very short period, with the high probability to block the involved human activities.

2.4 Landslide-induced damage

With regard to landslides, the available database all over the world show economic losses dealing with all types of movements ascribed to the field of

landslide phenomena. In this case, the annual economic losses are even associated with the alarming and highly considerable impact on natural environment, affecting morphology, forest and fauna (Schuster, 2007).



a)



b)



c)



d)



e)



f)

Figure 2.17 - Ancona (Italy) landslide in 1982 as reported in (Cotecchia, 2006). Damage to man-made structures caused by the landslide: (a) University Medical Faculty, (b)(d)(f) Flaminia road and (c)(e) Adriatic railway.

In the case of built structures damage analysis, it was observed that the maximum damage extent is caused by the impact with fast-moving landslides (such as debris flows and rock falls). Such a mass movement can even correspond to collapse of the entire structure or of some local members of it. On the other hand, slow-moving landslides represents a dangerous threat because their effects on architectural buildings are often underestimated in decision making processes but this kind of mass movement may severely affect facilities, so they deserve much more attention in future (Safeland Project, 2011).

Various factors are involved in the damage susceptibility for buildings subjected to slow-moving landslides. Among them, it is important to cite the most relevant, which are essentially: (a) the hazard level; (b) the rate of movement (relative slow to extremely slow moving landslides); (c) the triggering mechanism (intense rainfall, earthquake, erosion, construction activities etc); (d) the specific strength and stiffness characteristics of the exposed elements and (e) their position in relation to the potential sliding surface, and (f) the type of materials controlling the movement (Safeland Project, 2011). Several studies in literature showed that buildings and residential houses are able to accommodate higher slide velocities and total displacements compared to other facilities before experiencing serious damage while bridges were found to be the most weak (Gillon and Saul, 1996; Zhou, 2000; Esser, 2000; Nichol and Lowman, 2001; Moore, Watson and Martin, 2006; Fujisawa *et al.*, 2007; Bonnard, Tacher and Beniston, 2008; Clementino *et al.*, 2008; Malone *et al.*, 2008; Topal and Akin, 2008, 2009). In Italy, there are a lot of landslide affected cases studies are reported in literature. Among them, it is worth citing that of Ancona (Figure 2.17), where a reactivated rotational slide involving an huge area occurred in 1982 (Crescenti *et al.*, 1983; Cotecchia, 2006), and that occurred in, San Pietro in Guarano, a little town in southern Italy. This is a typical reactivation of the Western Sila massif affecting the intensely weathered gneiss rocks (Cascini and Gullà, 1992b, 1992a; Cascini and Di Maio, 1994; Cascini, Gullà and Sorbino, 2006).

During the last-mentioned event, the amount of damage suffered by a lot of buildings forced to evacuate or even demolish them. The most damaged facilities were deeply described in (Antronico *et al.*, 2003): a primary school mainly

suffered cracks in the beam, pillar and partitions, but also detached sections of spine wall (Figure 2.18a); a secondary school presented diagonal cracks in the spine wall due to the rigid body rotation of horizontal structures (Figure 2.18b); finally, a private building mainly suffered widespread cracking in the masonry walls (Figure 2.18c).

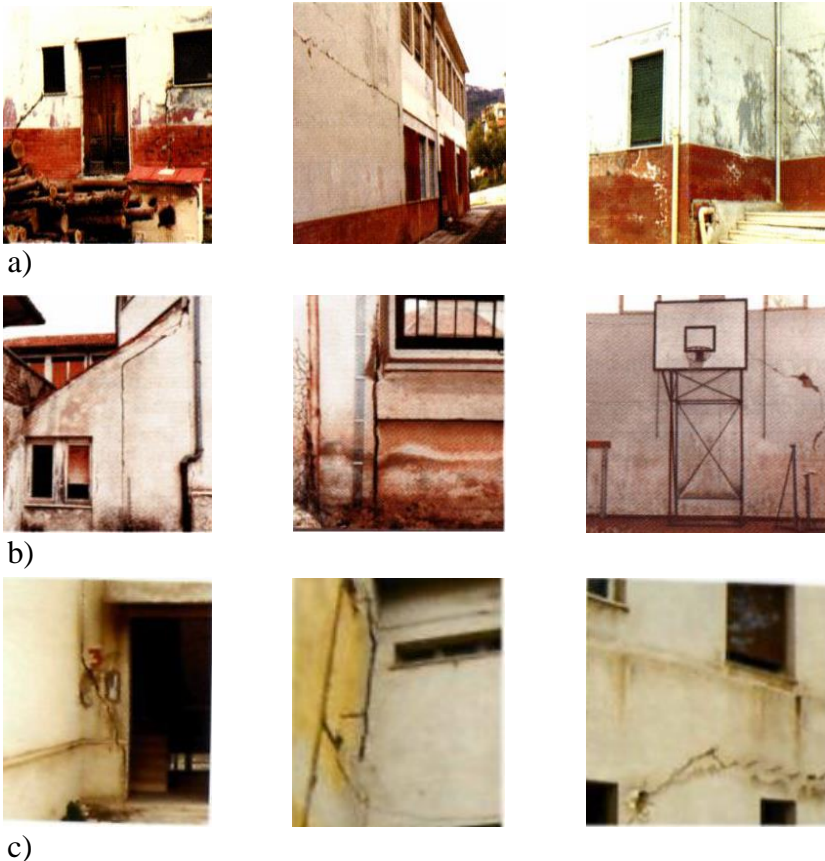


Figure 2.18 - San Pietro in Guarano (Italy) landslide in 1981 as reported in (Antronico *et al.*, 2003). Damage suffered by (a) a primary school, (b) a secondary school and (c) a private building subjected to the landslide.

In this framework, the recent Italian landslide events also include the reactivation of a complex landslide occurred in the early morning of March 7th 2005, after a

quite long period of rainfall-snowfall combination, in Cavallerizzo, Calabria region in the south of Italy (Figure 2.19).

According to the study carried out in (Iovine *et al.*, 2006), about thirty buildings suffered severe damage and were eventually destroyed by the mass movement and with roads completely blocked and hundreds of peoples evacuated to nearby villages.

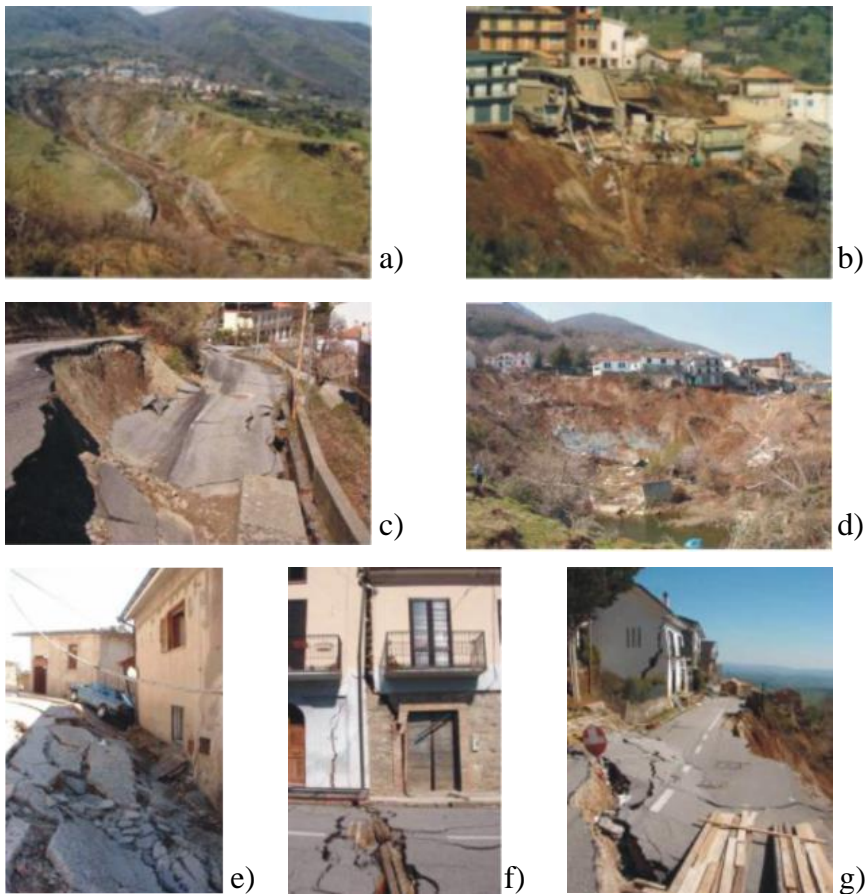


Figure 2.19 - Some photographs of the March 7th 2005 landslide at Cavallerizzo: (a) a panoramic view of the village (in foreground, the main earth flow); (b) view of buildings damaged along the crown; (c) view of damage to the provincial road; (d) view of the main scarp (in foreground, the landslide lake); (e)(f)(g) view of damage to the urbanized area, along the main scarp (Iovine *et al.*, 2006).

In the field of landslide analysis and investigation, the “Istituto Superiore per la Protezione e la Ricerca Ambientale” (ISPRA), with the partnership of Italian Regions and Self-Governing Provinces, carried out the IFFI project (Inventory of Landslide Phenomena in Italy). The IFFI project provides a detailed picture of landslide phenomena distribution in Italy. The inventory, online since 2005, represents a basic knowledge tool for landslide hazard evaluation which aims at giving relevant information to citizens, public administrations, research institutes and technicians operating in the sector of territorial planning of land protection measures. The need to have a national inventory of landslides in Italy has arisen following the catastrophic event of 5 May 1998, which caused heavy damage in the Municipalities of Sarno, Siano, Quindici, Bracigliano and S. Felice a Cancellò (Campania Region). The IFFI Inventory is an important base-knowledge tool to assess the landslide hazard of the River Basin Plans (PAI), the preliminary design of slope instability and flood mitigation works as well as protection of infrastructure networks. Moreover, IFFI contributes to the preparation of Civil Protection Emergency Plans.

The IFFI Inventory first aims at identifying and mapping landslides occurred in the whole Italian territory, following standardized criteria. IFFI has the scope, as well, to constitute an important base-knowledge tool to assess the landslide hazard of the River Basin Plans (PAI), for the preliminary design of slope instability and flood mitigation works as well as the protection of infrastructure networks. Moreover, IFFI contribute for the preparation of Civil Protection Emergency Plans.

The IFFI project has been financed in 1997 with 4.1 Mil. Euro by the Italian Committee of Ministries for the Land Protection. In 2004, APAT (nowadays ISPRA) allocated 650,000 Euro for the integration and update of the Italian Landslide Inventory database. In the period 2001-2008 the implementation of the Project took place through formal agreements. The first agreement (IFFI agreement) has been signed between November 2000 and May 2001 among the National Geological Survey and the Regions / Self-Governing Provinces and terminated in 2005 for almost all the Regions. The second agreement (II IFFI agreement), signed in 2005 between the APAT and the Autonomous Regions /

Self-Governing Provinces for database updating, was concluded between 2006 and 2008.

Since 2008, the Regions have provided ISPRA with updated information on landslides. Landslide data are updated to 2017 for the Umbria Region; 2016 for Emilia Romagna, Friuli Venezia Giulia, Liguria, Piedmont, Sicily, Valle d’Aosta and for the Autonomous Province of Bolzano; 2015 for Tuscany; 2014 for Basilicata and Lombardy. For the remaining regions, landslide data are updated to 2007. In 2012, the State-Regions Conference approved a technical and economic proposal to provide 7 million Euro in 3 years as further funds for the IFFI Inventory. The proposal was prepared by ISPRA and the Piedmont Region (leader in 2012 of the Regions for the Environment sector), and it is still waiting for funding. The Italian Landslide Inventory currently reports 620,808 landslides occurred in the Italian territory. Before the start of the IFFI Project, ca. 70,000 landslides were inventoried by the Regions and Self-Governing Provinces.

ISPRA reports are an important tool to study the landslide hazard in Italian territory. The last report was published in 2018, but one of the most complete and useful report is the one published in 2008. ISPRA Special Report 2018 is firstly devoted to the national mosaic of landslide hazard zones in Italy, based on the data available through the research of the River Basin Plans (PAI). The landslide hazard zones of the River Basin Plans (PAI) include areas of possible evolution of existing landslides and areas where new landslides potentially may occur, in addition to occurred landslides. River Basin Plans⁴ represent a fundamental tool for a correct land use planning through the application of land use restrictions and regulations (e.g. prohibition of building construction in high and very high hazard zones). River Basin Plans are dynamic instruments that may be subject to change over time by the River Basin Authorities (now River Basin District Authorities), following new studies and surveys, new landslide and flood events, completion of mitigation measures or requests of local authorities.

In order to update the landslide hazard map on the entire national territory, in 2017 ISPRA realised the new National Mosaic of the hazard zones provided by the River Basin District Authorities. According to the 2015 national mosaic (Trigila, Iadanza, Munafò, *et al.*, 2015), ISPRA introduced 5 hazard classes: very

high hazard *H4*, high *H3*, medium *H2*, moderate *H1* and attention zones *AA*. The study carried out by PAI revealed that the total area of landslide hazard zones and attention zones in Italy is 59,981 km² (19.9% of the national territory) as described in Table 2.7. In the case only the most hazardous classes (high *H3* and very high *H4*) are considered, the area is equal to 25,410 km², equal to 8.4% of the Italian territory (Table 2.8).

		Landslide hazard zones	
		km ²	% of national territory
H4	Very high	9.153	3.0%
H3	High	16.257	5.4%
H2	Medium	13.836	4.6%
H1	Moderate	13.953	4.6%
AA	Attention zones	6.782	2.2%
Total		59.981	19.9%

Table 2.7 - National mosaic of landslide hazard zones according to (River Basin Plans PAI).

The comparison between the 2017 and the 2015 national mosaics shows an increase of 2.9% of the total classified area (classes *H4*, *H3*, *H2*, *H1* and *AA*), an increase of 6.2% of the high and very high hazard classes (*H3* and *H4*) and a reduction of 19.5% of the attention zones, mainly reclassified as hazardous areas. The most significant increases of the high and very high hazard classes concerned the Tiber River Basin, the Sardegna Region, the Arno Basin, the Calabria, Marche and Abruzzo Regional Basins, the Po Basin in Lombardia Region, the Autonomous Province of Bolzano. These changes are mainly related to more detailed studies and mapping of new landslides described in the ISPRA Special Report 2018 (Trigila *et al.*, 2018).

The study carried in (Trigila *et al.*, 2018) also analysed the pressure of landslide risk on different categories, such as population, number of families and buildings. In the spirit of (Trigila *et al.*, 2018), the scope of the risk indicators is to provide an official reference framework for landslide risk in Italy and an important tool to support national mitigation policies by identifying intervention priorities, allocation of funds, programming mitigation measures and planning civil protection measures.

Region	Region area km ²	High and very high landslide hazard zones	
		H4 km ²	H3 %
Piemonte	25.387	1230.8	4.8%
Valle d' Aosta	3.261	2671.7	81.9%
Lombardia	23.863	1538.2	6.4%
Trentino-Alto Adige	13605	1476.7	10.9%
Bolzano-Bozen	7.398	131.7	1.8%
Trento	6.207	1345.0	21.7%
Veneto	18.407	105.6	0.6%
Friuli Venezia Giulia	7.862	19.5	2.4%
Liguria	5416	751.9	13.9%
Emilia Romagna	22.452	3277.7	14.6%
Toscana	22.987	3367.6	14.7%
Umbria	8.464	492.9	5.8%
Marche	9401	735.5	7.8%
Lazio	17232	953.3	5.5%
Abruzzo	10831	1678.2	15.5%
Molise	4460	716.9	16.1%
Campania	13671	2678.2	19.6%
Puglia	19541	594.8	3.0%
Basilicata	10073	511.6	5.1%
Calabria	15.222	545.6	3.6%
Sicilia	25832	394.6	1.5%
Sardegna	24100	1497.6	6.2%
Total	302066	25410	8.4%

Table 2.8 - High and very high landslide hazard zones on regional basis according to (River Basin Plans PAI).

The number of exposed people has been calculated with a proportional method (Trigila, Iadanza, Esposito, *et al.*, 2015). The population at risk represents the population living in landslide hazard zones exposed to the risk of damage. Vulnerability, i.e. the degree of loss of the element at risk that can be damaged during an event, has been assigned as 1, as its assessment would require knowledge of both landslide magnitude and behaviour of the population categories. Vulnerability may also vary based on the time of the year, the week and the time (day/night) in which the event occurs. Families, buildings and industry at risk have been estimated with a similar methodology. For the evaluation of cultural heritage at risk the georeferenced features of cultural sites have been intersected with the national mosaics of landslide hazard.

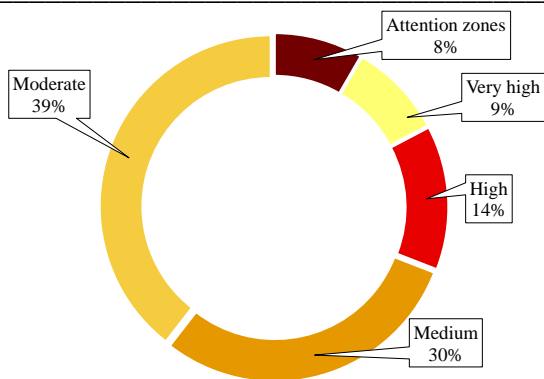


Figure 2.20 - Population exposed to landslide risk in Italy (Trigila et al., 2018).

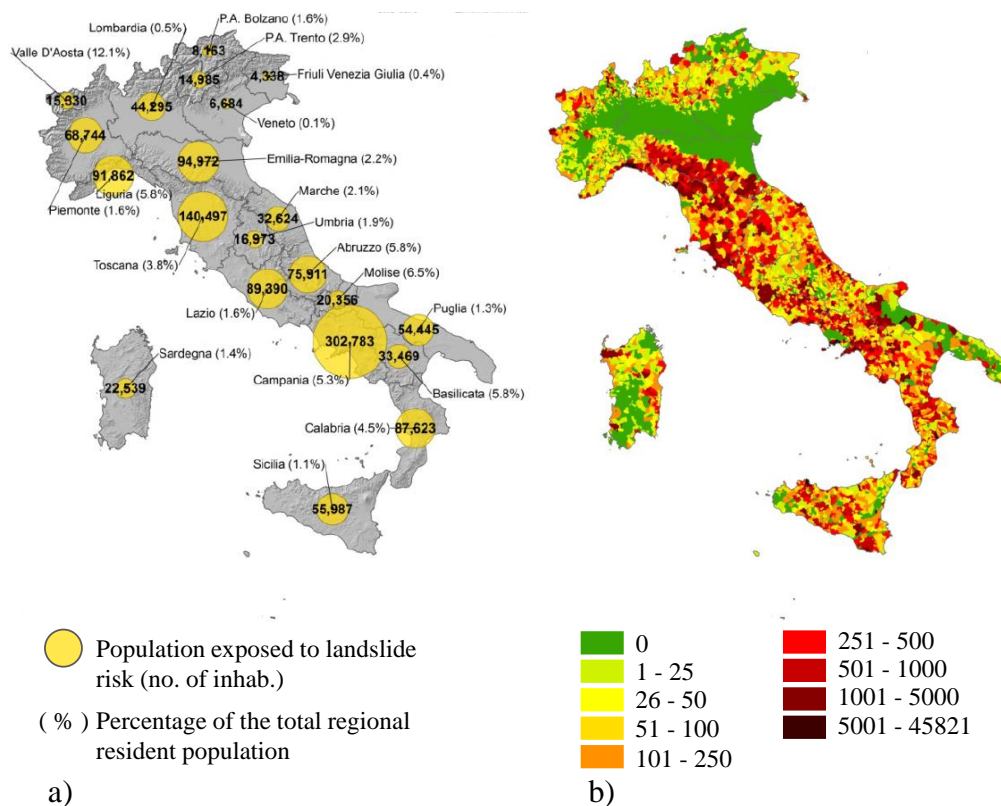


Figure 2.21 - Data collected in (Trigila et al., 2018): population at risk living in high and very high landslide hazard zones (no. of inhabitants) on (a) regional and (b) municipal basis.

Data collected in (Trigila *et al.*, 2018) have been used at national level for identification of intervention priorities, allocation of funds among the Regions and planning of mitigation measures (Plan for urban and metropolitan areas against floods - CIPE Resolution No. 32/2015; National plan for mitigation measures - Prime Minister Decree of 5th December 2016).

In Europe, the indicators have been selected for the evaluation of the effectiveness of the Structural Fund measures 2014-2020 (Dipartimento per lo Sviluppo e la Coesione economica, 2014). Population exposed to landslide risk indicators have been carried out within the framework of the project Environmental statistics for cohesion policies 2014-2020 (PON Governance and Institutional Capacity 2014-2020).

With reference to the population exposed to landslide risk, something like 1281970 Italians live in high (*H3*) and very high (*H4*) landslide hazard zone, i.e. about 2.2% of the total population in Italy (59433744 inhabitants according to ISTAT 2011 Census). Figure 2.20 shows the amount of population in Italy exposed to each type of landslide risk. population lives in *H3* and *H4* landslide hazard zones, as showed through the maps in Figure 2.21. The most affected population are those living in Campania, Toscana, Emilia-Romagna and Liguria Regions, where most of the. The comparison between 2015 and 2018 data reveals that population at risk increase of about 4.7% probably due to revision of the hazard zoning maps made by the River Basin District Authorities.

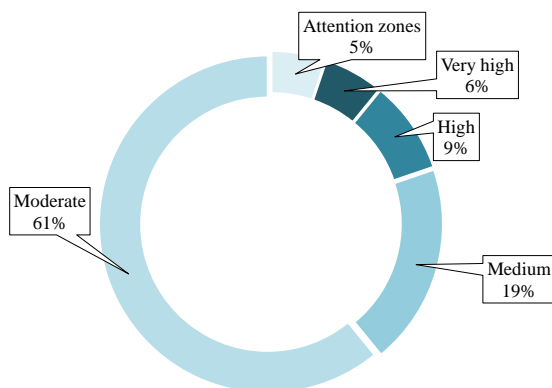


Figure 2.22 - Families exposed to landslide risk in Italy (Trigila *et al.*, 2018).

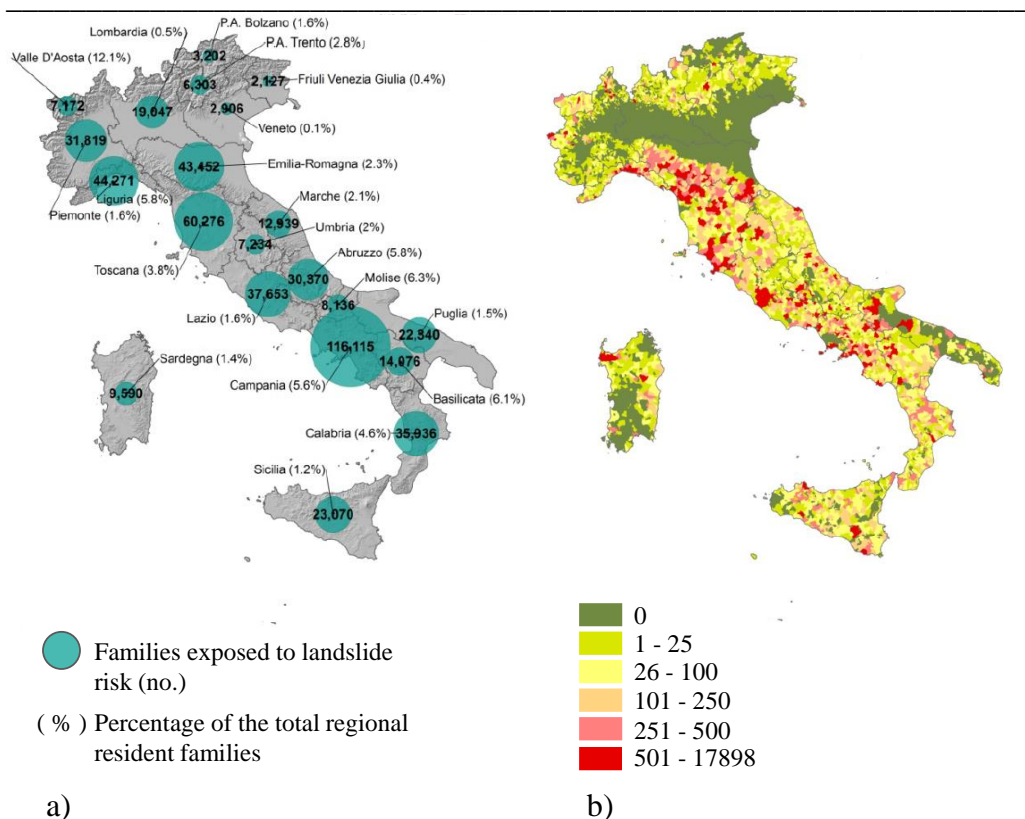


Figure 2.23 - Data collected in (Trigila et al., 2018): number of families at risk living in high and very high landslide hazard zones on (a) regional and (b) municipal basis.

Another important aspect investigated in the report published by ISPRA in 2018, there is also the statistic study of number of families exposed to the risk produced by landslide on the whole Italian territory. Such an investigation revealed that 538034 Italian families live in high (*H3*) and very high (*H4*) landslide hazard zone, i.e. about 2.2% of the total population in Italy (24611766 families according to ISTAT 2011 Census). Figure 2.22 shows the amount of families in Italy exposed to each type of landslide risk. The most affected families are those living in Campania, Toscana, Liguria and Emilia-Romagna Regions, in agreement with the results obtained in the case of the already described analysis of population exposed to landslide risk.

In the spirit of the present dissertation thesis, one of the most useful analysis performed by the (Trigila *et al.*, 2018) is related to the statistical investigation about the number of buildings exposed to landslide risk. At this regard, it is worth noting that in this report the term building is related to any type of use (residential, industrial, commercial, services, tourism, directional, tertiary, other). Also, in this case, the observed outcomes on the Italian territory are very severe and dangerous.

The statistical investigation revealed that 550723 buildings rise up on high (H3) and very high (H4) landslide hazard zone, i.e. about 3.8% of the total built structure in Italy (14515795 buildings according to ISTAT 2011 Census). In Figure 2.24 the amount of Italian buildings exposed to each type of landslide risk is represented, where it is possible to observe that most of buildings rises up on moderate (599813 buildings, equal to 32%) and medium (584500 buildings, equal to 29%). Also in this case, the most affected Regions in terms of exposed buildings are the same of the two previous analysed indicators, i.e. Campania, Toscana, Emilia-Romagna and Calabria. The only difference is the presence of Calabria in the place of Liguria. The distribution of buildings exposed to high and very high landslide risk zones among various Regions and Municipalities is represented in the maps of Figure 2.25.

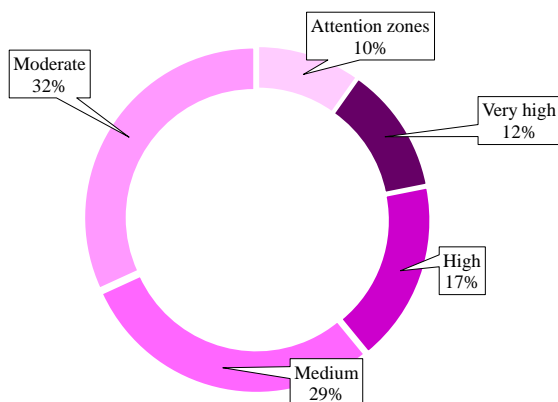


Figure 2.24 - Buildings exposed to landslide risk in Italy (Trigila *et al.*, 2018).

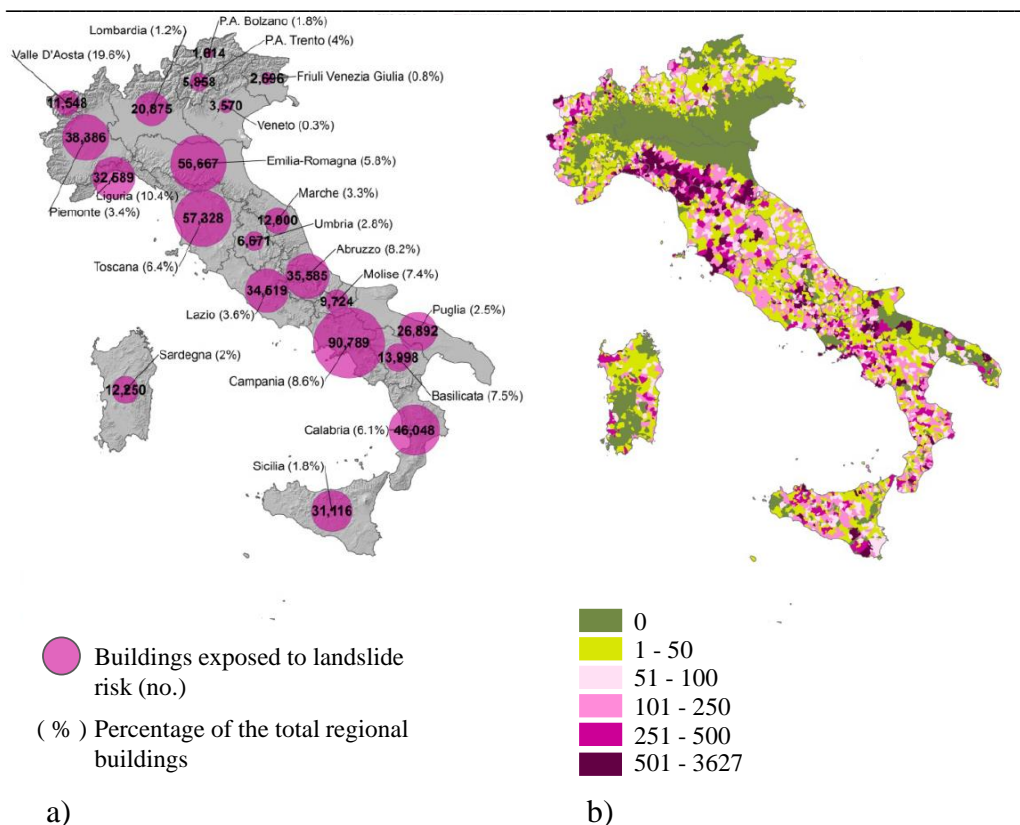


Figure 2.25 - Data collected in (Trigila et al., 2018): number of buildings at risk located in high and very high landslide hazard zones on (a) regional and (b) municipal basis.

The next analysed risk indicator is represented by industries and services local units, meaning a legal-economic unit or a part of it, located in a location that is topographically identified by an address and a street number. In this case the report studies in a statistic sense the number of industries and services local units exposed to landslide risk in Italy. Such an investigation revealed that 82948 Italian industries or services local units are located in high (*H3*) and very high (*H4*) landslide hazard zone, i.e. about 1.7% of the total number of industries or services in Italy (4806014 families according to ISTAT 2011 Census of Industry and Services). In terms of human life, this data corresponds to 217608 workers at risk.

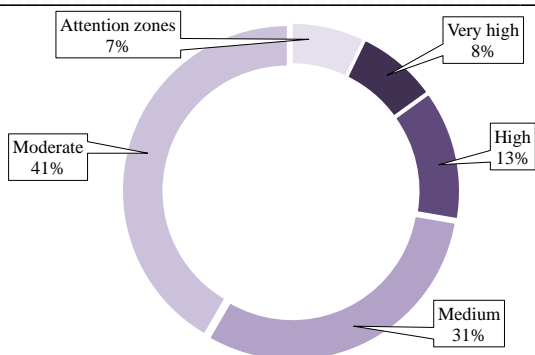


Figure 2.26 - Industry and services local units exposed to landslide risk in Italy (Trigila et al., 2018).

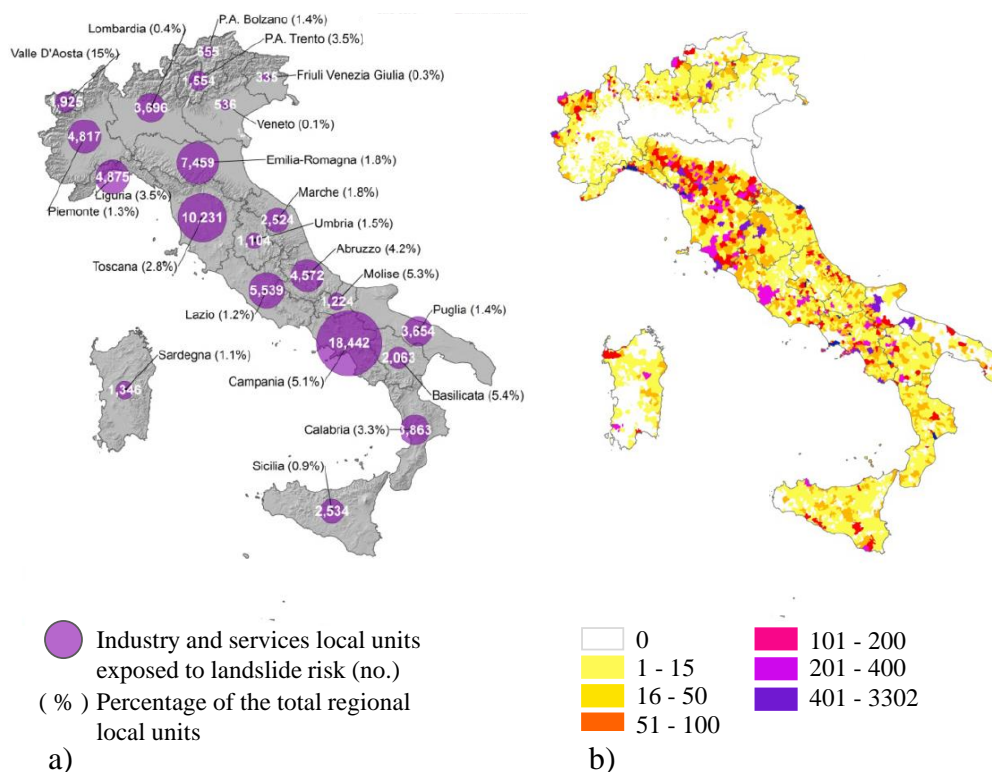


Figure 2.27 - Data collected in (Trigila et al., 2018): number of industry and services local units at risk located in high and very high landslide hazard zones on (a) regional and (b) municipal basis.

Figure 2.26 shows the number of industries and services local units in Italy exposed to each type of landslide risk, where it is possible to observe that most of involved industries/services rise up on moderate (168070 units, equal to 41%) and medium (123772 units, equal to 31%). The Regions with the highest number of industry and services local units located in high and very high landslide hazard zones are Campania, Toscana, Emilia-Romagna and Lazio, as showed in the maps of Figure 2.27.

With the scope of this thesis in mind, the most important investigated risk indicator in the (Trigila *et al.*, 2018) is represented by the analysis of Cultural Heritage exposed landslide risk. The statistical investigation revealed that the number of Cultural Heritage exposed to landslide risk are equal to 37847 corresponding to 18.6% of the total (203665 cultural heritage; VIR Database – ISCR), of which 11,712 (5.8%) are located in high and very high landslide hazard zones. Figure 2.28 shows the amount of families in Italy exposed to each level of landslide risk.

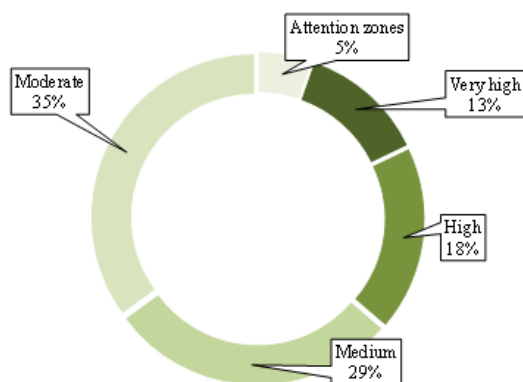


Figure 2.28 - Cultural Heritage exposed to landslide risk in Italy (Trigila *et al.*, 2018).

The highest number of Cultural Heritage located in high and very high landslide hazard zones is recorded in Toscana, Marche, Emilia-Romagna, Campania and Liguria Regions (Figure 2.29). There are numerous medieval villages affected by landslides that have been triggered or reactivated even in recent years, such as San Leo, Volterra and Civita di Bagnoregio. In recent decades, mitigation measures have been realised in several historic centres, as Certaldo, Todi and

Orvieto. Table 2.9 summarizes the results obtained for the investigated landslide risk indicators related to population, families, buildings, industry and services, cultural heritage according to (Trigila *et al.*, 2018).

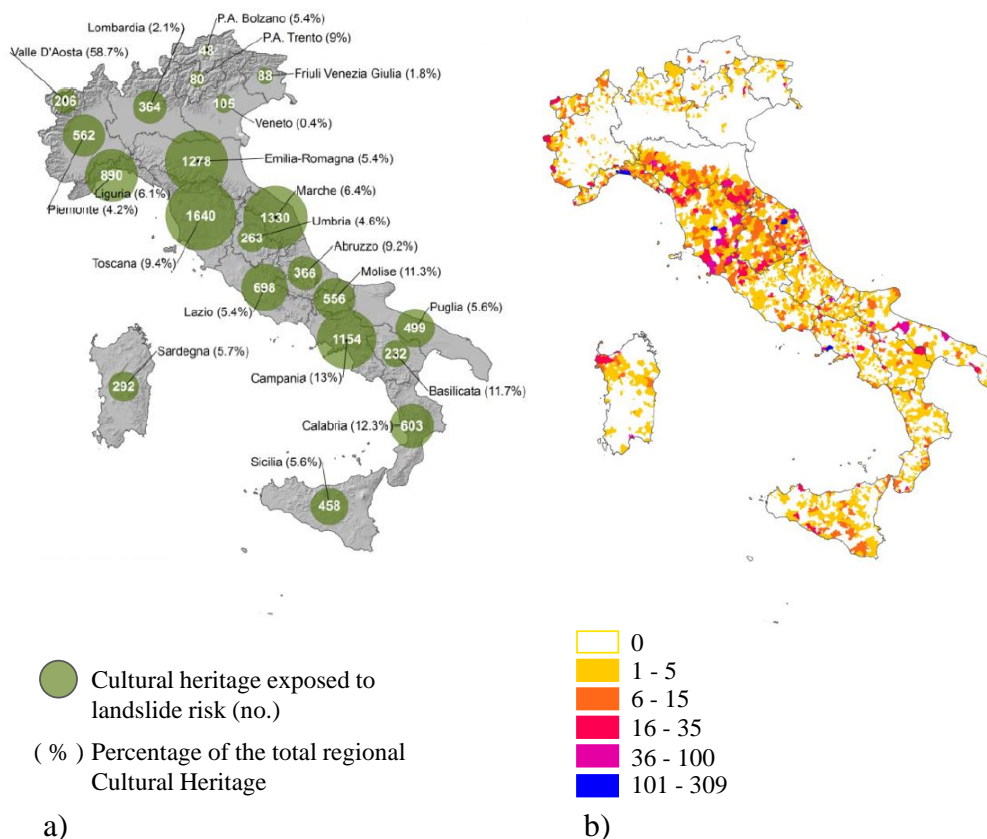


Figure 2.29 - Data collected in (Trigila *et al.*, 2018): number of Cultural Heritage at risk located in high and very high landslide hazard zones on (a) regional and (b) municipal basis.

The above-reported studies and research showed an important conclusion about the performance of buildings against landslide-induced mass movements. In most of the cases, structures exhibited a very high capacity to accommodate absolute horizontal movements up to several centimetres. This capacity is even higher when the landslides does not produce large differential deformations. The same cannot be said in the case of differential displacement, which can represent a

severe damage for the structure up to force to evacuate the inhabitants. The characterization of structural damage due to subsidence and landslide is a challenging topic in literature. Several factors influence the damage induced by this type of phenomena on buildings and monuments: local experiences; caution of professional engineer; occupancy type, market value and saleability of the property (Burland, 2008). In the next section, the possibility to obtain settlement values and profiles from the analysis of phenomena above described is investigated, with the scope to move on to the structural issues.

Region	Population at risk		Families at risk		Buildings at risk		Industry and services local units at risk		Industries and services workers at risk		Cultural Heritage at risk	
	No. ab.	%	No.	%	No.	%	No.	%	No.	%	No.	%
	in high and very high landslide hazard zones											
Piemonte	68744	1.6	31819	1.6	38386	3.4	4817	1.3	13966	1.0	562	4.2
Valle d'Aosta	15330	12.1	7172	12.1	11548	19.6	1,925	15.0	6364	15.0	206	58.7
Lombardia	44295	0.5	19047	0.5	10875	1.2	3696	0.4	12591	0.4	364	2.1
Trentino-Alto Adige	23148	2.2	9505	2.2	7472	3.1	2209	2.4	8669	2.4	128	7.2
Bolzano-Bozen	8163	1.6	3202	1.6	1614	1.8	655	1.4	2388	1.3	48	5.4
Trento	14985	2.9	6303	2.8	5858	4.0	1554	3.5	6281	3.6	80	9.0
Veneto	6684	0.1	2906	0.1	3570	0.3	536	0.1	1431	0.1	105	0.4
Friuli Venezia Giulia	4338	0.4	2127	0.4	2696	0.8	335	0.3	963	0.3	88	1.8
Liguria	91862	5.8	44271	5.8	32589	10.4	4875	3.5	12892	2.8	890	6.1
Emilia Romagna	94972	2.2	43452	2.3	56667	5.8	7459	1.8	20006	1.3	1278	5.4
Toscana	140497	3.8	60276	3.8	57328	6.4	10231	2.8	26922	2.3	1640	9.4
Umbria	16973	1.9	7234	2.0	6671	2.8	1104	1.5	2977	1.2	263	4.6
Marche	32624	2.1	12939	2.1	12000	3.3	2524	1.8	9919	2.0	1330	6.4
Lazio	89390	1.6	37653	1.6	34519	3.6	5539	1.2	13462	0.9	698	5.4
Abruzzo	75911	5.8	30370	5.8	35585	8.2	4572	4.2	11792	3.5	366	9.2
Molise	20356	6.5	8136	6.3	9724	7.4	1224	5.3	3262	5.2	556	11.3
Campania	302783	5.3	116115	5.6	90789	8.6	18442	5.1	43165	4.2	1154	13.0
Puglia	54445	1.3	22340	1.5	26892	2.5	3654	1.4	8068	1.0	499	5.6
Basilicata	33469	5.8	14076	6.1	13998	7.5	2063	5.4	4238	3.9	232	11.7
Calabria	87623	4.5	35936	4.6	46048	6.1	3863	3.3	7920	2.6	603	12.3
Sicilia	55987	1.1	23070	1.2	31116	1.8	2534	0.9	5683	0.7	458	5.6
Sardegna	22539	1.4	9590	1.4	12250	2.0	1346	1.1	3318	1.0	292	5.7
Total	1281970	2.2	538034	2.2	550723	3.8	82948	1.7	217608	1.3	11712	5.8

Table 2.9 - Landslide risk indicators related to population, families, buildings, industry and services, cultural heritage (Trigila et al., 2018).

2.5 From subsidence and landslide phenomena to field of settlement displacements

In the spirit of the present dissertation thesis, it is crucial to correlate the above-described natural phenomena to the promoted field of settlement displacements induced at the foundation of involved structures. The previous sections described in detail the distribution of subsidence and landslide events at the national and international scales as well as the damage induced by these phenomena. In this section, methods suggested in literature for the development of the movement profiles related to those phenomena are reported. It is worth noting that this point is a fundamental step in the scopes of this doctoral program: as a matter of fact, the next Chapters deal with numerical investigation of masonry panels subjected to movable support. In that case, the displacement profile will be directly assigned to the base, considering that its definition is the result of the application of one of the methods showed in this section. Three different groups will be identified on the base of the used technique for the displacement monitoring, namely in-situ, satellite and experimental monitoring displacement methods.

2.5.1 In-situ monitoring displacements

The first method to derive settlement profile from the analysis of ground movements and phenomena is represented by traditional in-situ monitoring technique for the displacement measurement. The use of surface marks, levelling rules and piezometers to monitor the movements of large portion of ground was widely spread in all over the world. Different contributions are available in literature, where the results obtained with these techniques were used to define settlement demand for buildings or structures affected by foundation movements.

In this spirit, a very useful contribution was provided in (Couto, Bento and Gomes, 2020), where the main scope of the authors is actually represented by the investigation of the seismic performance of residential buildings when they are even settlement affected. The paper focused on the case study of Lisbon's downtown, where the construction of underground structures associated with the fluctuation of the ground water level produced differential settlement at the

foundation of old masonry buildings which suffered severe damages. Several construction works were developed in the downtown of Lisbon in the last decades, causing an increase of load applications on the soil and so to surface settlements. Damages in the range from negligible to severe can be surveyed in the old building in this part of the city. In this framework, a monitoring plan was implemented by Lisbon City Council between 2004 and 2010 by using 54 surface marks, 15 levelling rules and 16 piezometers. As for the levelling rules, they were mainly installed in buildings, while the marks were mainly installed in presence of alluvial deposits. This monitoring step showed a strong relation between the groundwater level and the soil settlement: the accident occurred during the construction of the Terreiro do Paço subway station in 2000 caused a large amount of water and soils went in the tunnel, with a decrease of groundwater level and a surface settlement up to 23 cm.

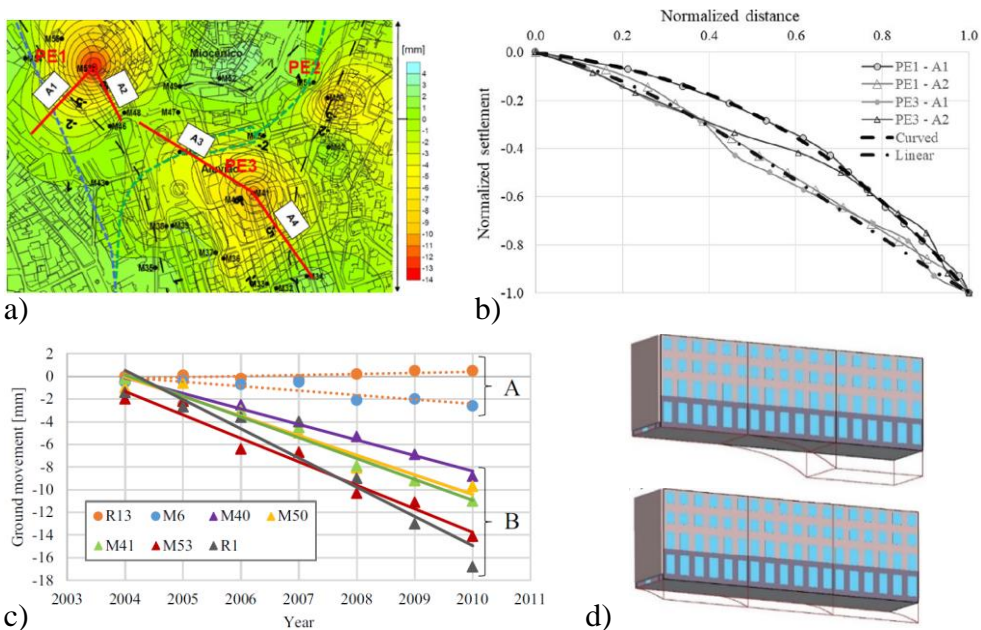


Figure 2.30 - Settlement profile derived by in-situ monitoring. The case study of Lisbon's downtown developed in (Couto, Bento and Gomes, 2020): (a) settlements isoline map of Lisbon's downtown; (b) normalized settlement profiles; (c) time evolution of settlements; (d) displacement configurations.

The preliminary work performed in (Couto, Bento and Gomes, 2020) to define settlement profiles for buildings in Lisbon’s downtown focused on the identification of the zones most affected by settlements by using a settlement map based on the in-situ measurements. Figure 2.30a shows that all of them are located near underground car parks: PE1—north of Praça dos Restauradores park (mark M53), PE2 south of Martim Moniz park (mark M50); and PE3 south of Praça da Figueira park (mark M41). With the scope to define the settlement profile to be used in the computational model, the settlement pattern for the identified zones was studied. In particular, four normalized hogging settlement profile were highlighted, corresponding to the upper and lower bound of PE1 and PE3. For an overall generalization of the problem, the settlement intensity and the length of the profiles were normalized using the maximum value. With this in mind, two settlement profile shapes were identified, which were smooth via polynomial regression, as showed in Figure 2.30b. The available data on the time evolution of the two marks allowed to identify two main behaviours represented in Figure 2.30c: the type A refers to stable evolution in time whereas the type B refers to increasing settlement in time.

2.5.2 Satellite monitoring displacements

The last decades have been showing many efforts to apply innovative satellite technologies to the study of the ground movements in order to overcome the limitations of the classical in-situ monitoring technique. An interesting and meaningful contribution is provided by (Arena, 2013), where an innovative technique based on DInSAR data is applied to study subsidence and landslide phenomena at different scales of analysis to investigate the related damage to urbanized area affected by these phenomena. For sake of clarity, the Differential SAR Interferometry (DInSAR) is a powerful satellite tool to quickly collect a high number of displacement measurements, both in time and space, based on data achieved by space-born Synthetic Aperture Radar (SAR). This interferometry technique is a fundamental branch of the so-called remote sensing, which represents a valid and innovative tool for the earth surface (and even atmosphere) observation from out of space by means of satellite (space born) or from the air through aircrafts (airborne). The main benefits of such a technique

can be listed as follow: the possibility to cover high spaces; the measurements of ground surface displacements with a very high accuracy thanks to large datasets of images acquired over about 30 years; the cost-effectiveness of this satellite monitoring technique compared with not affordable conventional in-situ techniques.

As for subsidence phenomena, the study carried out in (Arena, 2013) focused on Campania region at the small scale to arrive to single buildings at the detailed scale. At the small scale the goal is to identify the subsiding area by using available dataset, such as the Italian “Piano Straordinario di Telerivamento” (PST) based on data processed by ERS and ENVISAT satellite. The use of DInSAR allowed to double check the available ground movements and to define the cumulative settlements for the selected flat area as well as a global overall map derived from the application of a DEM procedure. Thanks to the satellite monitoring both horizontal and vertical velocity modulus of a discrete number of spread points (cells) can be calculated. By combine these vectors, the movement trend and features of the investigated area can be derived. The accuracy of the monitored data improves according to medium and large scale, where the relationship between the magnitude of settlement and the building damage occurrence is investigated. As a matter of fact, the gradient of displacements is computed by using a more refined cell grid, where each point is attached with a specific value of settlement measured by means of DInSAR technique. The detailed scale is the most interesting in the spirit of the present dissertation thesis, which deals with the analysis of single masonry types affected to foundation movements. The selected building is the one suffered the highest values of displacement gradient as for the analysis at the large and medium scales. With the scope to derive the applied settlement profile, the available DInSAR data are projected along the vertical direction and interpolated via a specific geometrical grid. The direction of profile is selected according to the maximum settlement change direction so that the settlement profiles applied to the investigated section can be retrieved. In the method proposed by (Arena, 2013) further important data are provided by the trends of the relative rotation calculated according to (Skempton and Mac Donald, 1956). The resulted were also compared with the crack observation via an in-situ damage survey.

In (Arena, 2013), the same procedure was also applied to the case of settlement profiles induced by landslide events. As already described in presence of subsidence, at large and medium scale the investigated area is chosen according to the distribution of slow-moving landslides causing losses of structures or infrastructures. At this scope, available inventory maps (MATTM, 2013) provide with detailed information dealing with location, type, state of activity and areal extension. At the large scale, a significant number of urbanized municipalities was selected and analysed in terms of homogenous aggregations of existing buildings. The next step consists of intersecting these data with the mapped slow-moving landslide affected areas with the goal to develop the vulnerable areas grouped according to the buildings' occupancy type. The identified vulnerable areas were then classified as damaged or not damaged area on the base of the number of damaged buildings located in each area: damaged areas present at least one damaged building. In order to better evaluate the intensity and the value of the applied displacements at the foundation of buildings, the analysis of the state of activity of landslide phenomena is also a crucial point. The cited method proposed in (Arena, 2013) groups the studied landslide in two classes, namely active and dormant, thanks to the DInSAR-Damage data. In this case, it is possible to classify the type of action which affects the investigated building, and the intensity and distribution of the landslide-induced settlement profile is suggested by the satellite data in terms of computed movements velocity of the fixed cells.

In (Arena, 2013) various example on Italian case studies were presented in order to validate the proposed approach via comparison with in-situ survey to observe visible cracks and damages. In this framework, three examples of application at detailed scale for subsidence were presented. The first one deals with the analysis of a single-floor reinforced concrete building located in Castel Volturno, already investigated in (Cascini *et al.*, 2013). The structure lies in a movable area according to the ERS-ENVISAT data at the medium scale in the period 1992-2010 (Figure 2.31a). The combination of three datasets allowed to develop the vertical displacement time series belonging to the cells located over the investigated building. As showed in Figure 2.31b, a cumulative vertical settlement of about 6 cm is computed for the analysed portion of building. The

interpolation of the vertical cumulative settlements over the building leads to define the settlement profile to be applied to the longitudinal cross-section of the building. According to (Arena, 2013), the introduced settlements only account for pure shear mode of deformation, neglecting the strain in the vertical direction. Under these assumptions, Figure 2.31c shows an increase of the absolute vertical settlements and of both sagging and hogging zones of the foundation.

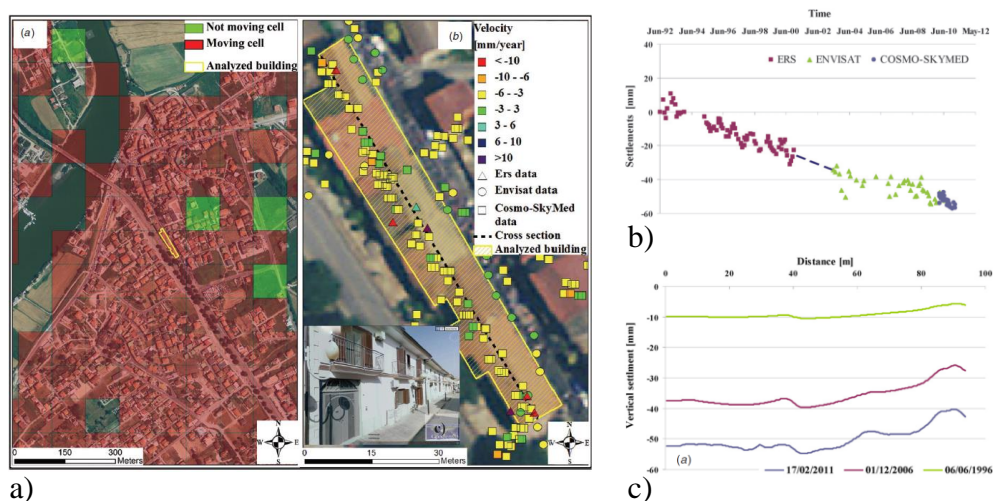


Figure 2.31 -Application at detailed scale for subsidence. The case study of a reinforced concrete building described in (Cascini *et al.*, 2013): (a) view of the Castel Volturno area with an indication of the grid of satellite covered cells and the analysed buildings; (b) example of cumulative vertical settlement obtained with three dataset time series; (c) vertical cumulative settlements to be applied along the longitudinal cross section of the building.

The second case study developed in (Arena, 2013) is represented by the subsidence occurred in Sarno and described in (Peduto, 2008; Cascini *et al.*, 2011a, 2011b). Two buildings were selected according to the map of cumulative settlement obtained using satellite acquisitions Figure 2.32a. Also in this case, the available satellite data were interpolated on a regular square grid aiming at the computation of the cumulative settlement trends. Important information about building performance can be obtained by investigating also the trends of other two parameters, i.e. the relative rotation and the deflection ratio according to the definition provided in (Skempton and Mac Donald, 1956). The results obtained

in (Cascini *et al.*, 2011a, 2011b) for the two mentioned buildings are showed in Figure 2.32b,c. The first building is characterized by the presence of weak sections causing highest relative values of the monitored parameters. As for the second building, the damage appears to be concentrated at the stairs.

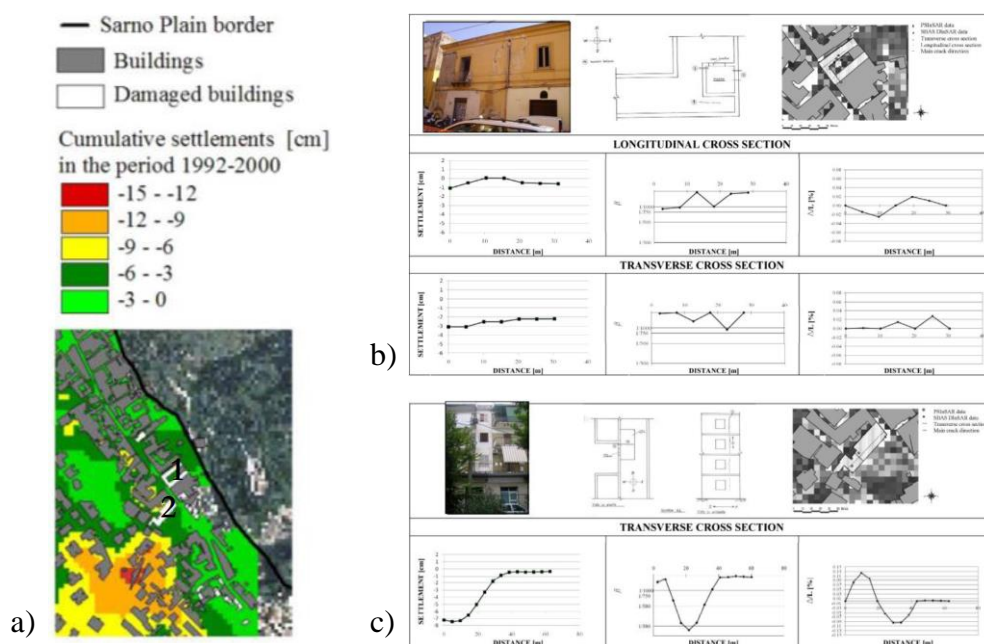


Figure 2.32 - Application at detailed scale for subsidence. The case study of two buildings in Sarno and described in (Cascini *et al.*, 2011a, 2011b): (a) map of the cumulative settlements; (b)(c) investigated buildings.

The last application described in (Arena, 2013) does not deal with a building or structure but with an infrastructural system located not far from Naples central station, made by a high-speed railway line and a highway viaduct, already investigated in (Cascini *et al.*, 2013). The procedure above described was again applied. First of all, moving cells were analysed in the specific area covered by satellite measurements Figure 2.33a. Since the satellite data can provide only linear features, velocity and displacement measured are assumed as occurring along the vertical direction. Under this assumption, Figure 2.33b shows the cumulative settlements computed over one-year monitoring considering three

different zones along the line. By using COSMO-SkyMed data, two settlement profiles were derived as possible movement for the two main cross sections. The results are showed in Figure 2.33c,d, where a maximum cumulative settlement of 20 mm and 10 mm is predicted for the railway line and viaduct respectively.

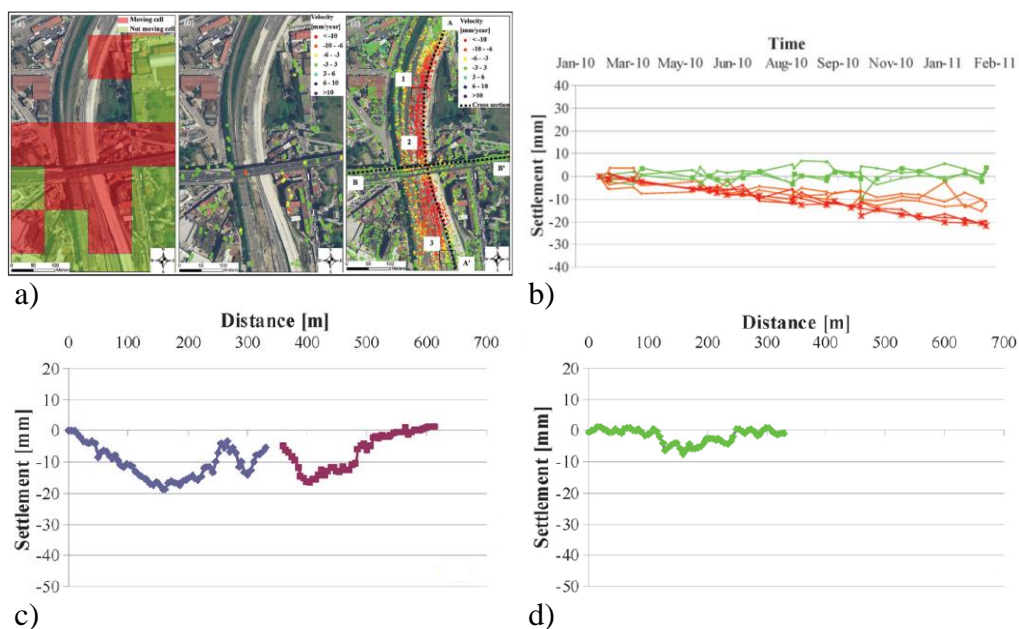


Figure 2.33 - Application at detailed scale for subsidence. The case study of a infrastructural system close to Naples described in (Cascini *et al.*, 2013): (a) zoom over the railway lines with the indication of the covered satellite cells; (b) one-year cumulative settlements computed along the vertical direction; the trend of cumulative vertical settlements for the (c) railway and (d) viaduct.

Another important application of this satellite monitoring technique was provided in (Reale *et al.*, 2019), where the innovative approach was tested on the monumental case study of the San Gerlando Cathedral in Agrigento (Sicily, Italy), a huge Roman Catholic cathedral founded in the 11th century. The city of Agrigento is affected by hydrogeological hazards and the specific geological and geomorphological features of this area have been causing a widespread ground instability reported in the landslide inventory map. As a consequence, the structure suffered various damages during the centuries mainly due to the slope

instability of the north side of the church. A detailed overview of the different suffered damages and relative strengthening interventions is developed in (Reale *et al.*, 2019).

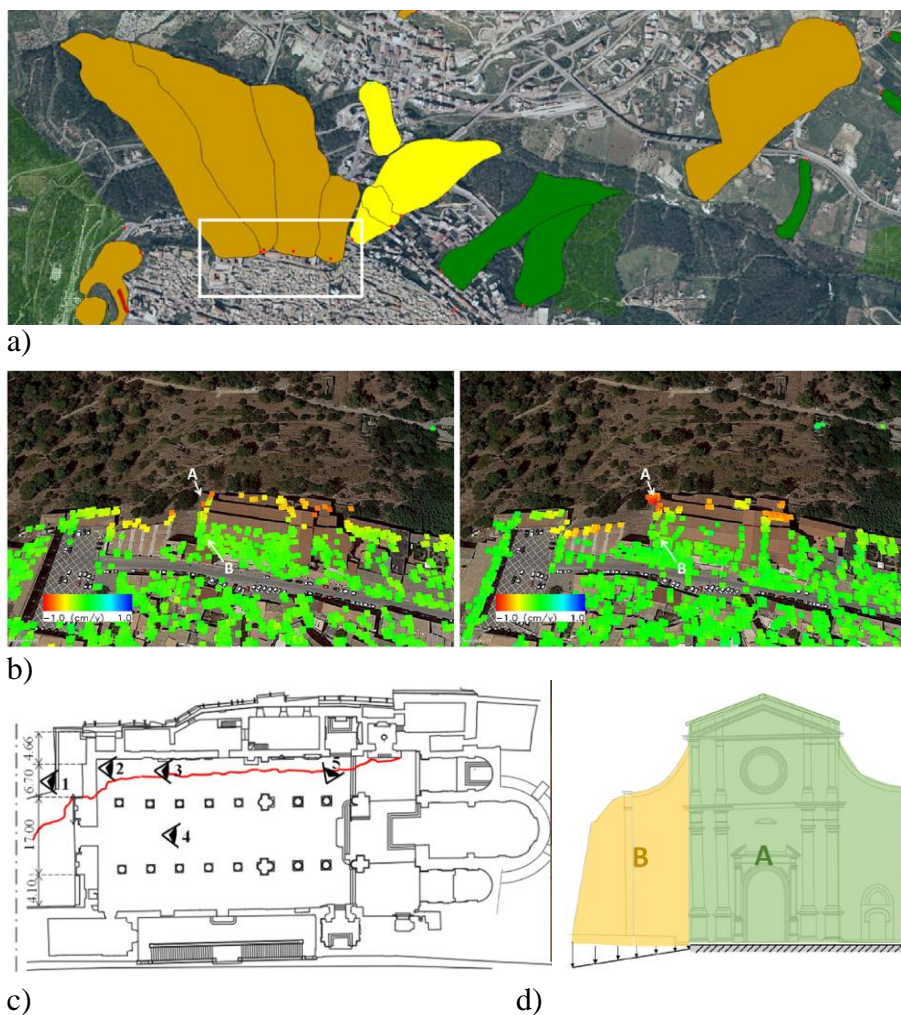


Figure 2.34 – Settlement profile derived by satellite monitoring. The case study of Agrigento Cathedral developed in (Reale *et al.*, 2019): (a) Landslide inventory map of the area of Agrigento; (b) estimated deformation mean velocity over the area of interest; (c) crack pattern; (d) settlement profile under the assumed macro-elements of the main façade.

In this case, the DInSAR measurements (obtained through data processing of VHR COSMO-SkyMed satellite) were also integrated with ground-based measurements and in-situ surveys. The possibility to study the Landslide inventory map of the area of Agrigento allowed to highlight the type of phenomena which is currently acting under the analysed structure. Then, the satellite acquisition showed the deformation velocity trend: in the case of the Agrigento Cathedral, it confirmed that the northern part (the one lying on unstable slope) of the church is characterized by a high deformation pattern. The post-processing satellite acquisition data can give information also about the displacement components in order to better define a proper displacement profile for the investigated structure.

In the case of Agrigento, the data estimated a deformation dominated by the vertical component, confirming the presence of significant differential settlements between Northern and Southern side of the church, which is consistent with the crack pattern observed via in-situ survey. The main façade appeared to be one of the most damaged elements of the church, and was deeply investigated in (Reale *et al.*, 2019). As for the façade, the integration of DInSAR distribution and in-situ measurements gave very interesting results. The analysis of satellite data along the façade showed that different velocities are observed over a huge vertical crack somehow originating two macro-elements subjected to a differential settlements profile. For sake of simplicity, the two macroblocks were analysed under a uniform kinematic behaviour with the ground instabilities simulated by a vertical and rotational settlement of one of them. Figure 2.34 summarizes the application to the case study of Agrigento Cathedral performed in (Reale *et al.*, 2019).

2.5.3 Experimental monitoring displacements

In the previous two sections, different techniques to derive settlement profile from the analysis of events related to ground movements were described. In this field, a research branch devoted to the experimental investigation of the settlement profile has been developing. It is worth mentioning that full-scale experimental tests are not easy to perform. With this in mind, centrifuge testing

usually are designed to study the effect of tunneling on masonry buildings. An experimental campaign was performed in (Dejong, 2016) to investigate the effect of building geometry, position and the influence of openings.

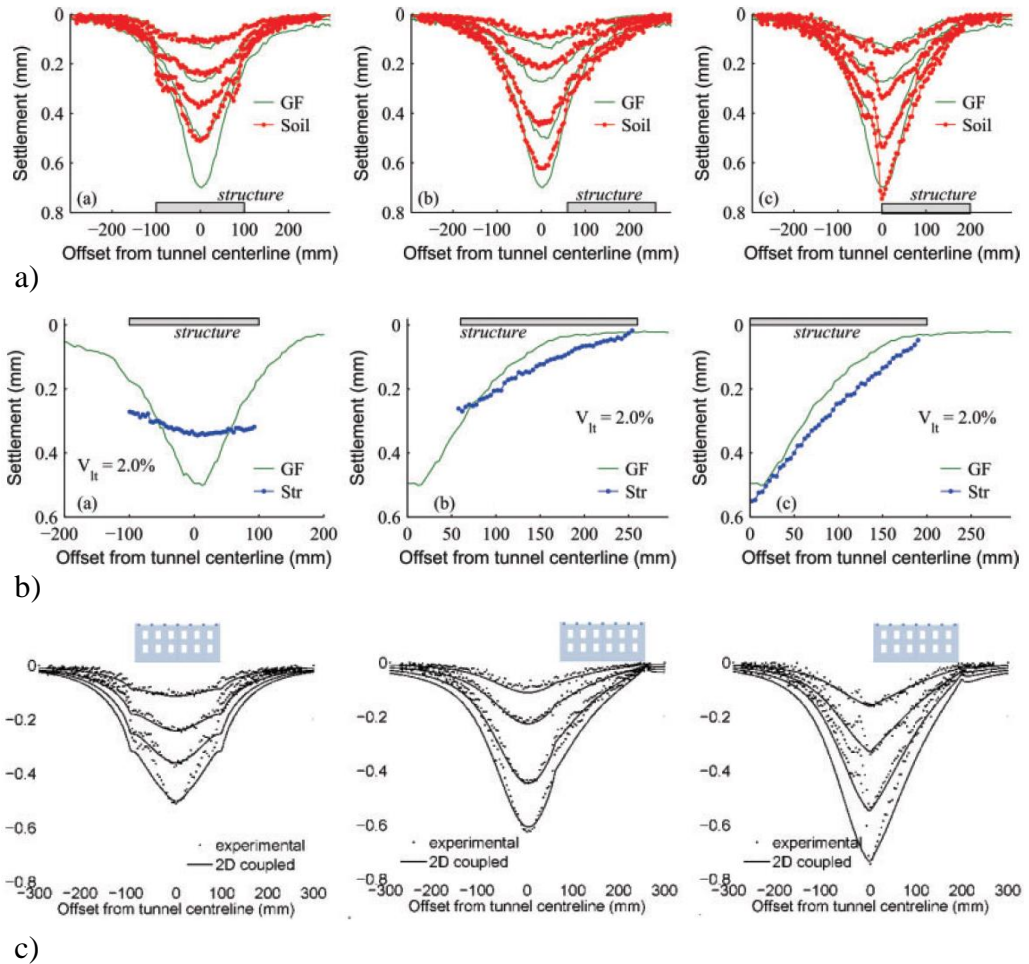


Figure 2.35 – Settlement profile derived by centrifuge test as described in (Dejong, 2016): (a) comparison of the vertical displacements at the soil surface for greenfield and building tests (volume loss=0.5%, 1%, 2%, 4%); (b) comparison of the vertical greenfield soil surface displacements to the vertical displacement of the base of the structure (volume loss=2%); (c) comparison with results obtained with a FEM computational model.

The work described in (Dejong, 2016) mainly focused on the influence of the building position with respect of the tunnel, analysing the settlement profiles of the soil surface for a greenfield test compared with the profile in the case of various percentages of volume losses. The results showed in Figure 2.35a revealed a high sensitivity of the settlement profile from the parameter of the volume loss. The comparison between greenfield settlement and 2% volume loss is also performed in (Dejong, 2016) showing that the curvature of the structure strongly reduced compared to the case with greenfield settlement profiles (Figure 2.35b). The experimental centrifuge tests were also compared with the results obtained by using computational methods based on FEM model, as showed in Figure 2.35c.

Conclusions

The present Chapter 2 was devoted to the overview on the settlement-induced damages aiming to provide an introduction for the next chapters where the analytical and numerical sections will be mainly focused on masonry structures affected by ground movements and settled foundations. The comprehensive description here reported is a crucial point to study the triggering action before to start with the investigation of the effects which is able to provoke on masonry structures.

In this spirit, the Chapter is dedicated to a large description of the most important natural and man-made hazards related to the possibility of settlement at the base of constructions. The deeper investigated causes are represented by subsidence and landslide, which are the main damaging geohazards. The two mentioned phenomena were described in detail in this Chapter: first, the morphological features of such events were reported in order to highlight the differences among them, avoiding any type of misunderstandings, and also to list the various type of events belonged to these two groups according to some important parameters such as the type of movement, the type of involved material, the intensity etc. On the side of man-made hazards, the main cause comes from the tunneling phenomena, which has been increasing in the last decades as a consequence of the development in several city centres where huge work of metro lines

construction is taking place, with strong influence on the subsoil constitution and stability which can affect structures and infrastructures in a very dangerous way.

The above-mentioned hazard phenomena were also described in terms of damage which can affect the involved buildings, especially masonry structures. In this case, a statistical research of the damages and distribution of these events at a national and international scales were performed with the goal to underline the role this risk has been playing in the last decades, especially in the field of the demand for measure of protection of structures with specific regard to the built Cultural Heritage.

Finally, the present Chapter ends with a description of possible solutions to monitor the above-described natural hazards and to derive a field of settlement displacements to be applied at the foundation level of the affected structures. The latter represents a crucial point to link with the topics discussed in the next chapters in order to better illustrate the nature of the applied actions (or displacements) at the base of the investigated masonry types.

References

- Allen, D. R. and Mayuga, M. N. (1970) ‘The Mechanics of Compaction and Rebound, Wilmington Oil Field, Long Beach, California, U.S.A’, in *Int Ass Sci Hydrol & UNESCO Land Subsidence Syrup.*
- Antronico, L. *et al.* (2003) *Linee guida per interventi di stabilizzazione di pendii in aree urbane da riqualificare.* Regione Calabria.
- Arena, L. (2013) *Analysis of DInSAR Data in urban areas affected by subsidence or slow-moving landslides.*
- Bell, F. G. (1993) *Engineering geology, Engineering geology.*
- Blong, R. J. (1973) ‘A numerical classification of selected landslides of the debris slide-avalanche-flow type’, *Engineering Geology*, 7(2), pp. 99–114. doi: 10.1016/0013-7952(73)90040-9.
- Bonnard, C. H., Tacher, L. and Beniston, M. (2008) ‘Prediction of landslide movements caused by climate change’, in *Landslides and Engineered Slopes. From the Past to the Future.* doi: 10.1201/9780203885284-c13.
- Booker, J. R., Carter, J. P. and Small, J. C. (1985) *Prediction of subsidence caused by pumping of groundwater., Res Rep Univ Sydney Sch Civ Min Eng.*
- Burland, J. B. (2008) ‘Foundation engineering’, *Structural Engineer*, pp. 45–51.
- Cascini, L. (2005) ‘Risk assessment of fast landslide—From theory to practice. General Report’, in Patron Editore (ed.) *Proc. Int. Conference on “Fast Slope Movements – Prediction and Prevention for Risk Mitigation”*, pp. 33–52.
- Cascini, L. *et al.* (2011a) ‘Monitoraggio con tecniche satellitari di aree urbanizzate in subsidenza.’, *Innovazione Tecnologica nell’Ingegneria Geotecnica*, 2, pp. 657–664.
- Cascini, L. *et al.* (2011b) ‘Tecniche innovative satellitari nel monitoraggio di opere interagenti con frane a cinematica lenta’, *Innovazione Tecnologica nell’Ingegneria Geotecnica*, 2, pp. 665–672.
- Cascini, L. *et al.* (2013) ‘Detection and monitoring of facilities exposed to subsidence phenomena via past and current generation SAR sensors’, *Journal of Geophysics and Engineering*, 10(6). doi: 10.1088/1742-2132/10/6/064001.

Cascini, L. and Gullà, G. (1992a) ‘Analisi di dettagli delle caratteristiche fisico meccaniche dei terreni prodotti dall’alterazione degli gneiss di San Pietro in Guarano (CS)’, *Geologia Applicata e Idrologia*, 27, pp. 49–76.

Cascini, L. and Gullà, G. (1992b) ‘Grado di alterazione e meccanismi di rottura nei terreni prodotti dall’alterazione degli gneiss di San Pietro in Guarano (CS)’, *CNR-IRPI, Rapporto N.363*.

Cascini, L., Gullà, G. and Sorbino, G. (2006) ‘Groundwater modelling of a weathered gneissic cover’, *Canadian Geotechnical Journal*, 43(11), pp. 1153–1166. doi: 10.1139/T06-066.

Cascini, L. and Di Maio, C. (1994) ‘Emungimento delle acque sotterranee e cedimenti nell’abitato di Sarno: analisi preliminare’, *Rivista Italiana di Geotecnica*, 3, pp. 217–231.

Clementino, R. *et al.* (2008) ‘Embankment Slope Stabilization Using Subhorizontal Drains At Highway 39 Near Drayton Valley, AB’, in *4th Canadian Conference on Geohazards: From Causes to Management*.

Cooper, A. H. (2008) ‘The classification, recording, databasing and use of information about building damage caused by subsidence and landslides’, *Quarterly Journal of Engineering Geology and Hydrogeology*, 41(3), pp. 409–424. doi: 10.1144/1470-9236/07-223.

Cotecchia, V. (2006) ‘The Second Hans Cloos Lecture. Experience drawn from the great Ancona landslide of 1982’, *Bulletin of Engineering Geology and the Environment*, 65(1), pp. 1–41. doi: 10.1007/s10064-005-0024-z.

Couto, R., Bento, R. and Gomes, R. C. (2020) ‘Seismic performance and fragility curves of historical residential buildings in Lisbon downtown affected by settlements’, *Bulletin of Earthquake Engineering*, 18(11), pp. 5281–5307. doi: 10.1007/s10518-020-00906-z.

Crescenti, U. *et al.* (1983) ‘La grande frana di Ancona del 1982’, in *Atti del XV Convegno Nazionale di Geotecnica*. Spoleto, Italy.

Cruden, D. M. (1991) ‘A simple definition of a landslide’, *Bulletin of the International Association of Engineering Geology - Bulletin de l’Association Internationale de Géologie de l’Ingénieur*, 43(1), pp. 27–29. doi: 10.1007/BF02590167.

Cruden, D. M. and Varnes, D. J. (1996) ‘Landslide types and processes’, *Special Report - National Research Council, Transportation Research Board*, 247, pp. 36–75.

Dejong, M. J. (2016) ‘Settlement effects on masonry structures’, *Structural Analysis of Historical Construction*, pp. 449–456.

Esser, A. J. (2000) ‘Case of a slope failure in lacustrine deposits. Landslides in research, theory and practice’, in *Proceeding of the 8th International Symposium on Landslides*. Cardiff, UK, pp. 531–536.

Fell, R. (1994) ‘Landslide risk assessment and acceptable risk’, *Canadian Geotechnical Journal*, 31(2), pp. 261–272. doi: 10.1139/t94-031.

Fujisawa, K. *et al.* (2007) *Landslide Detection, Monitoring, Prediction, Emergency Measures and Technical Instrumentation in a Busy City, Atami, Japan*.

Füssel, H.-M. *et al.* (2012) *Climate change, impacts and vulnerability in Europe 2012: an indicator-based report.*, *EEA Report*. doi: 10.2800/66071.

Gabrysch, R. K. (1984) *Ground-water withdrawals and land-surface subsidence in the Houston Galveston region, Texas, 1906-80*. Texas Department of water resources report, 64.

Giardina, G. (2013) *Modelling of settlement induced building damage*. Delft University of Technology.

Gillon, M. D. and Saul, G. J. (1996) ‘Cairnmuir Landslide infiltration protection stabilisation works’, *Transactions - Institution of Professional Engineers New Zealand: Civil Engineering Section*, 23(1), pp. 19–25.

Hungr, O. (1997) ‘Some methods of landslide hazard intensity mapping’, in *Landslide risk assessment Proceedings of the Workshop on Landslide Risk Assessment, Honolulu, Hawaii, USA, 19-21 February 1997*. Balkema. Rotterdam, pp. 215–226.

Hungr, O. *et al.* (2001) ‘A review of the classification of landslides of the flow type’, *Environmental and Engineering Geoscience*, 7(3), pp. 221–238. doi: 10.2113/gseegeosci.7.3.221.

Hutchinson, J. N. (1968) ‘Field meeting on the coastal landslides of Kent: 1–3

July 1966’, *Proceedings of the Geologists’ Association*, 79(2), pp. 227–237. doi: 10.1016/S0016-7878(68)80039-2.

Hutchinson, J. N. (1973) ‘The response of London Clay Clijfs to Differing Rates of Toe Erosion’, *Geologia Applicata e Idrologia*, 8, pp. 221–239.

Hutchinson, J. N. (1988) *General report: morphological and geotechnical parameters of landslides in relation to geology and hydrogeology, Landslides. Proc. 5th symposium, Lausanne, 1988. Vol. 1.*

Hutchinson, J. N. (2004) ‘Review of flow-like mass movements in granular and fine grained materials’, in *Proceedings of the International Workshop ‘Flows 2003 - Occurrence and mechanisms of flows in natural slopes and earthfill’*, pp. 3–16.

Hutchinson, J. N. and Gostelow, T. P. (1976) ‘The Development of an Abandoned Cliff in London Clay at Hadleigh, Essex’, *Philosophical Transactions of the Royal Society of London. Series A, Mathematical and Physical Sciences*, 283, pp. 557–604.

Iovine, G. *et al.* (2006) ‘The March 7th 2005 Cavallerizzo (Cerzeto) landslide in Calabria - Southern Italy.’, in *Geological Society of London*. Nottingham, UK, pp. 6–10.

Ireland, R. L., Poland, J. F. and Riley, F. S. (1984) ‘Land subsidence in the San Joaquin Valley, California, as of 1980.’, *US Geological Survey Professional Paper*. doi: 10.3133/pp437I.

ISPRA (2018) *Annuario dei date ambientali*. Edizione 2.

Jones, C. J. F. P. and Bellamy, J. B. (1973) ‘Computer prediction of ground movements due to mining subsidence’, *Geotechnique*, 23(4), pp. 515–530. doi: 10.1680/geot.1973.23.4.515.

Konagai, K. *et al.* (2013) ‘Maps of soil subsidence for Tokyo bay shore areas liquefied in the March 11th, 2011 off the Pacific Coast of Tohoku Earthquake’, *Soil Dynamics and Earthquake Engineering*, 53, pp. 240–253. doi: 10.1016/j.soildyn.2013.06.012.

Krahn, J. and Morgenstern, N. R. (1979) ‘The ultimate frictional resistance of rock discontinuities’, *International Journal of Rock Mechanics and Mining*

Sciences and, 16(2), pp. 127–133. doi: 10.1016/0148-9062(79)91449-9.

Leroueil, S. *et al.* (1996) ‘Geotechnical characterisation of slope movements’, in *Proceedings of the 7th International Symposium of Landslides*. Trondheim, pp. 53–74.

Leroueil, S. and Locat, J. (1998) *Slope movements – Geotechnical characterisation, risk assessment and mitigation*. Balkema. Edited by Geotechnical Hazards. Rotterdam.

López-Quiroz, P. *et al.* (2009) ‘Time series analysis of Mexico City subsidence constrained by radar interferometry’, *Journal of Applied Geophysics*, 69(1), pp. 1–15. doi: 10.1016/j.jappgeo.2009.02.006.

Malone, A. *et al.* (2008) ‘Post-failure movements of a large slow rock slide in schist near Pos Selim, Malaysia’, in *Landslides and Engineered Slopes. From the Past to the Future*. doi: 10.1201/9780203885284-c48.

MATTM (2013) *Ampliamento dei contenuti del Piano Straordinario di Telerilevamento (PST) per la ricognizione di dati ambientali*. Available at: <https://performance.gov.it/performance/obiettivo-strategico/422>.

Modoni, G. *et al.* (2013) ‘Spatial analysis of land subsidence induced by groundwater withdrawal’, *Engineering Geology*, 167, pp. 59–71. doi: 10.1016/j.enggeo.2013.10.014.

Moore, D. P., Watson, A. D. and Martin, C. D. (2006) *Deformation mechanism of a large rockslide inundated by a reservoir. Workshop on the mechanics and velocity of large landslides*. Italy.

Nelson, S. A. (2012) *Subsidence: Dissolution & Human Related Causes, EENS 3050 Natural Disasters*. Available at: http://www.tulane.edu/~sanelson/Natural_Disasters/subsidence.ht.

Nichol, D. and Lowman, R. D. W. (2001) ‘Stabilisation and remediation of a minor landslide affecting the A5 trunk road at Llangollen, North Wales, UK’, *Ground Improvement*, 5(2), pp. 49–56. doi: 10.1680/grim.5.2.49.39980.

Okumura, T. (1969) ‘Analysis of subsidence in Niigata.’, *Proceedings of the International Symposium on Land Subsidence*. Tokyo, Japan, pp. 130–143.

Ovando-Shelley, E. *et al.* (2003) ‘Effects on soil properties of future settlements

in downtown Mexico City due to ground water extraction’, *Geofisica Internacional*, 42(2), pp. 185–204.

Peck, R. B. (1969) ‘Deep Excavation and Tunneling in Soft Ground. State of the Art Report.’, in *7th International Conference on Soil Mechanics and Foundation Engineering*. Mexico City, pp. 225–290.

Peduto, D. (2008) *Analysis of ground deformations related to subsidence and landslide phenomena via DInSAR techniques*.

Phien-wej, N., Giao, P. H. and Nutalaya, P. (2006) ‘Land subsidence in Bangkok, Thailand’, *Engineering Geology*, 82(4), pp. 187–201. doi: 10.1016/j.enggeo.2005.10.004.

Picarelli, L. (2018) ‘Mechanisms and rates of slope movements in fine grained soils’, in *ISRM International Symposium 2000, IS 2000*.

Prokopovich, N. P. and Marriott, M. J. (1983) ‘Cost of subsidence to the Central Valley Project, California.’, *Bulletin of the Association of Engineering Geologists*, 20(3), pp. 325–332. doi: 10.2113/gseegeosci.xx.3.325.

Reale, D. *et al.* (2019) ‘A multi-disciplinary approach for the damage analysis of cultural heritage: The case study of the St. Gerlando Cathedral in Agrigento’, *Remote Sensing of Environment*, 235. doi: 10.1016/j.rse.2019.111464.

Ricceri, G. (2007) ‘Il futuro di Venezia tra subsidenza ed entusiasmo’, *Rivista Italiana di Geotecnica*, 3.

Sassa, K. (1988) *Special lecture: geotechnical model for the motion of landslides, Landslides. Proc. 5th symposium, Lausanne, 1988. Vol. 1*.

Schuster, R. L. (2007) *Establishment of the technical journal ‘landslides’ as the successor to ‘landslide news’, Progress in Landslide Science*. doi: 10.1007/978-3-540-70965-7.

Shi, X. *et al.* (2008) ‘Regional land subsidence simulation in Su-Xi-Chang area and Shanghai City, China’, *Engineering Geology*, 100(1–2), pp. 27–42. doi: 10.1016/j.enggeo.2008.02.011.

Skempton, A. W. (1953) ‘The colloidal activity of clays’, in *Proceeding of the 3rd International Conference on Soil Mechanics*. Zurich, pp. 7–61.

Skempton, A. W. (1970) ‘First-time slides in over-consolidated clays’,

Geotechnique, 20(3), pp. 320–324. doi: 10.1680/geot.1970.20.3.320.

Skempton, A. W. and Mac Donald, D. H. (1956) ‘Allowable Settlement of Structures’, in *Proc. Institute of Civil Engineers, Part III*, pp. 727–768.

Terzaghi, K. (1950) ‘Mechanism of Landslides’, *Application of Geology to Engineering Practice*. Edited by S. Paige. Geological Society of America. doi: 10.1130/Berkey.1950.83.

Topal, T. and Akin, M. (2008) ‘Investigation of a landslide along a natural gas pipeline (Karacabey-Turkey)’, in *Landslides and Engineered Slopes. From the Past to the Future*. doi: 10.1201/9780203885284-c226.

Topal, T. and Akin, M. (2009) ‘Geotechnical assessment of a landslide along a natural gas pipeline for possible remediations (Karacabey-Turkey)’, *Environmental Geology*. doi: 10.1007/s00254-008-1330-0.

Törnqvist, T. E. *et al.* (2008) ‘Mississippi Delta subsidence primarily caused by compaction of Holocene strata’, *Nature Geoscience*, 1(3), pp. 173–176. doi: 10.1038/ngeo129.

Trigila, A., Iadanza, C., Esposito, C., *et al.* (2015) ‘Comparison of Logistic Regression and Random Forests techniques for shallow landslide susceptibility assessment in Giampilieri (NE Sicily, Italy)’, *Geomorphology*, 249, pp. 119–136. doi: 10.1016/j.geomorph.2015.06.001.

Trigila, A., Iadanza, C., Munafò, M., *et al.* (2015) *Population exposed to landslide and flood risk in Italy, Engineering Geology for Society and Territory - Volume 5: Urban Geology, Sustainable Planning and Landscape Exploitation*. doi: 10.1007/978-3-319-09048-1_163.

Trigila, A. *et al.* (2018) *Dissesto idrogeologico in Italia: pericolosità e indicatori di rischio*. Edizione 2, ISPRA, *Rapporti* 287/2018. Edizione 2.

Trigila, A. and Iadanza, C. (2008a) *Landslides in Italy Special Report, Journal of Chemical Information and Modeling*. Available at: https://web.archive.org/web/20110717122241/http://www.apat.gov.it/site/_contentfiles/00153200/153292_RAPPORTO_83_08_Landslide.pdf.

Trigila, A. and Iadanza, C. (2008b) *Landslides in Italy Special Report, Journal of Chemical Information and Modeling*.

UNESCO WGS (2021) *The UNESCO Land Subsidence International Initiative (LaSII)*. Available at: <https://www.landsubsidence-unesco.org/>.

Varnes, D. J. (1958) 'Landslide types and processes', in *Landslides and Engineering Practice, National Academy of Sciences, Transportation Research Board Special Report*. Highway Research Board. Available at: <http://onlinepubs.trb.org/Onlinepubs/sr/sr29/29-003.pdf>.

Varnes, D. J. (1978) 'Slope movements: types and processes', in Schuster, R. L. and Krizek, R. J. (eds) *Landslide analysis and control, National Academy of Sciences, Transportation Research Board Special Report*.

Walker, B. F., Blong, R. J. and MacGre, J. P. (1987) *Soil slope instability and stabilisation*. Balkema.

Zhou, Y. (2000) 'Research and treatment of Shazhou landslide, Sichuan. Landslides in research, theory and practice.', in Bromhead et al. (EDS) (ed.) *Proceeding of the 8th International Symposium on Landslides*. Cardiff, UK, pp. 1647–1652.

Chapter 3

Overview on masonry structures and modelling approaches

3.1 Introduction

The present Chapter 3 is devoted to a comprehensive overview on masonry structures and to a detailed review of the modelling approaches proposed for the analysis of masonry structures. As for the first scope, this topic represents an appropriate introduction in the spirit of the dissertation thesis, which aims to face the challenging question of the masonry structural behaviour investigation and assessment. Any type of research dealing with the masonry like material cannot overlook the preliminary knowledge of the mechanical behaviour and of historical events related to this old and mysterious construction material.

The current engineering and architectural scenarios are strongly dominated by the use of two main constructive strategy based on reinforced concrete and steel respectively. The high potentialities and benefits these materials have been showing during the last decades in terms of structural response and performance are far from the possibility to be disregarded. Nevertheless, it is worth noting that

masonry was the first material to be applied for the construction since the dawn of the civilization. As soon as the man had started to feel the necessity to create an inner space, different from the outside world, he immediately began to build by using masonry materials, launching a thousand-year history, i.e. the history of masonry structures. Age by age the quality of the constructions improved, first using very rough materials, such as stone available in-situ, and then reaching highly advanced construction techniques, thanks to the improvements in terms of masonry mechanical properties knowledge and novel technologies. In such a described timeline the potentialities of masonry like material allowed to build some of the greatest building pieces of art, which are still living against the relentless time elapsing.

As for the mechanical properties and behaviour, masonry can be regarded as a very hard to be described building materials. The first issue in the mechanical behaviour deals with the heterogeneity composition of this material, which is usually based on the collaboration between mortar joints and block units, with the exception of the dry-jointed masonry structures which are also widely spread within the history. No codes and standards were designed until recent years and the knowledge of the masonry construction were passed from one generation to the next, mainly based on the so-called rules of thumb. This is another important point to be considered in the comparison among the typical materials applied in the building construction. As for recent materials, such as steel and reinforced concrete, their application in the engineering and architectural fields goes hand-in-hand with the scientific investigations and the codes developments. In this case, the dual procedure allows to quickly improve the knowledge and the performance of the involved materials, also due to the overall high technological level reached in the last centuries. The same is not possible to be ascribed in the case of masonry, because the application of masonry for construction started a long time before the first standard recommendation was introduced.

The second part of this Chapter is dedicated to a comprehensive review of the modelling approaches developed in literature for the investigation of the structural behaviour of masonry structures. The study of masonry using numerical and analytical tools is a recent and still open field in the scientific

literature. Centuries-old approach to study and build masonry structures is represented by the trial-and-error method based on the rules-of-thumb to be passed from one generation to the next. This long tradition allowed to develop a highly powerful empirical procedure to study masonry structures, which seems to be not requiring for mathematical predictive models. In this framework, the first attempts to evolve the historical and empirical techniques into innovative numerical applications were not successful and considered to be refused by the scientific community. This point was even exacerbated by another important aspects: new materials coming on the engineering scenario (especially steel and reinforced concrete) produced a lack of confidence upon masonry structures, mainly based on the idea that the material was expensive, low ductile, low seismic resistant and too much dependent on the workman abilities and knowledges. The consequences of all these considerations are essentially a lack of resources to be spent in masonry research, the absence of useful and complete national and international codes and a widespread very low knowledge of the structural behaviour of masonry structures. Nevertheless, the consideration that most of built Cultural Heritage is masonry-made brings to the conclusion that masonry structures has been asking for numerical and mathematical procedure in order to protect them against any type of undesired loss. In this spirit, the last decades saw many advances in the design of computational strategies aiming at the study of masonry structures. As for other structural materials research field, the possibility to develop a reliable and accurate numerical model is mainly dependent on the best knowledge of mechanical properties of base materials, meaning the necessity to associate the numerical model with experimental tests to better understand the real behaviour of such a structure. Especially in the case of masonry structures, the investigation of the serviceability condition is a fundamental topic. Aside from failure analysis, also the serviceability limit states are worth to be studied with numerical analyses, e.g. crack control and prevention for restrained shrinkage and differential movements.

In this framework, advance numerical models for the structural behaviour prediction for the linear stage as well as for the collapse, moving through cracking and strength degradation, can be considered highly useful tool not only for researchers but in the everyone interests. The possibility to predict collapse

mechanisms for masonry types and structures will allow for design of retrofitting system to protect and save them. The topic is more than challenging because of the innate complexity of masonry like material which completely delete any chance to adopt existing numerical tool already tested and validated in other engineering structures field, e.g. reinforced concrete and composite materials (Lourenço, 1996).

3.2 Masonry structures: a thousand-year history

Although masonry represents the oldest building material, it is still widely used in today's building processes. It is worth noting that the strategy to collect the brick units and mortar layers have been never changed compared to the ones originally developed thousands of years ago, even if numerous developments in masonry materials and applications occurred in the last decades. In this framework, innumerable variations of masonry materials, techniques and applications occurred during the course of time, mainly induced and promoted by various factors such as local culture and wealth, the knowledge of materials and tools, the availability of material and architectural reasons.

The centuries-old success of masonry can be identified with its natural simplicity, which allowed to build even huge and monumental pieces of arts by simple assembling pieces of stone or bricks on top of each other, either with or without cohesion using mortar. Some other fundamental properties must be put in addition to the above mentioned in order to better clarify the reason of the long-time presence of masonry in the architectural and engineering field, which are essentially the aesthetics, solidity, durability and low maintenance, versatility, sound absorption and fire protection. There is possible to identify severe examples of constructions where the use of structural masonry usually represents a competitive and powerful solution. Among them it is worth citing loadbearing walls, infill panels to resist seismic and wind loads, prestressed masonry cores and low-rise buildings. Although this framework depicts the structural masonry as a very-highly competitive material for construction, the last decades have revealed that very few innovative applications of structural masonry were developed, mainly due to the fact that the design rules did not evolve with the

same highly fast trend compared with the developments for innovative and recent structural materials such as concrete and steel. The main reason for such a sudden lack of interest in masonry application is to be ascribed to the poor insight and to the hardness to manage models for the complex response of units, mortar, joints and masonry as a composite material. Existing calculation methods are mainly of empirical and traditional nature and the use of numerical tools for the analysis or design of masonry structures is rather incipient. As suggested in (Lourenço, 1996) also the education of architects and engineers currently is not adequate in this specific field. It is worth noting that most of graduations courses in structural engineering does not even mention (or only in a minimal percentage) the design and knowledge of structural masonry. In this case, the limits are represented by our lack of knowledge rather than in the masonry properties itself.

The story of masonry went on together with the one of the mankind, whose cultural evolution is commonly classified by the archaeologists according to the main used material: they are essentially the Stone, Bronze and Iron Ages. The further economic and social development allowed to reach the actual civilization together with the construction of towns and cities, wherein a part of the population could engage in trade, industry and professional pursuits. It is possible to state that the history of masonry as a building technique started together with the one of architecture, which dates back to about ten thousand years ago, with the earliest civilization. At the beginning, mankind tried to make savage attempts to be safe against the elements and from attack included seeking shelter in rock caves, developing strategies to build tents of bark, skins, turves or brushwood and huts of wattle-and-daub. Primitive houses of stone, clay or timber were born thanks to these efforts. The mankind evolution is thus linked to the history of architecture (Musgrove and Fletcher, 1987), and the history of building materials (Davey, 1961).

It is commonly accepted that the stone was the first applied masonry material especially in the ancient Near East, gaining the step-by-step evolution of housing from huts to apsidal houses and finally to rectangular houses.

Dry-stone huts, circular and semisubterranean dated back to about 9000-8000 b.C. are officially recognized as the earliest examples of the first permanent stone

masonry houses: they are located near Lake Hullen (Israel) and are characterized by overall diameter in the range between 3.00 and 9.00 metres. A huge number of other assemblages of stone masonry survived until present as testimonies of ancient and medieval cultures. Among them, the huge and monumental masonry construction in the Mesopotamia area (about 7000 b.C.), the Egyptian architecture with its pharaonic pyramids (about 2800-2000 b.C.), the Roman and Romanesque architecture (about 0-1200 a.C.) with its temples, palaces, arches, columns, churches, bridges and aqueducts, the Gothic architecture (about 1200-1600 a.C.) with its magnificent cathedrals and many others. The Gothic Age represents the time when the art of cutting stone reached its highest peak, allowing to build the monumental Gothic cathedrals as a skeleton of piers, buttresses, arches and ribbed vaulting. The walls enclosed, but did not support, the structure and, indeed, they consisted, mainly, of glazed windows.

The use of stone was associated to the one of mud brick as a masonry material from the beginning of this structural history. Ancient and populated areas was asking for building materials and they arrived at the development of the brick thanks to the abundance of clay, the hot dry climate and the shortage of timber and building stones that did not require cutting. It is possible to identify various reason for the use of brick as a building material. It is easy to produce, lighter than stone and easy to work and assembly. In addition, it is also fire resistant and durable. During all the Egyptian Age (5000 b.C. – 50 a.C.) the main material for building houses was sun dried brick, commonly of Nile mud. The pure Nile mud shrinks over 30% in the drying process but the addition of chopped straw and sand to the mud prevented the formation of cracks.

The reason for the use of mud brick stands in the first observation that the brick near a cooking fire seemed to be stronger and more durable. Such an innovation demanded for an adequate supply of fuel to make burnt bricks, which may have partially accounted for the continued use of sun-dried bricks in the Near East. The most famous reference is found in the Bible, Genesis XI, 3-4, when the inhabitants of Babylonia “said to one another ‘Come, let us make bricks and bake them’. They used brick for stone and bitumen for mortar. Then they said: ‘Let us build ourselves a city and tower with its top in the heavens’”. And they were able

to build probably the first ever skyscraper, which is the seventh level of the Tower of Babel characterized by a height of 90 metres. In the centuries between 900 and 600 b.C., the Babylonians developed a high-level expertise in burning brick, producing patterned bricks and wall tiles with polychrome glazes. Nevertheless, the wide spread of brick only developed in the Roman times, thanks to the conditions created by a large, strong and centralized Empire. There were many kinds of clayey materials suitable for making bricks and tiles readily available in all the areas of the Roman Empire and the desire to obtain domination and homogenization of architecture and building techniques made the rest. During the Roman time, size and shapes of bricks started to be more standardized according to specific purposes.

In this particular tale about masonry structures, an important role was played by the Industrial Revolution as described by (Elliot, 1992). The development of the industrial activity led to the condition that traditional handwork procedures were replaced by machinery. The crucial step of the brick industry came in 1858 with the introduction of the Hoffman kiln which made possible all the steps of firing to be carried out concurrently and continuously. Starting with this event, the research has been progressively improving till to the present day, when it is possible to find units of different materials and shapes, different types of mortar and different techniques. The present scenario in the field of masonry is represented by the coexistence of ancient and new, of tradition and novelty. Modern units of concrete, lightweight concrete with expanded clay aggregate, aerated concrete, calcium-silicate or polystyrene, currently exist together with the traditional brick units of mud or clay. Recent and revived techniques as grouted masonry, reinforced masonry, prestressed masonry, prefabricated masonry panels, mortarless masonry or masonry with very large blocks coexist with the oldest technique of putting small bricks on top of each other. Recent mortars with admixtures, cement mortars and (retarded) ready-mix mortars coexist with the ancient clay, gypsum, lime and bitumen mortar.

In the last decades, some developments and attempts to combine improved building tools with modern machinery-based techniques allowed to increase the job productivity as well as a reduction of costs. As a matter of fact, it is to be

observed that masonry-like material has been progressive losing its structural function, especially in developed countries, mainly replaced by more competitive structural materials, such as reinforced concrete and steel. In this framework, in most of European and North American countries, masonry is used nowadays primarily as a cladding system or infill non-loadbearing walls. Exceptions are loadbearing reinforced masonry in North America and structural masonry used in low-rise buildings. With regard to Developing and Third World countries in Latin America, Asia and Africa, the structural masonry is still widely used in the field of architecture and engineering. Thus, it is a commonly shared idea that the decline of masonry as a structural material is not only due to economic issues but even to a lack of adequate masonry codes and shortcoming knowledge masonry structures behaviour and structural response.

It is worth noting that, contrary to other structural materials, the design rules and codes for masonry structures appeared only in the XIX century, thousands of year later the first application of masonry materials in the field of construction. Unfortunately, stone has currently received a new role in the building industry, becoming a prohibitive choice since it represents a heavy and expensive material.



Figure 3.1 – Timeline of the thousand-year history of structural masonry.

3.3 Material

Historical masonry buildings have something unique compared to others structural type: masonry should be regarded as a structure itself and not as a building material, such as steel, wood or reinforced concrete. Contrary to the above-mentioned materials, masonry is something like a system composed by an assemblage of various elements and materials, whose properties can also change from point to point in the same wall. Members arrangement is the main cause of the difference between masonry and others building materials. There are several uncertainties in the masonry structure definition: among these brick disposition and mortar thickness play a fundamental role. A similarity between compression-stressed masonry and tensile-stressed texture always exists. The two of them are not part of the field of “material” since they are “structures” composed by a collection of constitutive members. In the case of texture, the behaviour changes depending on geometrical, elastic and mechanical properties of combined members, as for masonry material.

The above-mentioned considerations induce to reject the idea of masonry like an ideal, homogenous and isotropic material. Moreover, masonry cannot even be compared to other composite materials, such as reinforced concrete. The latter is supposed to show differences only in the constituents (steel and concrete) properties but not in their assemblage. Once defined the type of steel and concrete and the bars position, strength and deformation properties of a reinforced concrete are known. The same cannot be ascribed to a masonry wall where a great uncertainty affects the strength capacity even though mortar and brick properties and assemblage technique are already known.

Mechanical properties assessment for masonry like material is a very hard challenge. The main features of masonry from a mechanical point of view can be briefly described:

- dis-homogeneity
- anisotropy
- asymmetry
- non-linearity

Dis-homogeneity is caused by the built-in mechanical differences between mortar and bricks. The prediction of masonry mechanical characteristics is not an easy task even if the components properties are known because of the crucial role played by the contact interfaces between mortar and bricks along the joints. The interface mechanical behaviour is very hard to predict as it also depends on several chemical and physical phenomena which cause an overall behaviour so far to be depended on those of the constitutive members. Finally, the masonry macroscopic mechanical behaviour is something like the outcome of mortar-brick interaction through the interfaces.

Anisotropy property deals with the influence of stressed direction on masonry mechanical properties as a consequence of bricks shape and proportion and way-to-compose the assemblage. Nowadays, modern masonry has courses-allocated regular blocks with continuous bed joints and staggered head joints to provide a good connection in the wall plane.

Asymmetry is due to the mechanical behaviour of the single components, each one of them has different behaviour in tension and compression. Also in this case, the contact interfaces play an important since the tensile strength is very low in the contact zone between mortar and block. This is the reason why the masonry is often modelled like no-tension strength material.

Non-linearity is the feature of masonry constitutive models and can be commented as the outcome of the above-mentioned characteristics. Both tension and compression fields are affected by the non-linearity.

It is very complicated to involve all the described properties in the numerical application. It may be stated that it is even not convenient to do it because of the computational efficiency: a full analysis is deeply time-consuming and the quality of the results is not so far from the one of the results obtained with simplified method which neglect some of the described masonry properties.

Dis-homogeneity in masonry also produces a separation between macroscopic and local mechanic properties. It is worth noting that micro-modelling approach demands for a material description based on individual components tests whereas macro-modelling works with results obtained by test performed on quite large

specimens assuming homogenized stress and strain states. Nevertheless, macroscopic stresses and strains do not correspond to those of mortar and bricks.

In this framework, a comprehensive overview of the main macroscopic mechanic properties for masonry-like material is described below whereas the micro-modelling approach is out of the scopes of this dissertation thesis.

3.3.1 Uniaxial compressive behaviour

Masonry most relevant mechanical property is represented by the compressive strength normal to the bed joints. It can be ascribed that masonry structural performance mainly depends on good compression behaviour. The stacked bond prism is the test traditionally used to obtain the uniaxial compressive strength, but this type of test still present unknown consequences in masonry strength prediction (Mann and Betzler, 1994). In this type of test, a masonry prism is loaded in compression in the direction normal to the bed joints, exhibiting an average compressive tension $\sigma = P/A$ and an average strain $\varepsilon = \Delta h/h_0$, where P is the prism weight, A is the prism gross area, Δh is the prism shortening parallel to the load application and h_0 is the specimen starting length. The test result is represented by the curve in Figure 3.2 in terms of strain against compressive stress, where the masonry behaviour is quite intermediate between those of tests performed separately on mortar and bricks.

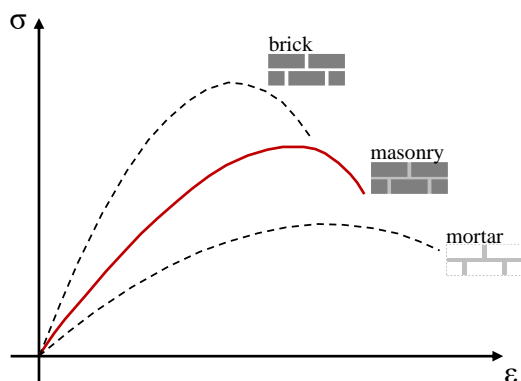


Figure 3.2 - Uniaxial compressive behaviour of masonry prism compared with those of mortar and brick.

Masonry compressive behaviour is affected by various causes. Among these, strength and strain and geometrical properties of bricks and mortar, joint thickness, brick capacity to absorb the water and mortar capacity to hold the water and brickwork geometry. The collapse in compression occurs with vertical cracks into the brick in the load direction due to the tension in the orthogonal direction caused by the co-action regime produced by mortar and brick different behaviour. Triaxial compression occurs in the mortar together with compression/biaxial tension in the blocks because of the uniaxial compression of masonry. Mortar triaxial confinement increased masonry compression strength compared with mortar uniaxial compression strength.

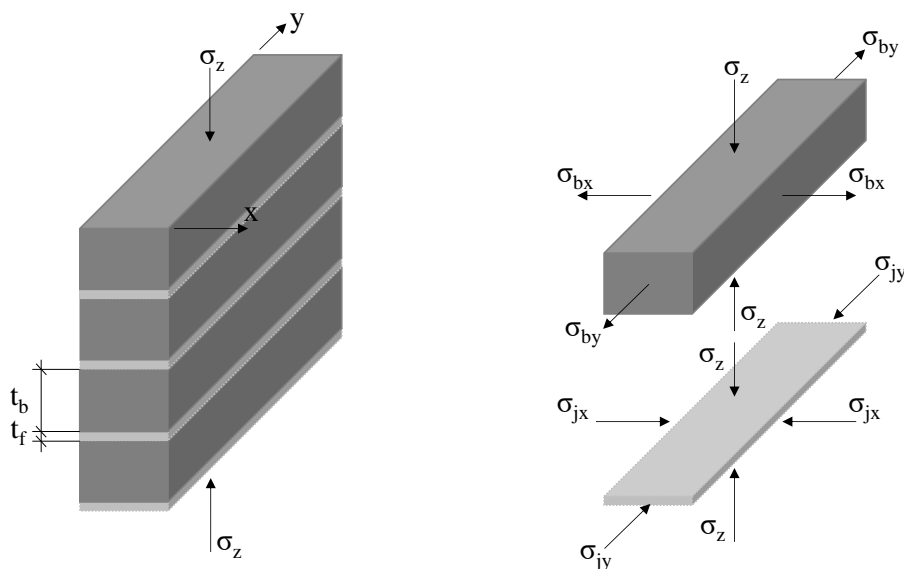


Figure 3.3 - Stacked bond prism model: stress state due to uniaxial compression.

Several methods were proposed to model masonry compressive behaviour. The elastic formulation (Francis, Horman and Jerrens, 1971; Tassios, 1988) assumes the stack bond prism model subjected to vertical compression under the assumption of linear elastic and isotropic mortar and units. Assuming Hooke principle, block and joints transversal deformations in x and y direction can be expressed:

$$\varepsilon_{bx} = \frac{1}{E_b} \cdot [\sigma_{bx} + \nu_b \cdot (\sigma_z - \sigma_{by})] \quad (3.1)$$

$$\varepsilon_{by} = \frac{1}{E_b} \cdot [\sigma_{by} + \nu_b \cdot (\sigma_z - \sigma_{bx})] \quad (3.2)$$

$$\varepsilon_{jx} = \frac{1}{E_j} \cdot [-\sigma_{jx} + \nu_j \cdot (\sigma_z - \sigma_{jy})] \quad (3.3)$$

$$\varepsilon_{jy} = \frac{1}{E_j} \cdot [-\sigma_{jy} + \nu_j \cdot (\sigma_z - \sigma_{jx})] \quad (3.4)$$

where:

- E_b and E_j are the Young modulus of blocks and joints respectively;
- ν_b and ν_j are the Poisson coefficient of blocks and joints respectively.

Congruence conditions guarantee the deformation equivalence between mortar and units whereas equilibrium conditions define the equivalence between mortar lateral compression and unit lateral tension. Naming α the joints to units thickness ratio, the following equations describe the equilibrium condition:

$$\sigma_{bx} = \alpha \cdot \sigma_{jx} \quad (3.5)$$

$$\sigma_{by} = \alpha \cdot \sigma_{jy} \quad (3.6)$$

Transversal tension stress in the units can be calculated as a function of vertical compression stress by the combination of equations from (3.1) to (3.6):

$$\sigma_{bx} = \sigma_{by} = \frac{\alpha \cdot (\nu_j - \beta \nu_b)}{1 + \alpha \beta - \nu_j - \alpha \beta \nu_b} \cdot \sigma_z \quad (3.7)$$

being β the joints to units Young modulus ratio. The value of the masonry compressive strength is obtained by assuming a linear relation between the transversal tensile stresses σ_{bx} , σ_{by} and vertical compressive stress σ_z :

$$f_u = \frac{1}{1 + \frac{\alpha \cdot (v_j - \beta v_b)}{\lambda(1 + \alpha\beta - v_j - \alpha\beta v_b)}} \cdot f_{bc} \quad (3.8)$$

being λ the block tension to compression strengths ratio.

The weakness of such a formulation is the assumption of linear elastic behaviour of masonry until the collapse. Other formulation tried to overcome this limit (Hilsdorf, 1969) assuming that masonry collapse occurs with a state of triaxial compression in the mortar and of compression/biaxial tension in the unit.

Important remarks turn out to be based on the previous formulation:

- masonry strength increases as the component strength grows in a non-proportional way;
- mortar quality is crucial to allow the masonry strength to increase as described in the previous point;
- masonry strength does not increase proportionally with mortar strength increase;
- the more joint thickness increases, the more masonry strength decreases, especially if the mortar quality is low.

3.3.2 Uniaxial tensile behaviour

Masonry tension behaviour is generally characterized by joint crack due to lack of cohesion at mortar-unit interface or to fracture in the joint thickness. Joint tension strength is in the range between 100% and few percentages of the mortar tension strength. Unit fracture can occur only in the case the mortar quality is high and unit strength is quite low. Tension strength is frequently neglected because of the big uncertainty. It's very hard to perform full tensile test so available experimental values were obtained by performing flexural-induced tensile test. There are two possible collapse modes in tensile test, depending on joints and units strength. The first one is characterized by zig-zag crack moving through head and bed joints. The second failure mode shows vertical cracks through units and head joints.



Figure 3.4 - Tension in the direction parallel to the bed joints: (a) failure occurs with a stepped crack through head and bed joints; (b) failure occurs vertically through head joints and units.

3.3.3 Biaxial behaviour

Anisotropy property caused the biaxial behaviour of masonry depends on the loading direction respect to the geometrical axes. When the stress state is located inside the wall average section, 2D-model can be applied to the stress state. In such a case, three parameters allow to fully describe the stress state, i.e. the principal stresses σ_1 and σ_2 and the rotation angle θ between the principal stresses and the material axes. Another possibility is to use the full stress vector (three components) in a fixed set of material axes, i.e. σ_n (perpendicular to bed joints), σ_p (parallel to bed joints) and τ (Figure 3.5). Experimental tests on masonry biaxial behaviour date back to Seventies and Eighties performed at the University of Newcastle in Australia (Page, 1982, 1983) and Edinburg in UK (Samarasinghe and Hendry, 1980).

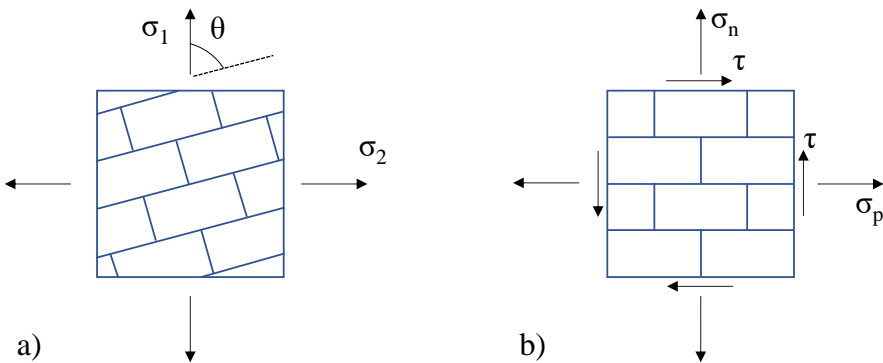


Figure 3.5 - Biaxial behaviour stress states: principal stress and rotation angle (a) and full stress vector (b).

The tests performed in Newcastle were carried out with half scale solid clay units. Failure mode and strength is highly affected by both the orientation of the principal stresses and the principal stress ratio. An overview of various modes of failure are illustrated in Figure 3.6.

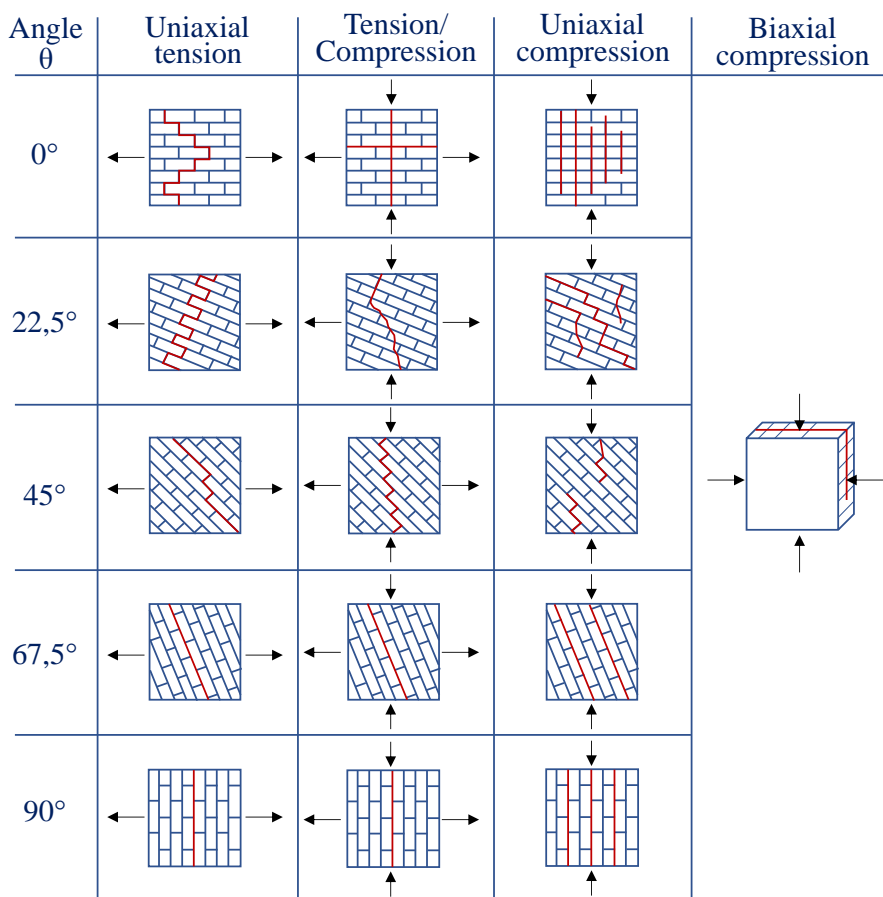


Figure 3.6 - Failure modes of solid clay units masonry under biaxial loading, (Dhanasekar, Page and Kleeman, 1985).

Shear and compression are also interesting stress state, especially in the case of walls subjected to lateral loads. Experimental tests showed three main failure modes for shear and compression (Mann and Muller, 1982):

-
- collapse inside the mortar joints, which occurs for very low value of σ_n ,
 - shear-tension collapse in the units, which occurs for intermediate value of σ_n ,

collapse due to masonry crushing, which occurs if the value of σ_n is very close to masonry uniaxial compression strength.

In the first failure mode, collapse occurs with zigzag cracks in the direction of both head and bed joints. Mortar joints are modelled with Coulomb friction criterion and the failure occurs when the bed joints achieve the condition below:

$$\tau_j = c + \mu \cdot \sigma_j \quad (3.9)$$

which includes the joint strength parameters (cohesion c and friction coefficient μ) and the joint local stresses σ_j and τ_j .

In the second case, the collapse occurs when the unit principal stress in tension reaches the mortar principal stress in tension. Finally, the third failure mode happens when the maximum stress in compression reaches masonry compressive strength f_u .

Mann and Muller assumed a masonry deformation mechanism to apply the macroscopic stress state at the local scale, under the assumption of mortar deformability so much greater compared to unit deformability. Such a mechanism brings to a different equilibrium equation against unit rotation, achieving different maximum and minimum normal compression stress in the bed joints. With this in mind, three failure condition describes the three failures mechanism above mentioned:

$$\tau = \bar{c} + \bar{\mu} \cdot \sigma_y \quad (3.10)$$

$$\tau = \frac{f_{bt}}{2.3} \cdot \sqrt{1 + \frac{\sigma_y}{f_{bt}}} \quad (3.11)$$

$$\tau = (f_u - \sigma_y) \cdot \frac{\Delta_x}{2 \cdot \Delta_y} \quad (3.12)$$

Equation (3.10) describes the first collapse mechanism for shear and compression, where:

$$\bar{c} = c \cdot \frac{1}{1 + \mu \cdot \frac{2 \cdot \Delta_y}{\Delta_x}} \quad (3.13)$$

$$\bar{\mu} = \mu \cdot \frac{1}{1 + \mu \cdot \frac{2 \cdot \Delta_y}{\Delta_x}} \quad (3.14)$$

Equation (3.11) describes the second collapse mechanism for shear and compression, where f_{bt} is the unit tensile strength.

Equation (3.12) describes the third collapse mechanism for shear and compression, where Δ_x and Δ_y are brick horizontal and vertical size respectively. The criteria above described assume zero-contribution of head joints to simulate a common condition for masonry structures with lower mortar filling in the head joints compared to bed joints. Figure 3.7 shows the collapse domain for a masonry panel subjected to shear and compression. Masonry shear deformability can be described by the shear modulus G . Very few experimental data are available on shear deformability. The shear modulus is usually associated to the Young modulus E in the direction of the head joints. A common value used is $G = 0,3 \div 0,4 \cdot E$.

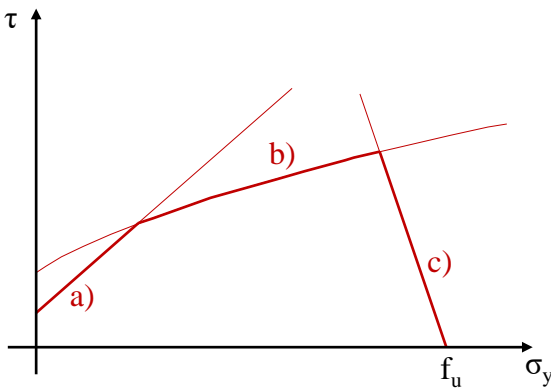


Figure 3.7 - Failure domain for a masonry panel subjected to shear (Dhanasekar, Page and Kleeman, 1985).

It is worth noting that the present Chapter aims to a material description suitable for the development of a macro-modelling approach, as in the purposes of this doctoral program. Therefore, the contents of these sections cannot be regarded as a complete description of masonry like material, which is pursued in (Hendry, 1990; Drysdale, Hamid and Baker, 1994).

The next section opens to the second topic discussed in the present Chapter, dealing with some preliminary observations for the correct classification of the several numerical solutions proposed in the last decades in literature to investigate the behaviour of masonry structures. This introductory digression is crucial to the best comprehension because the threshold between classes could be very thin, so it is important to deeply assimilate the types and the weights of the numerous factors to be accounted for the classification aiming to depict a full and comprehensive framework.

3.4 Preliminary observation to modelling approaches

The operation for a classification of the numerical procedures and solutions several authors proposed for the simulation, prediction and investigation of masonry types or structures still represents a difficult task for anybody. It is somewhat clear that the reason of this innate complexity relies in the further innate complexity of the material in question, i.e. the masonry, which is a very hard-to-analyse structural material in its nature. The previous sections dealt with the masonry-like material, showing the hardness to clearly describe its mechanical properties and behaviour. As a matter of fact, the effort to experimentally calculate the mechanical properties of masonry turns out on the simulation and implementation of the same parameters in numerical tools, especially in the case of in-house computational proposal, which is most of the cases. A large part of the issues in masonry mechanical characterization derived by the composite nature of this material, which is the result of the collaboration between two base components, the blocks (or units) and the mortar joints. Blocks are generally composed of quasi-brittle materials as stones or bricks and they are collected to create a specific bond-pattern with a very large number of possible solutions, depending on the used material, the time of construction etc. As largely

described above, both masonry components can be described as quasi-fragile materials both in tension and compression. The compression strength is highly larger than tension strength. The difference is so large that many numerical strategies even neglect the tension capacity, assuming a zero-tensile strength masonry model. Apart from this, the mechanical capacity of masonry structures is highly dependent on the block-to-mortar collaboration, but the interface between blocks and joints is typically very weak, characterized by a softening cohesive-frictional behaviour in shear and tension. It seems to be clear that the masonry global response is highly non-linear.

Masonry mechanical behaviour can be identified in terms of stiffness, strength and ductility according to the scale of material (Page, 1981, 1982, 1983) and the scale of structure (Magenes and Calvi, 1997; Calderini, Cattari and Lagomarsino, 2009; Beyer, 2012; Petry and Beyer, 2014; Messali and Rots, 2018). The level in the scale of material refers to the level of experimental characterization of masonry mechanical properties. The major difficulties are related to the study of existing buildings, especially in the case of historical protected masonry buildings where invasive in-situ testing are not allowed. With regard to the scale of structural elements, it is worth noting how the structural details influence the global mechanic behaviour. The most important structural details refer to the well-made connections between orthogonal walls and between walls and horizontal diaphragms, the in-plane stiffness of horizontal diaphragms and the quality of interaction with near buildings. In the case of historical existing buildings, the possibility to know the structural details is even more complicated because it is required to study all the story life of the building, with the several restoration designs, the changes in destination or spatial distribution, the damage suffered and the related reparations. This framework allows to understand how a specific survey campaign is required in the case of existing buildings, not only for the structural details investigation but also to better define the masonry structure geometry in historical buildings where the geometries are typically irregular and complex. In such a case, the first problem is the identification of the load-bearing system according to the observed geometry, an operation where a high expertise level is required. The structure identification issue is then associated with the geometry-to-structure compatibility issue, i.e. firstly a

software compatibility issue. The latter refers to the typical habit to model the geometry of a specific case study by using CAD software to be imported in structural analysis tool. Such an operation can create several problems of compatibility, especially for the mesh generation. The solutions to overcome this issue represents a still open and challenging task in literature (Castellazzi *et al.*, 2015, 2017; Korumaz *et al.*, 2017; Chiozzi, Grillanda, *et al.*, 2018; D’Altri *et al.*, 2018).

The numerical methods classification for masonry structure also required a description of the possible analysis approaches implemented in the numerical procedures. This means that the difference between two close numerical formulations sometimes relies in the adopted analysis approach. To this aim, in the field of masonry structure, there are essentially two families of analysis methods, namely incremental-iterative analysis and limit analysis. The first group, the incremental-iterative analysis represents the more complete methods where the structural behaviour investigation is going on with a step-by-step procedure, meaning the possibility to apply the loading conditions following a specific loading protocol, with a specific load increment per each step. The structural response is evaluated step-by-step as well. Such an analyses approach is so full to be able to consider also the non-linear mechanical and geometrical behaviour of masonry allowing to best predict the collapse capacity of the specific case study. In order to better evaluate the collapse response of the structure, some numerical formulations also include computational procedure for the analysis in the large displacement regime. According to the strategy adopted for the application and the evaluation of the loading conditions, the incremental-iterative solutions can be further grouped in non-linear static and non-linear dynamic time history analyses.

- Non-linear static analysis consists of a step-by-step load application including the maximum load and the post-peak softening loading step. There is any time consideration and both load and displacement control formulations can be assumed (Rots, Belletti and Invernizzi, 2008; DeJong *et al.*, 2009). The numerical problem is generally represented by a non-linear differential equations system. In most of the case, the non-linear

problem is solved by dividing the overall problem in linear steps introducing an iterative procedure. Several iteration procedures were proposed in literature, among them the Picard iteration method, the Newton-Raphson iteration methods and the Riks methods (Reddy, 2004) are widely adopted in proposed iterative formulations. The main scope of these iterative numerical procedures is represented by the as-known pushover analysis, which is a powerful and validated procedure for the assessment of seismic performance of masonry structures. The pushover analysis field will be deeply described in the next Chapter. For the time being, the thesis only reports that the basic assumptions of this method consist of the application of a horizontal forces load pattern, following the increasing displacement of a control node generally located at the top of the structure.

- With reference to the time history analysis, once again the method assumes a step-by-step incremental procedure, but the structural response is time-affected in terms of both inertial and damping effects. This means that non-linear dynamic analysis demands for the integration of differential time-dependent equations of motion. Several methods were developed in literature to approximate these highly hard to be solved equations, which are essentially grouped into explicit or implicit methods (Clough and Penzien, 2003). In the case of explicit method, the singular step structural response of the investigated model is function of the response resulting in the previous, while the explicit methods do not work with this step-to-step dependency, but values obtained in one step only concern with that specific step, assuming a trial starting value to be refined via iterative procedure. Several time integrations methods were proposed in literature, the most famous of them being the Euler-Gauss methods, Newmark Beta methods, second central difference procedure and linear acceleration methods (Clough and Penzien, 2003). It seems clear that this analysis group is very powerful because it is able to account for dynamic actions applied to masonry structures, allowing to implement really recorded accelerograms in the case of seismic response analysis.

The tradition of limit analysis formulation was born thanks to the pioneering work developed in (Heyman, 1966), where the classical theorem of limit analysis, namely the kinematic (or upper bound) and the static (or lower bound) theorems (Chiozzi, Milani and Tralli, 2017; Marmo and Rosati, 2017), was applied to masonry structures for the first time. The modelling theory proposed (Heyman, 1966) was based on three famous assumptions about the masonry mechanical behaviour:

1. Zero-tensile strength
2. Infinite compressive strength
3. Sliding failure condition cannot occur

The three basic assumptions of the Heyman's theory introduced a rigid no-tension model which was widely used in the following decades, especially in the case of masonry types stability analyses (M. Angelillo, 2014) by using graphic static solutions (Huerta, 2001) or kinematic chains approach for the failure modes calculation of masonry buildings (Giuffrè and Carrocci, 1993). Moving from these very simple modelling assumptions, many numerical tools and procedure were proposed in literature, some of them using the static theorem, others the kinematic one. These computational proposals usually express the numerical problem in terms of solution of an optimization mathematic programming problem (based on linear or non-linear programming). Aside the above-mentioned potentialities, it should be admitted that the numerical formulations based on limit analysis theorems are limited in terms of outcomes. Indeed, the only outcome of these models is represented by the failure modes and the value of the load factor promoting collapse. In this framework, the thesis aims to overcome this issue providing an example of the so-called non-linear kinematic analysis, a numerical procedure where it is possible to investigate also the displacement capacity of the masonry structures as well as the elastic and plastic post-peak behaviour. A comprehensive description of the latter will be provided with the Chapter 4.

3.5 Modelling approaches for masonry structures

The present Chapter aims to provide a review of the developed modelling methods for masonry structural behaviour investigation and prediction. In the last half-century, the scientific community devoted a consistent effort to the computational analysis of masonry structures, producing a huge number of numerical solutions and proposal that are very hard to be grouped in class characterized by common features. With the scope to make order in such a confuse computational framework, in this section the several approaches presented in scientific literature will be classified according to the level of accuracy in the description of masonry composite nature (Lourenço, 1996) and the modelling strategy (Roca *et al.*, 2010; D’Altri *et al.*, 2020). Then, an entire section is dedicated to just one modelling formulation, which is the rigid block limit analysis approach since it is the framework for the modelling proposals described in the next Chapter of this doctoral program.

As already stated in the introduction, the thesis aims at the assessment of masonry structures especially in the case of structures subjected to settlement-induced ground movements. Nevertheless, the modelling approaches and strategies reported later in the text do not refer only to numerical formulations specifically developed for the performance investigation of masonry buildings and types under settlement actions, but it can be regarded as an overall description of numerical and analytical solutions for the analysis of masonry structures against all possible loading and boundary conditions. As a matter of fact, most of the computational tools were particularly devoted to the seismic response investigation of masonry structures, being the seismic engineering a research field examined much more in depth in literature compared to the settlement vulnerability.

3.5.1 Classification according to masonry model

Modelling approaches devoted to the investigation of masonry structures can be classified according to the adopted assumptions for the description of the individual components (brick, joints etc.) properties. Based on the accuracy or

simplicity levels, the masonry structure performance under lateral seismic load or settlement-induced ground movements is currently assessed according to three modelling approaches at least (Lourenço, 1996; Gagliardo *et al.*, 2019). The differences between these approaches are ascribed to the interpretation of the complex behaviour of masonry, which exhibits variable mechanical properties according to the considered direction mainly due to weakness located at the mortar joint layers.

The most complex approach is a “detailed micro-model” (Figure 3.8a): this approach, particularly suitable for the finite element analysis, considers the separation between the mortar and bricks and requires two different constitutive laws. This means that Young modulus, Poisson ratio and inelastic properties of both mortar and units must be considered. In such a model, contact surfaces are potential crack or slip planes. It is closer to the real masonry behaviour but has the disadvantage of the slowness of calculation (D’Altri, Castellazzi and de Miranda, 2018; Sarhosis and Lemos, 2018). The “simplified micro-modelling” approach (Figure 3.8b) represents a good alternative where the mortar contribution is neglected, and the contact interfaces play an essential role in the failure modes definition. In this approach, the joint is changed in its morphology assuming the form of an average interface where the units are expanded to avoid any geometrical changes in the model. It can be said that such a formulation assumes elastic blocks and potential crack or slip lines along the joints. It is worth noting that this strategy is not highly accurate since the Poisson effect of mortar is neglected. This approach perfectly commits to the rigid block model analysis (Angelillo *et al.*, 2018). Both micro-modelling approaches work well in the case of small structural elements where stress and strain heterogeneity can be deeply investigated. The main scope of these kind of formulations is to study masonry properties with regard to the single constituent and interface. Finally, the “macro-modelling” approach (Figure 3.8c) does not consider the real masonry texture but makes use of homogenization criteria for the material, considering average properties (Marques and Lourenço, 2011; Pantò, Calì and Lourenço, 2018). In such a case, masonry material is represented by an anisotropic composite and a correlation between average stresses and strains is introduced.

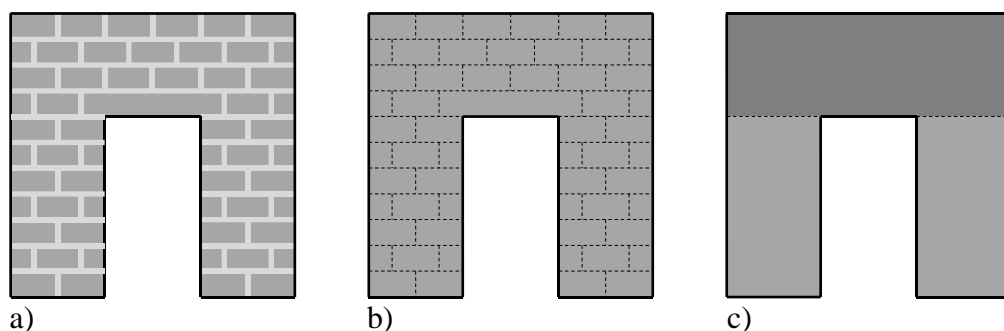


Figure 3.8 - Modelling approaches for masonry structures: a) detailed micro-modelling; b) simplified micro-modelling; c) macro-modelling. (Gagliardo *et al.*, 2019).

It is not possible to say which is the best strategies a-priori, because the choice of the most useful approach strictly depends on the field of application or the analysed case study. Both micro-modelling approaches are particularly suitable to investigate local behaviour of masonry structures, so they are to be preferred in the case of structural details applications or when the study involves walls or members with very few blocks or units. On the other hand, macro-models represent the adequate choice in the case of big structures made by solid walls provided with large dimensions to assume a uniform value for stresses across or along the length. Aside the mentioned differences, both models require a preliminary experimental investigation of involved materials. Nevertheless, their utility in the research field is now generally acknowledged as a powerful tool to be associated with the historical and empirical tradition of rules-of-thumb (Lourenço, 1996).

3.5.2 Classification according to modelling strategy

In this section, the existing modelling approaches are grouped according to the adopted strategy for the analysis of masonry structures behaviour/capacity. The contents showed in this section refers to the classification developed in (D’Altri *et al.*, 2020), as illustrated in Figure 3.9.

The formulations here described represent a comprehensive framework of all the possible modelling solution to be applied in the case of masonry structures,

without a unique reference to the type of investigated action or phenomenon. In such a case, it can be stated that most of them can be sufficiently applied to both seismic-induced lateral load case and settlement-activated foundation displacement. It is worth noting that the main scope of the present dissertation deals with the analysis of masonry structures subjected to ground movements or spreading supports. In this framework, this chapter also describes some numerical models specifically proposed with regard to the analysis of masonry panel and types when they are affected by settlement and foundation displacements. Among them, the Limiting Tensile Strain Method (LTSM) and the Load Path Method (LPM), which is part of the overall Strut-and-Tie Model (STM), are very powerful tools as described later in the Chapter.

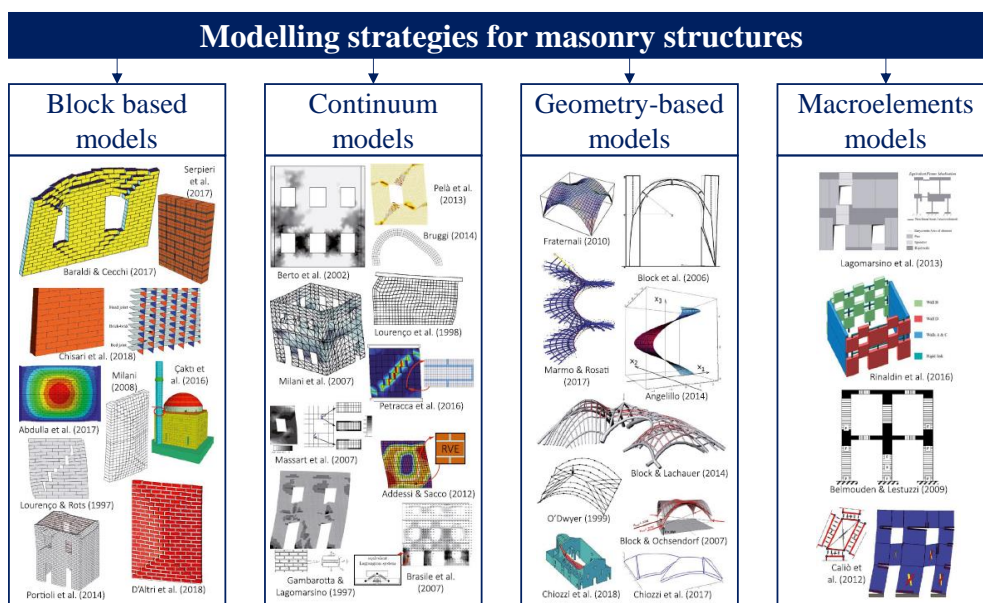


Figure 3.9 - Modelling strategies for masonry structures according to (D'Altri et al., 2020).

According to the adopted strategies, both numerical and analytical models for the capacity investigation of masonry structures can be identified. As for the numerical strategies four groups can be classified according to (D'Altri et al., 2020), that are essentially block-based models, continuum models, geometry

based models and macro elements models. The analytical formulations include models based on closed-form solution for the analysis of specific masonry types.

3.5.2.1 Numerical approaches

In this section a substantial review of the existing numerical approaches for masonry structures is developed, inspired to the classification already proposed in (D’Altri *et al.*, 2020). The last decades have been dominating by this kind of modelling strategy, which showed very high potentialities especially in the application to large and complicated structures, where analytical approach are usually not feasible at all. Both Finite element modelling (FEM) and Discrete element modelling (DEM) are variously applied in this field with the scope to investigate the structural capacity and response of building composed by a so hard and heterogenous material like masonry.

3.5.2.1.1 Block-based models

The strategy which allows to reach the most detailed outcome is represented by block-based models, where masonry is represented by a block-to-block bond pattern with the possibility to model the real texture. Both rigid or deformable block behaviour can be assumed, and different solutions were proposed to model the blocks interaction. This type of strategy exhibited high abilities in several studies presented in literature where the structural behaviour of full-scale masonry structures was investigated also in the case of challenging geometries and irregular bond pattern. Nevertheless, a limitation to be admitted for block-based models is represented by the high computational demand that makes such a numerical formulation not so suitable in the case of huge, monumental buildings. Considering this observation, the first identified strategy is very powerful for the investigation of specific mechanical features of masonry types allowing to obtain a starting solution for comparison with more simple models.

According to (D’Altri *et al.*, 2020), block-based models potentialities are represented by the next described aspects:

- the possibility to model the actual masonry bond pattern and the overall details of the case studies.

-
- mechanical properties derived by small-scale experimental tests.
 - the aptitude to collapse mechanisms analysis finalized to the identification of weaknesses of the studied model in order to better design strengthening measures.
 - masonry anisotropic behaviour is automatically involved and is not required to be modelled.
 - capability to analyse both in-plane and out-of-plane behaviour of masonry structures through 3D and 2D simple models.
 - also the wall-to-wall reaction transfer for 3D structural models is automatically involved further reducing the model weight.

On the other hand, block-based models also showed some limitations. Among them, it is worth citing the following:

- the huge computational demand can limit the field of applications only to the scale of panel structure, but it is possible to pass this issue in the near future thanks to the improvement of computational facilities.
- the strategy is not able to analyse 2D membrane models as scientific literature proved in the last decades.
- it is very complex to reproduce the real bond pattern in historical masonry case studies and the discretization needs to be approximated.
- the blocks collection is a time-consuming procedure.

According to (D'Altri *et al.*, 2020), block-based models can be grouped in different subcategories based on blocks interaction, that are essentially: interface element-based method (Rots, 1991, 1997; Lotfi and Shing, 1994; Lourenço and Rots, 1997; Gambarotta and Lagomarsino, 1997b; Casolo, 2000; Formica, Sansalone and Casciaro, 2002; Oliveira and Lourenço, 2004; Alfano and Sacco, 2006; Parrinello, Failla and Borino, 2009; Senthivel and Lourenço, 2009; Macorini and Izzuddin, 2011; Aref and Dolatshahi, 2013; Chisari *et al.*, 2015, 2018; Zhang, Macorini and Izzuddin, 2016; Dolatshahi and Aref, 2016; Calderón, Sandoval and Arnau, 2017; Wilding, Dolatshahi and Beyer, 2017; Malomo, Pinho and Penna, 2018; Minga, Macorini and Izzuddin, 2018; Dolatshahi, Nikoukalam and Beyer, 2018), contact-based method (Cundall and Strack, 1979; Cundall, 1980; Moreau, 1988; Shi, 1992; Jean, 1999; Thavalingam

et al., 2001; Papantonopoulos *et al.*, 2002; Munjiza, 2004; Lemos, 2007; Rafiee, Vinches and Bohatier, 2008; Tóth, Orbán and Bagi, 2009; Rafiee and Vinches, 2013; Smoljanović, Živaljić and Nikolić, 2013; Kuang and Yuen, 2013; Sarhosis and Sheng, 2014; Smoljanović, Nikolić and Živaljić, 2015; Çaktı *et al.*, 2016; Sarhosis, Lemos and Milani, 2016; Simon and Bagi, 2016; Lancioni *et al.*, 2016; Beatini, Royer-Carfagni and Tasora, 2017; Bui *et al.*, 2017; Lengyel, 2017; Miglietta, Bentz and Grasselli, 2017; Forgács, Sarhosis and Bagi, 2017; Sarhosis and Lemos, 2018; Smoljanović *et al.*, 2018; Foti, Vacca and Facchini, 2018), textured continuum-based method (Ali and Page, 1988; Petracca, Pelà, Rossi, Zaghi, *et al.*, 2017; Serpieri, Albarella and Sacco, 2017) and extended finite element method (Abdulla, Cunningham and Gillie, 2017; Zhai *et al.*, 2017). It is worth noting that the classification developed in (D’Altri *et al.*, 2020) also accounts for limit analysis approaches in the group of block-based models. In the present thesis, this class is not described yet since a specific section is devoted to rigid block limit analysis formulation later in this Chapter.

3.5.2.1.2 Continuum models

The field of masonry structural analysis using numerical tool is dominated by continuum models strategy. Scientific literature is teeming with several works on the topic of concerning direct approaches, isotropic crack and damage plasticity mechanical behaviour, especially in the field of assessment of historic masonry structures, where they are usually the only suitable method which allows to obtain relevant results. Nevertheless, the obtained outcomes need to be carefully investigated because continuum models tend to severely overestimate the displacement capacity especially against structural collapse. In this modelling categories both simplified homogenized FE limit analysis and homogenized discrete approaches represent powerful tools for the structural assessment of full-scale masonry structures. Another type of solution in the field of continuum models is represented by multi-scale approaches. Nevertheless, in most of the case they are devoted only to the analysis of 2D masonry structures. Another limitation is represented by the in-house nature of most of numerical codes, meaning few possibilities to be improved. 3D computational homogenization methods still not exist in scientific literature at all and the possibility to represent

in detail the structural configurations seems to be limited because these formulations usually assumes refined modelling strategies of a representative volume element (RVE) of the structure.

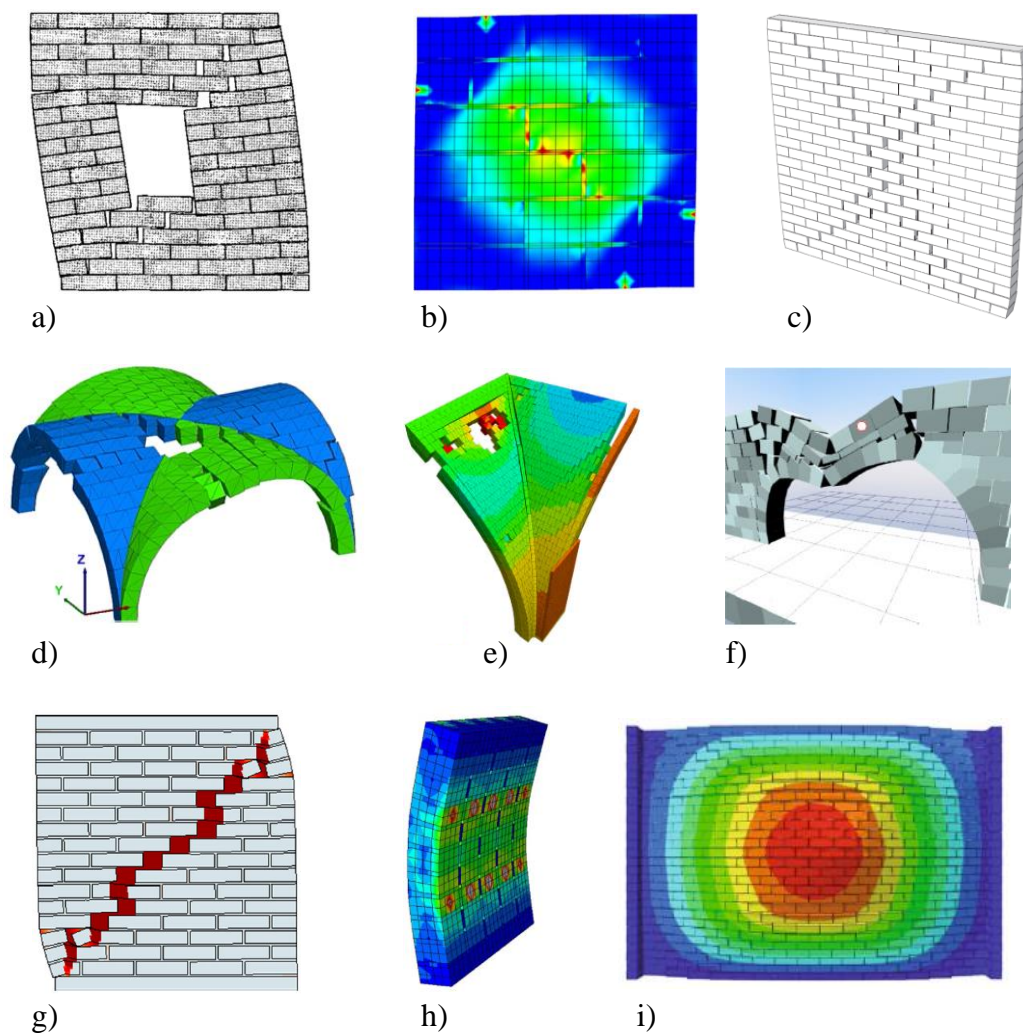


Figure 3.10 - Examples of block-based model: (a) (Lourenço and Rots, 1997); (b) (Sandoval and Arnau, 2017); (c) (Minga, Macorini and Izzuddin, 2018); (d) (Foti, Vacca and Facchini, 2018); (e) (Lengyel, 2017); (f) (Beatini, Royer-Carfagni and Tasora, 2017); (g) (Petracca, Pelà, Rossi, Zaghi, *et al.*, 2017); (h) (Serpieri, Albarella and Sacco, 2017); (i) (Abdulla, Cunningham and Gillie, 2017).

Continuum models look at masonry like a unique deformable body. This assumption helps in the mesh discretization because masonry heterogeneities are neglected and do not need to be modelled. This means a reduction in computational demands compared to the CPU effort required by other modelling categories such as block-based method. How to define the homogeneous constitutive model in order to simplify the mechanical complexities of masonry like material does not present only one answer in literature.

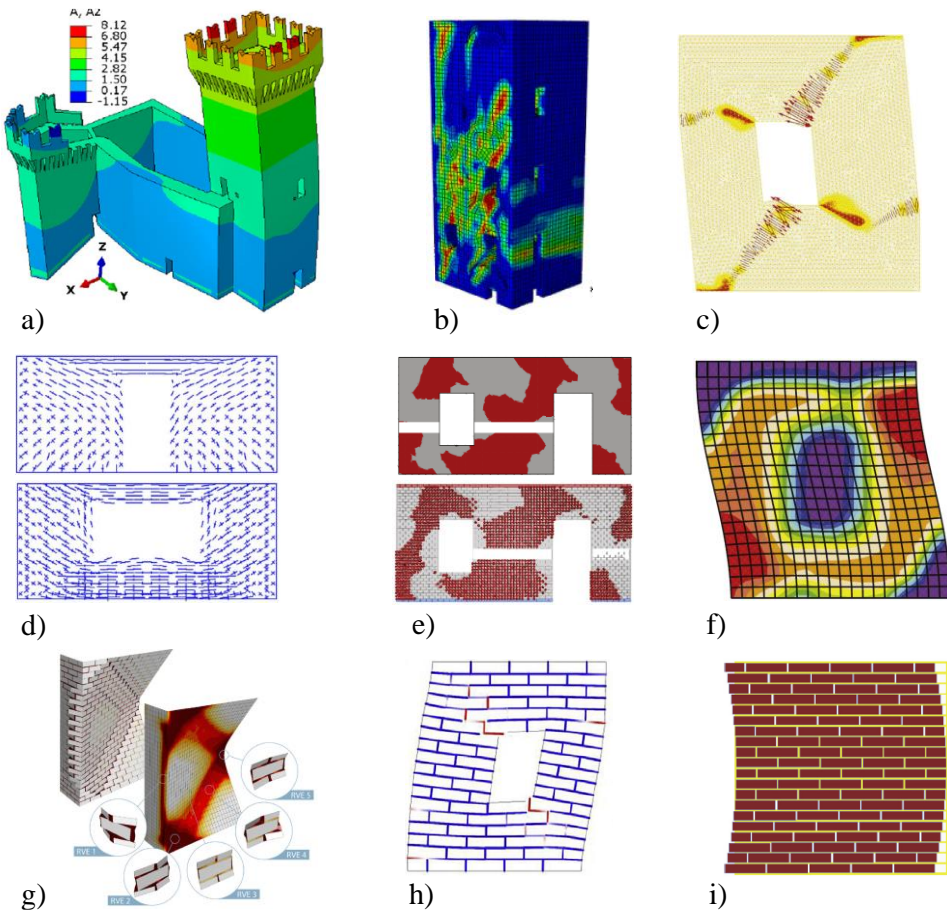


Figure 3.11 - Examples of continuum model: (a) (D’Altri, Castellazzi and de Miranda, 2018); (b) (Valente and Milani, 2016); (c) (Pelà, Cervera and Roca, 2013); (d) (Milani, P. B. Lourenço and Tralli, 2006a); (e) (Godio *et al.*, 2017); (f) (Addessi and Sacco, 2012); (g) (Petracca, Pelà, Rossi, Oller, *et al.*, 2017); (h) (Leonetti *et al.*, 2018); (i) (Brasile, Casciaro and Formica, 2007b).

According to the solution against this challenge, continuum models can be subdivided into two main families, namely 1) direct approaches and 2) homogenization procedures and multi scale approaches. In the case of direct approaches, the mechanical constitutive model is derived by experimental tests as described in (Heyman, 1966; Del Piero, 1989; Maier and Nappi, 1990; Lotfi and Shing, 1991; Angelillo, 1994; Lourenço, De Borst and Rots, 1997; Lourenço, Rots and Blaauwendraad, 1998; Lopez *et al.*, 1999; Alfano, Rosati and Valoroso, 2000; Cuomo and Ventura, 2000; Lucchesi, Padovani and Pasquinelli, 2000; Berto *et al.*, 2002; Pelà, Aprile and Benedetti, 2009; Reyes *et al.*, 2009; Pelà, Cervera and Roca, 2011, 2013; Betti and Vignoli, 2011; Milani *et al.*, 2012; Betti and Galano, 2012; M. Angelillo, 2014; Pelà *et al.*, 2014; Bruggi, 2014; Milani and Valente, 2015; Saloustros, Pelà and Cervera, 2015; Toti, Gattulli and Sacco, 2015; Zampieri, Zanini and Modena, 2015; Bruggi and Taliercio, 2015, 2018; Bartoli, Betti and Vignoli, 2016; Pantò *et al.*, 2016; Rots *et al.*, 2016; Tiberti, Acito and Milani, 2016; Valente and Milani, 2016; Castellazzi *et al.*, 2018; Elyamani *et al.*, 2017; Fortunato, Funari and Lonetti, 2017; Castellazzi *et al.*, 2017; D’Altri, Castellazzi and de Miranda, 2018; Pantò, Caliò and Lourenço, 2018; Saloustros *et al.*, 2018; Degli Abbatì *et al.*, 2019). The second group assumes that the mechanical behaviour is modelled by means a homogenization process dealing with both material and structural properties. It is possible to find a huge number of continuum numerical proposals based on homogenization procedures and multi-scale approach (Sacco, Addessi and Sab, 2018), but all of them can be grouped in three main families: a-priori homogenization methods (Pietruszczak and Niu, 1992; Anthoine, 1995; Masiani and Trovalusci, 1996; De Buhan and De Felice, 1997; Briccoli Bati, Ranocchiali and Rovero, 1999; Cecchi and Sab, 2009; Zucchini and Lourenço, 2002, 2004; Cecchi and Sab, 2002, 2007; Casolo, 2004; Cecchi, Milani and Tralli, 2005, 2007; Milani, P. B. Lourenço and Tralli, 2006a, 2006b; Milani, P. Lourenço and Tralli, 2006; Milani, Lourenço and Tralli, 2007; Mistler, Anthoine and Butenweg, 2007; Casolo and Peña, 2007; Kawa, Pietruszczak and Shieh-Beygi, 2008; Stefanou, Sulem and Vardoulakis, 2008; Cecchi and Milani, 2008; Wei and Hao, 2009; Milani, 2011; Cavalagli, Cluni and Gusella, 2011, 2013; Taliercio, 2014; Drougkas, Roca and Molins, 2015; Stefanou, Sab and Heck, 2015; Godio *et al.*, 2017; Silva, Lourenço and

Milani, 2017; Bertolesi, Milani and Casolo, 2018), step-by-step multi-scale methods (Papa, 1996; Gambarotta and Lagomarsino, 1997b, 1997a; Luciano and Sacco, 1997, 1998; Pietruszczak and Ushaksaraei, 2003; Calderini and Lagomarsino, 2006; Casolo, 2006; Massart, Peerlings and Geers, 2007; Brasile, Casciaro and Formica, 2007b, 2007a; Sacco, 2009; Salerno and de Felice, 2009; Zucchini and Lourenço, 2009; Addessi, Sacco and Paolone, 2010; Bacigalupo and Gambarotta, 2010, 2012; Mercatoris and Massart, 2011; de Bellis and Addessi, 2011; Addessi and Sacco, 2012; Marfia and Sacco, 2012; Addessi *et al.*, 2014; Petracca *et al.*, 2016; Petracca, Pelà, Rossi, Oller, *et al.*, 2017) and adaptive multi-scale methods (Brasile, Casciaro and Formica, 2007b; Lloberas-Valls *et al.*, 2012; Greco *et al.*, 2016; Leonetti *et al.*, 2018; Reccia *et al.*, 2018).

3.5.2.1.3 Macro-element models

In this section, the group of macro-element models is discussed in detailed, being this kind of formulation widely spread in literature thanks to their user-friendly features which makes them very suitable especially in the assessment of masonry buildings against seismic actions. On the other hand, the large approximation adopted by these models cause the risk to test their reliability in the prediction of the in-plane and out-of-plane mechanisms as well as the interaction of the two of them. The possibility to overcome this method limitations relies in ad-hoc designed experimental campaign.

The basic idea of these models is that the overall structure can be assumed as a sequence of panel-scale components which are essentially piers and spandrels. As a matter of fact, macro-element models are mainly devoted to the analysis of seismic global performance of masonry buildings. In this framework, the main limitations of this family are the lack of results in terms of local damage and failure modes and the complexity to extend the formulation to other type of structural investigation (e.g. masonry structures subjected to settlement or spreading supports). In this direction, one of the assumptions of macro-element methods is that no-local failure mode (e.g. overturning, horizontal flexural mode etc.) can occur. In such a model, the global structural capacity against settlement-induced lateral loads is governed by the panels in-plane performance and the well-designed rigid floor diaphragms. The global analysis here discussed

generally rely on incremental iterative static and dynamic formulation, especially in the case of 3D case studies, using the possibility to directly account for walls interaction in terms of load transfer.

The basic structural components involved in micro-element methods must be a priori identified in a previous step of the numerical procedure by in-situ observations of real buildings. Such a preliminary survey step helps to understand where the cracks are mainly located in both piers and spandrels. From a typological point of view, piers and spandrels can be immediately described, at least in the case of regular ordinary masonry structures (Dolce, 1991; Augenti, 2006; Moon *et al.*, 2006; Lagomarsino *et al.*, 2013, 2018; Parisi and Augenti, 2013; Parisi *et al.*, 2013; Calderoni *et al.*, 2015; Berti *et al.*, 2017; Quagliarini, Maracchini and Clementi, 2017): the term “pier” refers to vertical resisting elements with a specific capacity against both vertical and horizontal loads. Spandrel definition is then applied to the horizontal resisting elements in the structure which works to distribute the horizontal load among the various piers with regard to a specific building level. The same definitions cannot be correctly applied to the case of irregular masonry structures, with misaligned openings along vertical and horizontal direction that is the case of most of the observed historic masonry structures. As already mentioned in this section, the macro-element modelling is largely used in literature thanks to the quite-low computational demand and the speed in mechanical property characterization. On the other hand, it should be remembered that this modelling strategy is based on very simple and approximated assumptions for the definition of masonry behaviour investigation. The assumption to a-priori neglect the onset of any local out-of-plane collapse mechanism may represent an issue in the failure modes analysis of masonry structures, leading to wrong results and to overestimation of the global seismic capacity of the analysed model (Dolatshahi and Yekrangnia, 2015). Another drawback of this strategy is related to the issue of modelling the structural details of masonry structures, e.g. the connection between the orthogonal panels. Moreover, to be forced to identify each element in only two categories (spandrel or pier) can lead to define mechanical systems not coherent with the real one. The presence of all these drawbacks means the demand for a high expertise level in the field of macro-elements models.

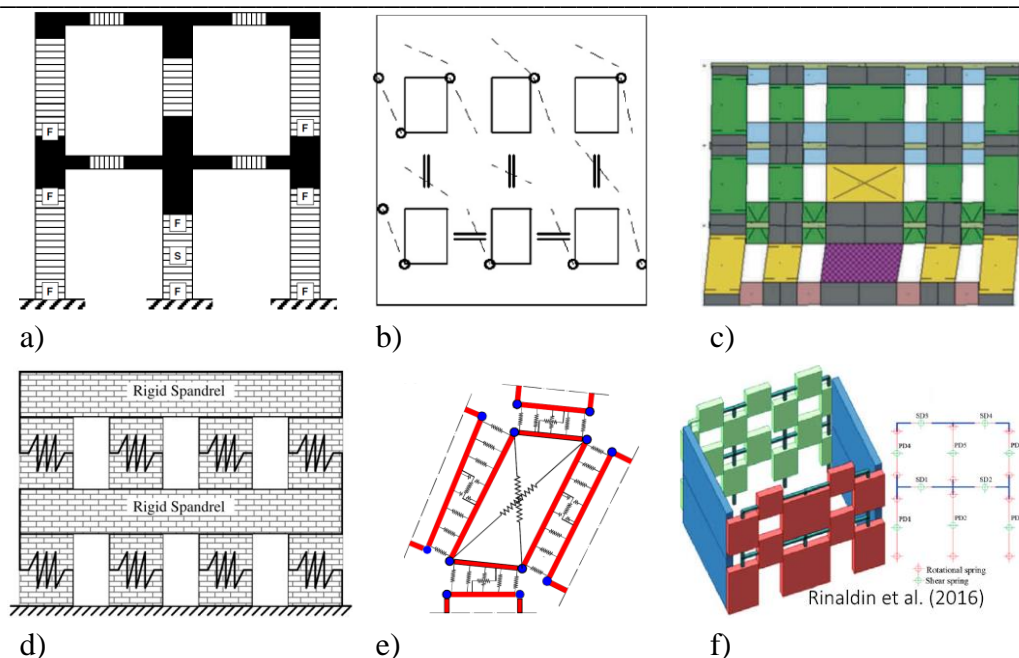


Figure 3.12 - Examples of macro-element model: (a) (Belmouden and Lestuzzi, 2009); (b) (Addessi, Mastrandrea and Sacco, 2014); (c) (Cattari *et al.*, 2018); (d) (Chen, Moon and Yi, 2008); (e) (Caliò, Marletta and Pantò, 2012); (f) (Rinaldin, Amadio and Macorini, 2016).

The group of macro-elements model is divided in two main families, namely equivalent beam-based models (Tomažević, 1978; Calderoni, Marone and Pagano, 1987; Dolce, 1991; Magenes and Della Fontana, 1998; Kappos, Penelis and Drakopoulos, 2002; Roca, Molins and Marí, 2005; Penelis, 2006; Pasticier, Amadio and Fragiaco, 2008; Belmouden and Lestuzzi, 2009; Grande, Imbimbo and Sacco, 2011; Lagomarsino *et al.*, 2013; Addessi, Mastrandrea and Sacco, 2014; Addessi, Liberatore and Masiani, 2015; Raka *et al.*, 2015; Liberatore and Addessi, 2015; Siano *et al.*, 2018; Cattari *et al.*, 2018) and spring-based models (Gambarotta and Lagomarsino, 1996, 1997b; Brenchic and Lagomarsino, 1998; Chen, Moon and Yi, 2008; Caliò, Marletta and Pantò, 2012; Lagomarsino *et al.*, 2013; Penna, Lagomarsino and Galasco, 2014; Caliò and Pantò, 2014; Rinaldin, Amadio and Macorini, 2016; Pantò *et al.*, 2016;

Aghababaie Mobarake, Khanmohammadi and Mirghaderi, 2017; Pantò, Caliò and Lourenço, 2018; Chácaras *et al.*, 2018).

3.5.2.1.4 Geometry-based models

This section is devoted to the description geometry-based models group. This type of formulations generally works in the limit analysis computational environment, by using the upper bound static theorem. The efficiency of geometry-based models was observed for both the investigation of equilibrium state analysis in the case of masonry vaulted structures as well as in the prediction of failure modes and collapse load factor in the case of full-scale masonry structures.

In this numerical strategy, the structure is represented by a single rigid body where the only required input are represented by structure geometry and loading conditions, being an approach generally based on limit analysis theorems to study the structural equilibrium and the collapse mode. Moving from the classical assumptions of the Heyman no-tension model (Heyman, 1966), the limit analysis-based approaches have been highly improving in the recent decades. Two families can be defined in the group of geometry-based models, each one of them using one of the two limit analysis theorems: statical (or lower bound) theorem (Heyman, 1966; O’Dwyer, 1999; Huerta, 2001; Block, Ciblac and Ochsendorf, 2006; Andreu, Gil and Roca, 2007; Block and Ochsendorf, 2007; Fraternali, 2010; Angelillo, Babilio and Fortunato, 2013; M. Angelillo, 2014; Block and Lachauer, 2014a, 2014b; Angelillo, 2015; Marmo and Rosati, 2017; Marmo, Masi and Rosati, 2018; Fraddosio, Lepore and Piccioni, 2019) and kinematical (or upper bound) theorem (Giuffrè, 1991; Milani, 2015; Chiozzi, Milani, *et al.*, 2018; Ministero delle infrastrutture e dei trasporti., 2018, 2019).

Apart from these two main approaches related to the theorem of limit analysis, in this field of the geometry-based models is possible to include also a third class of numerical models, mainly devoted to the analysis of masonry structures subjected to settlement-induced ground movements. The mentioned strategy is the so-called Strut-and-Tie Model (STM), originally formulated for the analysis of reinforced concrete beam subjected to shear stresses (Ritter, 1899), and successively applied to the investigation of masonry structures performance.

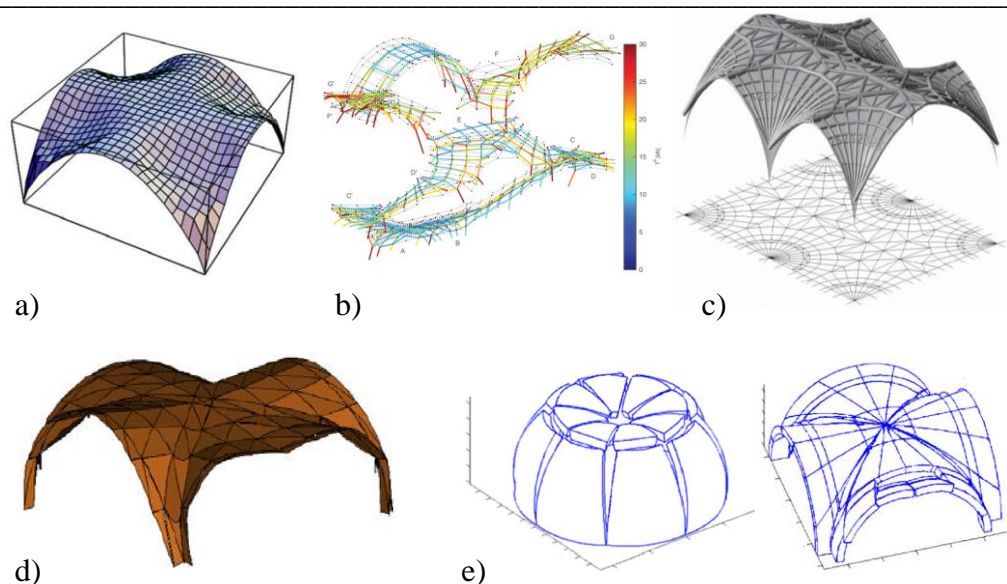


Figure 3.13 - Examples of geometry-based model: (a) (Angelillo, Babilio and Fortunato, 2013); (b) (Marmo, Masi and Rosati, 2018); (c) (Block and Lachauer, 2014a); (d) (Milani, 2015); (e) (Chiozzi, Milani and Tralli, 2017).

3.5.2.2 Analytical approaches

The present section contains some examples of the existing analytical methods for masonry structures. It is worth noting that analytical methods applied to the prediction of the structural response of masonry structures usually focus on the level of the structural element mainly due to the complexity in the analysis of large-scale structures. In this framework, analytical methods aim at closed-form solutions for the analysis of specific masonry types (e.g. walls, towers, arches etc.). As a matter of fact, many methods finally turn to computational algorithm to solve the equation system based analytical problem. With this in mind, two purely analytical approach are described in this section, mainly devoted to the analysis of settled masonry structures: the Limiting Tensile Strain Method (LTSM) and the Load Path Method (LPM), which is part of the overall Strut-and-Tie Model (STM).

3.5.2.2.1 The Limiting Tensile Strain Method (LTSM)

The so-called “Limiting Tensile Strain Method” (LTSM) is an analytical equivalent beam-based models specifically introduced for the prediction and investigation of masonry structures subjected to settlement-induced ground deformations. This empirical and analytical approach was extensively adopted as second level of assessment in the case of tunnelling-induced settlements (Mair, Taylor and Burland, 1996). For sake of clarity, the assessment procedures in the case of settlement analysis are generally grouped in three classes on the base of increasing level of complexity. The first class is represented by pure greenfield approaches based on expected soil deformation; the second class deals with empirical and analytical approaches accounting also for a simple model of the structures; the last one is represented by advanced numerical simulations to deeply investigate the settlement vulnerability of the case study. The LTSM is widely used thanks to its easy and flexible application, based on the following simplified assumptions (Giardina, 2013):

- the settlements are applied in two steps, a starting greenfield condition and the accounting for the isolated model of the structure, excluding the soil-structure interaction.
- the building is modelled as a linear elastic beam of the same size of the investigated building.
- the analysis is fully planar.
- the foundation system is not accounted for, being settlements applied directly to the equivalent beam model.
- openings (doors and windows) are neglected as well, assuming the equivalent beam stiffness in both bending and shear domain.

According to these easy assumptions, the Limiting Tensile Strain Method works in various sequential steps. In the first step, the ground movements promoting settlement is calculated in greenfield conditions, i.e. without accounting for the presence of any structure. The greenfield movements are calculated with reference to an influence area limited by the 1 mm settlement line, according to the suggestions provided with (Mair, Taylor and Burland, 1996). This means that in the case of very long buildings, a part of the building can be neglected because

it is not inside the considered influence area. Apart from this, the building length is commonly split according to the vertical settlement inflection point: some parts of the model suffer concave settlement profile (sagging mode) and the others suffer a convex settlement profile (hogging mode). The outcome of this starting procedure is represented by a settlement displacement protocol. The second step of the method consists of imposing the calculated greenfield displacements to the equivalent isotropic elastic beam model of the buildings. To this scope, the simplified model has the same length and height of the structure, where the height is calculated with reference to the distance between the foundation level and the top floor, being the roof usually neglected.

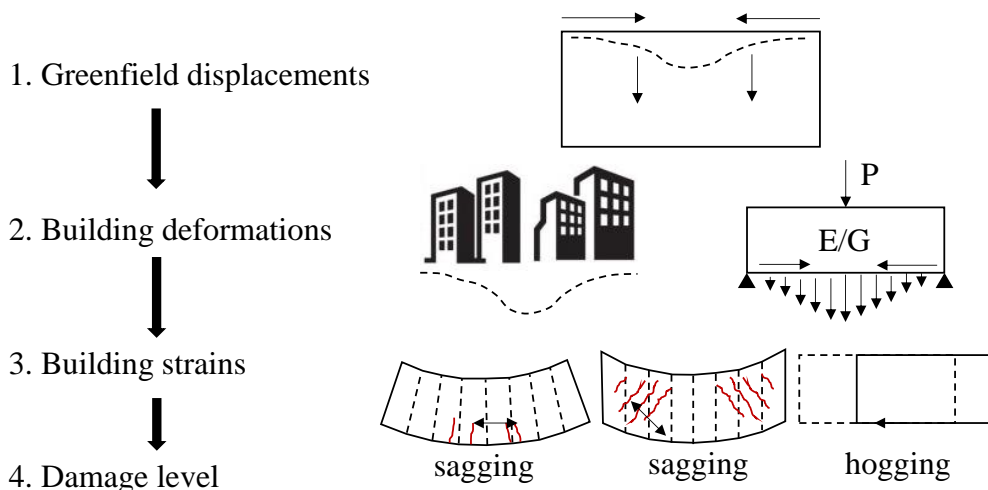


Figure 3.14 - Limit Tensile Strain Methods scheme, according to (Giardina, 2013).

In the case of long buildings, each split part of the building is modelled separately. The analysis of such a model, subjected to the specific displacement is the scope of the third procedure step, where both strains and stresses induced by the greenfield settlements in the equivalent beam model (or models in the case of split long buildings) are calculated. In the case of settlement acting in a not-orthogonal direction, the generic displacement can be uncoupled according to the vertical and horizontal axes. In such a condition, the bending and diagonal strains are calculated only for the vertical displacements and the horizontal strain is

calculated only for the horizontal settlements. Then, both the contributions are combined in order to evaluate the total bending and shear strains. Finally, the last step aims to relate the observed stress and strain distributions to a possible damage level of the masonry structures. Several approaches were proposed in literature for the classification of building damage due to settlements. A comprehensive description of these classification methods will be provided later in the text, in Chapter 7.

Although the LTSM showed to be a powerful and conservative assessment method for masonry structures subjected to ground movements, the various applications in literature of this method revealed that this method is also characterized by several limitations, as described in (Giardina, 2013). The first limitations relies on the nature of the method, which works in two separately steps: the assumption to model the settlement in greenfield conditions and only later applied the displacements to the isolated structural model, neglecting soil-structure interaction is an excessively simplification because the influence of the weights and stiffness of the building can produce a reduction in the values of differential settlements and deformations. (Franzius, 2003). On building side, the modelling assumption using linear elastic beam does not allow to account for the non-linear behaviour of masonry structure, which could promote a stress and strain redistribution. The risk is to predict incoherent collapse mechanisms and crack patterns due to the brittle nature of masonry, which is subjected also to localize cracks, where the stress and strain distribution can affect in a relevant way the local behaviour. Another important limitation is related to the planar approach of this method, which reduces the problem of the 3D interaction to a 2D analysis. Also, this assumption is too much simplified because the global performance of the analysed model could be affected in terms of underestimation of the predicted collapse mechanism. In the same context, the model neglects the soil-to-structure interaction effect, applying the displacement directly to the equivalent beam model. This assumption can be not so much conservative, especially in the case of horizontal settlements, where it can lead to underestimated outcomes in terms of structural capacity of masonry structures. Finally, the exclusion of openings in the equivalent beam model is highly not conservative because windows and doors can highly affect the structural response

of masonry structures in terms of crack pattern and damage concentration. Indeed, the corners of the openings usually show local damages which can influence the global structural response.

3.5.2.2.2 *The Load Path Method (LPM)*

In this section, an interesting analytical model is described, mainly devoted to the investigation of masonry structures affected by settlement-induced ground movements. The strategy refers to the so-called Load Path Method (LPM), which is a kind of numerical development of the early Strut-and-Tie Model (STM). The STM was initially introduced for the analysis and design of reinforced concrete beam subjected to shear stresses (Ritter, 1899). The idea proposed in (Ritter, 1899) is based on the observation that a beam under shear usually shows cracks due to diagonal tensile stresses. In this configuration, the beam can be idealized by a parallel chord truss with compressive strut in diagonal position with an angle of 45° inclination measured with respect to the longitudinal beam axis. This introduced idea was then investigated and extended in (Schlaich, Schaefer and Jennewein, 1987), where a global design approach based on STM is proposed. According to this approach, the structure modelled with respect to the strut-and-tie method is designed by using the static theorem of the limit analysis. The main challenge in this method is to find truss models to best reproduce the structure which is the object under investigation. It is worth noting that most of the cases, this step is not so complicated because it is possible to use examples already solved in other studies, which are comparable with the present one. Nevertheless, when the case study is not a standard one, the research for the optimum truss model represents a very challenging task demanding for high level of expertise and being a highly time-consuming process.

As already stated in the text, the theory of the STM relies on the lower bound theorem of the limit analysis, which is a theory to be applied to structural elements in order to investigate the structural response in the plastic regime. It is well-known by the literature that the application of a specific horizontal-and-vertical loads combination to a simple wall panel can activate several failure mechanisms of the panel. The failure response in this case can be even exacerbated by the onset of other mechanical phenomena, e.g. rocking motion,

block-to-block sliding at the interfaces due to frictional and cohesive behaviour, tensile cracking and compressive crushing in the units as well. All the mentioned failure modes can be modelled via plastic rules with a good approximation, with the exception of the brick tensile cracking which represents a brittle mechanism of course. This aspect shows an important limitation in the capability of the strut-and-tie method, which is not able to be applied in some cases. To overcome this issue, two solutions were proposed in literature (Roca *et al.*, 2011), namely primary models and residual models:

1. primary models can predict the maximum capacity of masonry wall panels when the collapse is only related to plastic performance. In this case, it is assumed that the ties are able to fully resist to any tensile forces, meaning that cracking is not possible to be exhibited.
2. residual models are devoted to the analysis of the brittle response of masonry types. Such a model is devoted to the analysis of structures where the ties contributions do not allow to absorb completely the tensile forces. To this aim, a generic residual model is designed without any ties or with a tie system incoherent with the cracks location.

In this framework, the Load Path Method (LPM) was introduced to solve the limitations of the Strut-and-Tie Method (especially the research of the optimum truss model) as a tool to find the best solution without a big energy and time consumption. Firstly introduced by (Schlaich, Schaefer and Jennewein, 1987), the LPM had been widely used in several applications and in different fields (De Tommasi, Monaco and Vitone, 2003; Palmisano, 2005; Palmisano *et al.*, 2007; Palmisano, Vitone and Vitone, 2008; Mezzina, Palmisano and Raffaele, 2010, 2012; Shi *et al.*, 2013). Following these experiences and the approach proposed in (Roca *et al.*, 2011) for the shear walls analysis, the possibility to apply the load path method to the structural behaviour investigation of masonry structures was explored in (Vitone, 2001; Palmisano, Vitone and Vitone, 2002, 2003; De Tommasi, Monaco and Vitone, 2003; Palmisano and Totaro, 2010; Palmisano, 2013, 2014; Palmisano and Elia, 2013, 2014). The latter introduced an approach somehow different from that in (Roca *et al.*, 2011) because the structural response of masonry structures is predicted by using equilibrium models and consistency.

In this framework, the main goal of such a model does not consist of prediction of the plastic ultimate response of the analysed masonry wall or structure but it is mainly devoted to the structural behaviour analysis and prediction in terms of damage and crack pattern initiation and propagation. The best outcome of LPM application is related to the search for the most coherent solution in the place of the exact one, meaning the solution represented by the path associated with the lowest value of the total strain energy among all the possible equilibrated load paths. The approach showed also to be very light in terms of computational and mathematical programming since the solution can be obtained by using very simple mathematical methods based on easy optimization algorithms. A valid example is represented by the so-called Bi-directional Evolutionary Structural Optimization method proposed in (Palmisano and Elia, 2015) for the application of the load path method in the case of masonry buildings subjected to landslide-induced settlements.

In (Palmisano and Elia, 2015; Palmisano, 2016), the key features of the load path method are described in detail. The method starts moving from the observation that the global forces transfer process inside a single element or structure can be affected by unexpected load path deviations which cause a thrust action. As a matter of fact, the thrust immediately demands for an equal reaction force applied along the same line but in the opposite direction. In this framework, the load path can be defined as the line where a force or one of its components moves on travelling by the loading application point until the element support. In this model, the generic force component of the specific load path has the same intensity along the overall path, being orthogonal to the thrust force in every deviation points. Such a definition leads to the conclusion that contrary to the travelling load force, the thrust intensity must change in each deviation node along the path. The outcome of this static equilibrium procedure based on the load flow is represented by approximated polygonal lines with a thrust vector per each deviation node. Figure 3.15 shows two schemes of the load path method in order to highlight the case without any deviation nodes and the case where there is only one deviation node with the corresponding thrust force. The letter used in Figure 3.15 are selected according to (Palmisano and Elia, 2015).

It seems to be clear that the stress regime predicted according to this proposed method depends on the directions of loads and paths: when loads and paths travel in the same direction the structure is stressed in compression (Figure 3.15c), while they travel in opposite directions, the structure is stressed in tension (Figure 3.15d). As already mentioned, the equilibrate load paths are unlimited and the LPM works to select the loads associated to vector investing the minimum value of the strain energy, which is the unique consistent and in equilibrium solution at the same time.

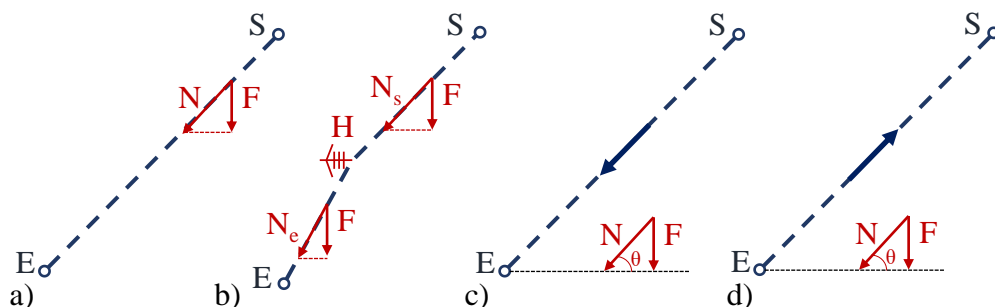


Figure 3.15 - Load Path Method in the case of (a) zero deviation and (b) only one deviation, according to (Palmisano and Elia, 2015). The representation of the stress regime in the case of (c) compressive and (d) tensile stress regime.

The above-mentioned approach is described in detail in (Palmisano and Elia, 2013, 2015; Palmisano, 2016). The idea is to consider the entire life of the structure, identifying a sequence of a certain number of configurations named “state” referred to specific transformations or evolutions suffered by the structure. In such a model, the overall structural behaviour can be studied as a step-by-step check of the single configuration. In the case of masonry structures, a five-state sequence is developed in (Palmisano, 2016):

- state 0, where the structure is not stressed.
- state 1, where the stress regime does not produce cracks on the structure.
- state 2, when the first cracks appear.
- state 2a, characterized by the propagation of the crack pattern.

-
- state 3, which represent the ultimate limit state, being the structure affected by severe damage and without further strength and stiffness capacity.

With regard to the assumptions for the identification of the foundation settlement to be applied to the structure, the model is based on the following hypothesis:

- applied settlement refers only to ground movements, being neglected any interaction between acting loads and foundation displacement.
- masses are concentrated.
- soil-structure interaction is neglected, assuming a full stiffness of the structure respect to the soil.
- soil mechanical behaviour is modelled with a perfectly plastic constitutive law for the ultimate limit state.

Under these assumptions, the LPM approach developed in (Palmisano and Elia, 2013) aims especially at the study of both brick-to-mortar contact behaviour and global response of the model, by using a macro-modelling strategy. In (Palmisano and Elia, 2015; Palmisano, 2016), the first three states (0, 1 and 2) were investigated assuming a linear behaviour for the material, neglecting the tensile strength. The aim is the prediction of the location and the causes of the first crack, which generally is also a fundamental indicator of the ultimate state behaviour at collapse. At the state 1, only downward loads are taken into account and no deviations of the travelling loads are introduced. The reason for the previous simplification relies in the macro-modelling nature of the proposed formulation, but in a micro-element environment, the contact surfaces among bricks and joints can promote some deviations in the load path. At the state 2 the load path can be represented by more than one possible configuration, meaning several equilibrated configurations.

First, the possible load paths are related to the type of settlement introduced: the generic wall can be subjected to a lateral settlement, when the involved area is limited to a lateral part of the total wall extension, a central settlement, when the involved area is located at the centre of the wall, a global settlement, when the displacement is applied to a length equal or of the same order of the geometrical

length of the wall. Furthermore, the settlement extension can also affect the response: e.g. in the case of a lateral settlement, it is possible to have a short, medium or long settlement according to the percentage of involved area compared to the geometrical length of the wall (Mastrodicasa, 1943). Apart from this, in (Palmisano and Elia, 2015; Palmisano, 2016), the settlement is introduced in the model in terms of a complete loss of contact between the soil and the involved side of the masonry panel. In such a way, the contact loss at soil-panel interface produces the sudden block of some of the possible load paths introduced at the state 1 and other static modification in order to assure the static global equilibrium per each step. The investigated case studies revealed that a masonry wall subjected to unsymmetrical settlement profile (e.g. lateral settlement applied to one wall end) can even exhibit a symmetrical structural response.

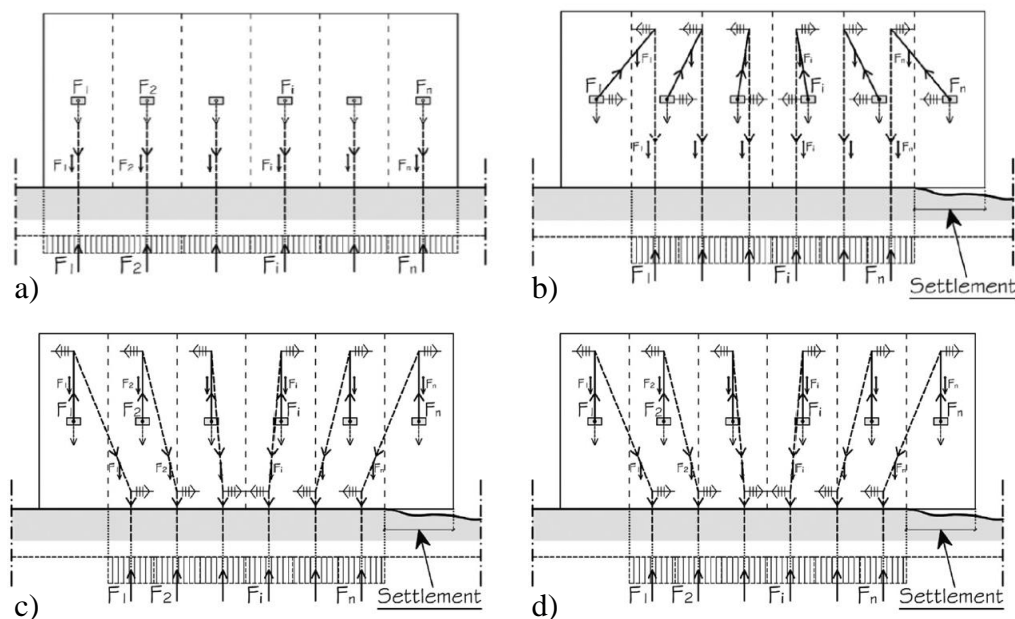


Figure 3.16 - Load Path Method in the case of a settlement located at one end of the masonry wall. Static equilibrium condition located at (a) state 1 and (b)(c)(d) state 2.

This section deeply described the field of Strut-and-Tie Model (STM), with particular regard to the application of the Load Path Method (LPM). The

possibility to assess the masonry structure and wall affected by landslide-induced settlements revealed many potentialities. Nevertheless, the simple hypothesis assumed in the model can generate some limitations. First of all, the current version of the model is able to analyse only the linear behaviour of the masonry structure capacity, but nothing can be predicted with regard to the ultimate limit state and for the plastic or post-peak capacity. This means that the only possible outcome the strategy is able to provide is represented by the position of first crack the structure exhibit. Also, the assumption to neglect the soil-structure interaction can cause some mistakes, i.e. predicting incoherent failure mode or even underestimate the global capacity. However, it is worth noting that the Load Path Method approach remains valid in the words of the authors due to two main reason. Firstly, the general procedure can solve both symmetrical and unsymmetrical case. Then, even in an unsymmetrical response, the load path shape in the area where the settlement is located is close the shape obtained in the case of the symmetrical response.

3.6 Rigid block models based on limit analysis

The two computational models proposed within the present dissertation in the next Chapter 4 essentially deal with rigid block limit analysis formulations and with the mathematical programming formulation of the classical bound theorems. The limit analysis formulation was developed in the framework of the theory of classical plasticity, which deals with rigid perfectly plastic materials that can be affected by plastic deformation when the value of the applied load reaches a specific value. According to the theory of plasticity, the plastic deformation, i.e. the collapse state, occurs as a result of flow when the stress point reaches the limit surface. The limit surface diagrams are typical depending on the material. In the case of elastic perfectly plastic model, the stress-to-strain behaviour can be represented by a bi-linear diagram with no softening or hardening ranges. In this framework, a specific material can be assumed to be perfectly plastic when the property of continuing plastic flow is exhibited. Such a material shows a purely plastic collapse strain, assuming a rigid perfectly plastic behaviour where the elastic properties are not accounted for at all.

3.6.1 State of art

The theory of limit analysis comes from the field of the material strength, which dates back to the far 1683 when Galileo Galilei finally found a way to calculate the ultimate moment of beam under the assumption of infinite compressive strength (Galilei, 1638). Then, Coulomb proposed criteria to determine the yielding of plastic soils in 1773. Tresca was a pioneer in the field of the investigation of the metals plasticity. In 1864 he proposed a formulation based on a comprehensive experimental campaign, stating that the plastic yielding for a metal occurs when the shear stress reaches a critical value (Tresca, 1864). The mathematical formulation of the theory of plasticity obtained a high contribution thanks to the research by de Saint Venant. He introduced a constitutive equations system for plastic materials (de Saint Venant, 1870). Lèvy followed the idea of de Saint Venant introducing 3D stress-plastic strain relations. Assuming yield condition proposed by Tresca, the flow rates are not forced to be normal to the limit yield surface (Lévy, 1870). Further improvements to the theory of plasticity were provided in 1909 by Haar and Von Karman, who proposed equations of plasticity based on a variational principle (Haar and von Karman, 1909). Many experimental tests were performed, resulting in several suggested yield criteria. As for metallic materials, the best solution was introduced by Von Mises in 1913 with a yield criterion fully based on mathematical procedures (von Mises, 1913). Close to the Von Mises proposals, the criteria suggested by Huber in 1904 and Hencky in 1924 introduced the assumption that the yielding occurs if the elastic shear strain energy reaches a critical value (Huber, 1904; Hencky, 1924). In 1925 Von Karman applied the plasticity theory to engineering practice for the first time with the investigation of the stress distribution during the rolling of a metal strip (von Kármán, 1925).

The Lèvy-Von Mises stress-strain relation was validated in 1926 thanks to the experimental campaign on metal tubes performed by Lode (Lode, 1926). In 1930 the work of Reuss allowed to generalize the theory of plasticity also involving the elastic range (Reuss, 1930). Then Schmidt and Odquist developed a strategy to modify the Lèvy-Von Mises equations in order to account for even the effect of strain-hardening (Schmidt, 1932; Odqvist, 1933). During the second half of

the XX century, the theory of plasticity widely spread and extended to field of both isotropic and anisotropic materials. In the case of soil materials, it was assumed that they could be eventually modelled by using Tresca and Mohr-Coulomb yield criteria (Drucker, Prager and Greenberg, 1952; Prager, 1952, 1959; Hodge, 1959).

The theory of plasticity was highly developed thanks to the introduction of the upper and lower bound theorems of the limit analysis. Although the earliest references to these theorems can be identified in (Hill, 1950; Gvozdev, 1960), the comprehensive formulation of the theorems was provided in (Drucker, Greenberg and Prager, 1951; Drucker, Prager and Greenberg, 1952). The theory of the limit analysis is based on the idea to calculate the collapse load of a structural system without any consideration about loading history and assuming a rigid perfectly plastic behaviour. In this framework, the theory of limit analysis does not deal with the prediction of the displacement capacity from the elastic to the plastic range. Such a theory is highly powerful especially in the field of engineering mechanics as a tool to assess the collapse state of a structure and the corresponding failure mode. Originally formulated to be mainly applied in mechanics, the limit analysis formulation has been improving also as a powerful tool for the prediction of the stability of structures thanks to the introduction of numerical approach based on mathematical programming formulations.

According to the classical lower bound theorem, a structure is said to be in a “statically admissible state” when the internal stresses are in equilibrium with the external forces and the yield conditions are fulfilled at all yield points. In such a condition, the structure is assumed to be safe. The value of the load factor is free to monotonically increase from zero to a specific point, i.e. the safety factor. Over this threshold the equilibrium or the yield conditions are not more fulfilled. As for the upper bound theorem, a mechanism is to be considered as “kinematically admissible” when the overall strains can be written as a linear combination of the associated plastic multipliers with a positive dissipation energy. The kinematic equilibrium is ensured by the compatibility condition, with respect to the displacement and flow rate. Dissipation energy corresponds to the work made by the applied loads, taken to be unity. According to the upper bound (or kinematic)

theorem of classic limit analysis, the safety factor is the smallest of all the kinematically admissible load factors. In 1950 Horne put together the two above-described theorems of the limit analysis, formulating the so-called uniqueness theorem (Horne, 1950). The lower bound theorem ensures that every internal stress distribution cannot be safe and statically admissible at the same time. On the other hand, the upper bound theorem shows that the value of load factor must be lower than the safety factor for any possible mechanism. The combination of these two considerations brings to the uniqueness theorem, which states that the largest of all the statically admissible load factors equals the smallest of all the kinematically admissible load factors and is thus the exact safety factor.

The last decades showed that the theory of the classical theorems of the limit analysis can be powerfully applied to the analysis of the structural response of discrete assemblage of rigid body elements. The discrete element methods (DEM) were originally devoted to the analysis of jointed and fractured masses (Cundall, 1971) being particularly suitable to investigate problems where most of deformation is due to the block-to-block relative motion. In this framework, the approach appears to be especially useful in the case of masonry structures, where the role of contact surface is fundamental. In (Trovalusci, 1992) experimental tests were performed to validate the use of discrete models, showing that the outcomes of such a formulation is strongly affected by the feature of the assemblage, such as shape, size and disposition of the rigid units. In the discrete modelling environment, the blocks can be considered as nodes and the internal forces are located at contact points. The internal forces are represented by normal and shear forces and by moment components. The approach is based on the assumption of rigid body, where the material is not accounted for as well as cracking and crushing failure conditions. The failure conditions assume a rigid perfectly plastic behaviour.

A formulation that can be used to build the discrete model is the so-called nodal formulation (Livesley, 1978; Baggio and Trovalusci, 1993, 1998; Ferris and Tin-Loi, 2001; Tran-Cao, 2009). The nodal approach is characterized by ease of automatic generation of problem data and was firstly introduced in (Livesley, 1978) where the technique previously developed for the analysis of rigid-plastic

structural frames was adapted to provide a formal procedure for finding the limit load of any structure formed from rigid blocks.

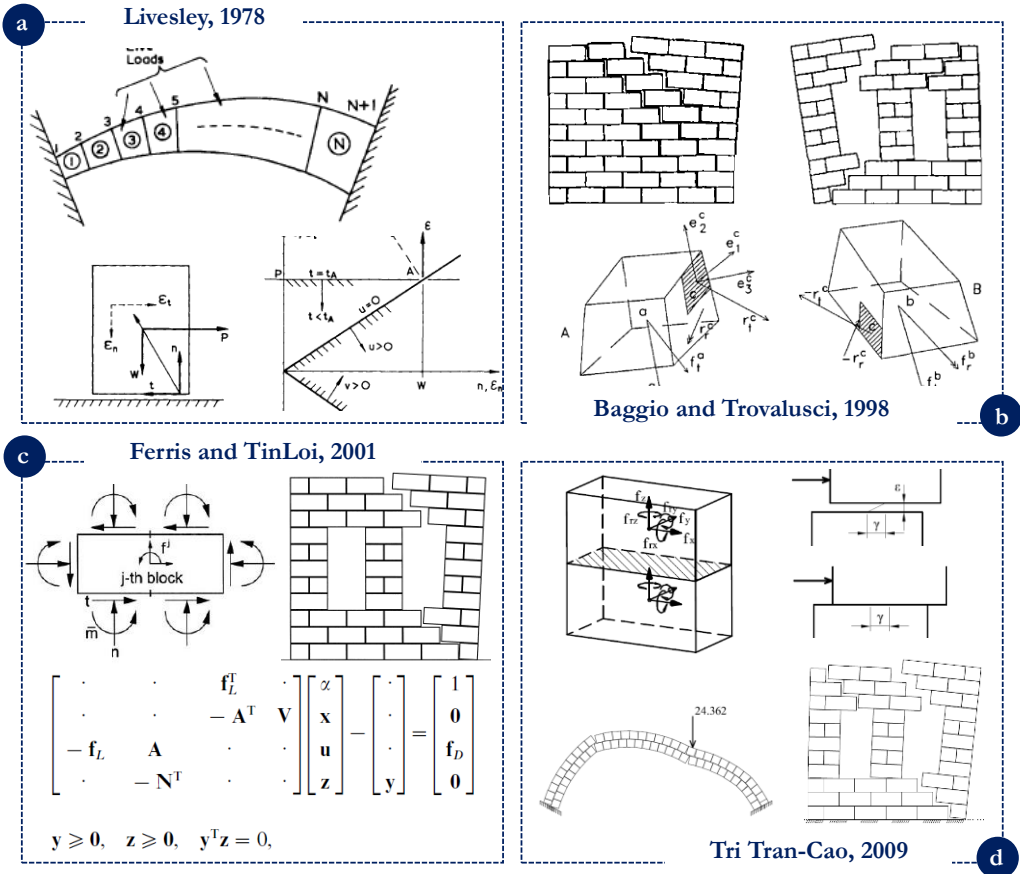


Figure 3.17 - Rigid block limit analysis proposed models: (a) (Livesley, 1978); (b) (Baggio and Trovalusci, 1998); (c) (Ferris and Tin-Loi, 2001); (d) (Tran-Cao, 2009).

A contribution to this formulation was provided in (Baggio and Trovalusci, 1993) where the mechanisms of hinging, sliding, and twisting at the interfaces were accounted for. The solution of the problem of non-linear programming is obtained by solving a problem of linear programming (LP). The research developed in (Fishwick, 1996; Ferris and Tin-Loi, 2001) showed that the

computation of the collapse loads of discrete rigid block systems can be solved as a constrained optimization problem, i.e. a Mathematical Program with Equilibrium Constraints (MPEC). Then in (Tran-Cao, 2009) both associated and non-associated flow rules were considered, using nonlinear programming, specifically mathematical programming with equilibrium constraints problems.

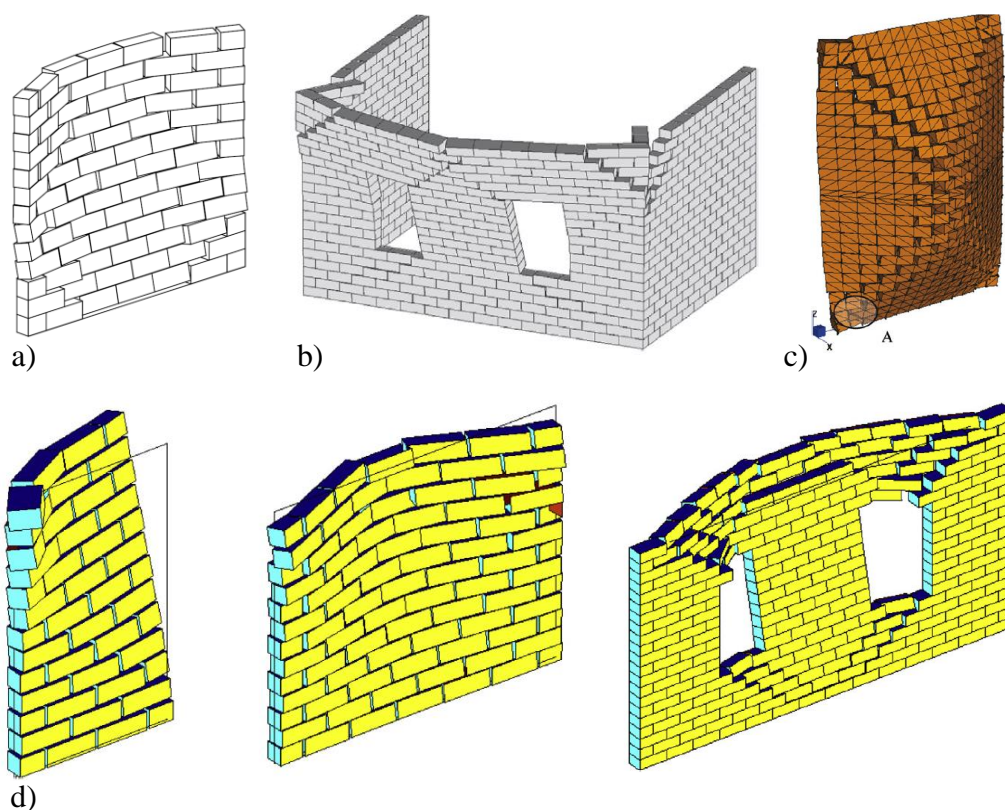


Figure 3.18 - Examples of proposed limit analysis approaches: (a) (Orduña and Lourenço, 2005a); (c) (Portioli *et al.*, 2014); (c) (Milani, 2008); (d) (Baraldi and Cecchi, 2017).

An interesting numerical experience in this field is represented by the computational technique implemented by (Sutcliffe, Yu and Page, 2001) based on the static theorem of limit analysis applied to the in-plane analysis of URM (unreinforced masonry) shear walls. In this case, linear programming and finite element were applied to introduce a Mohr-Coulomb mechanical behaviour at the

contact interfaces. This model is able to calculate the load factor (or collapse multiplier) through simple equilibrium equations. In this direction, (Orduña and Lourenço, 2005a, 2005b) introduced a numerical formulation based on the solution of the non-associative flow rule problem.

Other important contributions to the linear programming tools for the collapse mechanisms analysis of masonry structure have been proposed in (Gilbert, Casapulla and Ahmed, 2006; Portioli *et al.*, 2013, 2014), where the blocks interactions are represented through frictional no-tension contact interfaces. The potentialities of the block-based limit analysis approach in a FEM computational environment were tested by Milani (Milani, 2008) where a numerical formulation based on the kinematic problem of limit analysis is developed aiming at the study of in-plane and out-of-plane behaviour of masonry walls. Also, in this proposal, a Mohr-Coulomb failure criterion for the contact interfaces is adopted assuming a cohesion model with limited tensile and compressive strength for mortar joints. Masonry compressive crushing is also considered in this model.

This methodological class showed high potentialities in the application to real case study, but the limitations is represented by the high computational demands which could be a severe issue for large-scale masonry buildings. Some attempts to overcome these limitations were also developed in literature, as in the case of the full 3D rigid block model proposed in (Baraldi and Cecchi, 2017) where the material non-linearities are taken into account for a better prediction of the collapse mechanism and loading capacity of masonry structures modelled as collection of discrete and rigid blocks (Figure 3.18d).

3.6.2 Other proposed rigid block models

In this section, valid examples of proposed approaches in the field of rigid block limit analysis models are described in order to highlight the different ways suggested to face the modelling strategy which is the base of the formulations proposed in this research (in the next Chapter).

In this framework a significant contribution is provided in (Zampieri, Amoroso and Pellegrino, 2019) where the focus is represented by the collapse mechanism

analysis of circular masonry arch subjected to imposed settlement of one support by using the principle of virtual work and thrust-line analysis.

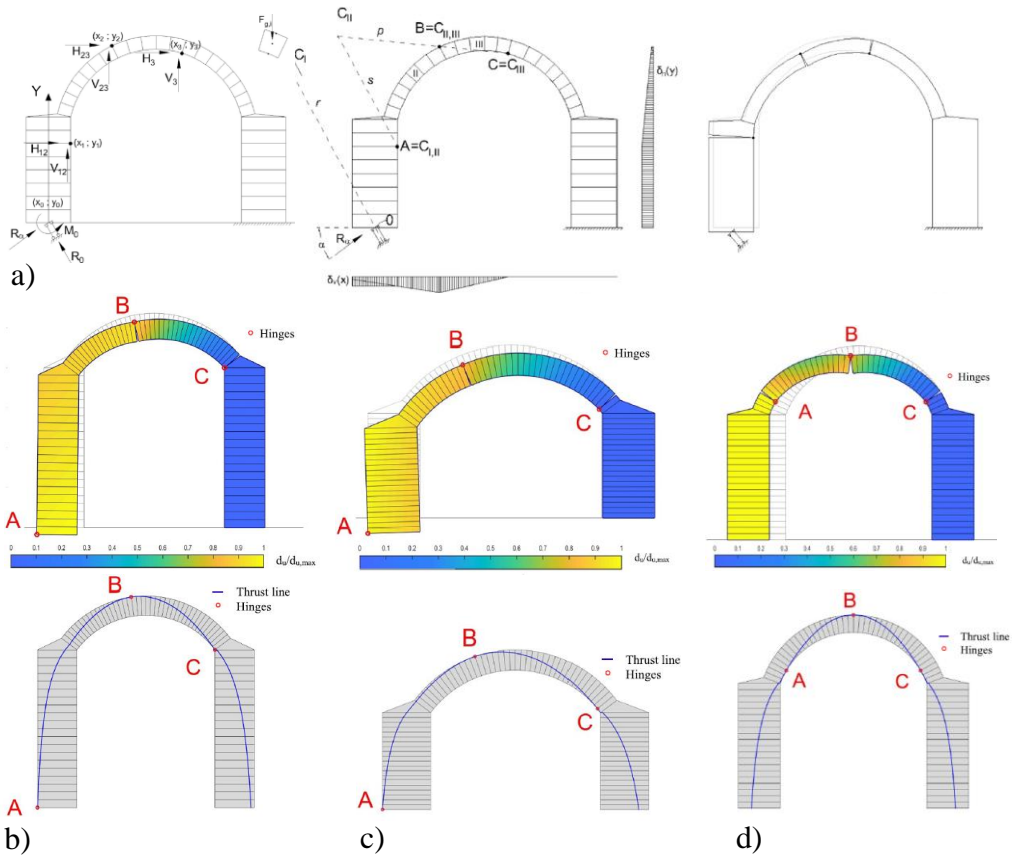


Figure 3.19 - Rigid block model proposed in (Zampieri, Amoroso and Pellegrino, 2019): (a) diagrams for the analytical proposal and (b)(c)(d) examples of predicted collapse mechanisms and corresponding thrust line.

The study also performed a parametric analysis to investigate the influence of the settlement angle and arch slenderness on the hinging failure configuration. The interesting suggestion developed in (Zampieri, Amoroso and Pellegrino, 2019) is represented by the introduction of two steps for the study of masonry arch subjected to foundation settlements: a first step ('Phase A') based on the rigid block equilibrium analysis with the scope to calculate the minimum support

reaction to create a hinging mechanism; a second step ('Phase B) where rigid block analysis is performed in order to study the load capacity of the settled masonry arch. It is worth noting that this second step is sometimes developed by using non-linear analysis, as described in (Zampieri *et al.*, 2017). The various mechanisms predicted according to the settlement angle and arch slenderness involve both displacements and rotations of the settled rigid blocks. The model of the investigated masonry buttressed arch is discretized into a certain number of rigid blocks and the collapse condition occurs with a three-hinge mechanism, whose position is a function of the above-mentioned tested parameters. Some examples of collapse mechanisms and corresponding thrust line presented in (Zampieri, Amoroso and Pellegrino, 2019) are showed in Figure 3.19b,c,d.

The investigation of the capacity of masonry arch subjected to spreading support by using rigid block limit analysis formulation is also the main topic performed in (Galassi *et al.*, 2018), where an innovative numerical procedure for the prediction of collapse mechanism and limit settlement is developed. In this model the search for proper hinges location promoting collapse is carried out by using both static and kinematic problem of the classical limit analysis formulation. As a consequence, the settlement capacity of the analysed arches is computed with equilibrium checks for each step of the increasing settlement. The numerical proposal is then validated against experimental test on small-scale arch models made of PVC blocks subjected to movable support. As for the rigid block model proposed in (Galassi *et al.*, 2018), the generic structure is considered as a system of n rigid blocks in contact by means $n+1$ interfaces. With regard to the interfaces, they are coincident with the bisectors of the joints and are made of two orthogonal links (at the intrados and extrados) and one longitudinal link (Figure 3.20a). Links behave according to a rigid-cracking model with respect to axial forces and perfectly rigid behaviour in shear. As for the constitutive model, the contact joints behave according to Heyman assumptions with infinite compressive and shear strengths and zero-tensile strength. The numerical procedure assigns to each settlement configuration the only mechanism kinematically compatible and in equilibrium with the loading condition, refusing the application of an optimization technique. Then, the compatible solutions are statically analysed in order to find the unique structure which is also in

equilibrium. The procedure ends with the estimation of the limit settlement via a series of static analyses on the structure subjected to increasing value of the applied settlement.

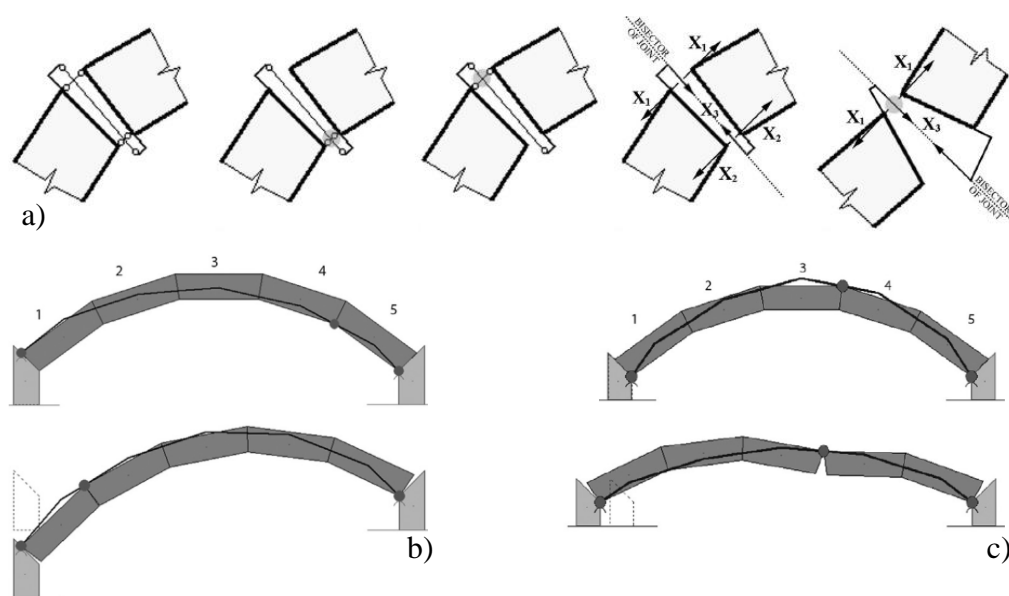


Figure 3.20 - Rigid block model proposed in (Galassi *et al.*, 2018): (a) interfaces model and involved forces; (b)(c) applications to arches subjected to movable support.

The two described model focuses on the study of arched masonry structures, a field highly investigated in literature also according to other modelling approaches (Forgács, Sarhosis and Ádány, 2019, 2021; Sarhosis, Forgács and Lemos, 2019, 2020). Nevertheless, rigid blocks formulations were also proposed in literature for the analysis of other structural types such as 2D building façades or sections. In this framework, the planar structural response of a masonry structure divided into rigid blocks, subjected to both uniform and linear settlements was analysed in (Maurizio Angelillo, 2014; Iannuzzo *et al.*, 2018), where a model for the prediction of fractures given by settlement is proposed, based on the solution of the kinematical problem by the minimum potential energy theorem. The idea proposed by the authors is based on the assumption that the potential fracture lines are located at the common block-to-block

boundaries. With this in mind, the model proposed in (Maurizio Angelillo, 2014; Iannuzzo *et al.*, 2018) is able to catch the mechanism that minimizes the energy by fixing a mesh geometry and the iterating a minimization algorithm assuming rigid body displacements. As a matter of fact, a minimal energy criterion is proposed which allows to detect the hinge position for the defined rigid block discretization and even to find the corresponding field of piecewise rigid displacement. Application of this rigid block approach to monumental 2D case study under settlement were also provided in (Maurizio Angelillo, 2014; Iannuzzo *et al.*, 2018) and are showed in Figure 3.21. The first case study is represented by the façade of a XVIII century tuff-masonry historical buildings located in Torre Annunziata (Naples) and the second one is represented by a XVII century church of Santa Maria Incoronatella della Pietà dei Turchini in Naples.

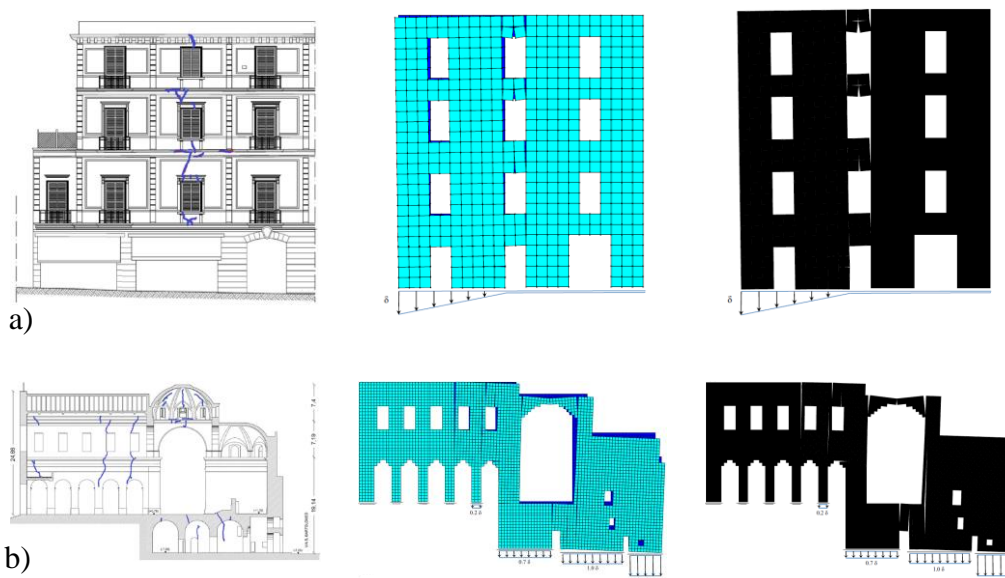


Figure 3.21 - Application of the rigid block model proposed in (Maurizio Angelillo, 2014; Iannuzzo *et al.*, 2018): (a) façade of a XVIII century building in Torre Annunziata (Naples); (b) cross section of XVII centuries church (Naples).

It is worth noting that this section only contains some examples of valid applications of rigid block limit analysis approach for the investigation of masonry structures capacity. Of course, this is not a full description of all the

proposed solutions in literature, which would be a huge work but is out of the scopes of the present dissertation.

Conclusions

This Chapter is dedicated to two main topics. The first one deals with a comprehensive overview on masonry structures with the scope to introduce the main features of the structural material adopted in this dissertation thesis, i.e. masonry. The large description here reported gives the image of a very complex material, from different points of view. It is worth noting that the study of the mechanical behaviour of such a hard material is a very difficult topic and the description performed in this Chapter does not expect to be an exhaustive and full text on this theme, aiming at only showing the main macroscopic mechanical features of masonry-like material.

The first point to be accounted for deals with the history of this specific material, which is the oldest building material. Although the high competitiveness by new building materials such as reinforced concrete and steel, masonry showed valid structural capacity as demonstrated by the huge number of monumental building (real pieces of arts) that still lives against the time elapsing. In this framework, the chapter is divided in two main sections. Firstly, an historical survey on the masonry structures is provided, a thousand-year tale which allows to assimilate the role the masonry played for centuries in the engineering world. Then, the investigation of the mechanical behaviour of masonry like material is performed, in order to clarify the response of this material according to the specific stress state and loading conditions according to masonry macroscopic behaviour.

The second discussed topic is represented by a comprehensive review of modelling approaches for the capacity investigation of masonry structures. The main scope is to provide an overall description of the several computational and analytical solutions proposed in literature in order to create a full background for the next Chapter, where the numerical procedures developed within this doctoral research will be presented. Although the present dissertation thesis is mainly focused on the topic of masonry structures subjected to movable foundation and

settlements, the review of modelling approaches performed in this Chapter can be regarded in a global framework, with no specific reference to only one type of load or support condition. The idea is to provide a complete description of the existing solutions for the overall analysis of masonry structures.

The various models were mainly classified on the base of two main factors, which are essentially the accuracy in the description of masonry like material and the adopted strategy for the analysis of structural response of masonry structures. According to the modelling material, the computational formulation can be divided in detailed micro-modelling, simplified micro-modelling and macro-modelling depending on the level of knowledge of components, i.e. units and mortar joints. The main difference between them is the assumption about the mechanical behaviour of the mortar joints, the possibility to neglect them and how to model the unit-to-joint contact interfaces. The various numerical applications proposed in literature in the last decades showed that detailed modelling approaches can better described the real mechanical behaviour of a so-complicated building material such as masonry. Nevertheless, these kinds of solutions demand for highly computational costs being time-consuming procedures. The latter is associated also with the observation that most of the time the outcomes obtained with such a detailed method are not so far from those obtained with a more simplified approach in terms of accuracy of results and agreement with experimental outcomes in the case of validation case studies.

According to the adopted modelling strategies this Chapter reported an extensive description of the huge number of solutions proposed in literature. In this case, computational formulations for the analysis of masonry structures can be firstly divided in numerical and analytical strategies. Both classes were further grouped in several sub-groups in order to list all the different solutions researchers found for the investigation of the structural response of masonry structures.

Finally, this Chapter dedicated a specific section to a particular approach for the analysis of masonry structures, i.e. the rigid block limit analysis approach. This choice is motivated by the fact that the numerical models proposed in this dissertation belong to this class. So, a comprehensive state of art of this modelling solution is performed and some examples available in literature are also reported.

According to the overview developed in Chapter 3, a highly crowded environment came to light with respect to the computational support for the masonry structure capacity analysis. This outcome is a consequence of the innate complexity of masonry like material, which open several opportunities to study and interpretate its mysterious mechanical behaviour, thus resulting in numerous modelling approaches and strategies. With this in mind, the next Chapter 4 will present two rigid block numerical formulation developed as in-house computational tool with the scope to contribute at the investigation of the structural response of masonry structures for both seismic-induced lateral loads and settlement-induced foundation movements.

This Chapter represents a fundamental step in this doctoral research because the topics here presented and described represent a fundamental theoretical background for all the contents to be discussed later. At this point of the dissertation, the preparatory knowledges and states of art were provided according to the type of investigated natural hazards, the structural object involved in the developed research study and the overview of the huge number of computational solutions proposed in literature to face the investigated structural issue.

References

Abdulla, K. F., Cunningham, L. S. and Gillie, M. (2017) ‘Simulating masonry wall behaviour using a simplified micro-model approach’, *Engineering Structures*, 151, pp. 349–365. doi: 10.1016/j.engstruct.2017.08.021.

Addessi, D. *et al.* (2014) ‘Modeling approaches for masonry structures’, *Open Civil Engineering Journal*, 8(1), pp. 288–300. doi: 10.2174/1874149501408010288.

Addessi, D., Liberatore, D. and Masiani, R. (2015) ‘Force-based beam finite element (FE) for the pushover analysis of masonry buildings’, *International Journal of Architectural Heritage*, 9(3), pp. 231–243. doi: 10.1080/15583058.2013.768309.

Addessi, D., Mastrandrea, A. and Sacco, E. (2014) ‘An equilibrated macro-element for nonlinear analysis of masonry structures’, *Engineering Structures*, 70, pp. 82–93. doi: 10.1016/j.engstruct.2014.03.034.

Addessi, D. and Sacco, E. (2012) ‘A multi-scale enriched model for the analysis of masonry panels’, *International Journal of Solids and Structures*, 49(6), pp. 865–880. doi: 10.1016/j.ijsolstr.2011.12.004.

Addessi, D., Sacco, E. and Paolone, A. (2010) ‘Cosserat model for periodic masonry deduced by nonlinear homogenization’, *European Journal of Mechanics, A/Solids*, 29(4), pp. 724–737. doi: 10.1016/j.euromechsol.2010.03.001.

Aghababaie Mobarake, A., Khanmohammadi, M. and Mirghaderi, S. R. (2017) ‘A new discrete macro-element in an analytical platform for seismic assessment of unreinforced masonry buildings’, *Engineering Structures*, 152, pp. 381–396. doi: 10.1016/j.engstruct.2017.09.013.

Alfano, G., Rosati, L. and Valoroso, N. (2000) ‘A numerical strategy for finite element analysis of no-tension materials’, *International Journal for Numerical Methods in Engineering*, 48(3), pp. 317–350. doi: 10.1002/(SICI)1097-0207(20000530)48:3<317::AID-NME868>3.0.CO;2-C.

Alfano, G. and Sacco, E. (2006) ‘Combining interface damage and friction in a cohesive-zone model’, *International Journal for Numerical Methods in*

Engineering, 68(5), pp. 542–582. doi: 10.1002/nme.1728.

Ali, S. S. and Page, A. W. (1988) ‘Finite element model for masonry subjected to concentrated loads’, *Journal of Structural Engineering (United States)*, 114(8), pp. 1761–1784. doi: 10.1061/(ASCE)0733-9445(1988)114:8(1761).

Andreu, A., Gil, L. and Roca, P. (2007) ‘Computational analysis of masonry structures with a funicular model’, *Journal of Engineering Mechanics*, 133(4), pp. 473–480. doi: 10.1061/(ASCE)0733-9399(2007)133:4(473).

Angelillo, M. (1994) ‘A finite element approach to the study of no-tension structures’, *Finite Elements in Analysis and Design*, 17(1), pp. 57–73. doi: 10.1016/0168-874X(94)90020-5.

Angelillo, M. (2014) *Mechanics of masonry structures*. Edited by Springer. Vienna.

Angelillo, Maurizio (2014) ‘Practical applications of unilateral models to Masonry Equilibrium’, in *CISM International Centre for Mechanical Sciences, Courses and Lectures*. doi: 10.1007/978-3-7091-1774-3_4.

Angelillo, M. (2015) ‘Static analysis of a Guastavino helical stair as a layered masonry shell’, *Composite Structures*, 119, pp. 298–304. doi: 10.1016/j.compstruct.2014.09.007.

Angelillo, M. *et al.* (2018) ‘Rigid block models for masonry structures’, *International Journal of Masonry Research and Innovation*, 3(4), pp. 349–368. doi: 10.1504/IJMRI.2018.095701.

Angelillo, M., Babilio, E. and Fortunato, A. (2013) ‘Singular stress fields for masonry-like vaults’, *Continuum Mechanics and Thermodynamics*, 25(2–4), pp. 423–441. doi: 10.1007/s00161-012-0270-9.

Anthoine, A. (1995) ‘Derivation of the in-plane elastic characteristics of masonry through homogenization theory’, *International Journal of Solids and Structures*, 32(2), pp. 137–163. doi: 10.1016/0020-7683(94)00140-R.

Aref, A. J. and Dolatshahi, K. M. (2013) ‘A three-dimensional cyclic meso-scale numerical procedure for simulation of unreinforced masonry structures’, *Computers and Structures*, 120, pp. 9–23. doi: 10.1016/j.compstruc.2013.01.012.

Augenti, N. (2006) ‘Seismic behaviour of irregular masonry walls’, in *1st*

European Conf. on Earthquake Engineering and Seismology.

Bacigalupo, A. and Gambarotta, L. (2010) ‘Second-order computational homogenization of heterogeneous materials with periodic microstructure’, *ZAMM Zeitschrift für Angewandte Mathematik und Mechanik*, 90(10–11), pp. 796–811. doi: 10.1002/zamm.201000031.

Bacigalupo, A. and Gambarotta, L. (2012) ‘Computational two-scale homogenization of periodic masonry: Characteristic lengths and dispersive waves’, *Computer Methods in Applied Mechanics and Engineering*, 213–216, pp. 16–28. doi: 10.1016/j.cma.2011.11.020.

Baggio, C. and Trovalusci, P. (1993) ‘Discrete models for jointed masonry walls’, in *The Sixth North American Masonry Conference*. Philadelphia, pp. 939–949.

Baggio, C. and Trovalusci, P. (1998) ‘Limit analysis for no-tension and frictional three-dimensional discrete systems’, *Mechanics of Structures and Machines*, 26(3), pp. 287–304. doi: 10.1080/08905459708945496.

Baraldi, D. and Cecchi, A. (2017) ‘A full 3D rigid block model for the collapse behaviour of masonry walls’, *European Journal of Mechanics, A/Solids*, 64, pp. 11–28. doi: 10.1016/j.euromechsol.2017.01.012.

Bartoli, G., Betti, M. and Vignoli, A. (2016) ‘A numerical study on seismic risk assessment of historic masonry towers: a case study in San Gimignano’, *Bulletin of Earthquake Engineering*, 14(6), pp. 1475–1518. doi: 10.1007/s10518-016-9892-9.

Beatini, V., Royer-Carfagni, G. and Tasora, A. (2017) ‘A regularized non-smooth contact dynamics approach for architectural masonry structures’, *Computers and Structures*, 187, pp. 88–100. doi: 10.1016/j.compstruc.2017.02.002.

de Bellis, M. L. and Addessi, D. (2011) ‘A cosserat based multi-scale model for masonry structures’, *International Journal for Multiscale Computational Engineering*, 9(5), pp. 543–563. doi: 10.1615/IntJMultCompEng.2011002758.

Belmouden, Y. and Lestuzzi, P. (2009) ‘An equivalent frame model for seismic analysis of masonry and reinforced concrete buildings’, *Construction and Building Materials*, 23(1), pp. 40–53. doi: 10.1016/j.conbuildmat.2007.10.023.

Berti, M. *et al.* (2017) ‘Unreinforced masonry walls with irregular opening layouts: reliability of equivalent-frame modelling for seismic vulnerability assessment’, *Bulletin of Earthquake Engineering*, 15(3), pp. 1213–1239. doi: 10.1007/s10518-016-9985-5.

Berto, L. *et al.* (2002) ‘An orthotropic damage model for masonry structures’, *International Journal for Numerical Methods in Engineering*, 55(2), pp. 127–157. doi: 10.1002/nme.495.

Bertolesi, E., Milani, G. and Casolo, S. (2018) ‘Homogenization towards a mechanistic Rigid Body and Spring Model (HRBSM) for the non-linear dynamic analysis of 3D masonry structures’, *Meccanica*, 53(7), pp. 1819–1855. doi: 10.1007/s11012-017-0665-6.

Betti, M. and Galano, L. (2012) ‘Seismic analysis of historic masonry buildings: The Vicarious Palace in Pescia (Italy)’, *Buildings*, 2(2), pp. 63–82. doi: 10.3390/buildings2020063.

Betti, M. and Vignoli, A. (2011) ‘Numerical assessment of the static and seismic behaviour of the basilica of Santa Maria all’Impruneta (Italy)’, *Construction and Building Materials*, 25(12), pp. 4308–4324. doi: 10.1016/j.conbuildmat.2010.12.028.

Beyer, K. (2012) ‘Peak and residual strengths of brick masonry spandrels’, *Engineering Structures*, 41, pp. 533–547. doi: 10.1016/j.engstruct.2012.03.015.

Block, P., Ciblac, T. and Ochsendorf, J. (2006) ‘Real-time limit analysis of vaulted masonry buildings’, *Computers and Structures*, 84(29–30), pp. 1841–1852. doi: 10.1016/j.compstruc.2006.08.002.

Block, P. and Lachauer, L. (2014a) ‘Three-dimensional (3D) equilibrium analysis of gothic masonry vaults’, *International Journal of Architectural Heritage*, 8(3), pp. 312–335. doi: 10.1080/15583058.2013.826301.

Block, P. and Lachauer, L. (2014b) ‘Three-dimensional funicular analysis of masonry vaults’, *Mechanics Research Communications*, 56, pp. 53–60. doi: 10.1016/j.mechrescom.2013.11.010.

Block, P. and Ochsendorf, J. (2007) ‘Thrust network analysis: A new methodology for three-dimensional equilibrium’, *Journal of the International Association for Shell and Spatial Structures*, 48(155), pp. 167–173.

Brasile, S., Casciaro, R. and Formica, G. (2007a) ‘Multilevel approach for brick masonry walls - Part I: A numerical strategy for the nonlinear analysis’, *Computer Methods in Applied Mechanics and Engineering*, 196(49–52), pp. 4934–4951. doi: 10.1016/j.cma.2007.06.021.

Brasile, S., Casciaro, R. and Formica, G. (2007b) ‘Multilevel approach for brick masonry walls - Part II: On the use of equivalent continua’, *Computer Methods in Applied Mechanics and Engineering*, 196(49–52), pp. 4801–4810. doi: 10.1016/j.cma.2007.06.020.

Brenchic, A. and Lagomarsino, S. (1998) ‘A macro-elements dynamic model for masonry shear walls’, *Proc. 4th Int. symp. computer methods in structural masonry (STRUMAS IV)*, pp. 67–75.

Briccoli Bati, S., Ranocchiani, G. and Rovero, L. (1999) ‘A micromechanical model for linear homogenization of brick masonry’, *Materials and Structures/Materiaux et Constructions*, 32(215), pp. 22–30. doi: 10.1007/bf02480408.

Bruggi, M. (2014) ‘Finite element analysis of no-tension structures as a topology optimization problem’, *Structural and Multidisciplinary Optimization*, 50(6), pp. 957–973. doi: 10.1007/s00158-014-1093-z.

Bruggi, M. and Taliercio, A. (2015) ‘Analysis of no-tension structures under monotonic loading through an energy-based method’, *Computers and Structures*, 159, pp. 14–25. doi: 10.1016/j.compstruc.2015.07.002.

Bruggi, M. and Taliercio, A. (2018) ‘Analysis of 3D no-tension masonry-like walls’, in *European mechanics society ESMC 2018*. Bologna.

De Buhan, P. and De Felice, G. (1997) ‘A homogenization approach to the ultimate strength of brick masonry’, *Journal of the Mechanics and Physics of Solids*, 45(7), pp. 1085–1104. doi: 10.1016/S0022-5096(97)00002-1.

Bui, T. T. *et al.* (2017) ‘Discrete element modelling of the in-plane and out-of-plane behaviour of dry-joint masonry wall constructions’, *Engineering Structures*, 136, pp. 277–294. doi: 10.1016/j.engstruct.2017.01.020.

Çaktı, E. *et al.* (2016) ‘Discrete element modeling of a scaled masonry structure and its validation’, *Engineering Structures*, 126, pp. 224–236. doi: 10.1016/j.engstruct.2016.07.044.

Calderini, C., Cattari, S. and Lagomarsino, S. (2009) ‘In-plane strength of unreinforced masonry piers’, *Earthquake Engineering and Structural Dynamics*, 38(2), pp. 243–267. doi: 10.1002/eqe.860.

Calderini, C. and Lagomarsino, S. (2006) ‘A micromechanical inelastic model for historical masonry’, *Journal of Earthquake Engineering*, 10(4), pp. 453–479. doi: 10.1142/S1363246906002608.

Calderón, S., Sandoval, C. and Arnau, O. (2017) ‘Shear response of partially-grouted reinforced masonry walls with a central opening: Testing and detailed micro-modelling’, *Materials and Design*, 118, pp. 122–137. doi: 10.1016/j.matdes.2017.01.019.

Calderoni, B. *et al.* (2015) ‘Problematiche di modellazione strutturale di edifici in muratura esistenti soggetti ad azioni sismiche in relazione all’utilizzo di software commerciali’, in *XVI convegno ANIDIS*. Aquila, Italy.

Calderoni, B., Marone, P. and Pagano, M. (1987) ‘Modelli per la verifica statica degli edifici in muratura in zona sismica’, *Ingegneria Sismica*, 3(3), pp. 19–27.

Caliò, I., Marletta, M. and Pantò, B. (2012) ‘A new discrete element model for the evaluation of the seismic behaviour of unreinforced masonry buildings’, *Engineering Structures*, 40, pp. 327–338. doi: 10.1016/j.engstruct.2012.02.039.

Caliò, I. and Pantò, B. (2014) ‘A macro-element modelling approach of Infilled Frame Structures’, *Computers and Structures*, 143, pp. 91–107. doi: 10.1016/j.compstruc.2014.07.008.

Casolo, S. (2000) ‘Modelling the out-of-plane seismic behaviour of masonry walls by rigid elements’, *Earthquake Engineering and Structural Dynamics*, 29(12), pp. 1797–1813. doi: 10.1002/1096-9845(200012)29:12<1797::AID-EQE987>3.0.CO;2-D.

Casolo, S. (2004) ‘Modelling in-plane micro-structure of masonry walls by rigid elements’, *International Journal of Solids and Structures*, 41(13), pp. 3625–3641. doi: 10.1016/j.ijsolstr.2004.02.002.

Casolo, S. (2006) ‘Macroscopic modelling of structured materials: Relationship between orthotropic Cosserat continuum and rigid elements’, *International Journal of Solids and Structures*, 43(3–4), pp. 475–496. doi: 10.1016/j.ijsolstr.2005.03.037.

Casolo, S. and Peña, F. (2007) ‘Rigid element model for in-plane dynamics of masonry walls considering hysteretic behaviour and damage’, *Earthquake Engineering and Structural Dynamics*, 36(8), pp. 1029–1048. doi: 10.1002/eqe.670.

Castellazzi, G. *et al.* (2015) ‘From laser scanning to finite element analysis of complex buildings by using a semi-automatic procedure’, *Sensors (Switzerland)*, 15(8), pp. 18360–18380. doi: 10.3390/s150818360.

Castellazzi, G. *et al.* (2017) ‘An innovative numerical modeling strategy for the structural analysis of historical monumental buildings’, *Engineering Structures*, 132, pp. 229–248. doi: 10.1016/j.engstruct.2016.11.032.

Castellazzi, G. *et al.* (2018) ‘Numerical insights on the seismic behavior of a nonisolated historical masonry tower’, *Bulletin of Earthquake Engineering*, 16(2), pp. 933–961. doi: 10.1007/s10518-017-0231-6.

Cattari, S. *et al.* (2018) ‘Masonry Italian Code-Conforming Buildings. Part 2: Nonlinear Modelling and Time-History Analysis’, *Journal of Earthquake Engineering*, 22(sup2), pp. 2010–2040. doi: 10.1080/13632469.2018.1541030.

Cavalagli, N., Cluni, F. and Gusella, V. (2011) ‘Strength domain of non-periodic masonry by homogenization in generalized plane state’, *European Journal of Mechanics, A/Solids*, 30(2), pp. 113–126. doi: 10.1016/j.euromechsol.2010.10.009.

Cavalagli, N., Cluni, F. and Gusella, V. (2013) ‘Evaluation of a Statistically Equivalent Periodic Unit Cell for a quasi-periodic masonry’, *International Journal of Solids and Structures*, 50(25–26), pp. 4226–4240. doi: 10.1016/j.ijsolstr.2013.08.027.

Cecchi, A. and Milani, G. (2008) ‘A kinematic FE limit analysis model for thick English bond masonry walls’, *International Journal of Solids and Structures*, 45(5), pp. 1302–1331. doi: 10.1016/j.ijsolstr.2007.09.019.

Cecchi, A., Milani, G. and Tralli, A. (2005) ‘Validation of analytical multiparameter homogenization models for out-of-plane loaded masonry walls by means of the finite element method’, *Journal of Engineering Mechanics*, 131(2), pp. 185–198. doi: 10.1061/(ASCE)0733-9399(2005)131:2(185).

Cecchi, A., Milani, G. and Tralli, A. (2007) ‘A Reissner-Mindlin limit analysis

model for out-of-plane loaded running bond masonry walls’, *International Journal of Solids and Structures*, 44(5), pp. 1438–1460. doi: 10.1016/j.ijsolstr.2006.06.033.

Cecchi, A. and Sab, K. (2002) ‘A multi-parameter homogenization study for modeling elastic masonry’, *European Journal of Mechanics, A/Solids*, 21(2), pp. 249–268. doi: 10.1016/S0997-7538(01)01195-0.

Cecchi, A. and Sab, K. (2007) ‘A homogenized Reissner-Mindlin model for orthotropic periodic plates: Application to brickwork panels’, *International Journal of Solids and Structures*, 44(18–19), pp. 6055–6079. doi: 10.1016/j.ijsolstr.2007.02.009.

Cecchi, A. and Sab, K. (2009) ‘Discrete and continuous models for in plane loaded random elastic brickwork’, *European Journal of Mechanics, A/Solids*, 28(3), pp. 610–625. doi: 10.1016/j.euromechsol.2008.10.007.

Chácará, C. *et al.* (2018) ‘Assessment of the dynamic response of unreinforced masonry structures using a macroelement modeling approach’, *Earthquake Engineering and Structural Dynamics*, 47(12), pp. 2426–2446. doi: 10.1002/eqe.3091.

Chen, S.-Y., Moon, F. L. and Yi, T. (2008) ‘A macroelement for the nonlinear analysis of in-plane unreinforced masonry piers’, *Engineering Structures*, 30(8), pp. 2242–2252. doi: 10.1016/j.engstruct.2007.12.001.

Chiozzi, A., Milani, G., *et al.* (2018) ‘A fast and general upper-bound limit analysis approach for out-of-plane loaded masonry walls’, *Meccanica*, 53(7), pp. 1875–1898. doi: 10.1007/s11012-017-0637-x.

Chiozzi, A., Grillanda, N., *et al.* (2018) ‘UB-ALMANAC: An adaptive limit analysis NURBS-based program for the automatic assessment of partial failure mechanisms in masonry churches’, *Engineering Failure Analysis*, 85, pp. 201–220. doi: 10.1016/j.engfailanal.2017.11.013.

Chiozzi, A., Milani, G. and Tralli, A. (2017) ‘A Genetic Algorithm NURBS-based new approach for fast kinematic limit analysis of masonry vaults’, *Computers and Structures*, 182, pp. 187–204. doi: 10.1016/j.compstruc.2016.11.003.

Chisari, C. *et al.* (2015) ‘An inverse analysis procedure for material parameter

identification of mortar joints in unreinforced masonry’, *Computers and Structures*, 155, pp. 97–105. doi: 10.1016/j.compstruc.2015.02.008.

Chisari, C. *et al.* (2018) ‘Identification of mesoscale model parameters for brick-masonry’, *International Journal of Solids and Structures*, 146, pp. 224–240. doi: 10.1016/j.ijsolstr.2018.04.003.

Clough, R. W. and Penzien, J. (2003) ‘Dynamics of Structures’, *Computers and Structures*.

Cundall, P. A. (1971) ‘A computer model for simulating progressive large-scale movements in blocky rock systems’, *Proceedings of the Symposium of the International Society of Rock Mechanics*. Nancy, France, 2, pp. 129–136.

Cundall, P. A. (1980) *UDEC - A generalised distinct element program for modelling jointed rock*, European Research Office.

Cundall, P. A. and Strack, O. D. L. (1979) ‘A discrete numerical model for granular assemblies’, *Geotechnique*, 29(1), pp. 47–65. doi: 10.1680/geot.1979.29.1.47.

Cuomo, M. and Ventura, G. (2000) ‘Complementary energy formulation of no tension masonry-like solids’, *Computer Methods in Applied Mechanics and Engineering*, 189(1), pp. 313–339. doi: 10.1016/S0045-7825(99)00298-4.

D’Altri, A. M. *et al.* (2018) ‘Stability analysis of leaning historic masonry structures’, *Automation in Construction*, 92, pp. 199–213. doi: 10.1016/j.autcon.2018.04.003.

D’Altri, A. M. *et al.* (2020) ‘Modeling Strategies for the Computational Analysis of Unreinforced Masonry Structures: Review and Classification’, *Archives of Computational Methods in Engineering*, 27(4), pp. 1153–1185. doi: 10.1007/s11831-019-09351-x.

D’Altri, A. M., Castellazzi, G. and de Miranda, S. (2018) ‘Collapse investigation of the Arquata del Tronto medieval fortress after the 2016 Central Italy seismic sequence’, *Journal of Building Engineering*, 18, pp. 245–251. doi: 10.1016/j.jobbe.2018.03.021.

Davey, N. (1961) *A history of building materials*. Edited by Phoenix House. London, UK.

Degli Abbati, S. *et al.* (2019) ‘Seismic assessment of interacting structural units in complex historic masonry constructions by nonlinear static analyses’, *Computers and Structures*, 213, pp. 51–71. doi: 10.1016/j.compstruc.2018.12.001.

DeJong, M. J. *et al.* (2009) ‘Shell elements for sequentially linear analysis: Lateral failure of masonry structures’, *Engineering Structures*, 31(7), pp. 1382–1392. doi: 10.1016/j.engstruct.2009.02.007.

Dhanasekar, M., Page, A. W. and Kleeman, P. W. (1985) ‘The failure of brick masonry under biaxial stresses’, *Proceedings of the Institution of Civil Engineers (London)*, 79(pt 2), pp. 295–313. doi: 10.1680/iicep.1985.992.

Dolatshahi, K. M. and Aref, A. J. (2016) ‘Multi-directional response of unreinforced masonry walls: experimental and computational investigations’, *Earthquake Engineering and Structural Dynamics*, 45(9), pp. 1427–1449. doi: 10.1002/eqe.2714.

Dolatshahi, K. M., Nikoukalam, M. T. and Beyer, K. (2018) ‘Numerical study on factors that influence the in-plane drift capacity of unreinforced masonry walls’, *Earthquake Engineering and Structural Dynamics*, 47(6), pp. 1440–1459. doi: 10.1002/eqe.3024.

Dolatshahi, K. M. and Yekrangnia, M. (2015) ‘Out-of-plane strength reduction of unreinforced masonry walls because of in-plane damages’, *Earthquake Engineering and Structural Dynamics*, 44(13), pp. 2157–2176. doi: 10.1002/eqe.2574.

Dolce, M. (1991) ‘Schematizzazione e modellazione degli edifici in muratura soggetti ad azioni sismiche’, *L’Industria delle costruzioni*, 25(242), pp. 44–57.

Drougkas, A., Roca, P. and Molins, C. (2015) ‘Analytical micro-modeling of masonry periodic unit cells - Elastic properties’, *International Journal of Solids and Structures*, 69–70, pp. 169–188. doi: 10.1016/j.ijsolstr.2015.04.039.

Drucker, D. C., Greenberg, H. J. and Prager, W. (1951) ‘The safety factor of an elastic plastic body in plane strain’, *Journal of Applied Mechanics*, 73, p. 371.

Drucker, D. C., Prager, W. and Greenberg, H. J. (1952) ‘Extended limit design theorems for continuous media’, *Quarterly of Applied Mathematics*, 9, pp. 381–389. doi: 10.1090/qam/45573.

Drysdale, R. G., Hamid, A. A. and Baker, L. R. (1994) *Masonry structures: Behavior and design*. New Jersey, USA: Prentice-Hall, Englewood Cliffs.

Elliot, C. D. (1992) *Technics and architecture: The development of materials and systems of buildings*. Edited by The MIT Press. Cambridge, Massachusetts, USA.

Elyamani, A. *et al.* (2017) ‘Seismic safety assessment of historical structures using updated numerical models: The case of Mallorca cathedral in Spain’, *Engineering Failure Analysis*, 74, pp. 54–79. doi: 10.1016/j.engfailanal.2016.12.017.

Ferris, M. C. and Tin-Loi, F. (2001) ‘Limit analysis of frictional block assemblies as a mathematical program with complementarity constraints’, *International Journal of Mechanical Sciences*, 43(1), pp. 209–224. doi: 10.1016/S0020-7403(99)00111-3.

Fishwick, R. J. (1996) *Limit analysis of rigid block structures*. University of Portsmouth.

Forgács, T., Sarhosis, V. and Ádány, S. (2019) ‘Numerical modelling of skew masonry arch bridges taking into account arch ring-backfill interaction’, *Masonry International*, 32(1), pp. 35–42.

Forgács, T., Sarhosis, V. and Ádány, S. (2021) ‘Shakedown and dynamic behaviour of masonry arch railway bridges’, *Engineering Structures*, 228. doi: 10.1016/j.engstruct.2020.111474.

Forgács, T., Sarhosis, V. and Bagi, K. (2017) ‘Minimum thickness of semi-circular skewed masonry arches’, *Engineering Structures*, 140, pp. 317–336. doi: 10.1016/j.engstruct.2017.02.036.

Formica, G., Sansalone, V. and Casciaro, R. (2002) ‘A mixed solution strategy for the nonlinear analysis of brick masonry walls’, *Computer Methods in Applied Mechanics and Engineering*, 191(51–52), pp. 5847–5876. doi: 10.1016/S0045-7825(02)00501-7.

Fortunato, G., Funari, M. F. and Lonetti, P. (2017) ‘Survey and seismic vulnerability assessment of the Baptistery of San Giovanni in Tumba (Italy)’, *Journal of Cultural Heritage*, 26, pp. 64–78. doi: 10.1016/j.culher.2017.01.010.

Foti, D., Vacca, V. and Facchini, I. (2018) ‘DEM modeling and experimental

analysis of the static behavior of a dry-joints masonry cross vaults’, *Construction and Building Materials*, 170, pp. 111–120. doi: 10.1016/j.conbuildmat.2018.02.202.

Fraddosio, A., Lepore, N. and Piccioni, M. D. (2019) *Lower Bound Limit Analysis of Masonry Vaults Under General Load Conditions*, *RILEM Bookseries*. doi: 10.1007/978-3-319-99441-3_118.

Francis, A. J., Horman, C. B. and Jerrens, L. E. (1971) ‘The Effect of Joint Thickness and Other Factors on the Compressive Strength of brickwork’, in British Ceramic Research Association (ed.) *Proc. Of the 2nd International Brick Masonry Conference*. Stoke-on-Trent, pp. 31–37.

Franzius, J. N. (2003) *Behaviour of buildings due to tunnel induced subsidence*. Imperial College.

Fraternali, F. (2010) ‘A thrust network approach to the equilibrium problem of unreinforced masonry vaults via polyhedral stress functions’, *Mechanics Research Communications*, 37(2), pp. 198–204. doi: 10.1016/j.mechrescom.2009.12.010.

Gagliardo, R. *et al.* (2019) ‘Blind-test numerical simulation of shake-table tests on three-leaf masonry walls: An application of LIA block_3D’, in *COMPADYN Proceedings*, pp. 4699–4706. doi: 10.7712/120119.7261.19695.

Galassi, S. *et al.* (2018) ‘Failure modes prediction of masonry voussoir arches on moving supports’, *Engineering Structures*, 173, pp. 706–717. doi: 10.1016/j.engstruct.2018.07.015.

Galilei, G. (1638) *Discourses on two new sciences*, trans. S. Drake 1974. The Univer. Madison.

Gambarotta, L. and Lagomarsino, S. (1996) ‘On the dynamic response of masonry panels’, in *Proceedings of the national conference on masonry mechanics between theory and practice*. Messina.

Gambarotta, L. and Lagomarsino, S. (1997a) ‘Damage models for the seismic response of brick masonry shear walls. Part I: the mortar joint model and its applications’, *Earthquake Engineering and Structural Dynamics*, 26(4), pp. 423–439. doi: 10.1002/(SICI)1096-9845(199704)26:4<423::AID-EQE650>3.0.CO;2-#.

Gambarotta, L. and Lagomarsino, S. (1997b) ‘Damage models for the seismic response of brick masonry shear walls. Part II: The continuum model and its applications’, *Earthquake Engineering and Structural Dynamics*, 26(4), pp. 441–462. doi: 10.1002/(SICI)1096-9845(199704)26:4<441::AID-EQE651>3.0.CO;2-0.

Giardina, G. (2013) *Modelling of settlement induced building damage*. Delft University of Technology.

Gilbert, M., Casapulla, C. and Ahmed, H. M. (2006) ‘Limit analysis of masonry block structures with non-associative frictional joints using linear programming’, *Computers and Structures*, 84(13–14), pp. 873–887. doi: 10.1016/j.compstruc.2006.02.005.

Giuffrè, A. (1991) *Lecture sulla meccanica delle murature storiche*. Kappa.

Giuffrè, A. and Carrocci, C. (1993) ‘Statica e dinamica delle costruzioni murarie storiche’, in, pp. 539–598.

Godio, M. *et al.* (2017) ‘A limit analysis approach based on Cosserat continuum for the evaluation of the in-plane strength of discrete media: Application to masonry’, *European Journal of Mechanics, A/Solids*, 66, pp. 168–192. doi: 10.1016/j.euromechsol.2017.06.011.

Grande, E., Imbimbo, M. and Sacco, E. (2011) ‘A beam finite element for nonlinear analysis of masonry elements with or without fiber-reinforced plastic (FRP) reinforcements’, *International Journal of Architectural Heritage*, 5(6), pp. 693–716. doi: 10.1080/15583058.2010.490616.

Greco, F. *et al.* (2016) ‘An adaptive multiscale strategy for the damage analysis of masonry modeled as a composite material’, *Composite Structures*, 153, pp. 972–988. doi: 10.1016/j.compstruct.2016.06.066.

Gvozdev, A. A. (1960) ‘The determination of the value of the collapse load for statically indeterminate systems undergoing plastic deformation’, *International Journal of Mechanical Sciences*, 1, pp. 322–333. doi: 10.1016/0020-7403(60)90051-5.

Haar, A. and von Karman, T. (1909) ‘Zur Theorie der Spannungszustände in plastischen und sandartigen Medien’, *Nachrichten von der Gesellschaft der Wissenschaften zu Göttingen, Mathematisch-Physikalische Klasse*, pp. 204–218.

Hencky, H. (1924) ‘Zur Theorie plastischer Deformationen und der hierdurch im Material hervorgerufenen Nachspannungen’, *ZAMM - Journal of Applied Mathematics and Mechanics / Zeitschrift für Angewandte Mathematik und Mechanik*, 4, pp. 323–334. doi: 10.1002/zamm.19240040405.

Hendry, A. W. (1990) *Structural masonry*. London, UK: Macmillan Education.

Heyman, J. (1966) ‘The stone skeleton’, *International Journal of Solids and Structures*, 2(2), pp. 249–279. doi: 10.1016/0020-7683(66)90018-7.

Hill, R. (1950) *The mathematical Theory of Plasticity*. Oxford Uni. London, UK.

Hilsdorf, H. K. (1969) ‘An Investigation Into the Failure Mechanism of Brick Masonry Loaded in Axial Compression’, in Johnson, F. B. (ed.) *Designing, Engineering and Constructing with Masonry Products*. Gulf Publ. Houston, pp. 34–41.

Hodge, P. G. (1959) *Plastic Analysis of Structures*. McGraw-Hil. New York.

Horne, M. R. (1950) ‘Fundamental Propositions in the Plastic Theory of Structures’, *Journal of the Institution of Civil Engineers*, 34, p. 174. doi: 10.1680/ijoti_1950_12895.

Huber, M. T. (1904) ‘Wlasciwa praca odkształcenia jako miara witezenia materialu’, *Czas. Techn. Lwów*, 22, pp. 38–81.

Huerta, S. (2001) ‘Mechanics of masonry vaults: The equilibrium approach’, *3rd International Seminar in Historical Constructions, Guimarães, Portugal*.

Iannuzzo, A. *et al.* (2018) ‘Modelling the cracks produced by settlements in masonry structures’, *Meccanica*. Springer Netherlands, 53(7), pp. 1857–1873. doi: 10.1007/s11012-017-0721-2.

Jean, M. (1999) ‘The non-smooth contact dynamics method’, *Computer Methods in Applied Mechanics and Engineering*, 177(3–4), pp. 235–257. doi: 10.1016/S0045-7825(98)00383-1.

Kappos, A. J., Penelis, G. G. and Drakopoulos, C. G. (2002) ‘Evaluation of simplified models for lateral load analysis of unreinforced masonry buildings’, *Journal of Structural Engineering*, 128(7), pp. 890–897. doi: 10.1061/(ASCE)0733-9445(2002)128:7(890).

von Kármán, T. (1925) ‘Beitrag zur Theorie des Walzvorganges’, *ZAMM -*

Journal of Applied Mathematics and Mechanics / Zeitschrift für Angewandte Mathematik und Mechanik, 5, p. 130. doi: 10.1002/zamm.19250050213.

Kawa, M., Pietruszczak, S. and Shieh-Beygi, B. (2008) ‘Limit states for brick masonry based on homogenization approach’, *International Journal of Solids and Structures*, 45(3–4), pp. 998–1016. doi: 10.1016/j.ijsolstr.2007.09.015.

Korumaz, M. *et al.* (2017) ‘An integrated Terrestrial Laser Scanner (TLS), Deviation Analysis (DA) and Finite Element (FE) approach for health assessment of historical structures. A minaret case study’, *Engineering Structures*, 153, pp. 224–238. doi: 10.1016/j.engstruct.2017.10.026.

Kuang, J. S. and Yuen, Y. P. (2013) ‘Simulations of masonry-infilled reinforced concrete frame failure’, *Proceedings of the Institution of Civil Engineers: Engineering and Computational Mechanics*, 166(4), pp. 179–193. doi: 10.1680/eacm.13.00002.

Lagomarsino, S. *et al.* (2013) ‘TREMURI program: An equivalent frame model for the nonlinear seismic analysis of masonry buildings’, *Engineering Structures*, 56, pp. 1787–1799. doi: 10.1016/j.engstruct.2013.08.002.

Lagomarsino, S. *et al.* (2018) ‘Seismic Assessment of Existing Irregular Masonry Buildings by Nonlinear Static and Dynamic Analyses’, in Pitilakis, K. (ed.) *Recent Advances in Earthquake Engineering in Europe. ECEE 2018. Geotechnical, Geological and Earthquake Engineering*. Springer, pp. 123–151.

Lancioni, G. *et al.* (2016) ‘Seismic vulnerability of ancient stone arches by using a numerical model based on the Non-Smooth Contact Dynamics method’, *Engineering Structures*, 119, pp. 110–121. doi: 10.1016/j.engstruct.2016.04.001.

Lemos, J. V. (2007) ‘Discrete element modeling of masonry structures’, *International Journal of Architectural Heritage*, 1(2), pp. 190–213. doi: 10.1080/15583050601176868.

Lengyel, G. (2017) ‘Discrete element analysis of gothic masonry vaults for self-weight and horizontal support displacement’, *Engineering Structures*, 148, pp. 195–209. doi: 10.1016/j.engstruct.2017.06.014.

Leonetti, L. *et al.* (2018) ‘A multiscale damage analysis of periodic composites using a couple-stress/Cauchy multidomain model: Application to masonry structures’, *Composites Part B: Engineering*, 141, pp. 50–59. doi:

10.1016/j.compositesb.2017.12.025.

Lévy, M. (1870) ‘Mémoire sur les équations générales des mouvements intérieurs des corps solides ductiles au delà des limites où l'élasticité pourrait les ramener à leur premier état’, *Comptes-rendus de l'académie des sciences*. Paris, France, 70, pp. 1323–1325.

Liberatore, D. and Addessi, D. (2015) ‘Strength domains and return algorithm for the lumped plasticity equivalent frame model of masonry structures’, *Engineering Structures*, 91, pp. 167–181. doi: 10.1016/j.engstruct.2015.02.030.

Livesley, R. K. (1978) ‘Limit analysis of structures formed from rigid blocks’, *International Journal for Numerical Methods in Engineering*, 12, pp. 1853–1871. doi: 10.1002/nme.1620121207.

Lloberas-Valls, O. *et al.* (2012) ‘Multiscale domain decomposition analysis of quasi-brittle heterogeneous materials’, *International Journal for Numerical Methods in Engineering*, 89(11), pp. 1337–1366. doi: 10.1002/nme.3286.

Lode, W. (1926) ‘Versuche über den Einfluß der mittleren Hauptspannung auf das Fließen der Metalle Eisen, Kupfer und Nickel’, *Zeitschrift für Physik*, 36, p. 913. doi: 10.1007/BF01400222.

Lopez, J. *et al.* (1999) ‘A homogeneous constitutive model for masonry’, *International Journal for Numerical Methods in Engineering*, 46(10), pp. 1651–1671. doi: 10.1002/(SICI)1097-0207(19991210)46:10<1651::AID-NME718>3.0.CO;2-2.

Lotfi, H. R. and Shing, P. B. (1991) ‘An appraisal of smeared crack models for masonry shear wall analysis’, *Computers and Structures*, 41(3), pp. 413–425. doi: 10.1016/0045-7949(91)90134-8.

Lotfi, H. R. and Shing, P. B. (1994) ‘Interface model applied to fracture of masonry structures’, *Journal of Structural Engineering (United States)*, 120(1), pp. 63–80. doi: 10.1061/(ASCE)0733-9445(1994)120:1(63).

Lourenço, P. B. (1996) *Computational strategies for masonry structures*, PhD Thesis.

Lourenço, P. B., De Borst, R. and Rots, J. G. (1997) ‘A plane stress softening plasticity model for orthotropic materials’, *International Journal for Numerical*

Methods in Engineering, 40(21), pp. 4033–4057. doi: 10.1002/(SICI)1097-0207(19971115)40:21<4033::AID-NME248>3.0.CO;2-0.

Lourenço, P. B. and Rots, J. G. (1997) ‘Multisurface interface model for analysis of masonry structures’, *Journal of Engineering Mechanics*, 123(7), pp. 660–668. doi: 10.1061/(ASCE)0733-9399(1997)123:7(660).

Lourenço, P. B., Rots, J. G. and Blaauwendraad, J. (1998) ‘Continuum model for masonry: Parameter estimation and validation’, *Journal of Structural Engineering*, 124(6), pp. 642–652. doi: 10.1061/(ASCE)0733-9445(1998)124:6(642).

Lucchesi, M., Padovani, C. and Pasquinelli, G. (2000) ‘Thermodynamics of no-tension materials’, *International Journal of Solids and Structures*, 37(45), pp. 6581–6604. doi: 10.1016/S0020-7683(99)00204-8.

Luciano, R. and Sacco, E. (1997) ‘Homogenization technique and damage model for old masonry material’, *International Journal of Solids and Structures*, 34(24), pp. 3191–3208. doi: 10.1016/S0020-7683(96)00167-9.

Luciano, R. and Sacco, E. (1998) ‘A damage model for masonry structures’, *European Journal of Mechanics, A/Solids*, 17(2), pp. 285–303. doi: 10.1016/S0997-7538(98)80087-9.

Macorini, L. and Izzuddin, B. A. (2011) ‘A non-linear interface element for 3D mesoscale analysis of brick-masonry structures’, *International Journal for Numerical Methods in Engineering*, 85(12), pp. 1584–1608. doi: 10.1002/nme.3046.

Magenes, G. and Calvi, G. M. (1997) ‘In-plane seismic response of brick masonry walls’, *Earthquake Engineering and Structural Dynamics*, 96, pp. 1091–1112. doi: 10.1002/(SICI)1096-9845(199711)26:11<1091::AID-EQE693>3.0.CO;2-6.

Magenes, G. and Della Fontana, A. (1998) ‘Simplified non-linear seismic analysis of masonry buildings’, *Proceedings of the British Masonry Society*, 8(8), pp. 190–195.

Maier, G. and Nappi, A. (1990) ‘A theory of no-tension discretized structural systems’, *Engineering Structures*, 12(4), pp. 227–234. doi: 10.1016/0141-0296(90)90021-J.

Mair, R. J., Taylor, R. N. and Burland, J. B. (1996) ‘Prediction of ground movements and assessment of risk of building damage due to bored tunnelling’, in Mair, R. J. and Taylor, R. N. (eds) *Geotechnical Aspects of Underground Construction in Soft Ground – Proceedings of the International Symposium on Geotechnical Aspects of Underground Construction in Soft Ground London*. Balkema. Rotterdam.

Malomo, D., Pinho, R. and Penna, A. (2018) ‘Using the applied element method for modelling calcium silicate brick masonry subjected to in-plane cyclic loading’, *Earthquake Engineering and Structural Dynamics*, 47(7), pp. 1610–1630. doi: 10.1002/eqe.3032.

Mann, W. and Betzler, M. (1994) ‘Investigations on the effect of different forms of tests samples to test the compressive strength of masonry’, in eds. N.G. Shrive and A. Huizer (ed.) *10th International Brick/Block Masonry Conference*. University of Calgary, Calgary, Alberta, Canada, pp. 1305–1313.

Mann, W. and Muller, H. (1982) ‘Failure of Shear-Stressed Masonry: An enlarged theory, tests and application to shear walls’, *Proceedings of the British Ceramical Society*, 30, pp. 223–235.

Marfia, S. and Sacco, E. (2012) ‘Multiscale damage contact-friction model for periodic masonry walls’, *Computer Methods in Applied Mechanics and Engineering*, 205–208(1), pp. 189–203. doi: 10.1016/j.cma.2010.12.024.

Marmo, F., Masi, D. and Rosati, L. (2018) ‘Thrust network analysis of masonry helical staircases’, *International Journal of Architectural Heritage*, 12(5), pp. 828–848. doi: 10.1080/15583058.2017.1419313.

Marmo, F. and Rosati, L. (2017) ‘Reformulation and extension of the thrust network analysis’, *Computers and Structures*, 182, pp. 104–118. doi: 10.1016/j.compstruc.2016.11.016.

Marques, R. and Lourenço, P. B. (2011) ‘Possibilities and comparison of structural component models for the seismic assessment of modern unreinforced masonry buildings’, *Computers and Structures*, 89(21–22), pp. 2079–2091. doi: 10.1016/j.compstruc.2011.05.021.

Masiani, R. and Trovalusci, P. (1996) ‘Cosserat and Cauchy materials as continuum models of brick masonry’, *Meccanica*, 31(4), pp. 421–432. doi:

10.1007/BF00429930.

Massart, T. J., Peerlings, R. H. J. and Geers, M. G. D. (2007) ‘An enhanced multi-scale approach for masonry wall computations with localization of damage’, *International Journal for Numerical Methods in Engineering*, 69(5), pp. 1022–1059. doi: 10.1002/nme.1799.

Mastrodicasa, S. (1943) *Dissesti statici delle strutture edilizie. Diagnosi e Consolidamento*. Edited by Ulrico Hoepli Editore. Milano.

Mercatoris, B. C. N. and Massart, T. J. (2011) ‘A coupled two-scale computational scheme for the failure of periodic quasi-brittle thin planar shells and its application to masonry’, *International Journal for Numerical Methods in Engineering*, 85(9), pp. 1177–1206. doi: 10.1002/nme.3018.

Messali, F. and Rots, J. G. (2018) ‘In-plane drift capacity at near collapse of rocking unreinforced calcium silicate and clay masonry piers’, *Engineering Structures*, 164, pp. 183–194. doi: 10.1016/j.engstruct.2018.02.050.

Mezzina, M., Palmisano, F. and Raffaele, D. (2010) ‘The design of r.c. bridge deck subjected to horizontal actions by strut-and-tie models’, in *Bridge Maintenance, Safety, Management and Life-Cycle Optimization - Proceedings of the 5th International Conference on Bridge Maintenance, Safety and Management*, pp. 2390–2397.

Mezzina, M., Palmisano, F. and Raffaele, D. (2012) ‘Designing simply supported R.C. bridge decks subjected to in-plane actions: Strut-and-Tie model approach’, *Journal of Earthquake Engineering*, 16(4), pp. 496–514. doi: 10.1080/13632469.2011.653866.

Miglietta, P. C., Bentz, E. C. and Grasselli, G. (2017) ‘Finite/discrete element modelling of reversed cyclic tests on unreinforced masonry structures’, *Engineering Structures*, 138, pp. 159–169. doi: 10.1016/j.engstruct.2017.02.019.

Milani, G. (2008) ‘3D upper bound limit analysis of multi-leaf masonry walls’, *International Journal of Mechanical Sciences*, 50(4), pp. 817–836. doi: 10.1016/j.ijmecsci.2007.11.003.

Milani, G. (2011) ‘Simple lower bound limit analysis homogenization model for in- and out-of-plane loaded masonry walls’, *Construction and Building Materials*, 25(12), pp. 4426–4443. doi: 10.1016/j.conbuildmat.2011.01.012.

Milani, G. *et al.* (2012) ‘Seismic assessment of a medieval masonry tower in Northern Italy by limit, nonlinear static, and full dynamic analyses’, *International Journal of Architectural Heritage*, 6(5), pp. 489–524. doi: 10.1080/15583058.2011.588987.

Milani, G. (2015) ‘Upper bound sequential linear programming mesh adaptation scheme for collapse analysis of masonry vaults’, *Advances in Engineering Software*, 79, pp. 91–110. doi: 10.1016/j.advengsoft.2014.09.004.

Milani, G., Lourenço, P. B. and Tralli, A. (2006a) ‘Homogenised limit analysis of masonry walls, Part I: Failure surfaces’, *Computers and Structures*, 84(3–4), pp. 166–180. doi: 10.1016/j.compstruc.2005.09.005.

Milani, G., Lourenço, P. B. and Tralli, A. (2006b) ‘Homogenised limit analysis of masonry walls, Part II: Structural examples’, *Computers and Structures*, 84(3–4), pp. 181–195. doi: 10.1016/j.compstruc.2005.09.004.

Milani, G., Lourenço, P. and Tralli, A. (2006) ‘Homogenization approach for the limit analysis of out-of-plane loaded masonry walls’, *Journal of Structural Engineering*, 132(10), pp. 1650–1663. doi: 10.1061/(ASCE)0733-9445(2006)132:10(1650).

Milani, G., Lourenço, P. and Tralli, A. (2007) ‘3D homogenized limit analysis of masonry buildings under horizontal loads’, *Engineering Structures*, 29(11), pp. 3134–3148. doi: 10.1016/j.engstruct.2007.03.003.

Milani, G. and Valente, M. (2015) ‘Failure analysis of seven masonry churches severely damaged during the 2012 Emilia-Romagna (Italy) earthquake: Non-linear dynamic analyses vs conventional static approaches’, *Engineering Failure Analysis*, 54, pp. 13–56. doi: 10.1016/j.engfailanal.2015.03.016.

Minga, E., Macorini, L. and Izzuddin, B. A. (2018) ‘Enhanced mesoscale partitioned modelling of heterogeneous masonry structures’, *International Journal for Numerical Methods in Engineering*, 113(13), pp. 1950–1971. doi: 10.1002/nme.5728.

Ministero delle infrastrutture e dei trasporti. (2018) *Decreto ministeriale 17 gennaio 2018 - Aggiornamento delle «Norme tecniche per le costruzioni»*.

Ministero delle infrastrutture e dei trasporti. (2019) *CIRCOLARE 21 gennaio 2019, n. 7 C.S.LL.PP - Istruzioni per l'applicazione dell'«Aggiornamento delle*

‘Norme tecniche per le costruzioni’».

von Mises, R. (1913) ‘Mechanik der festen Körper im plastisch-deformablen Zustand’, *Nachrichten von der Gesellschaft der Wissenschaften zu Göttingen, Mathematisch-Physikalische Klasse*, pp. 582–592.

Mistler, M., Anthoine, A. and Butenweg, C. (2007) ‘In-plane and out-of-plane homogenisation of masonry’, *Computers and Structures*, 85(17–18), pp. 1321–1330. doi: 10.1016/j.compstruc.2006.08.087.

Moon, F. L. *et al.* (2006) ‘Recommendations for seismic evaluation and retrofit of low-rise URM structures’, *Journal of Structural Engineering*, 132(5), pp. 663–672. doi: 10.1061/(ASCE)0733-9445(2006)132:5(663).

Moreau, J. J. (1988) ‘Unilateral Contact and Dry Friction in Finite Freedom Dynamics’, in Moreau, J. J. and Panagiotopoulos, P. D. (eds) *Nonsmooth Mechanics and Applications*. Springer. Vienna.

Munjiza, A. (2004) *The combined finite-discrete element method, The Combined Finite-Discrete Element Method*. doi: 10.1002/0470020180.

Musgrove, J. and Fletcher, B. (1987) *Sir Banister Fletcher’s: A history of architecture*. Edited by Butterworths. London, UK.

O’Dwyer, D. (1999) ‘Funicular analysis of masonry vaults’, *Computers and Structures*, 73(1–5), pp. 187–197. doi: 10.1016/S0045-7949(98)00279-X.

Odqvist, F. K. G. (1933) ‘Die Verfestigung von flußeisenähnlichen Körpern. Ein Beitrag zur Plastizitätstheorie’, *ZAMM - Journal of Applied Mathematics and Mechanics / Zeitschrift für Angewandte Mathematik und Mechanik*, 13(5), pp. 360–363.

Oliveira, D. V. and Lourenço, P. B. (2004) ‘Implementation and validation of a constitutive model for the cyclic behaviour of interface elements’, *Computers and Structures*, 82(17–19), pp. 1451–1461. doi: 10.1016/j.compstruc.2004.03.041.

Orduña, A. and Lourenço, P. B. (2005a) ‘Three-dimensional limit analysis of rigid blocks assemblages. Part I: Torsion failure on frictional interfaces and limit analysis formulation’, *International Journal of Solids and Structures*, 42(18–19), pp. 5140–5160. doi: 10.1016/j.ijsolstr.2005.02.010.

Orduña, A. and Lourenço, P. B. (2005b) ‘Three-dimensional limit analysis of rigid blocks assemblages. Part II: Load-path following solution procedure and validation’, *International Journal of Solids and Structures*, 42(18–19), pp. 5161–5180. doi: 10.1016/j.ijsolstr.2005.02.011.

Page, A. W. (1981) ‘An Experimental Investigation of the Biaxial Strength of Brick Masonry’, *Proceedings of the Institution of Civil Engineers*, 71(2), pp. 893–906.

Page, A. W. (1982) ‘An Experimental Investigation of the Biaxial Strength of Brick Masonry’, *6th International Brick Masonry Conference*, 71(2), pp. 893–906.

Page, A. W. (1983) ‘The Strength of Brick Masonry Under Biaxial Tension-Compression’, *International Journal of Masonry Construction*, 3(1).

Palmisano, F. (2005) ‘Form and structure in the harmonious complexity of the building process: From conceptual design to detailing in some reinforced concrete works’, *Structural Concrete*, 6(3), pp. 122–123.

Palmisano, F. *et al.* (2007) ‘Collapse of the Giotto Avenue Building in Foggia’, *Structural Engineering International: Journal of the International Association for Bridge and Structural Engineering (IABSE)*, 17(2), pp. 166–171. doi: 10.2749/101686607780680709.

Palmisano, F. (2013) ‘Interpretation of the behaviour of masonry arches and domes by simple models’, in *WIT Transactions on the Built Environment*, pp. 233–244. doi: 10.2495/STR130201.

Palmisano, F. (2014) ‘Assessment of masonry arches and domes by simple models’, *International Journal of Structural Engineering*, 5(1), pp. 63–75. doi: 10.1504/IJSTRUCTE.2014.058684.

Palmisano, F. (2016) ‘Rapid diagnosis of crack patterns of masonry buildings subjected to landslide-induced settlements by using the load path method’, *International Journal of Architectural Heritage*, 10(4), pp. 438–456. doi: 10.1080/15583058.2014.996922.

Palmisano, F. and Elia, A. (2013) ‘Structural behaviour of masonry buildings subjected to landslide: Load path method approach’, in *Structures and Architecture: Concepts, Applications and Challenges - Proceedings of the 2nd*

International Conference on Structures and Architecture, ICSA 2013, pp. 888–895.

Palmisano, F. and Elia, A. (2014) ‘Behaviour of masonry buildings subjected to landslide-induced settlements’, *International Journal of Structural Engineering*, 5(2), pp. 93–114. doi: 10.1504/IJSTRUCTE.2014.060891.

Palmisano, F. and Elia, A. (2015) ‘Shape optimization of strut-and-tie models in masonry buildings subjected to landslide-induced settlements’, *Engineering Structures*, 84, pp. 223–232. doi: 10.1016/j.engstruct.2014.11.030.

Palmisano, F. and Totaro, A. (2010) ‘Load Path Method in the interpretation of dome behaviour’, in *Structures and Architecture - Proceedings of the 1st International Conference on Structures and Architecture, ICSA 2010*, pp. 1880–1887.

Palmisano, F., Vitone, A. and Vitone, C. (2002) ‘Form & Structure The Rome Auditorium: Load path method’, *D’Architettura*, 18, pp. 168–173.

Palmisano, F., Vitone, A. and Vitone, C. (2003) ‘From load path method to classical models of structural analysis’, in Bomptemi, F. (ed.) *System-based Vision For Strategic and Creative Design*. Balkema. Rotterdam, pp. 589–596.

Palmisano, F., Vitone, A. and Vitone, C. (2008) ‘A first approach to optimum design of cable-supported bridges using load path method’, *Structural Engineering International: Journal of the International Association for Bridge and Structural Engineering (IABSE)*, 18(4), pp. 412–420. doi: 10.2749/101686608786455270.

Pantò, B. *et al.* (2016) ‘3D macro-element modelling approach for seismic assessment of historical masonry churches’, *Advances in Engineering Software*, 97, pp. 40–59. doi: 10.1016/j.advengsoft.2016.02.009.

Pantò, B., Calì, I. and Lourenço, P. B. (2018) ‘A 3D discrete macro-element for modelling the out-of-plane behaviour of infilled frame structures’, *Engineering Structures*, 175, pp. 371–385. doi: 10.1016/j.engstruct.2018.08.022.

Papa, E. (1996) ‘Unilateral damage model for masonry based on a homogenisation procedure’, *Mechanics of Cohesive-Frictional Materials*, 1(4), pp. 349–366. doi: 10.1002/(sici)1099-1484(199610)1:4<349::aid-cfm18>3.0.co;2-m.

Papantonopoulos, C. *et al.* (2002) ‘Numerical prediction of the earthquake response of classical columns using the distinct element method’, *Earthquake Engineering and Structural Dynamics*, 31(9), pp. 1699–1717. doi: 10.1002/eqe.185.

Parisi, F. *et al.* (2013) ‘Rocking response assessment of in-plane laterally-loaded masonry walls with openings’, *Engineering Structures*, 56, pp. 1234–1248. doi: 10.1016/j.engstruct.2013.06.041.

Parisi, F. and Augenti, N. (2013) ‘Seismic capacity of irregular unreinforced masonry walls with openings’, *Earthquake Engineering and Structural Dynamics*, 42(1), pp. 101–121. doi: 10.1002/eqe.2195.

Parrinello, F., Failla, B. and Borino, G. (2009) ‘Cohesive-frictional interface constitutive model’, *International Journal of Solids and Structures*, 46(13), pp. 2680–2692. doi: 10.1016/j.ijsolstr.2009.02.016.

Pasticier, L., Amadio, C. and Fragiaco, M. (2008) ‘Non-linear seismic analysis and vulnerability evaluation of a masonry building by means of the SAP2000 V.10 code’, *Earthquake Engineering and Structural Dynamics*, 37(3), pp. 467–485. doi: 10.1002/eqe.770.

Pelà, L. *et al.* (2014) ‘A localized mapped damage model for orthotropic materials’, *Engineering Fracture Mechanics*, 124–125, pp. 196–216. doi: 10.1016/j.engfracmech.2014.04.027.

Pelà, L., Aprile, A. and Benedetti, A. (2009) ‘Seismic assessment of masonry arch bridges’, *Engineering Structures*, 31(8), pp. 1777–1788. doi: 10.1016/j.engstruct.2009.02.012.

Pelà, L., Cervera, M. and Roca, P. (2011) ‘Continuum damage model for orthotropic materials: Application to masonry’, *Computer Methods in Applied Mechanics and Engineering*, 200(9–12), pp. 917–930. doi: 10.1016/j.cma.2010.11.010.

Pelà, L., Cervera, M. and Roca, P. (2013) ‘An orthotropic damage model for the analysis of masonry structures’, *Construction and Building Materials*, 41, pp. 957–967. doi: 10.1016/j.conbuildmat.2012.07.014.

Penelis, G. G. (2006) ‘An efficient approach for pushover analysis of unreinforced masonry (URM) structures’, *Journal of Earthquake Engineering*,

10(3), pp. 359–379. doi: 10.1080/13632460609350601.

Penna, A., Lagomarsino, S. and Galasco, A. (2014) ‘A nonlinear macroelement model for the seismic analysis of masonry buildings’, *Earthquake Engineering and Structural Dynamics*, 43(2), pp. 159–179. doi: 10.1002/eqe.2335.

Petracca, M. *et al.* (2016) ‘Regularization of first order computational homogenization for multiscale analysis of masonry structures’, *Computational Mechanics*, 57(2), pp. 257–276. doi: 10.1007/s00466-015-1230-6.

Petracca, M., Pelà, L., Rossi, R., Zaghi, S., *et al.* (2017) ‘Micro-scale continuous and discrete numerical models for nonlinear analysis of masonry shear walls’, *Construction and Building Materials*, 149, pp. 296–314. doi: 10.1016/j.conbuildmat.2017.05.130.

Petracca, M., Pelà, L., Rossi, R., Oller, S., *et al.* (2017) ‘Multiscale computational first order homogenization of thick shells for the analysis of out-of-plane loaded masonry walls’, *Computer Methods in Applied Mechanics and Engineering*, 315, pp. 273–301. doi: 10.1016/j.cma.2016.10.046.

Petry, S. and Beyer, K. (2014) ‘Influence of boundary conditions and size effect on the drift capacity of URM walls’, *Engineering Structures*, 65, pp. 76–88. doi: 10.1016/j.engstruct.2014.01.048.

Del Piero, G. (1989) ‘Constitutive equation and compatibility of the external loads for linear elastic masonry-like materials’, *Meccanica*, 24(3), pp. 150–162. doi: 10.1007/BF01559418.

Pietruszczak, S. and Niu, X. (1992) ‘A mathematical description of macroscopic behaviour of brick masonry’, *International Journal of Solids and Structures*, 29(5), pp. 531–546. doi: 10.1016/0020-7683(92)90052-U.

Pietruszczak, S. and Ushaksaraei, R. (2003) ‘Description of inelastic behaviour of structural masonry’, *International Journal of Solids and Structures*, 40(15), pp. 4003–4019. doi: 10.1016/S0020-7683(03)00174-4.

Portioli, F. *et al.* (2013) ‘Limit analysis by linear programming of 3D masonry structures with associative friction laws and torsion interaction effects’, *Archive of Applied Mechanics*, 83(10), pp. 1415–1438. doi: 10.1007/s00419-013-0755-4.

Portioli, F. *et al.* (2014) ‘Limit analysis of 3D masonry block structures with non-

associative frictional joints using cone programming’, *Computers and Structures*, 143, pp. 108–121. doi: 10.1016/j.compstruc.2014.07.010.

Prager, W. (1952) ‘The general theory of limit design’, in *Proceedings of the 8th International Congress of Theoretical and Applied Mechanics*, pp. 65–72.

Prager, W. (1959) *An Introduction to Plasticity*. Addison-Wesley Publishing Company.

Quagliarini, E., Maracchini, G. and Clementi, F. (2017) ‘Uses and limits of the Equivalent Frame Model on existing unreinforced masonry buildings for assessing their seismic risk: A review’, *Journal of Building Engineering*, 10, pp. 166–182. doi: 10.1016/j.jobe.2017.03.004.

Rafiee, A. and Vinches, M. (2013) ‘Mechanical behaviour of a stone masonry bridge assessed using an implicit discrete element method’, *Engineering Structures*, 48, pp. 739–749. doi: 10.1016/j.engstruct.2012.11.035.

Rafiee, A., Vinches, M. and Bohatier, C. (2008) ‘Application of the NSCD method to analyse the dynamic behaviour of stone arched structures’, *International Journal of Solids and Structures*, 45(25–26), pp. 6269–6283. doi: 10.1016/j.ijsolstr.2008.07.034.

Raka, E. *et al.* (2015) ‘Advanced frame element for seismic analysis of masonry structures: Model formulation and validation’, *Earthquake Engineering and Structural Dynamics*, 44(14), pp. 2489–2506. doi: 10.1002/eqe.2594.

Reccia, E. *et al.* (2018) ‘A multiscale/multidomain model for the failure analysis of masonry walls: A validation with a combined FEM/DEM approach’, *International Journal for Multiscale Computational Engineering*, 16(4), pp. 325–343. doi: 10.1615/IntJMultCompEng.2018026988.

Reddy, J. N. (2004) *An introduction to nonlinear finite element analysis*. Edited by Oxford University Press. Oxford.

Reuss, A. (1930) ‘Berücksichtigung der elastischen Formänderung in der Plastizitätstheorie’, *ZAMM - Journal of Applied Mathematics and Mechanics / Zeitschrift für Angewandte Mathematik und Mechanik*, 10(3), pp. 266–274.

Reyes, E. *et al.* (2009) ‘An embedded cohesive crack model for finite element analysis of brickwork masonry fracture’, *Engineering Fracture Mechanics*,

76(12), pp. 1930–1944. doi: 10.1016/j.engfracmech.2009.05.002.

Rinaldin, G., Amadio, C. and Macorini, L. (2016) ‘A macro-model with nonlinear springs for seismic analysis of URM buildings’, *Earthquake Engineering and Structural Dynamics*, 45(14), pp. 2261–2281. doi: 10.1002/eqe.2759.

Ritter, W. (1899) ‘Die Bauweise Hennebique’, *Schweizerische Bauzeitung*.

Roca, P. *et al.* (2010) ‘Structural analysis of masonry historical constructions. Classical and advanced approaches’, *Archives of Computational Methods in Engineering*, 17(3), pp. 299–325. doi: 10.1007/s11831-010-9046-1.

Roca, P. *et al.* (2011) ‘Capacity of shear walls by simple equilibrium models’, *International Journal of Architectural Heritage*, 5(4–5), pp. 412–435. doi: 10.1080/15583058.2010.501481.

Roca, P., Molins, C. and Mari, A. R. (2005) ‘Strength capacity of masonry wall structures by the equivalent frame method’, *Journal of Structural Engineering*, 131(10), pp. 1601–1610. doi: 10.1061/(ASCE)0733-9445(2005)131:10(1601).

Rots, J. G. (1991) ‘Numerical simulation of cracking in structural masonry’, *Heron*, 36(2), pp. 49–63.

Rots, J. G. (1997) *Structural masonry: an experimental/numerical basis for practical design rules*. Edited by AA Balkema. Leiden.

Rots, J. G. *et al.* (2016) ‘Computational modelling of masonry with a view to Groningen induced seismicity’, in *Structural Analysis of Historical Constructions: Anamnesis, diagnosis, therapy, controls - Proceedings of the 10th International Conference on Structural Analysis of Historical Constructions, SAHC 2016*, pp. 227–238.

Rots, J. G., Belletti, B. and Invernizzi, S. (2008) ‘Robust modeling of RC structures with an “event-by-event” strategy’, *Engineering Fracture Mechanics*, 75(3–4), pp. 590–614. doi: 10.1016/j.engfracmech.2007.03.027.

Sacco, E. (2009) ‘A nonlinear homogenization procedure for periodic masonry’, *European Journal of Mechanics, A/Solids*, 28(2), pp. 209–222. doi: 10.1016/j.euromechsol.2008.06.005.

Sacco, E., Addessi, D. and Sab, K. (2018) ‘New trends in mechanics of masonry’,

Meccanica, 53(7), pp. 1565–1569. doi: 10.1007/s11012-018-0839-x.

de Saint Venant, A. J. C. B. (1870) ‘Mémoire sur l’établissement des équations différentielles des mouvements intérieurs opérés dans les corps solides ductiles au delà des limites où l’élasticité pourrait les ramener à leur premier état.’, *Comptes-rendus de l’académie des sciences*. Paris, France, 70, pp. 473–480.

Salerno, G. and de Felice, G. (2009) ‘Continuum modeling of periodic brickwork’, *International Journal of Solids and Structures*, 46(5), pp. 1251–1267. doi: 10.1016/j.ijsolstr.2008.10.034.

Saloustros, S. *et al.* (2018) ‘An Enhanced Finite Element Macro-Model for the Realistic Simulation of Localized Cracks in Masonry Structures: A Large-Scale Application’, *International Journal of Architectural Heritage*, 12(3), pp. 432–447. doi: 10.1080/15583058.2017.1323245.

Saloustros, S., Pelà, L. and Cervera, M. (2015) ‘A crack-tracking technique for localized cohesive-frictional damage’, *Engineering Fracture Mechanics*, 150, pp. 96–114. doi: 10.1016/j.engfracmech.2015.10.039.

Samarasinghe, W. and Hendry, A. W. (1980) ‘The Strength of Brickwork under Biaxial Tensile and Compressive Stress’, in *Proceedings of the 7th International Symposium on Load Bearing Brickwork*. London, UK.

Sandoval, C. and Arnau, O. (2017) ‘Experimental characterization and detailed micro-modeling of multi-perforated clay brick masonry structural response’, *Materials and Structures/Materiaux et Constructions*, 50(1). doi: 10.1617/s11527-016-0888-3.

Sarhosis, V., Forgács, T. and Lemos, J. V. (2019) ‘A discrete approach for modelling backfill material in masonry arch bridges’, *Computers and Structures*, 224. doi: 10.1016/j.compstruc.2019.106108.

Sarhosis, V., Forgács, T. and Lemos, J. V. (2020) *Modelling Backfill in Masonry Arch Bridges: A DEM Approach, Structural Integrity*. doi: 10.1007/978-3-030-29227-0_16.

Sarhosis, V. and Lemos, J. V. (2018) ‘A detailed micro-modelling approach for the structural analysis of masonry assemblages’, *Computers and Structures*, 206, pp. 66–81. doi: 10.1016/j.compstruc.2018.06.003.

Sarhosis, V., Lemos, J. V and Milani, G. (2016) *Computational Modeling of Masonry Structures Using the Discrete Element Method, Civil and Industrial Engineering*.

Sarhosis, V. and Sheng, Y. (2014) ‘Identification of material parameters for low bond strength masonry’, *Engineering Structures*, 60, pp. 100–110. doi: 10.1016/j.engstruct.2013.12.013.

Schlaich, J., Schaefer, K. and Jennewein, M. (1987) ‘Toward a consistent design of structural concrete.’, *PCI Journal*, 32(3), pp. 74–150. doi: 10.15554/pcij.05011987.74.150.

Schmidt, R. (1932) ‘Über den Zusammenhang von Spannungen und Formänderungen im Verfestigungsgebiet’, *Ingenieur-Archiv*, 3, p. 215. doi: 10.1007/BF02079970.

Senthivel, R. and Lourenço, P. B. (2009) ‘Finite element modelling of deformation characteristics of historical stone masonry shear walls’, *Engineering Structures*, 31(9), pp. 1930–1943. doi: 10.1016/j.engstruct.2009.02.046.

Serpieri, R., Albarella, M. and Sacco, E. (2017) ‘A 3D microstructured cohesive–frictional interface model and its rational calibration for the analysis of masonry panels’, *International Journal of Solids and Structures*, 122–123, pp. 110–127. doi: 10.1016/j.ijsolstr.2017.06.006.

Shi, G.-H. (1992) ‘Discontinuous deformation analysis: A new numerical model for the statics and dynamics of deformable block structures’, *Engineering Computations*, 9(2), pp. 157–168. doi: 10.1108/eb023855.

Shi, H. *et al.* (2013) ‘Load path analysis of a floating concrete gate using finite element method’, *Structural Engineer*, pp. 38–41.

Siano, R. *et al.* (2018) ‘Numerical investigation of non-linear equivalent-frame models for regular masonry walls’, *Engineering Structures*, 173, pp. 512–529. doi: 10.1016/j.engstruct.2018.07.006.

Silva, L. C., Lourenço, P. B. and Milani, G. (2017) ‘Nonlinear discrete homogenized model for out-of-plane loaded masonry walls’, *Journal of Structural Engineering (United States)*, 143(9). doi: 10.1061/(ASCE)ST.1943-541X.0001831.

Simon, J. and Bagi, K. (2016) ‘Discrete element analysis of the minimum thickness of oval masonry domes’, *International Journal of Architectural Heritage*, 10(4), pp. 457–475. doi: 10.1080/15583058.2014.996921.

Smoljanović, H. *et al.* (2018) ‘Numerical analysis of 3D dry-stone masonry structures by combined finite-discrete element method’, *International Journal of Solids and Structures*, 136–137, pp. 150–167. doi: 10.1016/j.ijsolstr.2017.12.012.

Smoljanović, H., Nikolić, Z. and Živaljić, N. (2015) ‘A combined finite-discrete numerical model for analysis of masonry structures’, *Engineering Fracture Mechanics*, 136, pp. 1–14. doi: 10.1016/j.engfracmech.2015.02.006.

Smoljanović, H., Živaljić, N. and Nikolić, Ž. (2013) ‘A combined finite-discrete element analysis of dry stone masonry structures’, *Engineering Structures*, 52, pp. 89–100. doi: 10.1016/j.engstruct.2013.02.010.

Stefanou, I., Sab, K. and Heck, J.-V. (2015) ‘Three dimensional homogenization of masonry structures with building blocks of finite strength: A closed form strength domain’, *International Journal of Solids and Structures*, 54, pp. 258–270. doi: 10.1016/j.ijsolstr.2014.10.007.

Stefanou, I., Sulem, J. and Vardoulakis, I. (2008) ‘Three-dimensional Cosserat homogenization of masonry structures: Elasticity’, *Acta Geotechnica*, 3(1), pp. 71–83. doi: 10.1007/s11440-007-0051-y.

Sutcliffe, D. J., Yu, H. S. and Page, A. W. (2001) ‘Lower bound limit analysis of unreinforced masonry shear walls’, *Computers and Structures*, 79(14), pp. 1295–1312. doi: 10.1016/S0045-7949(01)00024-4.

Taliercio, A. (2014) ‘Closed-form expressions for the macroscopic in-plane elastic and creep coefficients of brick masonry’, *International Journal of Solids and Structures*, 51(17), pp. 2949–2963. doi: 10.1016/j.ijsolstr.2014.04.019.

Tassios, T. P. (1988) *Meccanica delle murature*. Edited by Liguori Ed. Napoli.

Thavalingam, A. *et al.* (2001) ‘Computational framework for discontinuous modelling of masonry arch bridges’, *Computers and Structures*, 79(19), pp. 1821–1830. doi: 10.1016/S0045-7949(01)00102-X.

Tiberti, S., Acito, M. and Milani, G. (2016) ‘Comprehensive FE numerical

insight into Finale Emilia Castle behavior under 2012 Emilia Romagna seismic sequence: Damage causes and seismic vulnerability mitigation hypothesis’, *Engineering Structures*, 117, pp. 397–421. doi: 10.1016/j.engstruct.2016.02.048.

Tomažević, M. (1978) *The computer program POR*.

De Tommasi, G., Monaco, P. and Vitone, C. (2003) ‘A first approach to the load path method on masonry structure behaviour’, in *Advances in Architecture*, pp. 287–296.

Tóth, A. R., Orbán, Z. and Bagi, K. (2009) ‘Discrete element analysis of a stone masonry arch’, *Mechanics Research Communications*, 36(4), pp. 469–480. doi: 10.1016/j.mechrescom.2009.01.001.

Toti, J., Gattulli, V. and Sacco, E. (2015) ‘Nonlocal damage propagation in the dynamics of masonry elements’, *Computers and Structures*, 152, pp. 215–227. doi: 10.1016/j.compstruc.2015.01.011.

Tran-Cao, T. (2009) *COLLAPSE ANALYSIS OF BLOCK STRUCTURES IN FRICTIONAL CONTACT*. The University of New South Wales, Sydney, Australia.

Tresca, H. (1864) ‘Memoir on the flow of solid bodies under strong pressure’, *Comptes-rendus de l’académie des sciences*. Paris, France, 59, p. 754.

Trovalusci, P. (1992) ‘No-tension discrete model with friction for jointed block masonry walls using interface elements’, in *Proceedings, ANSYS Technology Conference and Exhibition*. Pittsburgh, pp. 73–82.

Valente, M. and Milani, G. (2016) ‘Seismic assessment of historical masonry towers by means of simplified approaches and standard FEM’, *Construction and Building Materials*, 108, pp. 74–104. doi: 10.1016/j.conbuildmat.2016.01.025.

Vitone, C. (2001) *Il Load Path Method Per Il Restauro Strutturale Delle Opere Murarie*. Politecnico di Bari.

Wei, X. and Hao, H. (2009) ‘Numerical derivation of homogenized dynamic masonry material properties with strain rate effects’, *International Journal of Impact Engineering*, 36(3), pp. 522–536. doi: 10.1016/j.ijimpeng.2008.02.005.

Wilding, B. V., Dolatshahi, K. M. and Beyer, K. (2017) ‘Influence of load history on the force-displacement response of in-plane loaded unreinforced masonry

walls’, *Engineering Structures*, 152, pp. 671–682. doi: 10.1016/j.engstruct.2017.09.038.

Zampieri, P. *et al.* (2017) ‘Failure analysis of masonry arch bridges subject to local pier scour’, *Engineering Failure Analysis*, 79, pp. 371–384. doi: 10.1016/j.engfailanal.2017.05.028.

Zampieri, P., Amoroso, M. and Pellegrino, C. (2019) ‘The masonry buttressed arch on spreading support’, *Structures*, 20, pp. 226–236. doi: 10.1016/j.istruc.2019.03.008.

Zampieri, P., Zanini, M. A. and Modena, C. (2015) ‘Simplified seismic assessment of multi-span masonry arch bridges’, *Bulletin of Earthquake Engineering*, 13(9), pp. 2629–2646. doi: 10.1007/s10518-015-9733-2.

Zhai, C. *et al.* (2017) ‘Numerical Simulation of Masonry-Infilled RC Frames Using XFEM’, *Journal of Structural Engineering (United States)*, 143(10). doi: 10.1061/(ASCE)ST.1943-541X.0001886.

Zhang, Y., Macorini, L. and Izzuddin, B. A. (2016) ‘Mesoscale partitioned analysis of brick-masonry arches’, *Engineering Structures*, 124, pp. 142–166. doi: 10.1016/j.engstruct.2016.05.046.

Zucchini, A. and Lourenço, P. B. (2002) ‘A micro-mechanical model for the homogenisation of masonry’, *International Journal of Solids and Structures*, 39(12), pp. 3233–3255. doi: 10.1016/S0020-7683(02)00230-5.

Zucchini, A. and Lourenço, P. B. (2004) ‘A coupled homogenisation-damage model for masonry cracking’, *Computers and Structures*, 82(11–12), pp. 917–929. doi: 10.1016/j.compstruc.2004.02.020.

Zucchini, A. and Lourenço, P. B. (2009) ‘A micro-mechanical homogenisation model for masonry: Application to shear walls’, *International Journal of Solids and Structures*, 46(3–4), pp. 871–886. doi: 10.1016/j.ijsolstr.2008.09.034.

Chapter 4

Proposed rigid block models for linear and non-linear kinematic analysis

The contents of Chapter 4 are published in (Cascini, Gagliardo and Portioli, 2020; Gagliardo et al., 2021).

4.1 Introduction

In this chapter, two numerical models for the masonry structures analysis will be proposed and described, essentially a linear kinematic model with rigid contacts and a non-linear kinematic model with no-tension elastic contacts. The two formulations are somehow part of the same computational project developed at the University of Naples “Federico II” by Francesco Portioli and Lucrezia Cascini. Both models are MATLAB® based tools worked as rigid block-based strategy for the assessment of masonry types under seismic-induced lateral loads or settlement-induced support movements. As already declared in the objectives and motivations, the present dissertation thesis is mainly devoted to the analysis of masonry structures affected by ground movements related to foundation settlements. The analysis of the structural response of masonry buildings subjected to settlement demands for appropriate numerical models for masonry as well as accurate and reliable methods for damage assessment. In recent years, several modelling approaches were developed for this purpose (D’Altri *et al.*, 2020). The various numerical models look for the best way to account for the

heterogeneous and nonlinear behaviour of masonry, especially in the case of the low tensile strength in historic buildings (Foraboschi, 2019). Among these numerical approaches, it is worth mentioning the finite element models (Giardina *et al.*, 2013; Amorosi *et al.*, 2014; Reccia *et al.*, 2014; Alessandri *et al.*, 2015; Giardina, Hendriks and Rots, 2015; Milani *et al.*, 2016; Rossi, Calderini and Lagomarsino, 2016; D’Altri *et al.*, 2018, 2019; De-Felice and Malena, 2019), the distinct element models (Al-Heib, 2012; Bui and Limam, 2012; McInerney and Dejong, 2015; Bui *et al.*, 2017), the rigid body spring models (Galassi, Paradiso and Tempesta, 2013; Baraldi and Cecchi, 2017; Bertolesi, Milani and Casolo, 2018; Galassi *et al.*, 2018, 2020) and the multi-spring macro element models (Caliò *et al.*, 2013; Lagomarsino *et al.*, 2013; Pantò *et al.*, 2016; Nicodemo *et al.*, 2020). Limit analysis has been becoming as a valid alternative for the assessment of failure mechanisms and crack patterns in masonry structures subjected to settlement (Gilbert, 2001; Orduña and Lourenço, 2005a, 2005b; Angelillo *et al.*, 2018; Iannuzzo *et al.*, 2018; Angelillo, 2019; Nodargi, Intrigila and Bisegna, 2019; LimitState Ltd., 2020; Tiberti *et al.*, 2020). In this framework, a comparison among various numerical approaches was provided in (Pepe, Pingaro, *et al.*, 2020; Pepe, Sangirardi, *et al.*, 2020). With the scope to overcome shortages of the classical assumptions of limit analysis – i.e. infinitesimal displacement field –, analytical and numerical formulations based on sequential limit analysis were also proposed in literature with the goal to account for the structural performance in the large displacement regime (Block, Ciblac and Ochsendorf, 2006; Ochsendorf, 2006; Coccia, Di Carlo and Rinaldi, 2015; Di Carlo, Coccia and Rinaldi, 2018; Zampieri *et al.*, 2018; Zampieri, Amoroso and Pellegrino, 2019; Di Carlo and Coccia, 2020; Tralli *et al.*, 2020).

As already declared, this chapter describes two rigid block-based numerical proposal aiming at showing their numerical features in terms of geometrical and mechanical assumption and in terms of specific input and output data. It is worth noting that the computational project developed in this thesis is framed within the tradition and the theoretical background described in detail in the previous Chapter in the section devoted to the state of art of rigid block limit analysis approach.

The first numerical proposal is a linear kinematic rigid block model with rigid contacts based on the lower bound theorem of limit analysis (Cascini, Gagliardo and Portioli, 2020). The formulation is condensed in an in-house computational tool, namely LiABlock_3D which is provided with a very simple Graphical User Interface (GUI). The software can investigate the structural behaviour of 3D masonry structures made by polyhedral blocks. The type of action the code is able to simulate are both lateral live loads and displacement at the base support. The latter means the numerical procedure is able to investigate the structural masonry behaviour for both seismic action and settlement effects. The outcome this proposal can provide are essentially the value of the load factor (or collapse multiplier) and the value of the collapse loads.

The second numerical proposal can be ascribed as an extension of the previous limit analysis model to the large-displacement regime (Gagliardo *et al.*, 2021), namely a non-linear kinematic rigid block model with no-tension elastic contacts. The idea is to develop an iterative step-by-step numerical procedure where the starting configuration per each step corresponds to the mechanism predicted in the previous step. In such a case, the computational tool implements a non-linear kinematic analysis. With regard to the consistency of the model, the second proposed procedure is currently able to analyse only planar case studies. In this case the tool is not provided with a dedicated Graphical User Interface, but the analysis is performed directly running in the MATLAB® command window. Furthermore, the non-linear kinematic model is mainly devoted to the analysis of the structural response of masonry structures subjected to foundation settlement. So, the model in the current form is not able to investigate the seismic performance of the specific case study. The reason for this kind of limitation is that the second numerical procedure was developed for the first time within the activities of the present doctoral program, which is mainly devoted to the assessment and prediction of collapse mechanism for masonry structures affected by landslide (or subsidence) induced ground movements. It is worth noting that the two numerical proposals (especially the second one) are part of an on-going computational project, so it is expected to improve their capabilities and fields of application.

The next sections are devoted to the description of the two proposed rigid block numerical formulations. The linear kinematic analysis approach is based on the implementation of a classic lower bound formulation of limit analysis applied to 2D or 3D collection of rigid blocks with rigid contacts whereas the non-linear kinematic model is formulated as a linear complementarity problem in the field of large displacements with unilateral elastic contact interfaces for the analysis of 2D case studies. The two computational proposals are deeply described below, with regard to the adopted mathematical formulation.

4.2 Rigid block model with rigid contacts for linear kinematic analysis

The first proposed numerical proposal deals with a rigid block limit analysis model, based on a linear kinematic approach for the investigation of structural response of masonry structures. The numerical formulation was condensed in an in-house code, named LiABlock_3D and described in (Cascini, Gagliardo and Portioli, 2020). The software is particularly suitable for the analysis of monumental buildings made of large masonry blocks or stones and masonry assemblages with regular or complex bond patterns, such as arched structures and vaults, under the assumption of negligible mortar contribution. The software is a MATLAB® based tool with a Graphical User Interface (GUI) and implements a limit equilibrium analysis problem. The input data consists of a geometric 3D-model, which can be generated in a Computer Aided Design (CAD) environment, ensuring in such way a very high flexibility in terms of structural configurations and masonry texture. The GUI provides a simple interface to initialize the masonry properties (friction coefficient and weight per unit volume) as well as boundary and loading conditions (Amorosi *et al.*, 2014).

LiABlock_3D is able to analyse 3D structures made of polyhedral blocks in contact by means of quadrilateral interfaces. The routine implemented consists in creating the geometry of the assemblage in AutoCAD, exporting relevant data to a Microsoft Excel data sheet and importing them in LiABlock_3D for the generation of the numerical model. For a given 3D block structure, the first steps are to identify the block types used to discretize the structural assemblage (i.e.,

rectangular and polyhedral blocks) and the associated contact interfaces. Block types are modelled as Autodesk CAD blocks with attributes. The information required for each block type are the Cartesian coordinates of the vertexes of the polyhedron, which define the geometry, its centroid, and the coordinates of vertexes associated to each contact interface. In the CAD block editor, object “points” are used to represent the above-mentioned points and position attributes are assigned to them. Additional attributes are attached to the block types to store the block volume and the labels of contact interface.

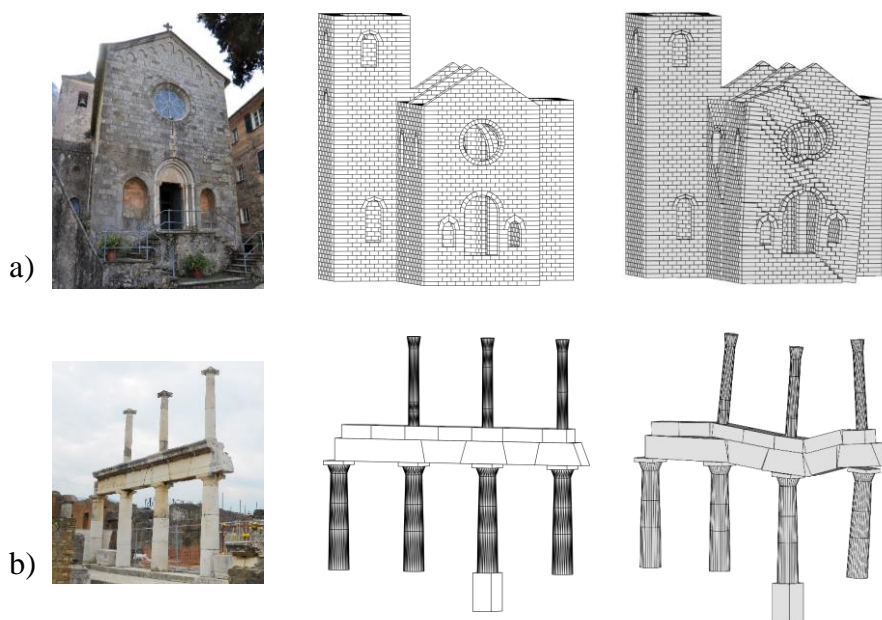


Figure 4.1 - Application examples of LiABlock_3D to historic masonry structures under (a) lateral loads and (b) settlement (Cascini, Gagliardo and Portioli, 2020).

Figure 4.2 reports an example of block types identification for a simple portal arch made of regular polyhedral blocks. In such a case, the definition of three block types only is required to model the entire structure. In particular, a voussoir block (type A in Figure 4.2b) with eight primary vertexes and two contact interfaces is created to model the arch. Two rectangular block types are created to model the arch springers (type B in Figure 4.2b with eight primary vertexes,

ten potential contact points, and three interfaces) and piers (type C in Figure 4.2b with eight primary vertexes and potential contact points and two interfaces), respectively. To model blocks with more than four sides per each base, an additional attribute can be defined, named “base”, where a different number of vertexes can be assigned. Once the basic blocks with attributes are defined, the model geometry is created by simply assembling the block types in the AutoCAD model space. By launching the data Extraction wizard of AutoCAD, the creation of an output file starts.

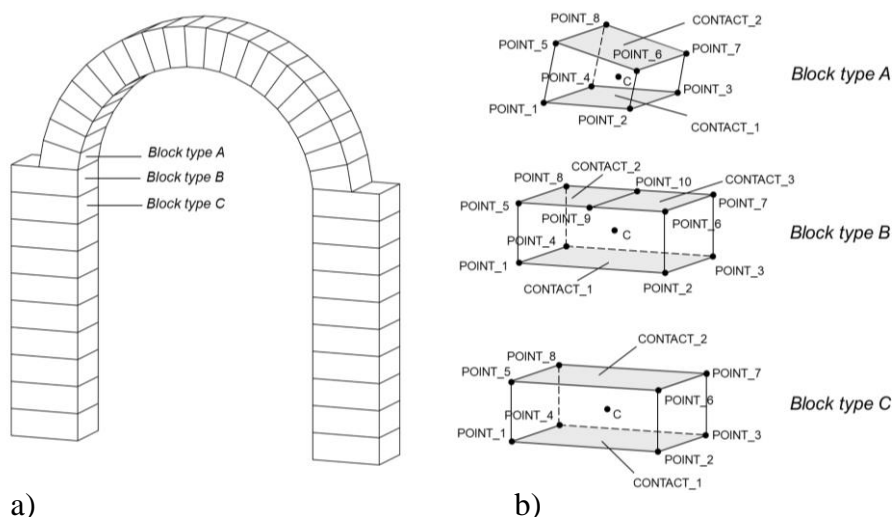


Figure 4.2 – (a) CAD model of a simple portal arch made of polyhedral blocks and (b) block types with contact interfaces and attributes (Cascini, Gagliardo and Portioli, 2020).

The result is a datasheet with as many rows as many polyhedral blocks are in the model and as many columns as the attributes defined. The first row reports the labels of attributes (extracted in any order). From the second row on, all the information created in the form of attributes will be reported for each block composing the assemblage, namely: block type, coordinates of points used to define the geometry of the polyhedral blocks and associated to contact interfaces, coordinates of the centroid and block volume. The creation of the geometry of the model is completed by importing in LiABlock_3D the data reported in the spreadsheet. The tool is provided with a standard routine which acquires the data

from the spreadsheet and allocates them in an internal structure array with predefined fields.

Block type	POINT_1	POINT_10	CONTACT_1	CONTACT_2	CONTACT_3	CENTROID	VOL.
Type_A	x_{A1}, y_{A1}, z_{A1}	...	empty cell	1, 2, 3, 4	5, 6, 7, 8	empty cell	x_A, y_A, z_A	V_A
Type_B	x_{B1}, y_{B1}, z_{B1}	...	$x_{B10}, y_{B10}, z_{B10}$	1, 2, 3, 4	6, 7, 9, 10	9, 10, 5, 8	x_B, y_B, z_B	V_B
Type_C	x_{C1}, y_{C1}, z_{C1}	...	empty cell	1, 2, 3, 4	5, 6, 7, 8	empty cell	x_C, y_C, z_C	V_C

Table 4.1 - The scheme of the Excel spreadsheet obtained using the AutoCAD data Extraction.

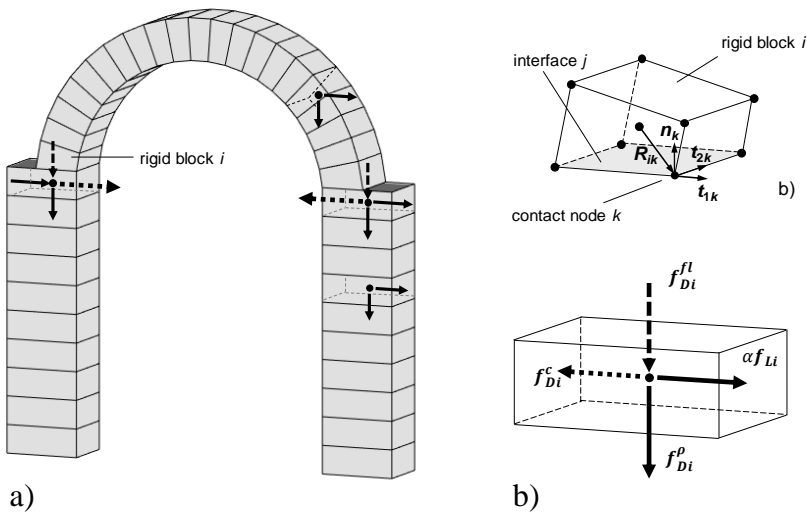


Figure 4.3 – (a) CAD model of a simple portal arch made of polyhedral blocks and (b) block types with contact interfaces and attributes (Cascini, Gagliardo and Portioli, 2020).

4.2.1 Formulation of limit equilibrium problem

Once the geometry of the model has been created and imported in LiABlock_3D, the GUI allows to launch the routine that builds the equilibrium matrix A governing the limit analysis problem associated to the rigid block model. The coefficients of the equilibrium matrix are determined assuming a “point” contact model for interactions, with internal forces (i.e., contact or static variables) acting at each contact point k located at the vertices of the interface j . The internal forces are represented by the shear force components t_{1k}, t_{2k} along local coordinate axes and by the normal force n_k . With static variables collected in the vector $x_k =$

$[t_{1k} \ t_{2k} \ n_k]^T$, the contact equilibrium matrix associated to the 6 degrees of freedom (DOFs) of block i and to contact point k can be expressed as:

$$A_{ik} = - \begin{bmatrix} \hat{t}_{1k} & \hat{t}_{2k} & \hat{n}_k \\ R_{ik} \times \hat{t}_{1k} & R_{ik} \times \hat{t}_{2k} & R_{ik} \times \hat{n}_k \end{bmatrix} \quad (4.1)$$

where A_{ik} is a (6 x 3) matrix; \hat{t}_{1k} , \hat{t}_{2k} , and \hat{n}_k are, respectively, the column vectors with components of tangent and normal to contact interface; R_{ik} is the position vector of contact point k with respect to the block centroid (Figure 4.3b). For the assemblage of matrix A corresponding to the whole structure, LiABlock_3D assumes that the discrete rigid block models are simply supported to the ground (support layer at $z = 0$). Alternatively, support layers at different heights above ground level can be also imposed (i.e., in the case of flying arches). Once the support condition has been specified in the relevant box, the contacts among the blocks are automatically detected, then sequentially numbered and a contact matrix, collecting the information about the contacts, is created.

LiABlock_3D assumes two contacts failure modes: opening and sliding of interfaces at contact points. Assuming shear failure governed by a Coulomb type criterion with isotropic friction and no cohesive behaviour, two inequalities govern the contact failure condition:

$$-n_k \leq 0 \quad (4.2)$$

$$\sqrt{t_{1k}^2 + t_{2k}^2} - \mu \cdot n_k \leq 0 \quad (4.3)$$

The only required input parameter for the contact failure condition is the friction coefficient μ .

Each rigid block is loaded by an external load f_i applied to the centroid of the solid element and expressed as the sum of the dead load f_{Di} and of the live load f_{Li} , increased by an unknown scalar multiplier α . The simple GUI allows to set the live loads direction along the three global coordinates axes, applied to the whole assemblage or to a selection of rigid blocks.

$$f_i = f_{Di} + \alpha \cdot f_{Li} \quad (4.4)$$

LiABlock_3D automatically computes the self-weight of each rigid block on the basis of the unit weight of material ρ and block volume attribute V_i and assumes it as dead load $f_{Di} = f_{Di}^\rho$, where:

$$f_{Di}^\rho = [0 \quad 0 \quad -\rho V_i \quad 0 \quad 0 \quad 0]^T \quad (4.5)$$

Additional dead loads of known magnitude can be applied to a selection of rigid blocks to simulate the effect of other permanent actions. Those include downward vertical loads f_{Di}^{fl} to model the actions induced by floors and constant loads f_{Di}^c , which can be applied along any global axis, to model the effect of other imposed forces, such as those associated to tie elements or static thrusts due to arches or vaults. As such, the vector of dead loads is expressed as:

$$f_{Di} = f_{Di}^\rho + f_{Di}^{fl} + f_{Di}^c \quad (4.6)$$

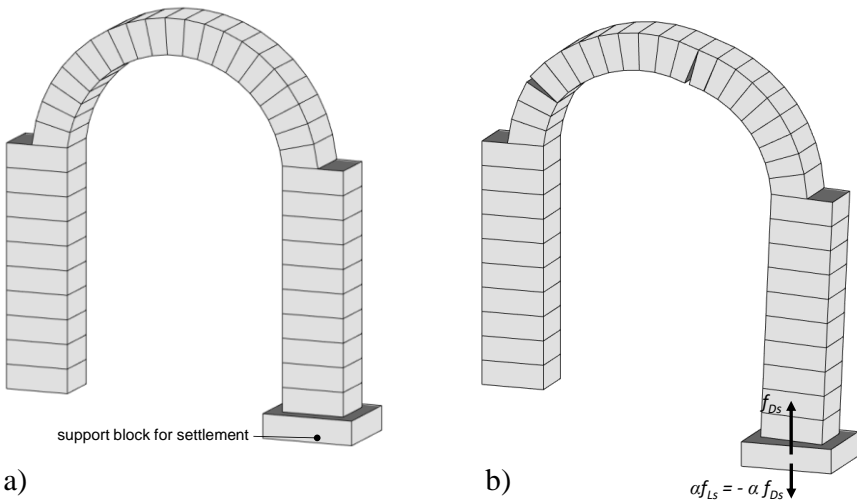


Figure 4.4 - Example of settlement analysis on a portal arch: (a) geometrical model and (b) failure mode (Cascini, Gagliardo and Portioli, 2020).

Live loads f_{Li} can be applied in any direction along the global coordinate axes, to the whole assemblage or to a selection of rigid blocks. The magnitude of live loads is expressed as the sum of block unit weight f_{Di}^ρ and floor loads f_{Di}^{fl} . The

available options for the floor loads, live loads, and constant loads can be specified in the relevant editable white boxes and interactive pop-up menus. LiABlock_3D includes also a module to evaluate the behaviour of masonry assemblages subjected to uniform settlements. In such a case, a support block s is used to introduce ground movement effects on the structure (Figure 4.4). The collapse load multiplier is used to vary the reaction at the support block (which is expressed as a function of dead loads) up to the activation of the failure mechanism (Portioli and Cascini, 2016). In particular, the following expression is adopted for the external force f_s at the support block:

$$f_s = (1 - \alpha) \cdot f_{Ds} \quad (4.7)$$

being f_{Ds} a starting value of the base reaction which is automatically assigned in the tool as a function of the total dead load acting on the model (Figure 4.4b).

To activate the settlement module in LiABlock_3D, the proper option in the relevant pop-up menu has to be selected. In this case, it is assumed by default that the support block s corresponds to the last block number in the list of the Excel spreadsheet obtained using the AutoCAD data Extraction wizard from the geometric model of the masonry assemblage.

LiABlock_3D provides a two-step procedure for the solution of the limit analysis problem. The first step is the solution of the mathematical programming problem which arises from the formulation of the limit analysis problem when an associative friction behaviour is assumed. The assumption of associative behaviour involves dilatancy when sliding occurs at a contact point (i.e., normal displacement rates ε_k accompanying tangential displacement rates γ_k , as shown in Figure 4.5a and Figure 4.5c). Under these conditions, the load factor is unique, and it can be calculated according to a static or kinematic formulation of the limit analysis problem. LiABlock_3D implements the lower bound problem of limit analysis according to the following formulation:

$$\begin{aligned} \max \quad & \alpha \\ \text{s. t.} \quad & A \cdot x = f_D + \alpha \cdot f_L \\ & x \in C \end{aligned} \quad (4.8)$$

where x is the vector of the internal static variables at contact interfaces, A is the equilibrium matrix, f_D and f_L are the vector of dead and live loads, and C is the convex cone. In the above optimization problem, the first constraint represents the equilibrium conditions of the 3D rigid block assemblage. The second constraint includes failure conditions extended to the whole assemblage.

The Mosek optimization software (www.mosek.com) is used to solve the mathematical programming problem. It is well known that the collapse load multiplier obtained under the assumption of associative friction represents an upper bound on the multiplier corresponding to non-associative friction model, i.e., to zero-dilatancy sliding behaviour (Figure 4.5b and Figure 4.5d). To take into account the non-associative frictional behaviour and to compute safe values of the collapse load multiplier, an iterative procedure is implemented which solves a series of cone programming sub-problems, according to (Portioli *et al.*, 2014). Starting from the associative solution, values of normal forces computed at previous iterations are used to define a fictitious failure condition for which the associative (i.e., normal) flow rule leads to zero-dilatancy behaviour. By default, in order to reproduce a non-dilatant behaviour under the assumption of normality flow rule, LiABlock_3D assumes that sliding behaviour at contacts is governed at each iteration by a cylindrical failure surface with a zero angle of friction and an effective cohesion intercept calculated as follows (Figure 4.5d):

$$c_{k,iter+1} = [\beta \cdot n_{k,iter} + (1 - \beta) \cdot n_{k,iter-1}] \cdot (1 + \xi) \cdot \tan \varphi_k + c_k^0 \quad (4.9)$$

where β is an algorithm parameter used to calculate normal forces $n_{k,iter+1}$ at iteration no. $iter+1$ on the basis of normal forces computed at previous iterations; φ_k is the angle of friction; and c_k^0 is a small cohesion value which can be introduced to overcome numerical convergence problems, according to (Gilbert, Casapulla and Ahmed, 2006; Portioli *et al.*, 2014). The parameter ξ governs the angle of friction of the fictitious failure surface (posed equal to 0 to obtain a zero angle of friction as shown in Figure 4.5d). To improve convergence characteristics in case of numerical problems, different values of the algorithm parameters β , ξ and c_k^0 can be assigned in a specific window inside the Graphical User Interface. This windows also allows to modify the tolerance used to exit

from the iterative solution procedure and the maximum number of iterations in the case of convergence problems.

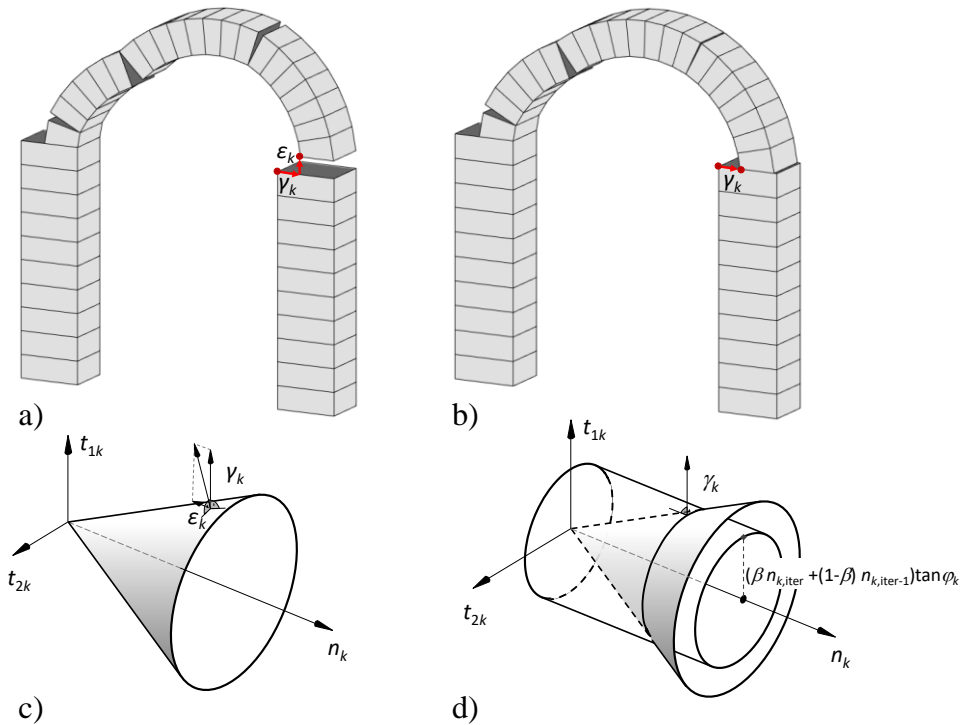


Figure 4.5 - (a) Associative (dilatant) and (b) non-associative (non-dilatant) collapse mechanisms of a masonry block arch subjected to sliding failure at the right end support; (c) Coulomb failure surface used for the associative solution; and (d) fictitious failure surface adopted in the iterative solution procedure for the non-associative behaviour (Cascini, Gagliardo and Portioli, 2020).

The output is the collapse mechanism and the value of the corresponding load factor for the considered loading condition. Utility functions are available to plot failure mechanism configurations increasing or decreasing the scale of displacement rates. Convergence plots, which report the load factor calculated at each iteration, are also available. Other functionalities involve the possibility to plot the geometric configuration of the structure or to highlight loaded blocks. Considering that limit analysis is based on the assumption of infinitesimal and indefinite displacements, it is clear that the plot of the failure mechanism is

indicative of the collapse mode only rather than of the displaced configuration in terms of finite values of displacements. It is also worth noting that the formulation implemented refers to the initial geometric configuration for the calculation of load factor and failure mechanism. As such, the geometric nonlinearities related to large displacements in the case of rocking structures subjected to lateral loads or masonry arches under spreading supports are not taken into account. Nevertheless, it should be noted that incremental formulations based on mathematical programming are also available in the literature which could be conveniently used to take into account the effects of large displacements and for the prediction of load factor displacement curves, as showed in the next section (Portioli and Cascini, 2017, 2018; Gagliardo *et al.*, 2021).

4.3 Rigid block model with no-tension elastic contacts for non-linear kinematic analysis

The second numerical model proposed in this dissertation thesis aims to extend the capabilities of the limit analysis method described in the previous section to the field of the large displacement regime. The main scope of this numerical progress is the possibility to develop numerical capacity curve for masonry structure subjected to foundation movements (Gagliardo *et al.*, 2021). The thesis objective is to use the capacity curve as the main analysis tool for the proposal of a performance-based assessment method for historic masonry Cultural Heritage subjected to settlements, mainly focused on masonry panels such as walls and façades. With this in mind and differently from the linear kinematic formulation, the numerical model based on non-linear kinematic analysis is mainly devoted to the analysis of numerical or experimental case study of masonry types subjected to settlements rather than to seismic lateral loads.

From a theoretical point of view, the non-linear kinematic analysis is based on the three key words: demand, capacity and performance. The demand is the entity of strain or deformation imposed to the structure by the loads; the capacity evaluates the ability of the structure to withstand the demand; the performance governs the interaction between the demand and the capacity based on a specific limit state. With this in mind, the dissertation thesis aims to introduce an

evolution of the common push-over analysis to the contest of settlement failure modes investigation of historic masonry structures. In the seismic analysis field, the push-over analysis method was highly investigated. For the seismic scenario, the demand is represented by the acceleration-displacement response spectrum (ADRS) and the capacity is represented by the so-called “push-over” curve, being the relation between the base shear force and the roof displacement. Trying to apply such formulation to hydrogeological hazard analysis for structures subjected to support ground movements, the parameters of interest are so different since the issue now deals with the entity of the vertical ground movement and the distribution of the settlement at the foundation layer. The output of such numerical analysis can be better represented by a capacity curve, named “push-down curve”, which allows to analyse the investigated damage parameter (maximum settlement, angular deflection, etc.) against the loss of the base reaction. The capacity push-down curve must be numerically defined also in the elastic range in order to fulfil one of the main scopes of the present dissertation, i.e. the settlement-induced damage assessment of historical masonry structures. In this regard, the possibility to investigate the elastic behaviour in the early damage state is a crucial challenge compared to the incipient collapse behaviour which is a performance state far to be reached because of the known high resilience of settled masonry structure to accommodate high displacement before to reach an ultimate configuration.

In this framework, a planar rigid block model with unilateral contact interfaces is proposed for the investigation of behaviour of masonry structures subjected to settlement from the early crack opening until the collapse. Also in this model, the structure is idealized into an assemblage of rigid blocks i interacting at contact interfaces j (see Figure 4.6). A no-tension behaviour with finite friction strength is assumed at interfaces. Interactions are modelled as concentrated forces at the vertices k of each contact pair j . Additional rigid blocks s are used to model the settling foundation with imposed displacements. It is worth noting that the implemented modelling approach is formulated in the large displacement regime and is based on a pure static formulation. In this scenario, one of the greatest potentialities of the proposed non-linear numerical formulation is that the equilibrium conditions are expressed in terms of static forces, so that there is no

need to introduce inertia effects for the analysis of the failure mechanisms, as for most of discrete element models, such as distinct element method.

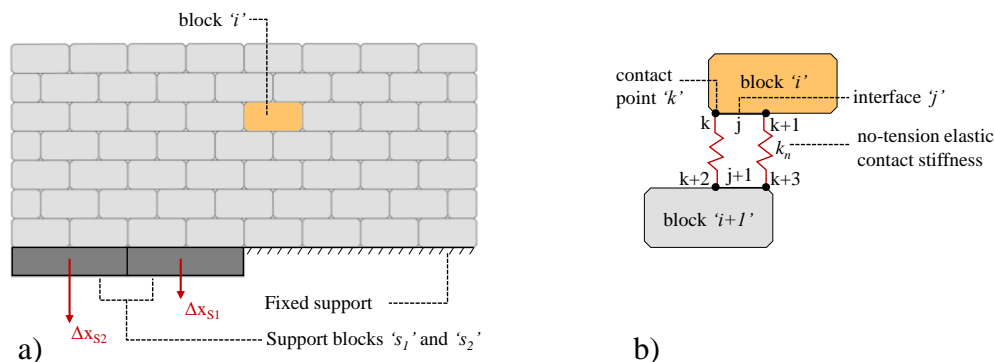


Figure 4.6 - Rigid block model with elastic contact interfaces: (a) block assemblage; (b) rigid block 'i', interface 'j', contact point 'k' and no-tension elastic normal stiffness 'kn' (Gagliardo et al., 2021).

Important novelties of this numerical model, respect to works inside the numerical project conducted at the University of Naples “Federico II” (Portioli and Cascini, 2017), are the ability to take into account elastic behaviour at interfaces and the possibility to model different displacements history for settlements. It is worth noting that the model accounts for a unilateral normal elastic behaviour at contact points, while a rigid behaviour is assumed for sliding. The model is provided with the possibility to adopt a settlement protocol discretized into displacement increments, where the size of the displacement imposed at each support block depends on the shape and history of settlement. The model was implemented in an in-house MATLAB® code using a variational formulation for the contact problems associated to unilateral contact interfaces with elastic behaviour in compression, as detailed later in the dissertation thesis.

4.3.1 Formulation of incremental static contacts problem

The formulation is based on the solution of two dual quadratic programming problems, corresponding to a force-based and to a displacement-based problem, which are equivalent to the system of equilibrium, failure and complementarity conditions governing the rigid block model. This is a noticeably simplification

which allows efficient solution algorithms to be used, with low computational costs. For an assemblage of b rigid blocks interacting at c contact points (see also Figure 4.8), the force-based optimization problem was formulated as follows (Lloyd Smith, 1990; Krabbenhoft *et al.*, 2012; Meng *et al.*, 2017; Portioli, 2020):

$$\begin{aligned} \max \quad & -\frac{1}{2}c^T Cc - g_0^T c \\ \text{s. t.} \quad & A_0 c = f \\ & Y^T c \leq 0 \end{aligned} \tag{4.10}$$

where:

- c is the $(2c \times 1)$ vector of the unknown contact forces at interfaces which collects subvectors $c_k = [t_k \ n_k]^T$, with entries corresponding to the shear force component t_k and the normal force n_k at each contact point k , which is taken to be positive in compression.
- C is the $(2c \times 2c)$ diagonal matrix of contact compliances collecting submatrices $C_k = \text{diag}(0 \ 1/k_n)$, being k_n the normal stiffness.
- g_0 is $(2c \times 1)$ the vector of contact gaps which collects subvectors $[0 \ g_{0k}]^T$.
- f is the $(3b \times 1)$ vector of external forces collecting subvectors $f_i = [f_{xi} \ f_{zi} \ m_{yi}]^T$ with force components applied at the centroid of block i .
- A_0 is the $(3b \times 2c)$ equilibrium matrix, with coefficients determined by the position of contact points and geometry of rigid blocks.
- Y^T is the $(3c \times 2c)$ matrix of failure conditions.

With reference to contact point k and according to notation used in (Ferris and Tin-Loi, 2001), the limit conditions for sliding and opening failure can be written in matrix form as:

$$Y_k^T = \begin{bmatrix} 1 & -\mu \\ -1 & -\mu \\ 0 & -1 \end{bmatrix} \begin{bmatrix} t_k \\ n_k \end{bmatrix} \leq \begin{bmatrix} 0 \\ 0 \\ 0 \end{bmatrix} \tag{4.11}$$

Similar to the lower bound formulation of limit analysis, the two constraints of problem given by Equation (4.10) represent the equilibrium and failure

conditions, respectively. The equilibrium equations are expressed with reference to the configuration related to a displacement increment of the sequential solution procedure. With regard to the failure conditions, the numerical model is based on concave contact formulation, so the behaviour at contact points undergoing sliding failure is governed by failure conditions which are expressed according to the Coulomb friction law (Figure 4.7).

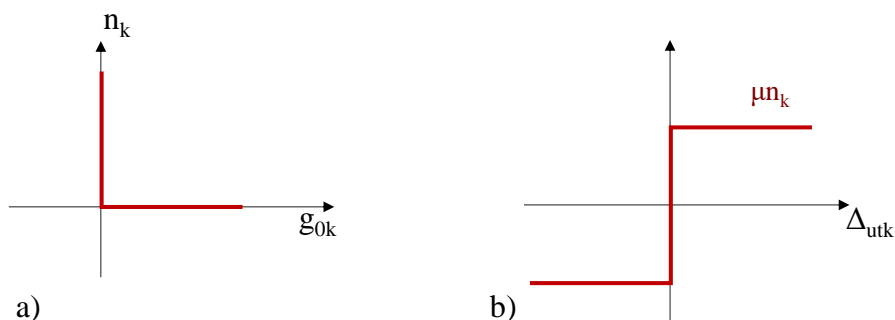


Figure 4.7 - Contact laws for normal reaction force (a) and shear force (b) at point k .

The dual displacement-based optimization problem is:

$$\begin{aligned}
 \min \quad & \frac{1}{2} e^T K e - f^T \Delta x \\
 \text{s. t.} \quad & A_0^T \Delta x - Y \lambda - g_0 - e = 0 \\
 & \lambda \geq 0
 \end{aligned} \tag{4.12}$$

where $K = C^{-1}$ and $e = Cc$ is the vector of contact interpenetrations.

The vector $\Delta x = x - x_0$ collects the unknown displacements at the block centroid, being x_0 the vector of block centroid coordinates associated to the initial configuration. λ is the vector of non-negative flow multipliers associated to each failure condition, namely opening and sliding failure modes. In the problem given by Equation (4.12), the objective function represents the total potential energy, whilst the constraints represent the geometric compatibility conditions between the displacements Δu at contact points expressed as a function of the displacement vector Δx ($\Delta u = A_0^T \Delta x$) and as a function of the assumed flow rule. The assumed flow rule is an associative flow rule and defines the relationship between displacement rates and flow multipliers as a function of the transpose of the

matrix associated to failure conditions Y , taking into account contact gaps and interpenetrations ($\Delta u = Y\lambda + g_0 + e$). With reference to contact point k , the flow rule can be written as:

$$\begin{aligned} \Delta u_{tk} &= \lambda_{sk+} - \lambda_{sk-} \\ \Delta u_{nk} &= -\mu\lambda_{sk+} - \mu\lambda_{sk-} - \lambda_{ok} + g_{0k} + C_k C_k \end{aligned} \tag{4.13}$$

where λ_{sk+} , λ_{sk-} and λ_{ok} are the flow multipliers corresponding to positive and negative sliding, respectively, and contact opening. It is interesting to note that, when g_{0k} is omitted, previous optimization problems reduce to the standard forms of upper and lower bound formulations of limit analysis theorems presented in the previous section about the first numerical model.

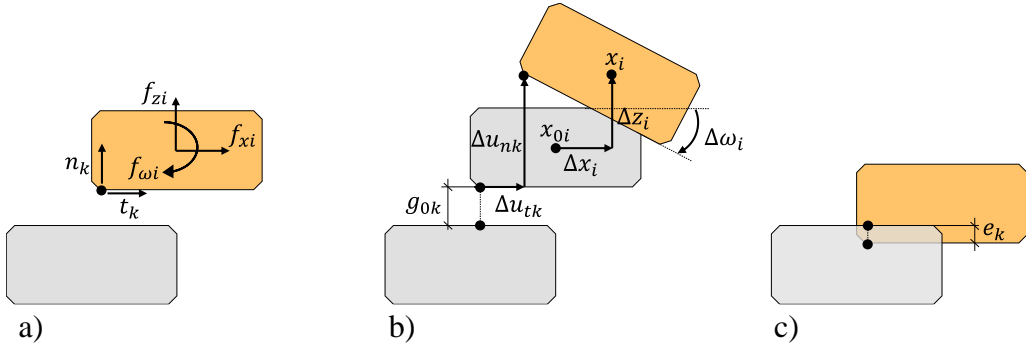


Figure 4.8 – (a) External and contact forces; (b) Initial gap at contact point k and kinematic variables at block centroid i and contact point k ; (c) Elastic contact interpenetration (Gagliardo et al., 2021).

It is also worth noting that the above optimization problems are similar to those which arise for contact dynamics when the effect of inertial and dynamics forces are neglected. Static variables and collapse load multipliers were obtained from the solution of the optimization problem (25). The kinematic variables in (23) were derived as Lagrange multipliers associated to the solution of the static problem (25), according to the procedure illustrated in the next sub-section.

An incremental solution procedure was developed for push-down analysis. The procedure is based on the solution of the displacement-based problem stated in Equation (4.12) when given displacement increments are applied at the moving

supports. The static variables associated to the force-based problem are calculated directly from the Lagrange multipliers associated to the solution of the same displacement-based problem with no need to explicitly solve the optimization problem in Equation (4.10).

The incremental solution procedure is organized as follows:

- (i) Solve the displacement-based optimization problem defined in Equation (4.12) at configuration x_0 , with initial gaps g_0 , and obtain block displacements Δx contact forces c and the collapse load multiplier α corresponding to the support reaction.
- (ii) Determine new positions of the blocks $x = x_0 + \Delta x$ and contact gaps g .
- (iii) Obtain contact forces c and support reactions in Equation (4.10) from Lagrange multipliers associated to the solution of the displacement-based problem.
- (iv) Set up a new optimization problem on the basis of the new configuration at configuration x and repeat from step (i).

For the purpose of the present dissertation thesis, the incremental solution procedure starts from the position of the displacement-based problem. In such a way, it is possible to directly apply different displacement rates to each moving rigid block at supports by simply adding additional constraints to the relevant variables. In addition, the solution procedure is more stable because, imposing displacement at moving supports – rather than varying support reactions – allows to follow the entire path of the force-displacement curve, as shown in the validation and application reported in the next sections.

4.3.2 Input data for the model

The non-linear kinematic formulation is able to analyse 2D structures made of CAD polylines in contact by means simple lines. The routine implemented consists in creating the geometry of the assemblage in AutoCAD, exporting relevant data to a DXF file and importing them in MATLAB® for the generation of the numerical model and the analysis. The MATLAB® routine allows to

import the so-defined DXF file and to pull out the information for the units geometry and for the potential contact lines. Additional data required by the numerical routine are essentially the value of the weight for unit volume, the friction coefficient (with the possibility to set various values for vertical head joints and horizontal bed joint frictional properties), the value of the normal stiffness at contact points, the number of iterations and the full analysis time and finally the investigated settlement protocol defined as described in the next section. For a given planar block structure, the first steps are to identify the block types used to discretize the structural assemblage and the associated contact lines. The geometrical input is much lighter and speed compared with that required for the previously described limit analysis numerical formulation, where block types were modelled as Autodesk CAD blocks with a series of attributes regarding the geometrical properties and the contact interfaces definition. In this new formulation, the single element is fully described by simple drawing a CAD polyline with intermediate points in the position where the block interacts with the neighbouring bricks (Figure 4.9).

The block (or blocks) devoted to the ground displacement is (are) modelled by the same procedure and insert at the foundation level under the base layer. The only requirement for the support blocks consists in the need to insert them at the end of the modelling process. In such a way the implemented numerical routine recognizes the blocks devoted to the vertical settlement displacement because they are at the end places of the vector of the blocks that are part of the input DXF file. The number of the movable foundation block is free and depends on the type of settlement profile to be assumed in the numerical analysis. In the example of Figure 4.10, where a linear settlement of one side of the panel is defined, at least two support blocks must be modelled, each one with a different settlement displacement protocol.

The proposed numerical formulation for the rigid block large displacement analysis with elastic contact interfaces also allows to model several laws of settlement displacements. The novelty is an important development in the field of the analysis of historic masonry structure subjected to foundation movements because it allows to better pick the real behaviour of the foundation soils.

The model is provided with the possibility to assume a settlement protocol characterized by several steps, where the user can describe the $(1 \times n \text{ steps})$ vector of the settlement displacement freely selecting the amount of vertical displacement for each step. Several displacements vectors can be created and applied to different support blocks in order to model the required settlement law. Figure 4.10 shows an example of a settlement protocol in the case of a linear settlement law. Two support blocks were added at the foundation layer and two different settlement vectors were applied to these blocks, where the amount of the step displacement was selected in order to simulate the linear displacement law showed in Figure 4.10a.

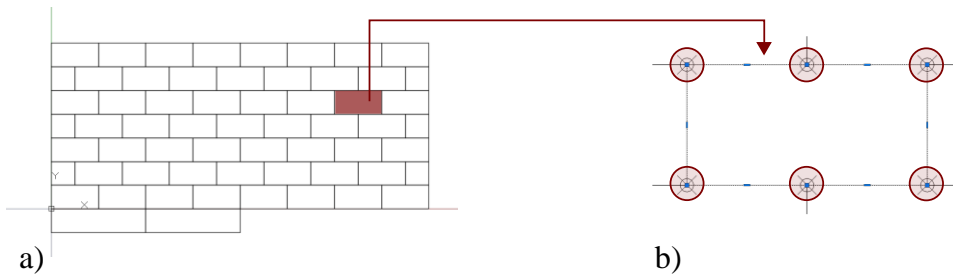


Figure 4.9 - Non-linear kinematic analysis formulation: (a) block assemblage in the case of a wall sample and (b) definition of a block by a simple CAD polyline.

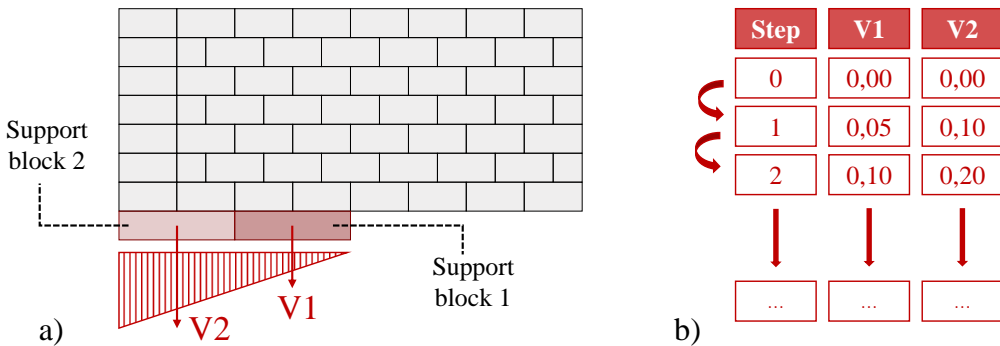


Figure 4.10 - Settlement protocol in the case of a linear settlement law: (a) definition of the support blocks at the foundation layer and (b) vectors of settlement displacements for the support blocks.

4.4 Conclusions

In the present chapter, the numerical formulation proposed for the simulation of masonry types and structures investigated in this thesis were described. Two models were presented, a rigid block linear kinematic model with rigid contacts based on the lower bound theorem of the classical problem of the limit analysis and a rigid block non-linear kinematic model with no-tension elastic contacts to study the structural response of settled masonry structures in the large displacement regime. Both models are devoted to the analysis of collection of rigid blocks in contact via no-tension frictional contact interfaces. The limit analysis model is devoted to the analysis of 2D or even 3D models in the case of seismic-induced live loads or settlement-induced foundation movements. The non-linear kinematic model is actually able to investigate only 2D assemblage of rigid blocks and only in the case of foundation settlements, that is the main topic of this dissertation thesis.

The second model proposed in this Chapter represents the true novelty carried out in this research. The role of this formulation is crucial within the scopes of this thesis because the non-linear kinematic model allows for the generation of capacity curves (namely push-down curves) which are the numerical basis to formulate a displacement-based approach for the proposal of a set of performance (and damage levels) typical of masonry structures subjected to settlement of the foundation system, as described later in Chapter 7. In the next Chapters 5 and 6, several applications of both computational proposals will be presented with the aim to validate them against numerical and experimental comparisons and to deeply show the potentialities and the limitations of the above-described numerical tools.

References

- Al-Heib, M. (2012) ‘Distinct Element Method Applied on Old Masonry Structures’, in Miidla Peep (ed.) *Numerical Modelling*. doi: 10.5772/36255.
- Alessandri, C. *et al.* (2015) ‘Crack patterns induced by foundation settlements: Integrated analysis on a renaissance masonry palace in Italy’, *International Journal of Architectural Heritage*, 9(2), pp. 111–129. doi: 10.1080/15583058.2014.951795.
- Amorosi, A. *et al.* (2014) ‘Tunnelling-induced deformation and damage on historical masonry structures’, *Geotechnique*, 64(2), pp. 118–130. doi: 10.1680/geot.13.P.032.
- Angelillo, M. *et al.* (2018) ‘Rigid block models for masonry structures’, *International Journal of Masonry Research and Innovation*, 3(4), pp. 349–368. doi: 10.1504/IJMRI.2018.095701.
- Angelillo, M. (2019) ‘The model of Heyman and the statical and kinematical problems for masonry structures’, *International Journal of Masonry Research and Innovation*, 4(1–2), pp. 14–21. doi: 10.1504/IJMRI.2019.096820.
- Baraldi, D. and Cecchi, A. (2017) ‘A full 3D rigid block model for the collapse behaviour of masonry walls’, *European Journal of Mechanics, A/Solids*, 64, pp. 11–28. doi: 10.1016/j.euromechsol.2017.01.012.
- Bertolesi, E., Milani, G. and Casolo, S. (2018) ‘Homogenization towards a mechanistic Rigid Body and Spring Model (HRBSM) for the non-linear dynamic analysis of 3D masonry structures’, *Meccanica*. doi: 10.1007/s11012-017-0665-6.
- Block, P., Ciblac, T. and Ochsendorf, J. (2006) ‘Real-time limit analysis of vaulted masonry buildings’, *Computers and Structures*, 84(29–30), pp. 1841–1852. doi: 10.1016/j.compstruc.2006.08.002.
- Bui, T. T. *et al.* (2017) ‘Discrete element modelling of the in-plane and out-of-plane behaviour of dry-joint masonry wall constructions’, *Engineering Structures*, 136, pp. 277–294. doi: 10.1016/j.engstruct.2017.01.020.
- Bui, T. T. and Limam, A. (2012) ‘Masonry walls under membrane or bending loading cases: Experiments and discrete element analysis’, in *Civil-Comp*

Proceedings. doi: 10.4203/ccp.99.119.

Caliò, I. *et al.* (2013) ‘Evaluation of foundation settlements in masonry buildings using non-linear static analysis carried out with 3DMacro Software’, in *XV Convegno ANIDIS – L’Ingegneria Sismica in Italia*.

Di Carlo, F. and Coccia, S. (2020) ‘Collapse state of elliptical masonry arches after finite displacements of the supports’, *Engineering Failure Analysis*, 114.

Di Carlo, F., Coccia, S. and Rinaldi, Z. (2018) ‘Collapse load of a masonry arch after actual displacements of the supports’, *Archive of Applied Mechanics*, 88(9), pp. 1545–1558. doi: 10.1007/s00419-018-1386-6.

Cascini, L., Gagliardo, R. and Portioli, F. (2020) ‘LiABlock_3D: A Software Tool for Collapse Mechanism Analysis of Historic Masonry Structures’, *International Journal of Architectural Heritage*, 14(1), pp. 75–94. doi: 10.1080/15583058.2018.1509155.

Coccia, S., Di Carlo, F. and Rinaldi, Z. (2015) ‘Collapse displacements for a mechanism of spreading-induced supports in a masonry arch’, *International Journal of Advanced Structural Engineering*, 7(3), pp. 307–320. doi: 10.1007/s40091-015-0101-x.

D’Altri, A. M. *et al.* (2018) ‘A 3D detailed micro-model for the in-plane and out-of-plane numerical analysis of masonry panels’, *Computers and Structures*, 206, pp. 18–30. doi: 10.1016/j.compstruc.2018.06.007.

D’Altri, A. M. *et al.* (2019) ‘Historic Barrel Vaults Undergoing Differential Settlements’, *International Journal of Architectural Heritage*. doi: 10.1080/15583058.2019.1596332.

D’Altri, A. M. *et al.* (2020) ‘Modeling Strategies for the Computational Analysis of Unreinforced Masonry Structures: Review and Classification’, *Archives of Computational Methods in Engineering*, 27(4), pp. 1153–1185. doi: 10.1007/s11831-019-09351-x.

De-Felice, G. and Malena, M. (2019) ‘Failure pattern prediction in masonry’, *Journal of Mechanics of Materials and Structures*, 14(5), pp. 663–682. doi: 10.2140/jomms.2019.14.663.

Ferris, M. C. and Tin-Loi, F. (2001) ‘Limit analysis of frictional block assemblies

as a mathematical program with complementarity constraints’, *International Journal of Mechanical Sciences*, 43(1), pp. 209–224. doi: 10.1016/S0020-7403(99)00111-3.

Foraboschi, P. (2019) ‘Masonry does not limit itself to only one structural material: Interlocked masonry versus cohesive masonry’, *Journal of Building Engineering*, 26. doi: 10.1016/j.jobbe.2019.100831.

Gagliardo, R. *et al.* (2021) ‘A rigid block model with no-tension elastic contacts for displacement-based assessment of historic masonry structures subjected to settlements’, *Engineering Structures*, 229. doi: 10.1016/j.engstruct.2020.111609.

Galassi, S. *et al.* (2018) ‘Failure modes prediction of masonry voussoir arches on moving supports’, *Engineering Structures*, 173, pp. 706–717. doi: 10.1016/j.engstruct.2018.07.015.

Galassi, S. *et al.* (2020) *Analysis of masonry pointed arches on moving supports: A numeric predictive model and experimental evaluations*, *Lecture Notes in Mechanical Engineering*. doi: 10.1007/978-3-030-41057-5_163.

Galassi, S., Paradiso, M. and Tempesta, G. (2013) ‘Non-Linear Analysis of Masonry Structures Subjected to External Settlements’, *Open Journal of Civil Engineering*, pp. 18–26. doi: 10.4236/ojce.2013.32a003.

Giardina, G. *et al.* (2013) ‘Numerical analysis of a masonry façade subject to tunnelling-induced settlements’, *Engineering Structures*, 54, pp. 234–247. doi: 10.1016/j.engstruct.2013.03.055.

Giardina, G., Hendriks, M. A. N. and Rots, J. G. (2015) ‘Sensitivity study on tunnelling induced damage to a masonry façade’, *Engineering Structures*, 89, pp. 111–129. doi: 10.1016/j.engstruct.2015.01.042.

Gilbert, M. (2001) ‘RING : A 2D rigid-block analysis program for masonry arch bridges’, in *3rd International Arch Bridges Conference (ARCH01)*, pp. 459–464.

Gilbert, M., Casapulla, C. and Ahmed, H. M. (2006) ‘Limit analysis of masonry block structures with non-associative frictional joints using linear programming’, *Computers and Structures*, 84(13–14), pp. 873–887. doi: 10.1016/j.compstruc.2006.02.005.

Iannuzzo, A. *et al.* (2018) ‘Modelling the cracks produced by settlements in

masonry structures’, *Meccanica*, 53(7), pp. 1857–1873. doi: 10.1007/s11012-017-0721-2.

Krabbenhoft, K. *et al.* (2012) ‘Granular contact dynamics with particle elasticity’, *Granular Matter*, 14(5), pp. 607–619. doi: 10.1007/s10035-012-0360-1.

Lagomarsino, S. *et al.* (2013) ‘TREMURI program: An equivalent frame model for the nonlinear seismic analysis of masonry buildings’, *Engineering Structures*, 56, pp. 1787–1799. doi: 10.1016/j.engstruct.2013.08.002.

LimitState Ltd. (2020) *LimitState : RING Manual*. Sheffield, UK.

Lloyd Smith, D. (1990) *Mathematical programming methods in structural plasticity*, *Mathematical Programming Methods in Structural Plasticity*. doi: 10.1007/978-3-7091-2618-9.

McInerney, J. and Dejong, M. J. (2015) ‘Discrete Element Modeling of Groin Vault Displacement Capacity’, *International Journal of Architectural Heritage*, 9(8), pp. 1037–1049. doi: 10.1080/15583058.2014.923953.

Meng, J. *et al.* (2017) ‘Granular contact dynamics with elastic bond model’, *Acta Geotechnica*, 12(3), pp. 479–493. doi: 10.1007/s11440-016-0481-5.

Milani, G. *et al.* (2016) ‘Tilting plane tests on a small-scale masonry cross vault: Experimental results and numerical simulations through a heterogeneous approach’, *Engineering Structures*, 123, pp. 300–312. doi: 10.1016/j.engstruct.2016.05.017.

Nicodemo, G. *et al.* (2020) *Damage to Masonry Buildings Interacting with Slow-Moving Landslides: A Numerical Analysis*, *Lecture Notes in Civil Engineering*. doi: 10.1007/978-3-030-21359-6_6.

Nodargi, N. A., Intrigila, C. and Bisegna, P. (2019) ‘A variational-based fixed-point algorithm for the limit analysis of dry-masonry block structures with non-associative Coulomb friction’, *International Journal of Mechanical Sciences*, 161–162. doi: 10.1016/j.ijmecsci.2019.105078.

Ochsendorf, J. A. (2006) ‘The masonry arch on spreading supports’, *Structural Engineer*, pp. 29–35.

Orduña, A. and Lourenço, P. B. (2005a) ‘Three-dimensional limit analysis of

rigid blocks assemblages. Part I: Torsion failure on frictional interfaces and limit analysis formulation’, *International Journal of Solids and Structures*, 42(18–19), pp. 5140–5160. doi: 10.1016/j.ijsolstr.2005.02.010.

Orduña, A. and Lourenço, P. B. (2005b) ‘Three-dimensional limit analysis of rigid blocks assemblages. Part II: Load-path following solution procedure and validation’, *International Journal of Solids and Structures*, 42(18–19), pp. 5161–5180. doi: 10.1016/j.ijsolstr.2005.02.011.

Pantò, B. *et al.* (2016) ‘3D macro-element modelling approach for seismic assessment of historical masonry churches’, *Advances in Engineering Software*, 97, pp. 40–59. doi: 10.1016/j.advengsoft.2016.02.009.

Pepe, M., Sangirardi, M., *et al.* (2020) ‘Discrete and Continuous Approaches for the Failure Analysis of Masonry Structures Subjected to Settlements’, *Frontiers in Built Environment*, 6. doi: 10.3389/fbuil.2020.00043.

Pepe, M., Pingaro, M., *et al.* (2020) ‘Micromodels for the in-plane failure analysis of masonry walls: Limit analysis, FEM and FEM/DEM approaches’, *Frattura ed Integrità Strutturale*, 14(51), pp. 504–516. doi: 10.3221/IGF-ESIS.51.38.

Portioli, F. *et al.* (2014) ‘Limit analysis of 3D masonry block structures with non-associative frictional joints using cone programming’, *Computers and Structures*, 143, pp. 108–121. doi: 10.1016/j.compstruc.2014.07.010.

Portioli, F. and Cascini, L. (2016) ‘Assessment of masonry structures subjected to foundation settlements using rigid block limit analysis’, *Engineering Structures*. Elsevier Ltd, 113, pp. 347–361. doi: 10.1016/j.engstruct.2016.02.002.

Portioli, F. and Cascini, L. (2017) ‘Large displacement analysis of dry-jointed masonry structures subjected to settlements using rigid block modelling’, *Engineering Structures*, 148, pp. 485–496. doi: 10.1016/j.engstruct.2017.06.073.

Portioli, F. and Cascini, L. (2018) ‘Contact Dynamics of Masonry Block Structures Using Mathematical Programming’, *Journal of Earthquake Engineering*, 22(1), pp. 94–125. doi: 10.1080/13632469.2016.1217801.

Portioli, F. P. A. (2020) ‘Rigid block modelling of historic masonry structures using mathematical programming: a unified formulation for non-linear time history, static pushover and limit equilibrium analysis’, *Bulletin of Earthquake*

Engineering, 18(1), pp. 211–239. doi: 10.1007/s10518-019-00722-0.

Reccia, E. *et al.* (2014) ‘Full 3D homogenization approach to investigate the behavior of masonry arch bridges: The Venice trans-lagoon railway bridge’, *Construction and Building Materials*, 66, pp. 567–586. doi: 10.1016/j.conbuildmat.2014.05.096.

Rossi, M., Calderini, C. and Lagomarsino, S. (2016) ‘Experimental testing of the seismic in-plane displacement capacity of masonry cross vaults through a scale model’, *Bulletin of Earthquake Engineering*, 14(1), pp. 261–281. doi: 10.1007/s10518-015-9815-1.

Tiberti, S. *et al.* (2020) ‘A Genetic Algorithm adaptive homogeneous approach for evaluating settlement-induced cracks in masonry walls’, *Engineering Structures*.

Tralli, A. *et al.* (2020) ‘Masonry structures in the presence of foundation settlements and unilateral contact problems’, *International Journal of Solids and Structures*, 191–192, pp. 187–201. doi: 10.1016/j.ijsolstr.2019.12.005.

Zampieri, P. *et al.* (2018) ‘Collapse displacements of masonry arch with geometrical uncertainties on spreading supports’, *Computers and Structures*, 208, pp. 118–129. doi: 10.1016/j.compstruc.2018.07.001.

Zampieri, P., Amoroso, M. and Pellegrino, C. (2019) ‘The masonry buttressed arch on spreading support’, *Structures*, 20, pp. 226–236. doi: 10.1016/j.istruc.2019.03.008.

Chapter 5

Numerical applications using linear kinematic analysis

The contents of Chapter 5 are published in (Gagliardo, Cascini, et al., 2019; Gagliardo, Terracciano, et al., 2019; Malena, Portioli, Gagliardo et al., 2019; Cascini, Gagliardo and Portioli, 2020; Landolfo, Gagliardo et al., 2020).

5.1 Introduction

The present Chapter 5 is dedicated to the application of the rigid block model for linear kinematic analysis proposed in the previous Chapter 4 to a large number of case studies, involving masonry panels, simple connections, curved structures and monumental analytical and real case studies. The main scope is to investigate to which extent this in-house tool can be applied in the study of structural response of masonry structures.

In this framework, the following sections are dedicated to the applications related to the limit analysis based numerical model, i.e. the software LiABlock_3D. In this case, both seismic and settlement responses of masonry structures is investigated. To this scope, it is worth noting that the settlement analysis is the crucial one accounting for the spirit of the present thesis. Nevertheless, the seismic field is not neglected because one of the further developments of the work performed in the thesis is represented by the seismic-to-settlement interaction in terms of masonry structures capacity and vulnerability. In this framework, the case studies presented in the section devoted to linear kinematic model deals with

lateral and vertical live loads and support base movements aiming at the validation of the tool against both seismic and settlements.

5.2 Applications of rigid block model for linear kinematic analysis

This section deals with the description of the applications related to the first proposed computational tool, which is a numerical model based on a rigid block limit analysis formulation, condensed in an in-house software named LiABlock_3D. Numerical and experimental case studies of masonry types and structures subjected to lateral live loads and spreading supports are analysed with the aim to show the capability of the limit analysis formulation in structural capacity investigation of several types of masonry structures (simple panels, panels connection, curved structures and monumental full-scale case studies) under different loading conditions. As already described in the previous Chapter 4, the outcomes such a numerical model is able to predict are essentially the plot of the predicted collapse mechanism (and of the corresponding crack pattern) and the values of both collapse load factor and collapse load. In the spirit of the classical limit analysis theorems, the numerical model can only predict the structural capacity of the investigated case study against collapse or near collapse state, meaning that damage initiation and propagation is not accounted for in this model.

As for the specific numerical formulation, both associative and non-associative flow rule plasticity will be considered in the analysed case studies. The first obtained solution deals with an associative flow rule assumption, which can be considered an upper bound value of the numerical response in terms of collapse load factors. Non-associative solution allows to predict a collapse where the dilatancy at the blocks contact interfaces is not allowed to develop. As already described in Chapter 4, the proposed computational tool is able to account for the non-associative solution thanks to an iterative procedure implemented for the cohesive behaviour at contact interfaces in order to obtain a zero-dilatancy numerical behaviour. With the aim to homogenize the outcomes of the several described case studies, the parameters to be set in the algorithm for the step-by-

step procedure will be constant in the next applications, with only some changes when sensitivity analysis to these parameters will be performed in the case of very few case studies. In this framework, the algorithm parameters β and ξ for non-associative solution were taken as 0.6 and 0.0, the fictitious cohesion c_k^0 was equal to $1e-5 \times n_{max}$, where n_{max} is the largest normal force calculated at a given iteration. The values of the algorithm parameters were set in accordance to (Gilbert, Casapulla and Ahmed, 2006; Portioli *et al.*, 2014) to avoid convergence problems when the normal force at a contact is zero and to reduce cycling in the iterative solution procedure (i.e., to reduce the number of iterations required to converge). The convergence tolerance was 10^{-3} , and a maximum number of iterations equal to 10 was used. In the same homogenization spirit, the analyses were performed using the same workstation, characterized by a 3.50 GHz Intel Xeon Processor E5-1650 with 16.0 GB of RAM.

5.2.1 Lateral and vertical live loads

5.2.1.1 Circular arches and vault subjected to vertical live loads

The circular arches and the barrel vault shown in Figure 5.1 were analysed for testing the numerical procedure. The same case studies were also analysed in (Tran-Cao, 2009) using different formulations for the mathematical programming problems underlying the limit analysis problem and also using different solvers. The friction coefficient used for numerical analysis is equal to 0.75 and the unit weight is 25.0 kN/m^3 .

The first case study is a circular arch subjected to a point live load (Figure 5.1a). The arch is made of 16 voussoir blocks with 17 rectangular contact interfaces. The variable point load f_l is assigned as a factor of the self-weight f_D of the loaded block, equal to 0.29 kN. The second case study is a double ring voussoir arch. The dimensions of the inner ring are the same of the single ring arch. Contact points are used along the surfaces between the two rings. Also, in this case a vertical, variable point load is applied to the outer ring. The third case study is a barrel vault with dimensions and block arrangement shown in Figure 5.1e. Two block types were defined in AutoCAD to generate in LiABlock_3D the entire

geometry of the vault, which comprises 63 full rigid blocks, 18 half blocks, and 215 rectangular contact faces. The vault is loaded by variable forces distributed on four blocks expressed as a factor of the self-weight of the four blocks, equal to 1.16 kN, as indicated in Figure 5.1e.

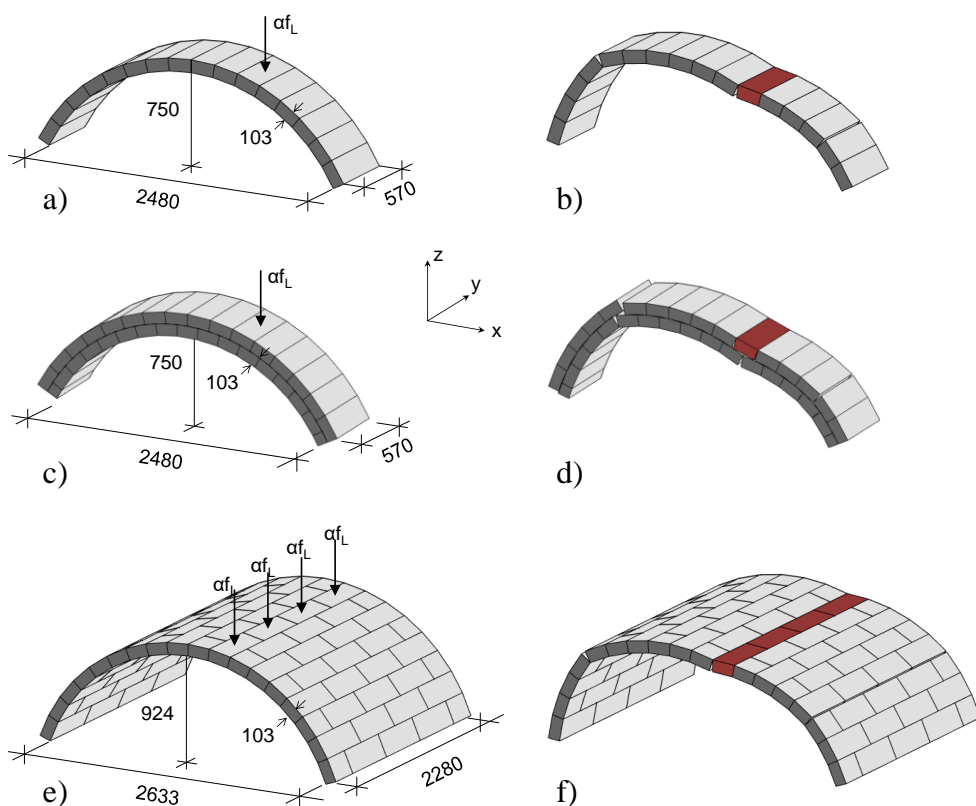


Figure 5.1 - (a) Circular arch dimensions; (b) circular arch collapse mechanism; (c) two-ring arch dimensions; (d) two-ring arch collapse mechanism; (e) barrel vault dimensions; and (f) barrel vault collapse mechanism (Cascini, Gagliardo and Portioli, 2020).

The predicted failure mechanisms are shown in Figure 5.1b, Figure 5.1d and Figure 5.1f and corresponding load factors are reported in Table 5.1. In all cases the collapse occurs by a four-hinge failure mechanism. In the case of the single ring arch and the barrel vault, the values of the collapse load factors for the associative and non-associative solution are the same, due to the nature of the

failure mode activated, which in this case does not involve sliding at contact points. A difference of 6% between the non-associative and associative solution is obtained in the case of the double ring arch due to the sliding at the contact interfaces between the two rings.

Model	Model size (b × c)	α (Tran-Cao, 2009)	Associative		Non-associative formulation		Analytical solution α
			α_{assoc}	CPU Time (s)	$\alpha_{\text{non assoc}}$	CPU Time (s)	
Circular arch	16 x 68	4.45	4.45	0.02	4.45	0.05	4.45
Two rings arch	33 x 268	17.29	15.12	0.03	14.19	0.18	15.1
Barrel vault	81 x 860	3.06	2.48	0.06	2.48	0.18	2.48

Table 5.1 - Masonry arches and vaults under vertical live loads: comparison of numerical results.

The comparison of results with those obtained in (Tran-Cao, 2009) shows a perfect agreement in the case of the single ring arch, both in terms of failure mechanism and load factor. In contrast, a remarkable difference of the results between LiABlock_3D and those reported in (Tran-Cao, 2009) can be noted for the other case studies. In the case of the barrel vault, this is because a different failure mechanism is obtained in (Tran-Cao, 2009), with different position of the hinges.

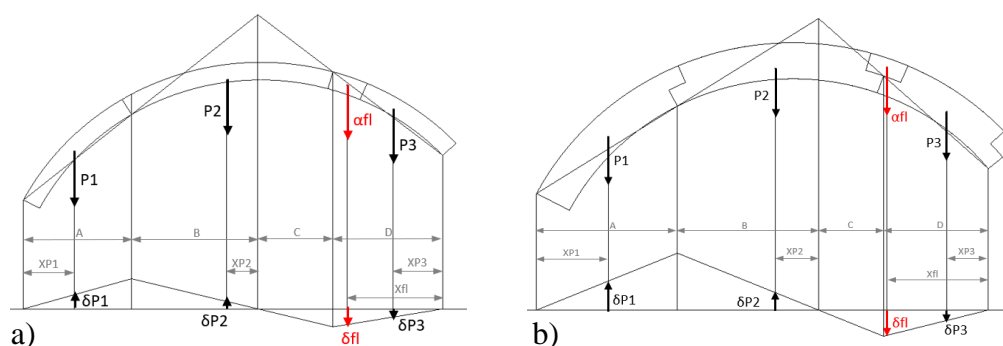


Figure 5.2 – Sketches of the analytical solutions in the case of (a) circular arch and (b) two-ring arch.

However, in the interests of safety, it should be noted that the lower value of the collapse load multiplier obtained with LiABlock_3D was also validated against the analytical solution which was obtained using rigid body mechanism analysis

and virtual work principle (Figure 5.2). The differences observed in the case of the double ring arch can be ascribed to the different formulation of the limit analysis problem and solver adopted in (Tran-Cao, 2009).

The case study of a circular arch subject to eccentric load was also considered to point out the ability of the proposed formulation to capture 3D behaviour associated to torsion failure on curved assemblages. The arch configuration and dimensions were inspired to the case studies presented in (Livesley, 1992) and (Tran-Cao, 2009). The model is made of four blocks subject to dead loads applied to the centroid of each block and corresponding to unit weight (Figure 5.3a). An additional rigid block was generated to apply an eccentric live load according to the configuration presented in (Tran-Cao, 2009) and expressed as a factor of the unit weight of the loading block.

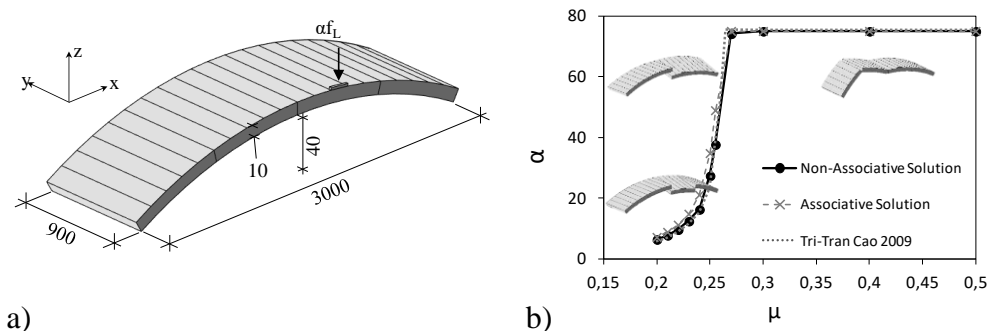


Figure 5.3 - Four block arch subjected to eccentric live load: (a) configuration and (b) sensitivity analysis to friction coefficient (Cascini, Gagliardo and Portioli, 2020).

The results of the numerical analysis obtained when varying the friction coefficient in the range 0.50–0.20 are shown in Figure 5.3b. A four hinges failure mechanism is obtained when the friction coefficient is larger than 0.270. For lower values of the friction coefficient, twisting mechanisms occur which involve two blocks, or a single block as indicated in Figure 5.3b. The failure mechanisms obtained and collapse load multipliers are in a good agreement with those reported in (Tran-Cao, 2009).

5.2.1.2 A skew arch subjected to point live load

In this section, the limit analysis numerical formulation is applied to the case of an experimental specimen of a skew arch, named Skew2 in (Wang, 2004), already investigated in (Forgács, Sarhosis and Bagi, 2018) using DEM software. Masonry arch bridges do not always span the distances perpendicularly but with an angle depending on the conditions at the site. Two most common construction techniques for skew masonry arch bridges are helicoidal skew and false skew. The specimen is represented by a masonry arch with 45° skew and 3 m span. For the geometrical features, the arch is 670 mm width and 220 mm thick and it is made up of two brickwork rings connected by headers.

The arch was constructed using Class A engineering bricks on two reinforced concrete abutments representing rigid supports. In the test, a concentrated load P was applied under force control at the three-quarter span mid-width of the arch barrel as schematically shown in Figure 5.4. The load was monotonically increased up to $P_{u,exp} = 17.4$ kN when collapse occurred due to the formation of five cracks extending in the mortar joints through the whole width of the arch. These divided the arch into four blocks of brickwork rotating about the lines of fracture. The cracks were not parallel due to the specific geometry of the arch and the orientation of the mortar joints giving rise to a 3D failure mode typical of skewed masonry arches.

Two different numerical models were developed on this case study. The first one is represented by a simplified model, where the south and north abutments are perpendicular to the arch span and the arch is represented by a single ring. A geometrical model representing the brickwork skew arch tested in the laboratory was created. The rigid elements are represented by 3D polyhedral blocks separated by zero thickness interfaces in order to reproduce mortar layers. The rigid block model is showed in Figure 5.4. The geometrical model was created in a Computer Aided Design environment and consist of 234 rigid blocks and 2300 contact points. Unit weight and friction coefficient used for the computational model was set according to (Wang, 2004). The unit weigh is equal to 2240 kg/m^3 and the friction coefficient was set equal to 0.65 since the experimental value of

the friction angle was equal to 33° . The live load was expressed as a factor of the weight of the corresponding loaded blocks.

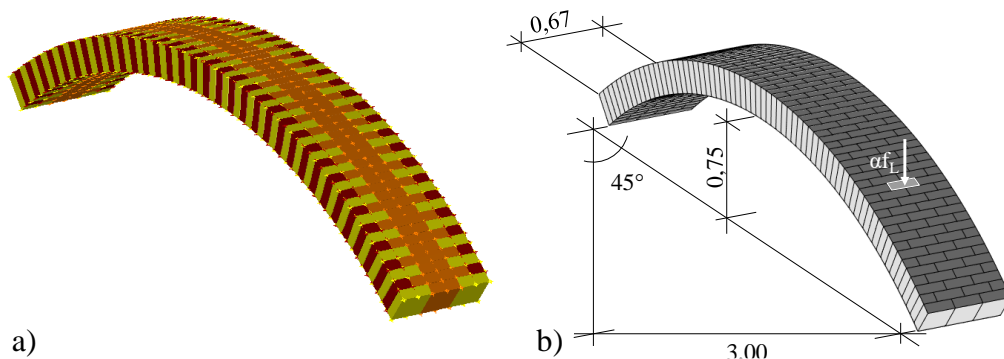


Figure 5.4 - Skew arch first type: geometrical model in AutoCAD (a) and rigid block model (b).

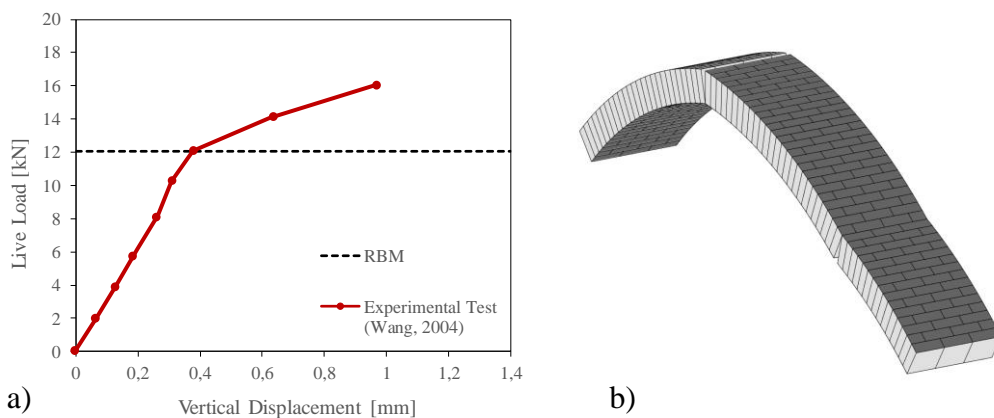


Figure 5.5 - Skew arch first type: numerical vs experimental comparison in terms of load-displacement curve (a) and RBM failure mode (b).

The comparison between numerical and experimental results was carried out in terms of collapse load against vertical displacement of the reference point on the arch, as suggested by the test. Figure 5.5a shows the results of the comparison. It is possible to notice that the rigid block model returns a lower value of the collapse load compared with the experimental results. The numerical formulation underestimated the ultimate strength of the skew arch under vertical loads. The reason why is probably because of the geometrical simplified assumption of the

model, where the blocks interaction along the surface is not as performant as in the experimental configuration. The collapse mechanisms and the cracks pattern obtained with the discrete model is showed in Figure 5.5b.

The second numerical model developed for the case study of the skew arch is based on the idea to better reproduce the real geometry of the tested specimen. The second model does not consider the simplified assumption of abutments perpendicular to the arch span and the bricks are modelled in order to be located in the same position and with the same direction of those in the test. The rigid block model (Figure 5.6) is made by 197 rigid blocks and 1388 contact points.

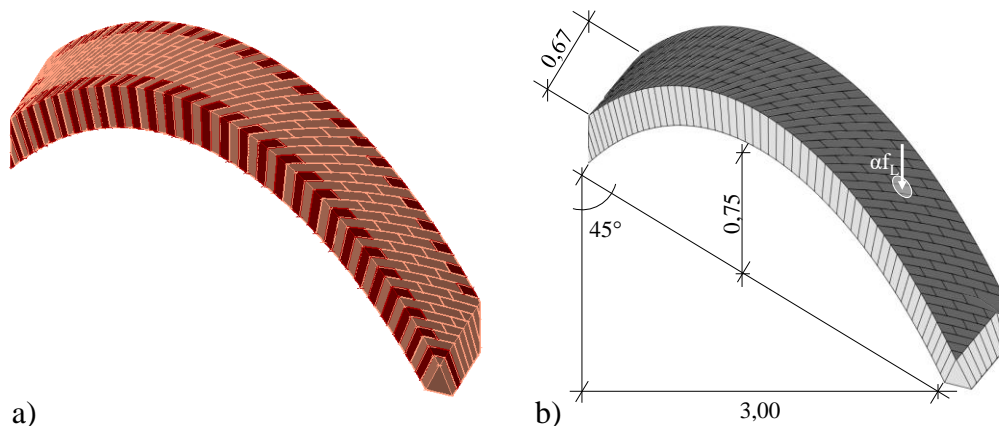


Figure 5.6 - Skew arch second type: geometrical model in AutoCAD (a) and rigid block model (b).

Figure 5.7a shows the comparison between the numerical analysis and the experimental test performed in (Wang, 2004) in terms of collapse load and vertical displacement of the reference point on the arch, considering a value of 0.4 for the friction coefficient in the rigid block model. The Figure 5.7b deals with the failure mode activated in the rigid block simulation: the cracks openings are in good agreement with the experimental test performed in (Wang, 2004). However, it should be noted that the numerical analysis showed high sensitivity of the collapse load to the value of the friction coefficient, and higher values of the collapse load multiplier were obtained when using larger values of the friction

coefficient, such as those measured in the experimental tests. This aspect is worth of further investigation.

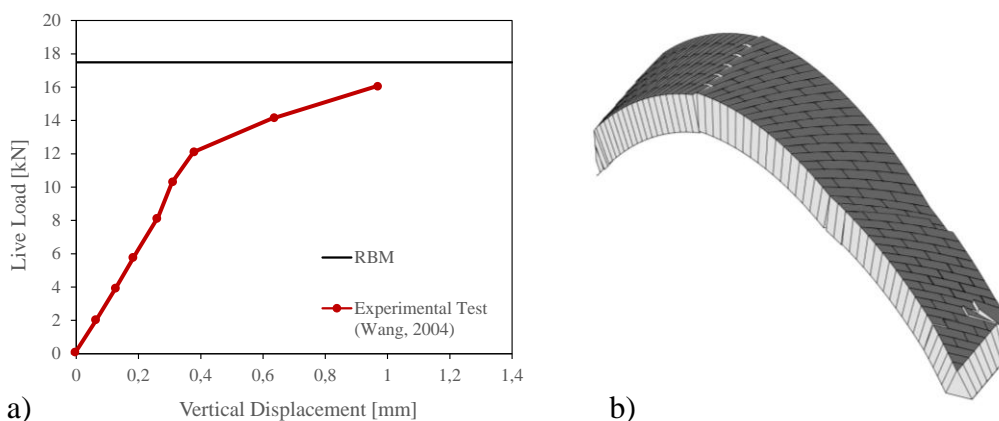


Figure 5.7 - Skew arch second type: numerical vs experimental comparison in terms of load-displacement curve (a) and RBM failure mode (b).

5.2.1.3 Masonry dome subjected to horizontal live loads

The dome considered is a small scale specimen made of dry-stacked plaster blocks (Zessin, 2012). The dimensions of the dome are shown in Figure 5.8a. The exterior radius is equal to 164.0 mm and thickness is equal to 32.8 mm. The dome was tested on a tilting table in order to investigate failure mechanism and acceleration value promoting the collapse under a uniform distribution of lateral accelerations (Zessin, 2012). The rigid block numerical model is made of 137 blocks and 1276 contact points located along bed joint interfaces. The numerical model was generated in AutoCAD from 8 block types which were obtained by dividing the dome into seven rings and a central cap using polar angles as indicated in (Zessin, 2012). The value of friction coefficient was taken as 0.7, according to (Quinonez *et al.*, 2010; Zessin, Lau and Ochsendorf, 2010; Zessin, 2012), and a unit weight of 12.5 kN/m^3 was used. To reproduce experimental loading conditions, each block was subjected to horizontal live loads expressed as a factor of the block unit weight. The computed collapse load factor and predicted failure mechanism are presented in Table 5.2 and Figure 5.8b. The dome collapses with a five hinges failure mechanism along the meridian sections,

also involving opening and sliding failures distributed along vertical and bed joint interfaces, respectively.

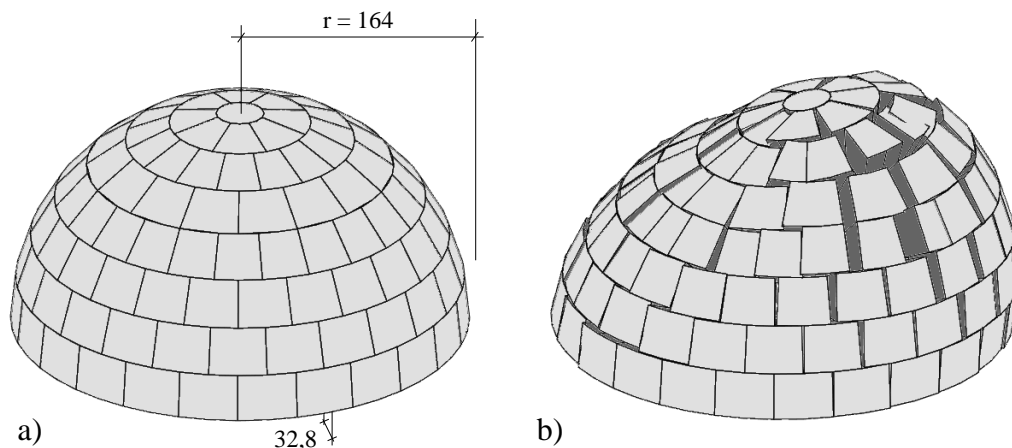


Figure 5.8 - (a) Hemispherical dome dimensions and (b) hemispherical dome collapse mechanism (Cascini, Gagliardo and Portioli, 2020).

Model	Model size (b × c)	α (Zessin, 2012)	Associative		Non-associative formulation		Diff. α %
			$\alpha_{assoc.}$ (kN)	CPU Time (s)	$\alpha_{non-assoc.}$ (kN)	CPU Time (s)	
Dome	137×1276	0.460	0.589	0.9	0.536	2.4	16.5

Table 5.2 - Masonry dome under horizontal live loads: comparison of numerical and experimental results.

The comparison with the experimental tests presented in (Zessin, 2012) shows a quite good agreement with numerical results. The angles of extrados and intrados hinge positions are slightly different from those observed experimentally (Zessin, 2012). For example, whereas the location of an intrados hinge was observed experimentally between the second and third row of blocks on the right end side of the dome, multiple hinge locations are predicted by the numerical model at the upper block rows. Moreover, significant sliding failures were observed experimentally between lower block rows just before collapse, which can be also associated to the large displacement regime rather than to the onset (i.e., initiation) of the failure mechanism, where small displacement can be assumed in accordance to the numerical model. The difference of numerical and

experimental collapse load multipliers is 16.5%, which can be likely ascribed to the influence of geometric imperfections (i.e., corner rounding and construction) on test results. In terms of computational efficiency, the numerical analyses took only a few seconds to obtain a solution, as reported in Table 5.2 for the associative and non-associative solution.

5.2.1.4 Small scale wall components

5.2.1.4.1 Single-leaf masonry walls

Numerical simulations based on two tilting tests carried out at the University of Pavia (Restrepo Vélez, Magenes and Griffith, 2014) on 1:5 scale dry-stone masonry prototypes are presented in this section. A sensitivity analysis to friction coefficient, block size ratio and numerical starting conditions was also carried out to evaluate the effects on the predicted response (Malena *et al.*, 2019).

The two tests were selected to compare the predicted response for both the in-plane and the out of plane behaviour. The first prototype analysed is the S22, made of a main wall and three partition walls with openings. The main wall was 21 bricks high and 14 bricks wide, while the partition walls were 21 bricks high and 10 bricks wide with one opening each, 15 bricks high and 2 bricks wide. The second numerical simulation deals with the S5 prototype, made of a main wall and two partition walls. The main wall is 21 bricks high and 8 bricks wide, while the partition walls are 21 bricks high and 4 bricks wide. Masonry prototypes were made of blocks whose dimensions are equal to $30 \times 80 \times 40 \text{ mm}^3$, the unit weight of the masonry is 26.8 kN/m^3 , while the friction coefficient μ was assumed equal to 0.7.

Numerical simulations of the tilting tests were performed considering that blocks were subject to self-weight loading and to varying horizontal loads associated to blocks self-weight and tilt angle. In the case of the rigid block model, this loading condition was simply reproduced considering horizontal live loads expressed as a function of the load factor α and block self-weight. In Figure 5.9 the results obtained for the S22 experimental test are represented in terms of failure modes obtained for the associative and non-associative solutions. At collapse, the main feature of the crack pattern was the strong concentration of in plane joint opening

in the partition walls close to the door: different crack patterns can be noted in the spandrels above the openings for the non-associative solution, which are very similar to those observed experimentally.

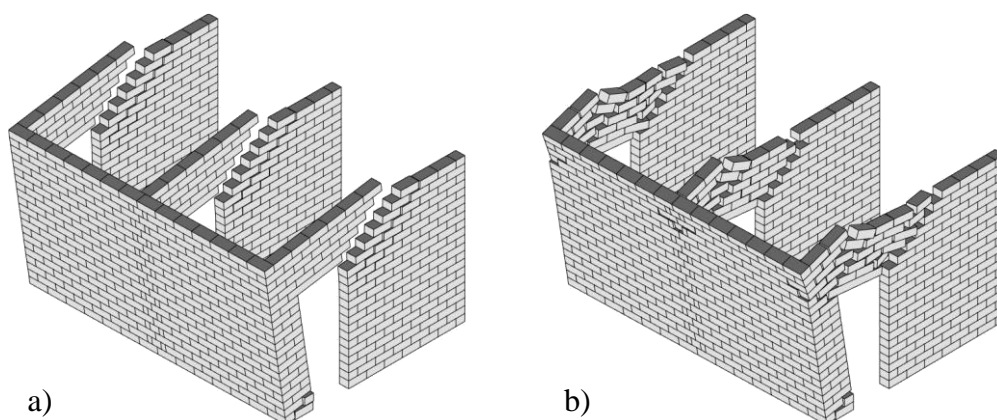


Figure 5.9 - Test S22 (Restrepo Vélez, Magenes and Griffith, 2014): (a) associative and (b) non-associative failure mechanisms using rigid block limit analysis (Malena, Portioli, Gagliardo *et al.*, 2019).

The failure mechanisms derived from the simulation of the S5 experimental test are presented in Figure 5.10. The crack pattern at the collapse was characterized mainly by the bending opening of the head joints in the central portion of the main wall interested by out of plane overturning and by the in plane opening of the head joints in the partition walls. About the comparison between experimental test and predicted collapse load multipliers, the discrepancy in terms of load factor was equal to +5.6% and -5.6% for test S22 and +28.4% and +8.9% for test S5, for the associative and non-associative behaviour, respectively. While the numerical outcomes for the test S22 match quite well with the observed behaviour, the results for the S5 are affected by a larger difference. This difference can be mainly ascribed to the simple contact model adopted in the case of the rigid block model, which produces an overestimation of the load factor when torsion behaviour is involved (Tran-Cao, 2009; Casapulla and Maione, 2018).

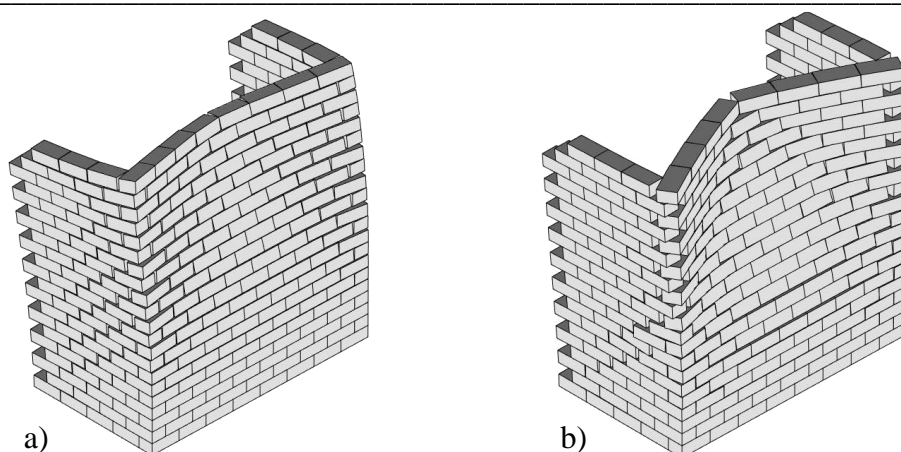


Figure 5.10 - Test S5 (Restrepo Vélez, Magenes and Griffith, 2014): (a) associative and (b) non-associative failure mechanisms using rigid block limit analysis (Malena, Portioli, Gagliardo *et al.*, 2019).

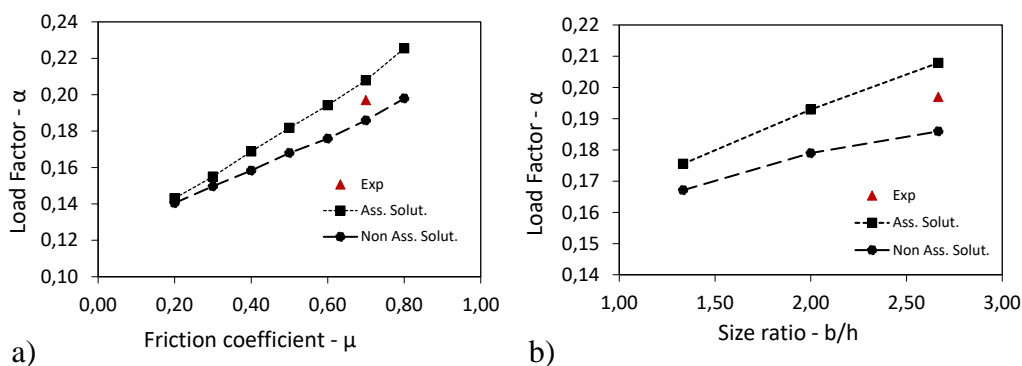


Figure 5.11 - Test S22: (a) sensitivity analyses to the friction coefficient and (b) to the block size ratio (Malena, Portioli, Gagliardo *et al.*, 2019).

Sensitivity analyses to friction coefficient and to the block size ratio were carried out with rigid block model. The results obtained in terms of load factor in the case of S22 are presented in Figure 5.11. As expected, lower values of the load factor are obtained when reducing the friction coefficient, for both the models. In terms of crack pattern at the collapse, the reduction of the friction coefficient

caused the development of a wider area involved in the opening of the joints, as shown in Figure 5.12, where the outcomes for $\mu = 0.4$ are reported.

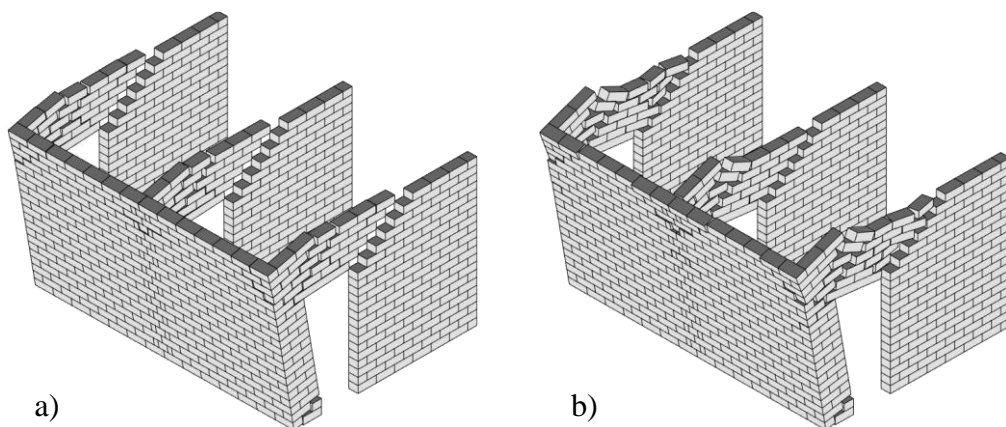


Figure 5.12 - Test S22: sensitivity analyses to the friction coefficient ($\mu = 0.4$ in the Figure). (a) associative and (b) non-associative failure modes predicted with the rigid block model (Malena, Portioli, Gagliardo *et al.*, 2019).

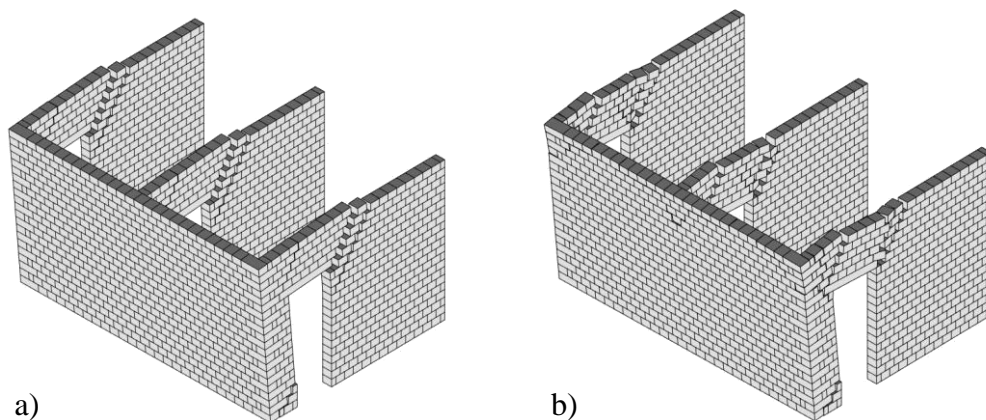


Figure 5.13 - Test S22: sensitivity analyses to the size ratio ($b = 40$ mm in the Figure). (a) associative and (b) non-associative failure modes predicted with the rigid block model (Malena, Portioli, Gagliardo *et al.*, 2019).

When varying the width b to height h ratio and more in detail fixing the height equal to 30 mm and reducing the width, lower values of the load factor are

obtained (Figure 5.11). In Figure 5.13 the results in terms of crack pattern at the collapse are reported for 40 mm block width, where a wider area involved into the in-plane joints opening can be noted.

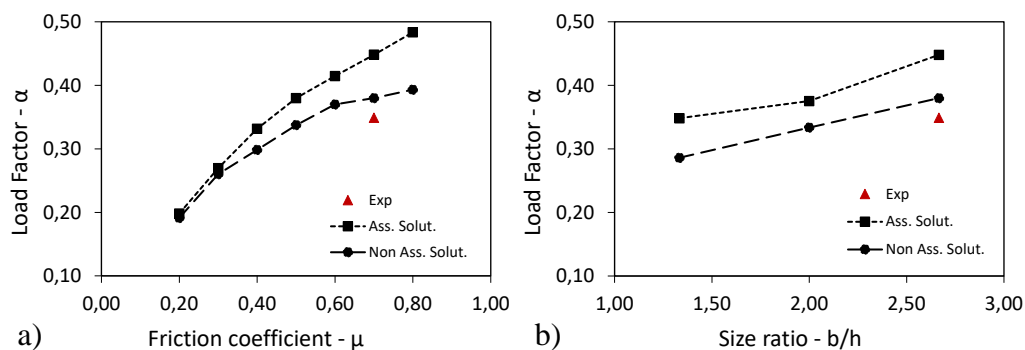


Figure 5.14 - Test S5: (a) sensitivity analyses to the friction coefficient and (b) to the block size ratio (Malena, Portioli, Gagliardo *et al.*, 2019).

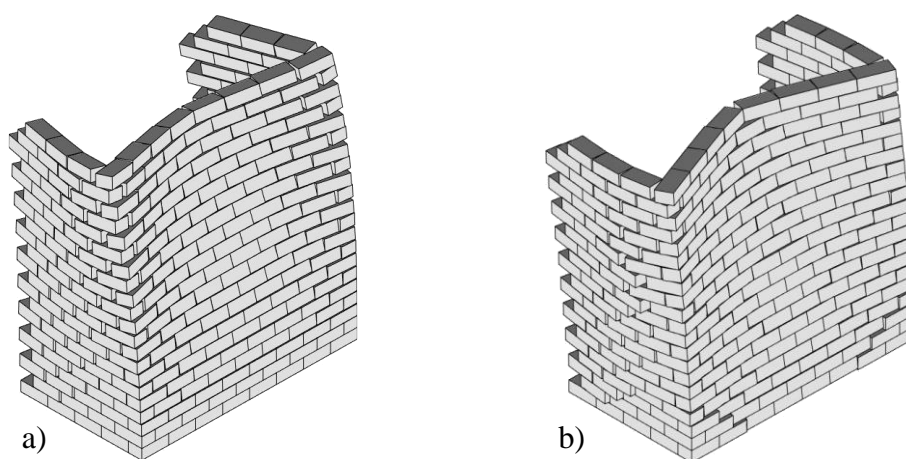


Figure 5.15 - Test S5: sensitivity analyses to the friction coefficient ($\mu = 0.4$ in the Figure). (a) associative and (b) non-associative failure modes predicted with the rigid block model (Malena, Portioli, Gagliardo *et al.*, 2019).

The results of sensitivity analyses carried out on test S5 are shown in Figure 5.14. Also in this case, lower values of the load factor are obtained when reducing the friction coefficient, for both the models. In terms of crack pattern at the collapse,

the reduction of the friction coefficient caused an overturning of the main wall less localized in its upper part, as highlighted in Figure 5.15 where the results for $\mu = 0:4$ are reported. Also in this case, lower values of the load factor are obtained when the size ratio b/a is reduced. In Figure 5.16, the results in terms of crack pattern at the collapse for the case with 40 mm block width are shown. The reduction of the size ratio does not affect the portion of the main wall involved in the overturning but increases the intensity of the joints opening.

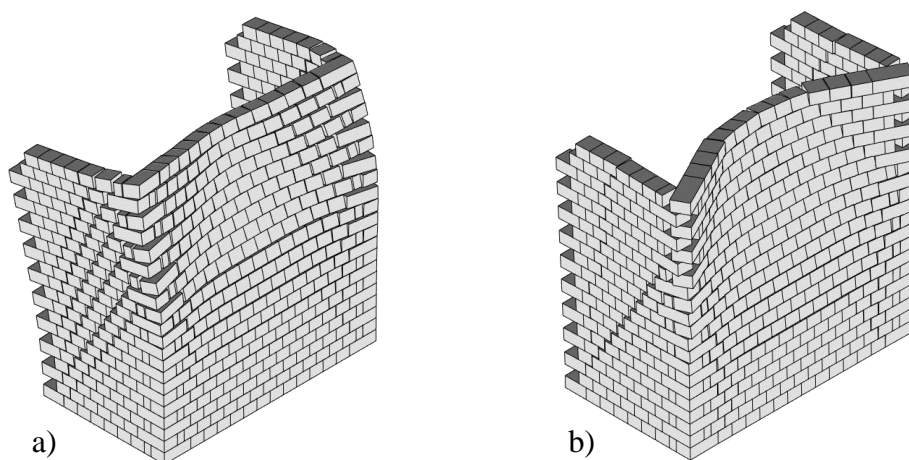


Figure 5.16 - Test S5: sensitivity analyses to the size ratio ($b = 40$ mm in the Figure). (a) associative and (b) non-associative failure modes predicted with the rigid block model (Malena, Portioli, Gagliardo *et al.*, 2019).

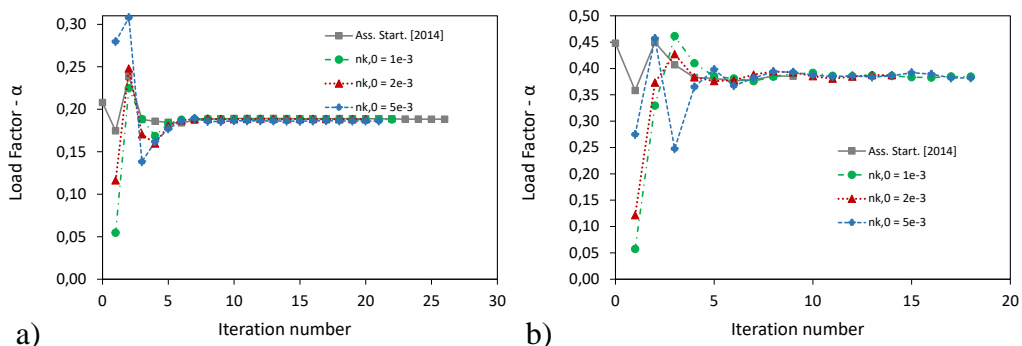


Figure 5.17 - Convergence plots and sensitivity analyses to starting conditions for (a) Test S22 and (b) Test S5 (Malena, Portioli, Gagliardo *et al.*, 2019).

In the case of the small-scale wall components, a sensitivity analysis to starting conditions was carried out for the iterative solution procedure used to take into account non-associative sliding behaviour. The results show that the convergence behaviour is only slightly influenced by starting conditions when varying the initial value of the normal forces in the range considered (Figure 5.17). In the case of specimen S22, it was observed that the number of iterations required to converge was less than that required for the standard iterative procedure using the associative solution as a starting point. However, in general CPU times were only slightly affected by the starting value of normal forces, also due to the limited number of blocks comprised in these case studies.

5.2.1.4.2 Three-leaf masonry walls

In this section, the rigid block limit analysis tool is applied to the blind-test prediction of experimental shake-table tests on two small-scale three-leaf masonry walls in order to evaluate the software reliability in the prediction of seismic-induced collapse mechanisms (Gagliardo, Cascini, *et al.*, 2019).

The case studies comprise two experimental shake-table tests developed at the University of Chieti-Pescara “Gabriele D’Annunzio” on two small-scale masonry walls. For sake of clarity, it is worth noting that experimental tests have not been yet carried out and therefore only the numerical outcomes are described. With this in mind, the numerical application represents a blind-test prediction on three-leaf masonry walls made of two panels outside and an internal filling. The panels are 140 mm width and are made of stone blocks with dimensions 350 x 140 x 140 mm and mortar joints of 15 mm thickness. The internal filling is 170 mm width. The first case study is a simple wall and the second is a T-wall. The specimen is provided of a steel frame on the top for the application of a 6 tons additional mass. In the case of the T-wall, only in-plane load was contemplated. Figure 5.18 shows the geometry and loading condition for the two case studies. Experimental campaign was carried on in order to obtain the mechanical properties of both mortar and stones. The shear tests return the value of the stone’s properties involved in the sliding failure: the cohesion c , the friction coefficient μ and the sliding shear strength f_{vk0} was measured as 0.11 MPa, 0.21 and 0.091 MPa respectively. The Gazli earthquake record was selected as seismic

input in the experimental tests. The Gazli earthquake dates to the 17th of May in 1976, with a magnitude equal to 6.8. Both horizontal and vertical acceleration component will be considered during the shake-table test.

The numerical models were generated through the proposed micro-modelling approach and then analysed in LiABlock_3D. The block size follows the experimental data with a difference: seeing as how the formulation is not considering the mortar contribution, the brick size was increased in order to cover the mortar joints. Ad hoc blocks were generated to model the internal filling. The first case study (Figure 5.18a) is made of 150 rigid blocks and 1812 contact points. The second case study (Figure 5.18b) is made of 241 rigid blocks and 2988 contact points. With respect to mechanical parameters, the weight per unit volume was set equal to 24 kN/m^3 (average value for the selected stone type, *pietra di Pacentro*), the friction coefficient was set in the range between 0.4 (the value suggested by the Italian code (Ministero delle infrastrutture e dei trasporti., 2018)) and 0.6, and the cohesion was set equal to 0.00.

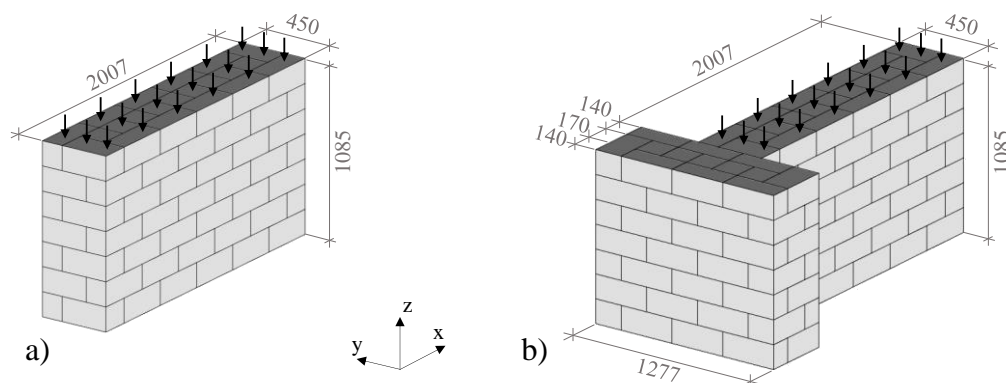


Figure 5.18 - Three-leaf masonry walls geometry and loading condition: a) simple wall; b) T-wall (Gagliardo, Cascini, *et al.*, 2019).

Both loading directions along the x-axis was analysed in order to simulate the cyclic behaviour of the seismic input considered in the experimental shake-table tests. Figure 5.19, Table 5.3 and Table 5.4 summarize the numerical outcomes obtained by the rigid block model. Figure 5.19 shows the collapse mechanisms activated when a lateral live load is applied along the x-axis in both directions

and a value of coefficient friction equal to 0.40 is used. The prevalent failure condition is the sliding at the contact points, except for the mechanism showed in Figure 5.19b, where the model exhibits the overturning of the side wall. Table 5.3 and Table 5.4 contains the output of the analysis in LiaBlock_3D.

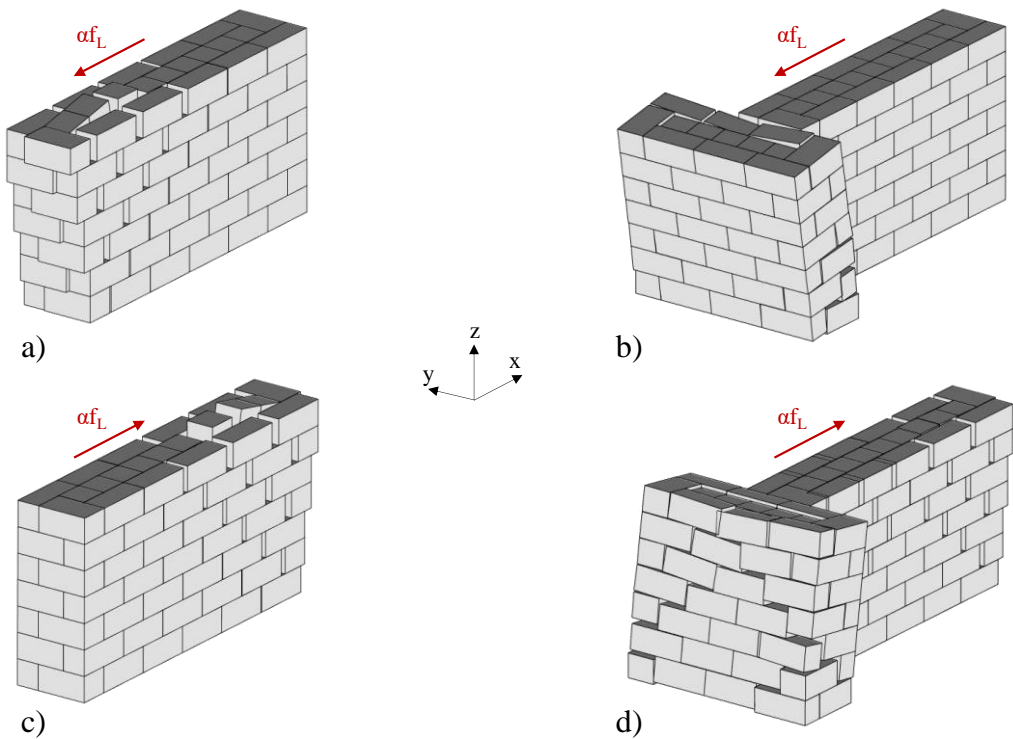


Figure 5.19 - Collapse mechanism induced by live load applied along x-axis in both directions: (a)(c) simple wall; (b)(d) T-wall (Gagliardo, Cascini, et al., 2019).

Model size (b x c)	ρ [kN/m ³]	c [N/mm ²]	Load directions	μ [-]	Numerical Solution		
					α [-]	αf_L [N]	CPU Time [s]
150 x 1812	24	0.00	positive x-axis	0.40	0.38	31103.48	1.31
				0.50	0.45	37478.94	1.57
				0.60	0.56	46423.97	0.20
			negative x-axis	0.40	0.38	31068.96	1.36
				0.50	0.45	37478.94	1.58
				0.60	0.56	46423.97	0.30

Table 5.3 - The case study of the simple wall: numerical output using rigid block limit analysis.

Figure 5.20 shows the sensitivity analysis to the friction coefficient for both simple wall and T-wall specimens in terms of collapse load factor versus iteration number. As above mentioned, three values of friction coefficient were selected. Higher values of friction coefficient return higher value of the load factor and of the corresponding shear force at collapse.

Model size (b x c)	ρ [kN/m ³]	c [N/mm ²]	Load directions	μ [-]	Numerical Solution		
					α [-]	αf_L [N]	CPU Time [s]
241 x 2988	24	0.00	positive x-axis	0.40	0.35	13522.47	2.83
				0.50	0.42	16405.84	2.76
				0.60	0.50	19229.06	1.92
			negative x-axis	0.40	0.27	10504.92	2.15
				0.50	0.29	11270.83	2.61
				0.60	0.31	12027.33	1.63

Table 5.4 - The case study of the T-wall: numerical output using rigid block limit analysis.

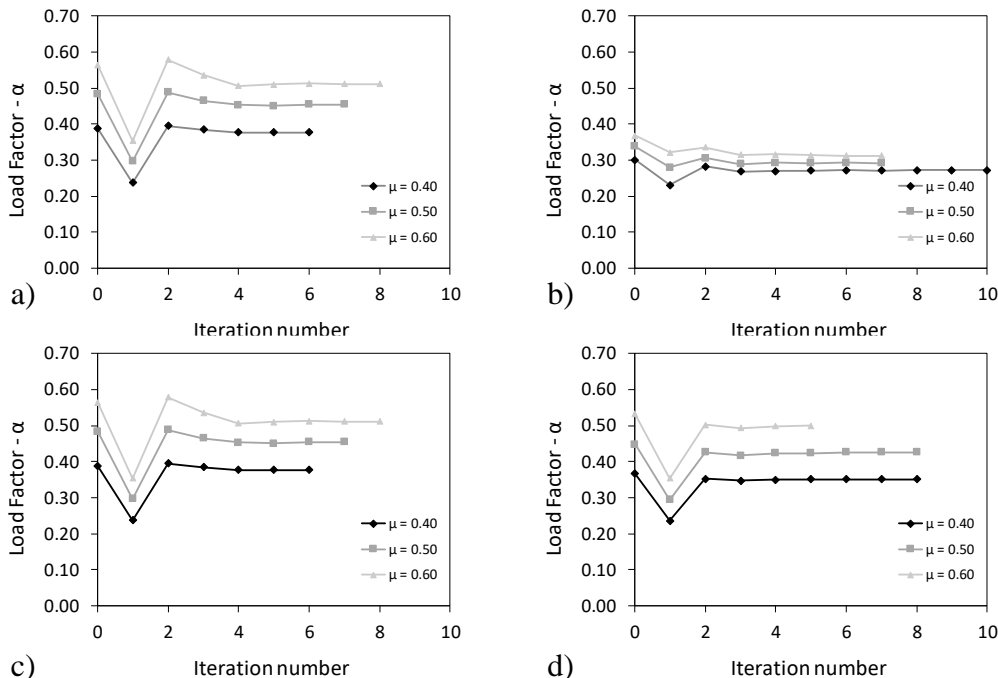


Figure 5.20 - Collapse load factor vs iteration number for both simple wall (a)(c) and T-wall (b)(d) numerical simulation considering live loads applied along both negative (a)(b) and positive (c)(d) x-axis (Gagliardo, Cascini, et al., 2019).

The numerical analysis showed that the collapse could be expected for a load applied along both directions of the x-axis based on the shake-table shaking and the failure could occur with the overturning of the side wall along the negative direction or with the sliding in the opposite directions. The value of the acceleration promoting collapse in the experimental test should be derived by the value of the collapse load factor and the value of the behaviour factor. Following the assessment method of force-based approach, the estimated peak ground acceleration (PGA) at collapse should be in the range between 0.8g and 1.0g, considering a behaviour factor equal to 2.

5.2.1.5 Application to monumental historical masonry buildings

In this section, the numerical formulation based on limit analysis is tested against the structural behaviour investigation of monumental historical masonry buildings, which are part of the built Cultural Heritage. The case studies below described are: Ponti della Valle di Maddaloni (Gagliardo, Terracciano, *et al.*, 2019) and the Church of San Nicolò di Capodimonte (Malena *et al.*, 2019).

5.2.1.5.1 Ponti della Valle di Maddaloni

The case study is the so-called “Ponti della Valle di Maddaloni” that is a part of the Caroline Aqueduct designed by Luigi Vanvitelli on commission of the Bourbon King, Charles III. Built between the 1753 and 1770 to supply water to the Royal Palace and Gardens of Caserta and the industrial complex of San Leucio, the aqueduct transports water from the slopes of Mount Taburno to the Royal Palace, covering a mostly underground route of 38 kilometres length. This infrastructure is considered one of the most important expression of the Architecture and Engineering of the XVIII century. This extraordinary hydraulic engineering work is listed by UNESCO as World Heritage Site since 1997.

The viaduct *Ponti della Valle* (Figure 5.21) represents the most famous structure of the aqueduct above-ground. It is still perfectly preserved in its original structure and material, although it suffered three severe seismic events in the last centuries. The structure is made of tuff masonry, with 3 arches order and 44 squared pillars. It is 528 meters long and the maximum height is equal to 55.80

meters (UNESCO World Heritage List, 1997). In this study, a portion of the whole structural system between three pillars is considered.



Figure 5.21 - Aqueduct Carolino - “I Ponti della Valle di Maddaloni”.

The analytical model is composed of 3344 polyhedral rigid blocks (b) and 38224 contact points (c), (Figure 5.22 and Figure 5.23). The block size was set according to the average block size ratio of the real structure. The dimensions of the blocks are 1720 x 2400 x 600 mm, except for the blocks of the arches and buttresses. The weight per unit volume ρ of the masonry was assumed equal to 16 kN/m³ and the value of the friction coefficient μ was set equal to 0.6. The behaviour of the structural system was investigated for in-plane and out-of-plane horizontal forces. In both cases the horizontal live load is a factor of the block self-weight. In the present study, a single pillar was loaded against lateral loads for a preliminary comparison of the rigid block and finite element model. The LiABlock_3D output is summarized in Table 5.5. For each load direction, the table contains the collapse load factor calculated for the associative and non-associative solution, as defined in Section 2, the collapse load αf_L and the CPU Time (Gagliardo, Terracciano, *et al.*, 2019).

As for the non-associative solution, the algorithm parameters β and ξ were set equal to 0.6 and 0.0, respectively; the fictitious cohesion c_k^0 was fixed equal to $1e^{-5}$ times the largest normal force calculated at a given iteration. The algorithm

was set in accordance to (Gilbert, Casapulla and Ahmed, 2006; Portioli *et al.*, 2014) to avoid convergence problems and optimize the iterative solution procedure in terms of number of iterations to obtain the convergence. The convergence tolerance was $1e^{-3}$, using a number of iterations equal to 10.

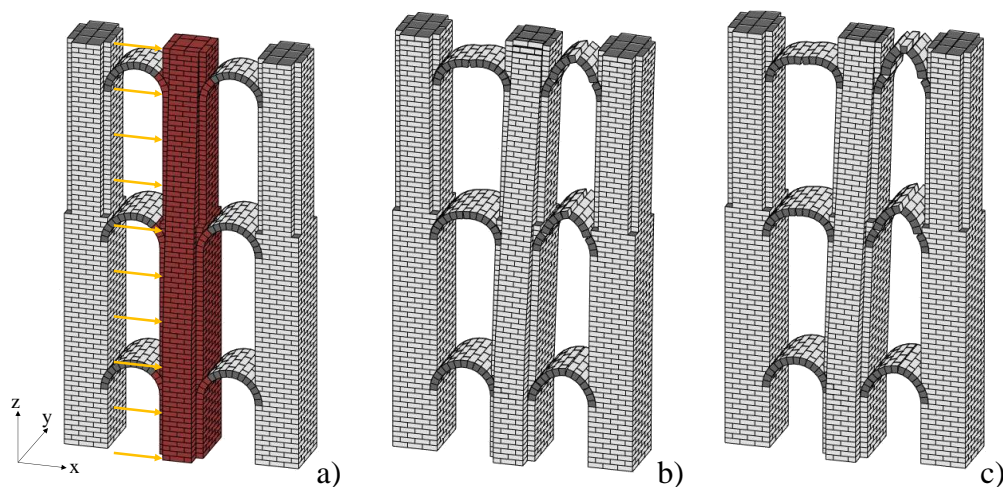


Figure 5.22 - In-plane collapse mechanism: a) Geometry and load; b) Associative plot; c) Non-Associative plot (Gagliardo, Terracciano, *et al.*, 2019).

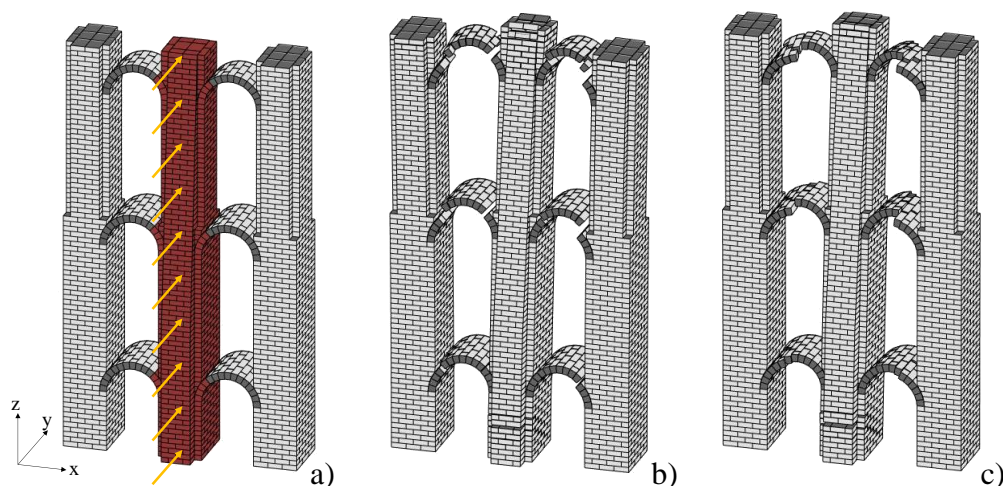


Figure 5.23 - Out-of-plane collapse mechanism: a) Geometry and load; b) Associative plot; c) Non-Associative plot (Gagliardo, Terracciano, *et al.*, 2019).

Figure 5.22 and Figure 5.23 show the collapse mechanisms corresponding to the in-plane and out-of-plane loading condition, respectively. Both associative and non-associative solutions are plotted. For the in-plane loading condition the collapse occurs by a four-hinge failure mode in the arches of the two spans (Figure 5.22b and Figure 5.22c). For the out-of-plane loading condition the failure mechanism involves the overturning of the central pillar (Figure 5.23b and Figure 5.23c).

Model size (b x c)	Load direction	Associative Solution			Non-Associative Solution		
		α [-]	αf_L [kN]	CPU Time [s]	α [-]	αf_L [kN]	CPU Time [s]
3344 x 38224	in plane	0.185	6027.98	4.64	0.183	5978.39	71.08
	out of plane	0.296	9649.60	4.79	0.284	9267.62	29.24

Table 5.5 - Numerical outcomes for in-plane and out-of-plane collapse mechanisms analysis of Ponti della Valle di Maddaloni.

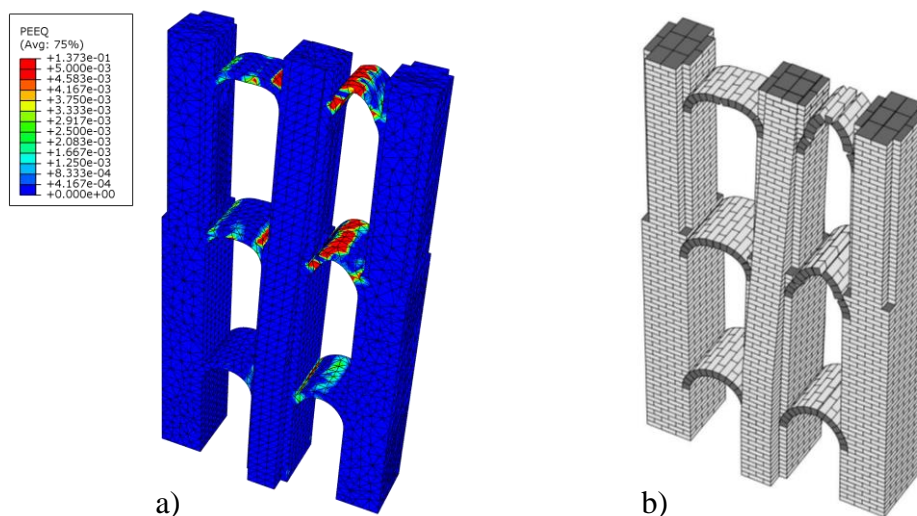


Figure 5.24 - In-plane loading condition. Comparison between the distribution of the equivalent plastic strain (PEEQ) in the FEM model and cracks position in the rigid block model (Gagliardo, Terracciano, et al., 2019).

The predictive capabilities of the software were assessed by means of the comparison with a continuum modelling approach. The structural system presented before was analysed by the finite element software Abaqus (Simulia,

2014). Quadratic tetrahedral elements were selected to model the masonry structure. A total of 40312 C3D10 elements connected with 63179 nodes were used to model the structural system. The pillars were assumed to be fully restrained at their base. As for the mechanical characterization of the material, the masonry was treated as a homogeneous, isotropic continuum with a nonlinear behaviour simulated by the concrete damaged plasticity (CDP) model. At this aim, the average compressive strength was fixed equal to 2 N/mm^2 and the tensile resistance was assumed equal to 0.06 N/mm^2 .

Static analysis under force control was used to investigate both in-plane and out-of-plane behaviour of the structure, subjected to increasing horizontal loads on the central pillar. Figure 5.24 and Figure 5.25 show the equivalent plastic strains for the in-plane (Figure 5.24a) and out-of-plane (Figure 5.25a) loading condition. Tension cracks were observed in the arches for in-plane loads, while tension cracks in the arches and at base of the central pillar appeared in case of out-of-plane actions. Such results are in good agreement with the rigid block limit analysis outcomes presented in Figure 5.24b and Figure 5.25b.

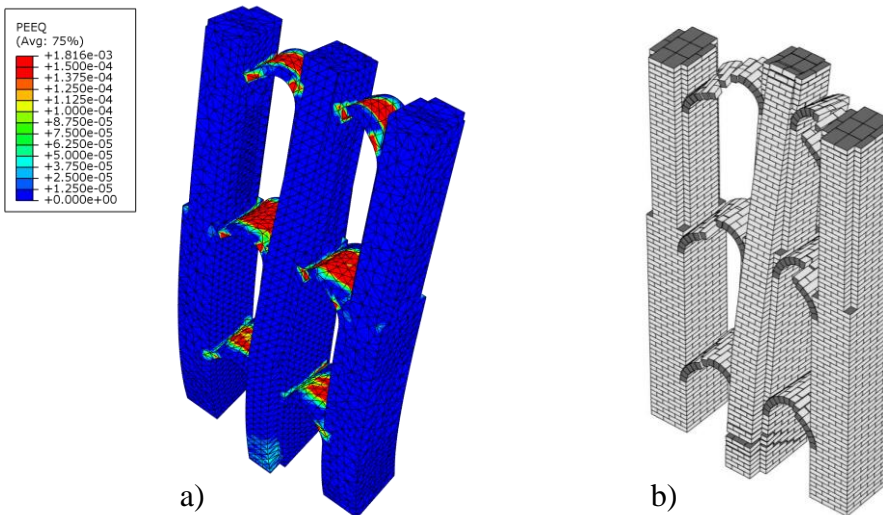


Figure 5.25 - Out-of-plane loading condition. Comparison between the distribution of the equivalent plastic strain (PEEQ) in the FEM model and cracks position in the rigid block model (Gagliardo, Terracciano, *et al.*, 2019).

Conversely, the ultimate loads are different for the compared procedures. According to the continuum approach the collapse load factor α associated with the in-plane and out-of-plane mechanisms are equal to 0.13 and 0.21. Such results compared with non-associative solutions provided by the rigid block limit analysis shown in Table 5.5, highlight an overestimation of the collapse loads by LiABlock_3D. This circumstance could be due to compressive crushing at the base of pillars not accounted in LiABlock_3D as basic assumption but considered in the FE analysis because of the DCP material model. In order to investigate this point, a second numerical simulation of the finite element model was performed assuming infinite compressive strength. As it happens, no relevant differences were observed in terms of distribution of the equivalent plastic strain and collapse load factors. This basically demonstrated that plasticity zones only deal with tensile stress.

5.2.1.5.2 Church of San Nicolò di Campodimonte

The numerical case study under investigation in this section is a masonry construction representative of a typical ancient church characterized by a longitudinal plan, in the form of the Latin Cross, already studied in (Malena *et al.*, 2019). The case study was inspired by the church of San Nicolò di Capodimonte (Camogli, Genova, Italy), mainly for the dimensions of the different part of the buildings, the type of macro-elements (i.e. the façade, the triumphal arches, the nave, the transept, the apse and the bell tower) as well as for the texture of the limestone block masonry which was used in this case. A long single nave, of about 18 m, is crossed by a transept 14 m large (Figure 5.26). A chapel and a bell tower are located in the transept next to the apses. The bell tower is about 17.0 m height while the nave is 14.0 m height. The roof structure was not taken into account in the analysis because the focus of the present study was to compare the two modelling approaches on the basis of the response of vertical bearing structures only, rather than to perform a capacity assessment of the real building. Moreover, it should be noted that possible rubble masonry sections which could be reasonably used in thicker parts of the real case study were treated as single leaf walls to restrict the number of configurations and geometric parameters affecting the response of the numerical models.

The discrete rigid block model of the church is made of 5161 blocks and 49,976 contacts. The average block size is 570 x 900 x 275 mm. The unit weight of masonry blocks for numerical simulation is 18.0 kN/m³ and the friction coefficient at block interfaces is 0.6. A distribution of lateral loads expressed as a factor of the self-weight was considered to simulate the effects induced by seismic actions. This distribution of lateral loads was set in accordance with code provisions comprising verification of local failure mechanisms, where a single multiplier (i.e. the load factor) is generally used to magnify lateral loads as a function of the corresponding vertical loads at different levels. However, it should be noted that alternative force distribution such as those corresponding to linearly varying accelerations might be used, especially for the analysis of global failure mechanisms, which could strongly affect the estimation of the load factor associated to the onset of collapse behaviour.

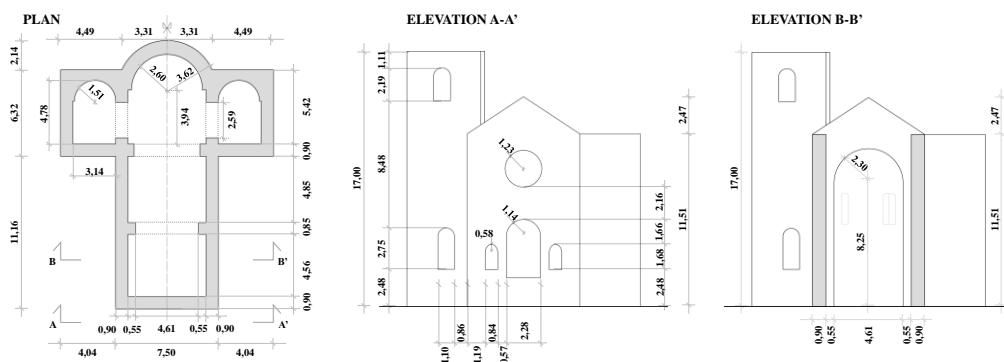


Figure 5.26 - Dimensions of the numerical case study of an ancient masonry church building.

Two different loading directions were considered for horizontal loads: the transverse direction (x-axis in Figure 5.27a), parallel to the transept, and the longitudinal direction (y-axis in Figure 5.27b) parallel to the nave. In Figure 5.27a, the failure mechanism obtained with the rigid block model are reported for the lateral loads acting along the x-axis. The numerical model predicts a collapse mechanism that essentially involves in-plane failures in the main facade and in the triumphal arches parallel to the main facade. The formation of diagonal cracks is observed in the façade between the openings, while the longitudinal walls parallel to y-z plane remain almost undamaged. With respect to the second

loading condition, Figure 5.27b reports the failure mechanism obtained for lateral loads along the y-axis and, in this case, the numerical model predicts the overturning of the main façade and of a portion of the sidewalls.

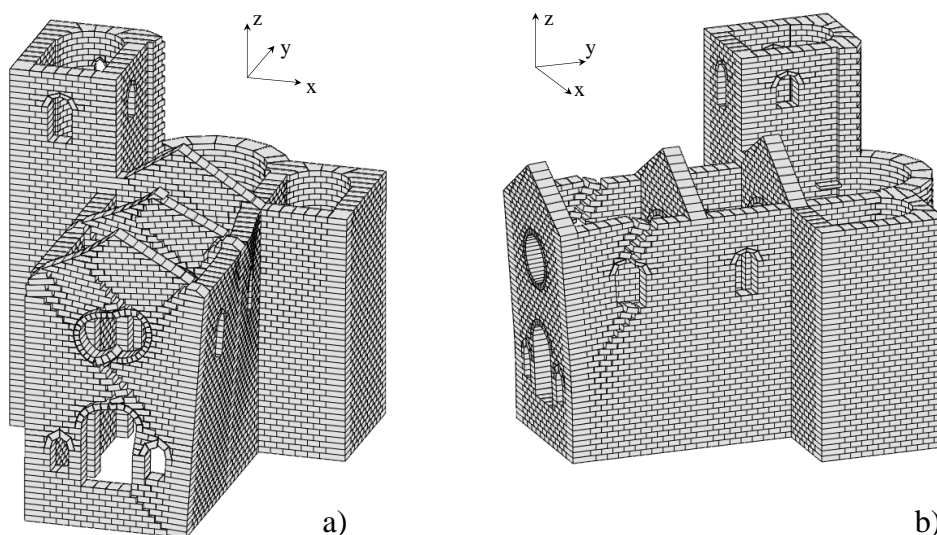


Figure 5.27 - Rigid block model of the church: non-associative failure modes for lateral load applied along the (a) x-axis and (b) along y-axis (Malena, Portioli, Gagliardo *et al.*, 2019).

The outcomes in terms of failure load multipliers are summarized in Table 5.6. Both the associative and non-associative solutions are reported. It is worth noting that the difference of associative and non-associative collapse load multipliers is up to 10 percent. It is also interesting to note that the associative solution is obtained in about 12 s, which is a reasonable CPU time considering the number of variables associated to the numerical model.

Lateral loads	μ	Rigid block model			
		Associative		Non-associative formulation	
		α_{assoc}	CPU Time (s)	$\alpha_{\text{non assoc}}$	CPU Time (s)
x-axis	0.6	0.221	12.5	0.201	126.1
y-axis	0.6	0.237	12.3	0.224	118.9

Table 5.6 - Numerical outcomes for lateral loads-induced collapse mechanisms analysis of a single-nave masonry church.

As reported in Table 5.6, the average CPU time evaluated on the total number of load steps is about 25–27 s. Considering the high number of variables needed to define the model, the results can be considered reasonable.

In the present case study of the single-nave masonry church, starting values of normal forces corresponding to a uniform distribution of normal forces n_0 are also used as an alternative to the normal force distribution n_{assoc} : corresponding to the associative solution, as it was in the iterative solution procedure generally used in the other case studies above presented. The uniform normal force distribution was used to check sensitivity of results to starting conditions and also to explore the possibility to save CPU time in case of large-scale problems. In Figure 5.28 the sensitivity to starting conditions is also shown for the rigid block model. Also, in this case, the results show that the predicted value of the load factor is not affected by starting conditions. As for computational efficiency, in most cases the number of iterations required to converge is larger than that required for the associative starting solution procedure. Thus, the CPU time which is saved in the first iteration when a uniform force distribution is used for starting rather than calculating the associative solution is spent on the larger number of iterations required to converge.

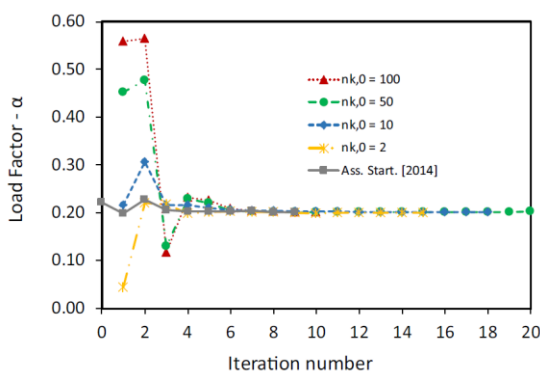


Figure 5.28 - Rigid block model convergence plot and sensitivity analysis to starting conditions (Malena, Portioli, Gagliardo *et al.*, 2019).

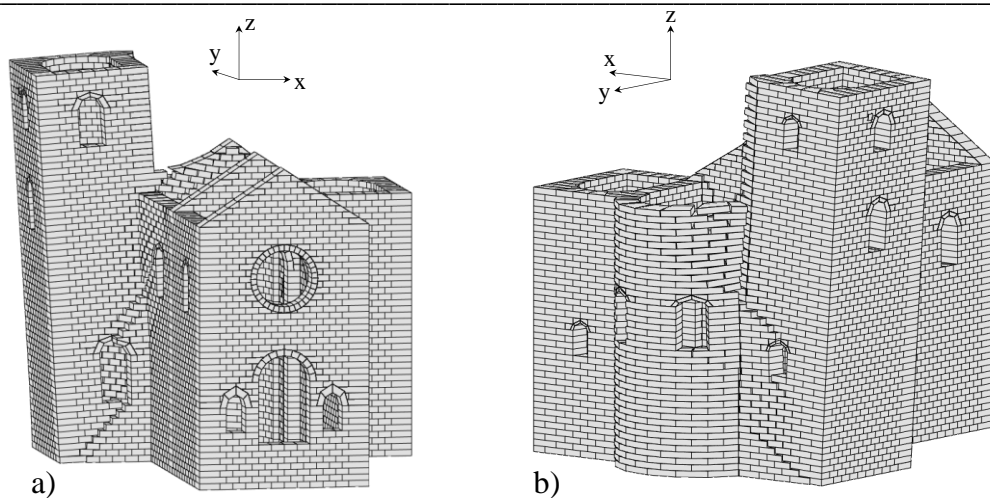


Figure 5.29 - Lateral load applied only to the bell tower along the x -axis: (a) front and (b) back views of non-associative failure mode (Malena, Portioli, Gagliardo *et al.*, 2019).

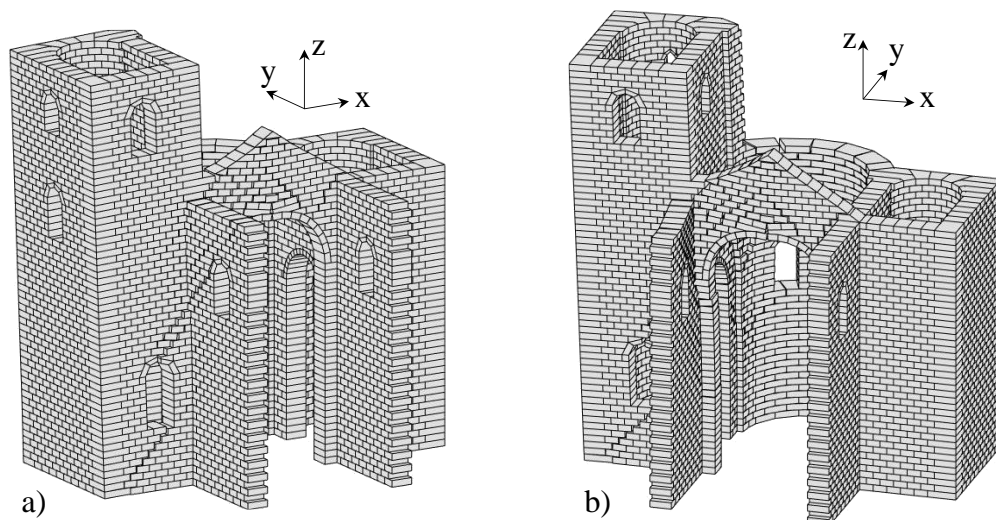


Figure 5.30 - Lateral load applied only to the bell tower along the x -axis: failure mechanism at the triumphal arch between the nave and the transept (Malena, Portioli, Gagliardo *et al.*, 2019).

In order to capture possible local failure mechanisms, collapse mechanism analyses considering lateral loads acting only to the bell tower along the x -axis,

were carried out. The results of the analyses are reported in Figure 5.29, where the plot shows that the rigid block model returns a failure mechanism involving the apse and the lower part of the bell tower. As a consequence of the bond pattern adopted in geometrical model to connect the bell tower, the collapse mechanism also involves the triumphal arch with sliding and opening failures in the piers and at the top. To this scope, Figure 5.30 shows an internal view of the failure mode obtained in the case of lateral loads applied only to the bell tower. It is worth observing that the failure load multiplier corresponding to this last analysis ($\alpha_{non-assoc} = 0.339$) was higher than those deriving from the previous nonlinear analyses.

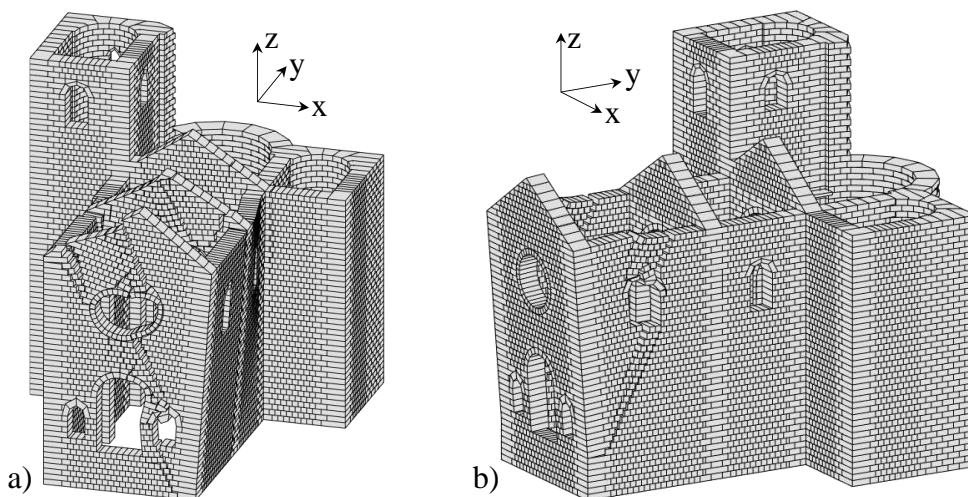


Figure 5.31 - Lateral load applied along the (a) x-axis and (b) y-axis. Non-associative rigid block failure mechanism for the reduced block size (Malena, Portioli, Gagliardo *et al.*, 2019).

Finally, sensitivity analysis to block size were carried out in this case study to evaluate the effects on the predicted failure mechanism and corresponding load factors. The results obtained adopting blocks with the same height but splitting in half their base are shown in Figure 5.31 in the case of lateral loads acting along both axes. As for the refined mesh, the discrete rigid block model of the church is made of 7216 blocks and 66084 contact points. It is shown that the collapse modes are only slightly affected by the block size: as expected in the case of lateral load applied along x-axis (Figure 5.31a), the crack pattern is now

characterized by an almost vertical crack above and below the rose windows while in the previous case the crack exhibits a diagonal trend from the upper left corner up to the lower right corner of the façade. The value of the collapse load factor for the reduced block size is equal to 0.161 for the non-associative solution, resulting with a reduction equal to about 20% compared with the previous adopted mesh. Figure 5.31 shows the failure mode when the seismic load acts in the y-direction in the case of reduced block mesh. The collapse mechanism is very close to that obtained with the larger block size, with a diagonal crack in the lateral walls, moving through the arch window. In the reduced-mesh case the above-mentioned crack is longer because the bottom end is closer to the model base compared with the failure mode predicted in the case of large mesh (Figure 5.31b). The reduced mesh analysis returns a value of collapse load factor equal to 0.178, with a reduction of about 21% compared to the large mesh analysis.

The outcomes obtained with the proposed rigid block formulation on the case study of the single-nave masonry church were also compared with those derived with the simulation by a non-linear three-dimensional finite element model (Malena *et al.*, 2019). Such a model represents the masonry wall as an elasto-perfectly plastic homogenized Love-Kirchhoff plate (Sab, 2003; Sab, Dallot and Cecchi, 2007). The model, formulated in the framework of multi-surface plasticity, is implemented in a FE code for the path-following analysis, by means of a minimization algorithm directly derived from the Haar-Karman principle. The comparison between the numerical outcomes from the two models was carried out in terms of failure modes and deformed configurations, as well as in terms of lateral loads promoting the collapse when varying mechanical and algorithm parameters. A good agreement of failure mechanisms was observed, indicating the ability of the discrete and the continuous models to capture similar local behaviour and damages in the case of in-plane as well as in the case of out-of-plane collapse. Discrepancies in the predicted failure mechanism from the two models were observed only when the continuum model was not able to capture the masonry bond patterns considered in the rigid block model, as it was in the case of the church bell tower. Also, the computed load factors were very similar in the case of in-plane failure mechanisms and in a good agreement with experimental outcomes, with differences up to about 5 percent. In Figure 5.32,

the plot of the load multiplier versus the displacement at the control point, for the finite element analyses, is represented, for both the directions, x and y, of the lateral loads (Malena *et al.*, 2019). The control point was located in all the cases at the maximum displacement point, that was the same for the two lateral loads directions, that is the higher point of the façade. With the aim to compare the numerical formulations, the results in terms of failure load multiplier of rigid block analyses are represented, too.

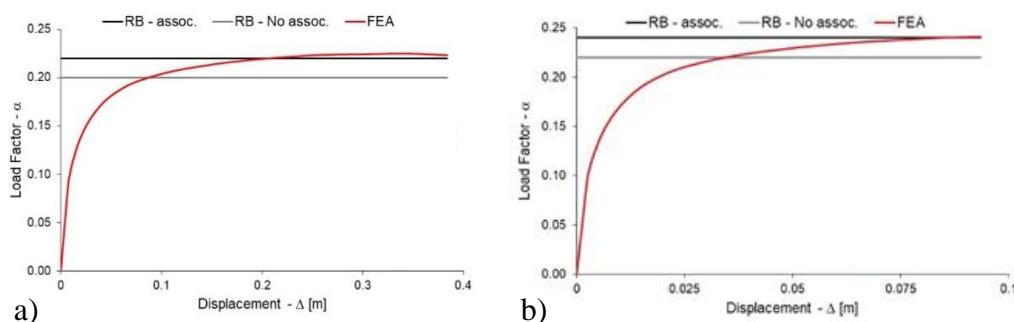


Figure 5.32 - Comparison between the proposed rigid block model and a finite element model (Malena *et al.*, 2019) in terms of load factor vs displacement: (a) x-axis; (b) y-axis (Malena, Portioli, Gagliardo *et al.*, 2019).

As for computational efficiency, the comparison between the two numerical formulations showed the high speed of calculation of the proposed rigid block model in place of the finite element method where longer CPU time is needed to obtain a solution, considering that the continuum model requires a dense mesh to describe strong localization of plastic strains. As for the sensitivity to mesh size, the comparison also showed that the finite element model underestimates the load factor predicted with the rigid block model, in accordance with the adopted homogenization theory.

5.2.2 Spreading supports and settlements

5.2.2.1 Circular arch subjected to spreading support

The case study of a circular arch on spreading supports was considered in order to validate the settlement module of the developed software. The rigid block

model developed for numerical simulation is shown in Figure 5.33a. The mean radius of the arch is 220 mm and the radial thickness is 50 mm. The unit weight is 25.0 kN/m^3 and friction coefficient is equal to 0.7. The additional rigid block indicated in Figure 5.33a is used to simulate the spreading support.

The dimensions and unit weight of the arch are the same of the voussoir arch tested in (Ochsendorf, 2006) under spreading supports till collapse. The same arch was also analysed in (Coccia, Di Carlo and Rinaldi, 2015) to test the accuracy of other numerical and analytical formulations based on limit analysis theorems. The predicted failure mechanism and the minimum thrust are reported in Figure 5.33b and Table 5.7. Outward movement of the support block induces the opening of three hinges, which are associated to a stable rigid body mechanism. The predicted position of the three hinges and the value of the associated reaction f_s (i.e., the minimum thrust) are in full accordance with analytical results and outcomes of experimental tests presented in (Ochsendorf, 2006; Coccia, Di Carlo and Rinaldi, 2015).

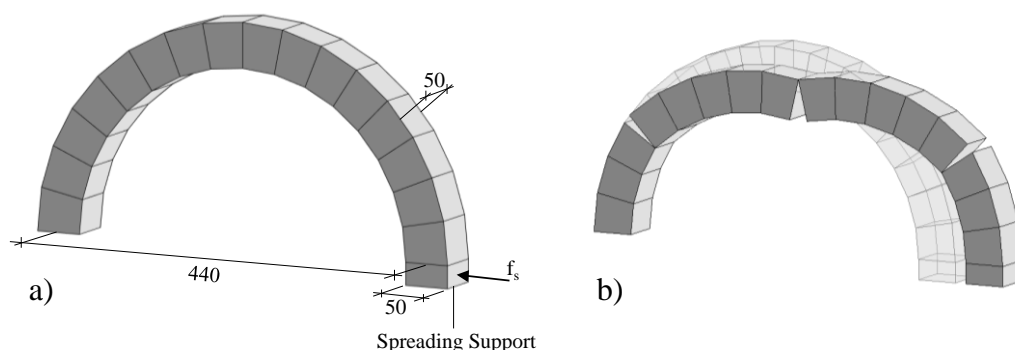


Figure 5.33 - (a) Voussoir circular arch on spreading support and (b) predicted failure mechanism (Cascini, Gagliardo and Portioli, 2020).

Model	Model size (b × c)	f_s Analytical (kN)	Associative f_s		Non-associative formulation		Diff. α %
			$f_{s \text{ assoc}}$ (kN)	CPU Time (s)	$f_{s \text{ non assoc}}$ (kN)	CPU Time (s)	
Circular arch	17 × 68	6.14	6.14	0.03	6.14	0.04	0.0

Table 5.7 - Circular arch subjected to spreading support: comparison of numerical and analytical results.

5.2.2.2 Cross vault subjected to support movement

The experimental case study investigated in this section is the scale model of a cross vault tested under spreading supports presented in (Rossi, Calderini and Lagomarsino, 2016). The specimen was made of plastic blocks with dry joints. The block unit weight was 27.0 kN/m^3 and the friction coefficient was 0.56. The specimen was tested under imposed displacements at the supports in order to reproduce a simple shear failure mechanism in the horizontal plane. The numerical model of the cross vault is shown in Figure 5.34a and was generated on the basis of the CAD model used for 3D printing in (Rossi, Calderini and Lagomarsino, 2016). It comprises 91 block types, 1131 blocks, and 17,544 contact points. The rigid block used to simulate the shear type displacements imposed experimentally at the supports is shown in Figure 5.34a. The obtained failure mechanism is shown in Figure 5.34b.

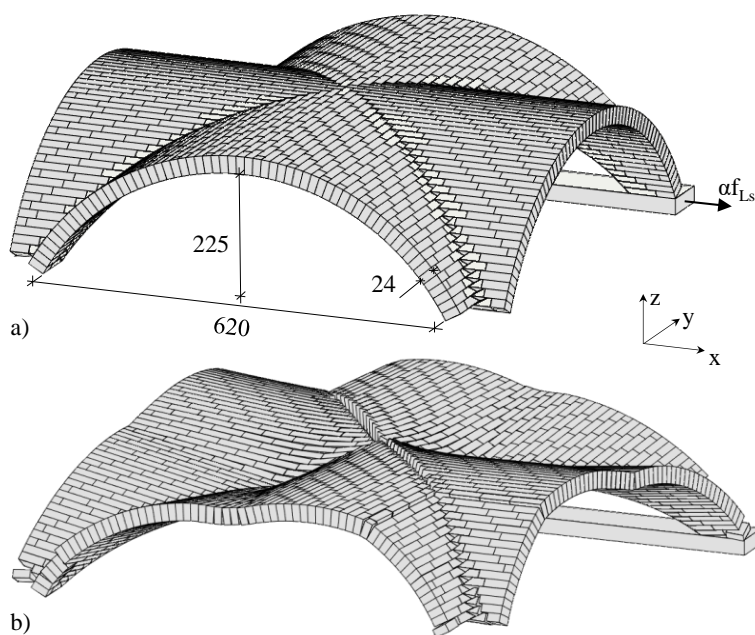


Figure 5.34 - Cross vault (Rossi, Calderini and Lagomarsino, 2016) (a) size and (b) collapse mechanism (Cascini, Gagliardo and Portioli, 2020).

The result is in a good agreement with experimental outcomes, where a four hinges failure mechanism was observed, with opposite webs having inverted signs. In Figure 5.35 the collapse horizontal reactions at the moving support for the associative and non-associative solution are compared with the force/displacement curves presented in (Rossi, Calderini and Lagomarsino, 2016), the forces being expressed as a percentage the total weight W . The results show that the reaction at the moving support corresponding to the dilatant and non-dilatant behaviour differ of about 20.5 and 7.1% from experimental values.

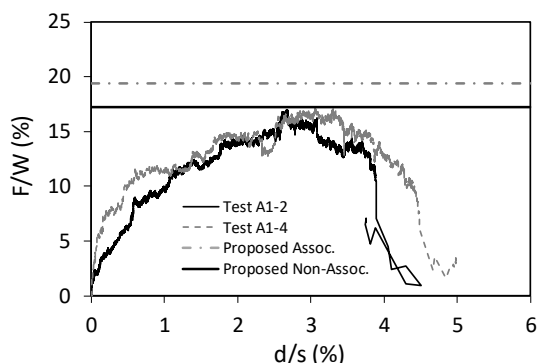


Figure 5.35 - Cross vault: comparison of numerical and experimental results (Rossi, Calderini and Lagomarsino, 2016).

5.2.2.3 Two-story masonry façade

In this section, the numerical case study of a masonry façade subjected to settlement and already investigated in (Landolfo *et al.*, 2020) is presented. The configuration and size of the façade are inspired to tuff masonry buildings in the area of Naples, Italy, dating back to XVIII century (Iannuzzo *et al.*, 2018). The façade consists of two stories with overall height of 12.0 m, length of 20.0 m and thickness equal to 0.5 m (Figure 5.36). A first analysis considers the façade without openings, while the subsequent analyses take into account the presence of two levels of openings with the goal of evaluating their effects on the settlement-induced failure mode. In the case of façade with openings, the lintels were modelled in order to reproduce the pattern and the effect of flat arches: blocks with an inclination angle of the head joints are adopted.

It should be noted that the inclination of the joints in the lintels might affect the response of the investigated wall panels, especially if sliding failure is also taken into account, as it was in the present case. However, the analysis of the influence of the inclination angle and of the friction coefficient was out of the scope of the present study.

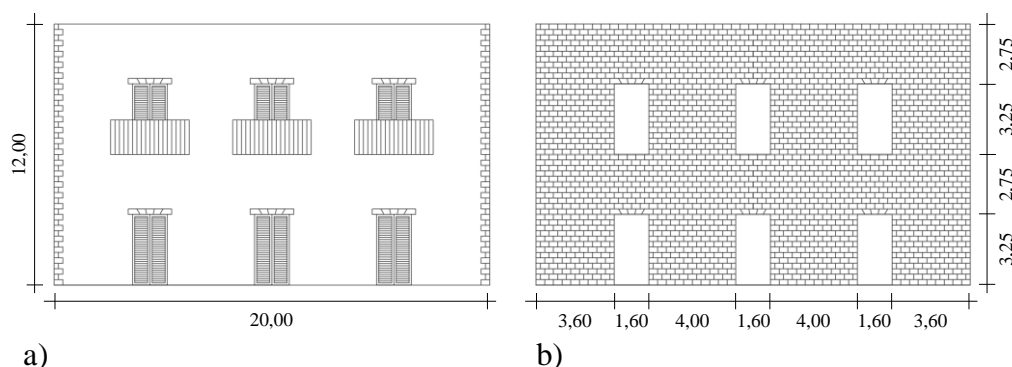


Figure 5.36 - The case study of a masonry façade subject to settlement: (a) the front side of the building; (b) rigid block model (Landolfo, Gagliardo *et al.*, 2020).

A parametric analysis is carried out to investigate the response when changing the width of ground settlement (Figure 5.37), the block size and shape, the load provided by the slabs over the wall, and the presence of openings, as mentioned above. Based on the parameters selected, either a local or a global failure mode is activated: the local failure is characterized by a uniform vertical displacement of the wedge located over the movable support, which detaches from the wall and fails according to a rigid body translation; the global failure mode is characterized by a more complex failure pattern, involving a greater portion of the wall and combining displacements and rotations of the block units. According to (Mastrodicasa, 1943), three movable ground support lengths are considered, namely short, medium and long settlement, corresponding respectively to 33%, 83% and 117% of the front height and to the 20%, 50% and 70% of the total length of the façade (Figure 5.37).

Two masonry types are introduced aiming at studying to what extent the block shape could affect the failure pattern. The masonry tuff stones used in Naples during the modern and contemporary ages have been considered. The first tuff

block shape, which is typical of the first decades of the XIX century, has height in the range 13-21 cm and height-to-length ratio equal to 1:2. The second tuff block shape, used in Naples at the end of the XVIII century, has height in the range 11-14 cm and length in the range 25-30 cm. Accordingly, both the discrete and the continuous model have considered blocks with 25 cm height and 40 cm length (1st typology) and 12 cm height and 25 cm length (2nd typology). The mechanical properties have kept constant for both typologies: weight per unit volume equal to 16 kN/m³ and friction coefficient equal to 0.6. In this case, two different assumptions were adopted at the contact interfaces in order to further investigate the abilities and flexibility of the proposed numerical model: a non-associative behaviour with no friction on the vertical interfaces (type A), and an associative behaviour with finite friction on the vertical interfaces (type B).

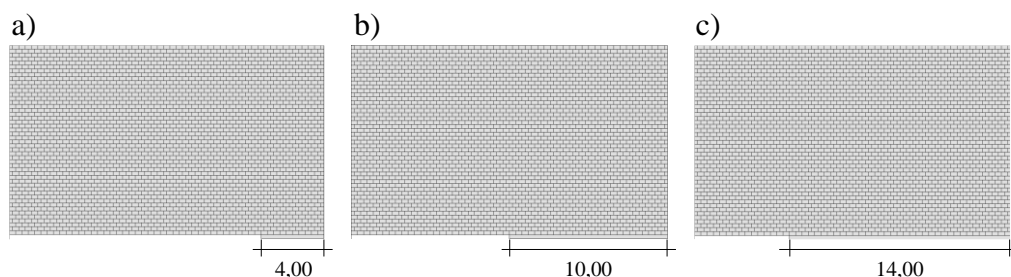


Figure 5.37 - The settlement configurations on the base of movable support block length: (a) short settlement, (b) medium settlement and (c) long settlement.

5.2.2.3.1 The façade without openings

The first case study consists in the façade with no openings described in the previous section. The two block stone types are adopted with both the numerical models. In the case of rigid block model, when a 40x25 cm block sizes is used, the model is made by an assemblage of 2425 rigid blocks and 28684 contact points, while, when a 25x12 cm block size is adopted, the model consists of 8050 blocks and 95800 contact points. Both the vertical contact cases previously described are considered: the case with the same friction behaviour for the vertical and the horizontal interfaces and the case where the vertical contacts have a friction coefficient equal to zero.

Figure 5.38 shows the failure mechanisms derived from the simulation with the rigid block limit analysis for both the block typologies, in the case of short settlement. According to (Mastrodicasa, 1943), as results of all the numerical simulations only the lower part of the façade over the moving support is involved in the settlement showing a local failure mechanism. In the case of ‘Type A’ contact interfaces, the failure mechanism is characterized by a slightly more localized fracture than for the ‘Type B’ contact interfaces. The adoption of different block dimensions, in this specific case, involved only small changes in failure mechanisms.

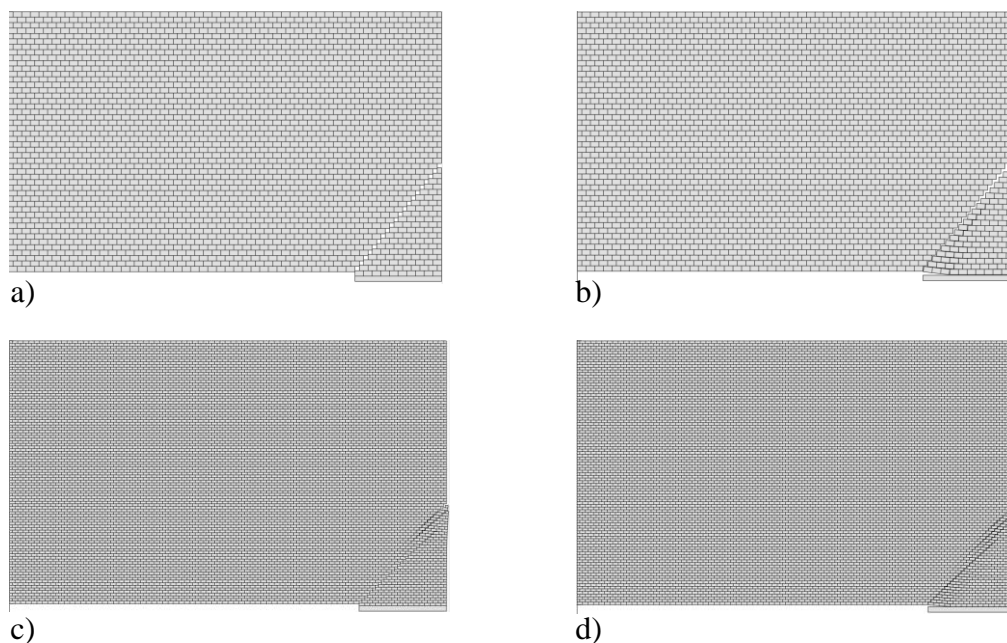


Figure 5.38 - Failure modes of the façade without openings subjected to short settlement and for the two block sizes (40x25 cm first row and 25x12 cm second row). (a), (c): non-associative solution with no friction on vertical contacts (Type A); (b), (d): associative solution with friction on vertical contacts (Type B) (Landolfo *et al.*, 2020).

Table 5.8, Table 5.9 and Table 5.10 collect the values of vertical reaction at failure at the base of the masonry structure involved in the settlement for both the numerical models in the case of short, medium and long settlement, respectively.

In the same Tables, the CPU time for the analyses is reported. When the friction on the vertical contact interfaces is not involved, the value of the reaction at failure is greater than that provided by the same non-linear model when the friction in the vertical contacts interfaces is involved.

Block size [cm]	ρ [kN/m ³]	μ [-]	No friction on vertical contacts (Type A)		Friction on vertical contacts (Type B)	
			fs [kN]	CPU Time [s]	fs [kN]	CPU Time [s]
40x25	16	0.6	83.79	17.68	66.30	25.48
25x12			64.46	130.87	55.20	134.77

Table 5.8 - Base reaction and CPU Time in the case of the façade without openings subjected to short settlements.

Block size [cm]	ρ [kN/m ³]	μ [-]	No friction on vertical contacts (Type A)		Friction on vertical contacts (Type B)	
			fs [kN]	CPU Time [s]	fs [kN]	CPU Time [s]
40x25	16	0.6	515.18	50.75	428.79	7.95
25x12			488.32	613.26	423.99	54.24

Table 5.9 - Base reaction and CPU Time in the case of the façade without openings subjected to medium settlements.

Block size [cm]	ρ [kN/m ³]	μ [-]	No friction on vertical contacts (Type A)		Friction on vertical contacts (Type B)	
			fs [kN]	CPU Time [s]	fs [kN]	CPU Time [s]
40x25	16	0.6	892.30	23.94	753.70	8.72
25x12			847.33	652.83	767.98	52.20

Table 5.10 - Base reaction and CPU Time in the case of the façade without openings subjected to long settlements.

Figure 5.39 shows the failure mechanisms derived from the simulation in the case of medium settlement. As observed, the two contact formulations return two different failure modes: the model with no friction on vertical contacts predicts a collapse mechanism where the upper part of the wall shows a vertical crack while in the lower part a diagonal crack develops. This failure pattern is a typical global failure mode, derived from the combination of displacements and rotations of the block units, for the medium settlement (Mastrodicasa, 1943). It is worth noting that the ‘type B’ contact interface is characterized by a more local behaviour. Also in this case, the block size does not change significantly the shape of mechanism, for both the numerical models.

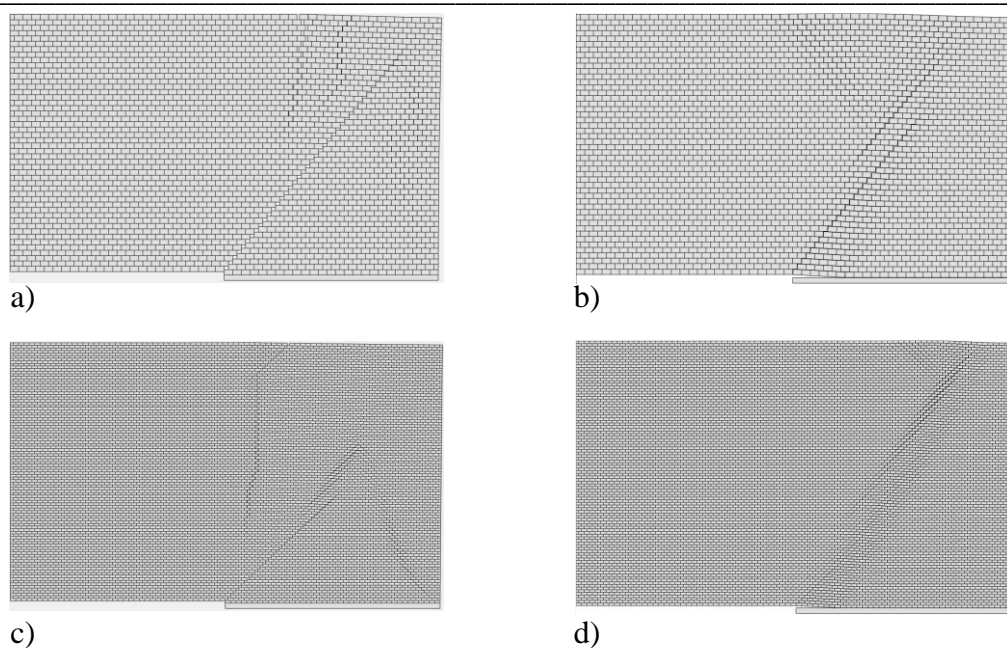


Figure 5.39 - Failure modes of the façade without openings subjected to medium settlement and for the two block sizes (40x25 cm first row and 25x12 cm second row). (a), (c): non-associative solution with no friction on vertical contacts (Type A); (b), (d): associative solution with friction on vertical contacts (Type B) (Landolfo, Gagliardo *et al.*, 2020).

Figure 5.40 shows the failure modes for both the block typologies in the case of long settlement. All numerical simulations provide a failure pattern with a diagonal crack developing from the left end side of the moving support up to the upper edge of the wall dividing the masonry wall into two parts, except to for the results obtained from the model based on a contact type A and 25x12 block size (Figure 5.40c), where a more vertical crack is observed at failure. This last failure mode should be expected according to (Mastrodicasa, 1943), and the discrepancy could be due to the simple model used to simulate the ground settlement.

A set of numerical analyses to consider the effects of distributed loads corresponding to the floors were also carried out. The loads were applied on courses at 6.00 and 12.00m height and a magnitude of 24.0 kN/m was considered. The results showed that the failure mechanisms are not affected by the floor load.

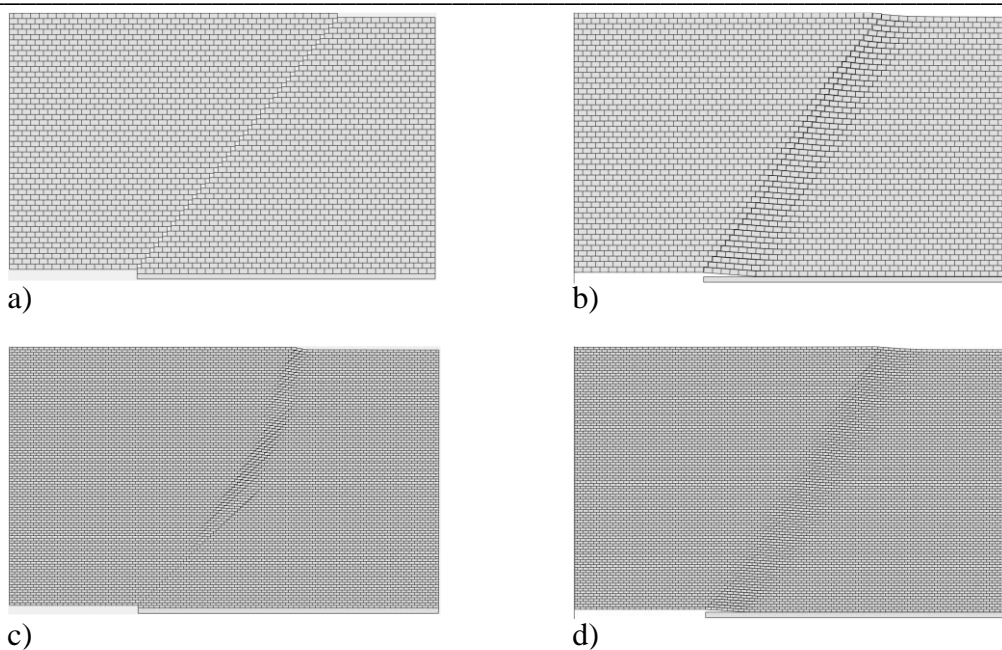


Figure 5.40 - Failure modes of the façade without openings subjected to long settlement and for the two block sizes (40x25 cm first row and 25x12 cm second row). (a), (c): non-associative solution with no friction on vertical contacts (Type A); (b), (d): associative solution with friction on vertical contacts (Type B) (Landolfo, Gagliardo et al., 2020).

5.2.2.3.2 The façade with openings

The second case study is represented by the façade with openings on the front, above described, subject to settlements. Also in this case, the same two block typologies are used in this application. When a 40x25 cm block size is used, the model is made by an assemblage of 2148 rigid blocks and 24608 contact points, while, when a 25x12 cm block size is adopted, the model consists of 7156 blocks and 83520 contact points. The masonry walls are involved in a short, a medium and a long settlement and both the vertical contact type, A and B, are considered.

Figure 5.41 shows the failure mechanisms derived for both the block typologies in the case of façade with openings subjected under short settlement. The presence of the openings changes the structural response to the short settlement. The part of the façade involved into the mechanism at failure is the portion of the

wall over the moving support with the development of cracks above the two openings. The mechanism is not strongly influenced by the contact type adopted. Further the size block only affects in a slight way the results.

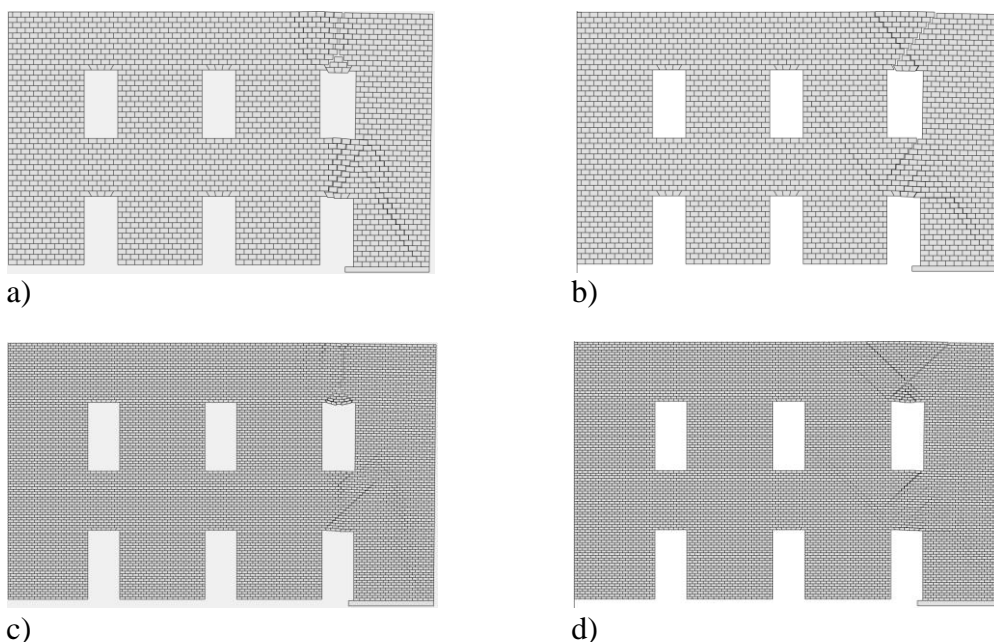


Figure 5.41 - Failure modes of the façade with openings subjected to short settlement and for the two block sizes (40x25 cm first row and 25x12 cm second row). (a), (c): non-associative solution with no friction on vertical contacts (Type A); (b), (d): associative solution with friction on vertical contacts (Type B) (Landolfo, Gagliardo *et al.*, 2020).

Table 5.11, Table 5.12 and Table 5.13 collect the values of vertical reaction at failure at the base of the masonry structure involved in the settlement for both the numerical models in the case of short, medium and long settlement, respectively. In the same Table, the CPU time for the analyses is reported. The same considerations for the case of façade without openings are still valid: when the friction on the vertical contact interfaces is not involved, the value of the reaction at the base of the movable support is greater than that provided by the same model when the friction in the vertical contacts interfaces is involved.

Block size [cm]	ρ [kN/m ³]	μ [-]	No friction on vertical contacts (Type A)		Friction on vertical contacts (Type B)	
			fs [kN]	CPU Time [s]	fs [kN]	CPU Time [s]
40x25	16	0.6	278.46	21.83	259.60	4.03
25x12			273.66	397.06	251.85	29.30

Table 5.11 - Base reaction and CPU Time in the case of the façade with openings subjected to short settlements.

Block size [cm]	ρ [kN/m ³]	μ [-]	No friction on vertical contacts (Type A)		Friction on vertical contacts (Type B)	
			fs [kN]	CPU Time [s]	fs [kN]	CPU Time [s]
40x25	16	0.6	638.05	47.45	604.67	4.42
25x12			644.73	233.12	610.34	40.43

Table 5.12 - Base reaction and CPU Time in the case of the façade with openings subjected to medium settlements.

Block size [cm]	ρ [kN/m ³]	μ [-]	No friction on vertical contacts (Type A)		Friction on vertical contacts (Type B)	
			fs [kN]	CPU Time [s]	fs [kN]	CPU Time [s]
40x25	16	0.6	873.30	14.04	734.92	5.50
25x12			808.60	575.01	745.14	43.42

Table 5.13 - Base reaction and CPU Time in the case of the façade with openings subjected to long settlements.

Figure 5.42 shows the collapse mode predicted from the simulation with the rigid block limit analysis for both the block typologies in the case of medium settlement. The failure pattern is mainly characterized by a diagonal crack above the two central openings in the case of model with contact type B. When contact type A is adopted a diagonal crack above the central opening at the first floor develops up to the second floor. The block typology affects only in a slight way the results: when 25x12 block size is adopted, more localized fractures than for 40x25 cm block size, develops.

Finally, Figure 5.43 shows the crack pattern and failure mode derived from the proposed numerical model for both the block typologies in the case of long settlement. Failure pattern, for both contact types, is characterized by a diagonal crack from the end side of the movable block up to central opening at the second floor and by a diagonal crack above the same opening. In this case, the size block

does not affect the failure mode. As for the effects of floor loads, also in this case similar results were observed in terms of failure modes to those obtained on the wall panel subjected to self-weight only.

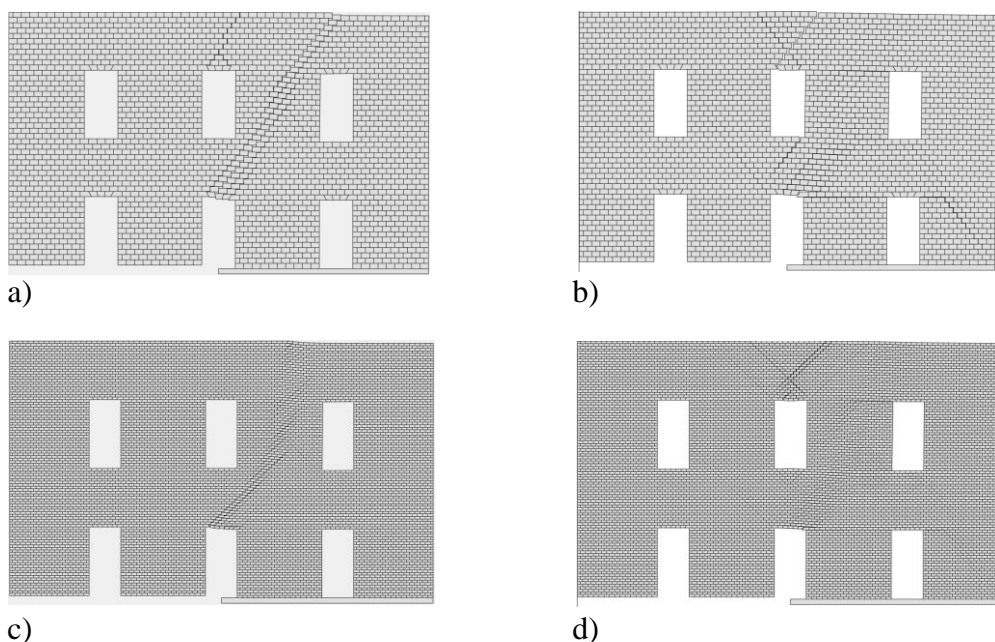


Figure 5.42 - Failure modes of the façade with openings subjected to medium settlement and for the two block sizes (40x25 cm first row and 25x12 cm second row). (a), (c): non-associative solution with no friction on vertical contacts (Type A); (b), (d): associative solution with friction on vertical contacts (Type B) (Landolfo, Gagliardo *et al.*, 2020).

In conclusion, the analysis performed on the masonry façade revealed that the failure mode is only slightly affected by the floor loads, while is strongly affected by the presence and disposition of openings and by the width of the settled area. Depending on the width of the moving support, the failure mechanism turns from local to global. The numerical results of both contact interface approaches are in a good agreement with the experimental outcomes reported in the literature (Mastrodicasa, 1943), showing the appearance of a diagonal and vertical crack patterns. Some non-negligible differences were found in the case of long settlements, where the models predict diagonal cracks from the side of the

moving support to the upper edge of the wall, instead of vertical cracks, as expected. The discrepancy can be ascribed to the rough simulation of the ground settlement, consisting in a uniform vertical displacement at the moving support.

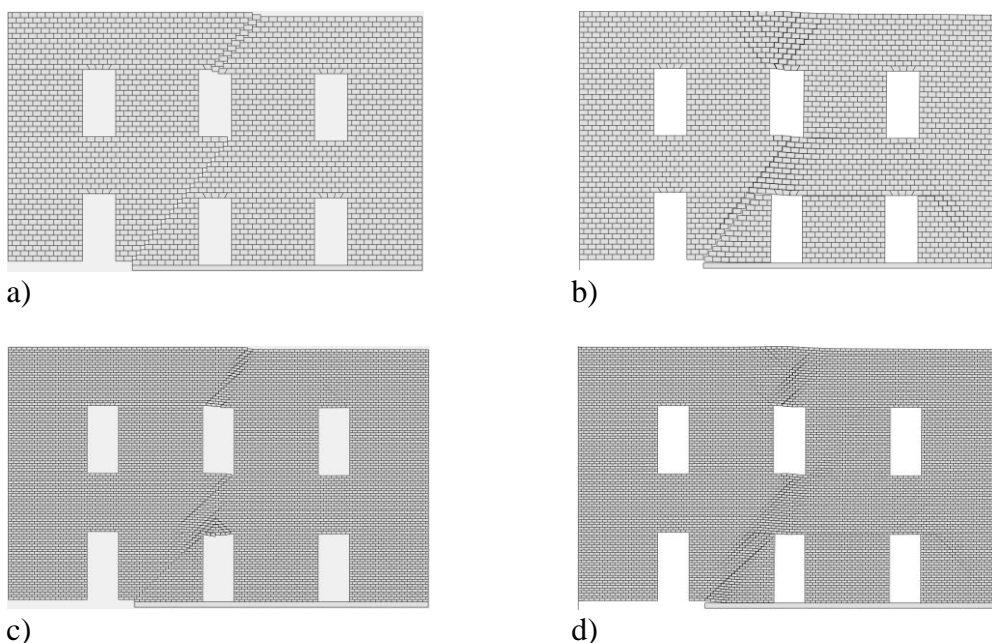


Figure 5.43 - Failure modes of the façade with openings subjected to long settlement and for the two block sizes (40x25 cm first row and 25x12 cm second row). (a), (c): non-associative solution with no friction on vertical contacts (Type A); (b), (d): associative solution with friction on vertical contacts (Type B) (Landolfo, Gagliardo *et al.*, 2020).

The outcomes obtained with the proposed rigid block formulation on the case study of the masonry façade subjected to uniform settlements were also compared with those derived with the simulation by a non-linear 3D finite element model (Landolfo *et al.*, 2020). Formulated in the framework of multi-surface plasticity and implemented in a FE code for the path-following analysis, the numerical model was already described in the section about the case study of the church of San Nicolò di Capodimonte. The comparison showed a good agreement of the two approaches in the prediction of the failure mode and in the reduction of the reaction at the foundation that activates the failure mechanism, when varying the shape of the masonry units, the wall openings and the width of the settled area.

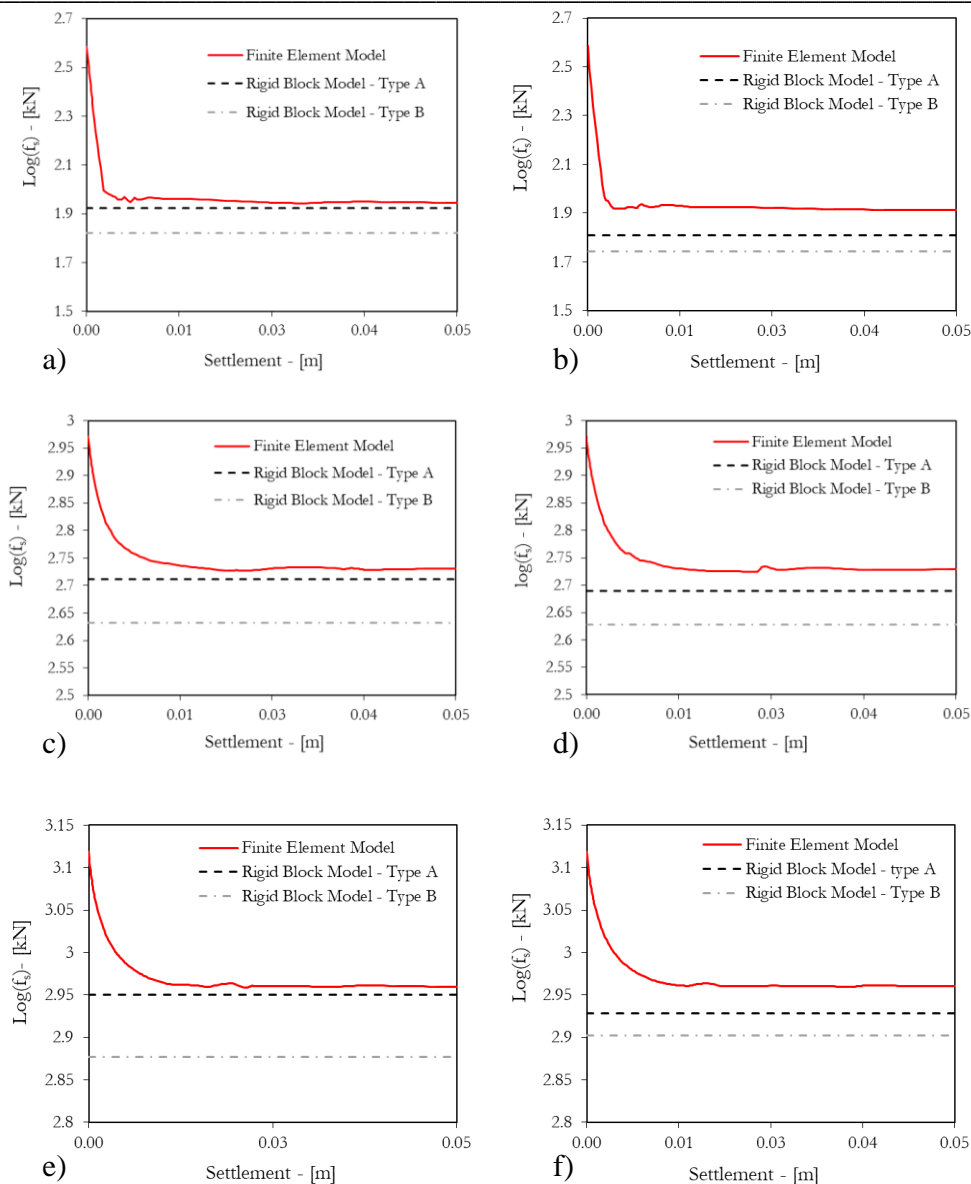


Figure 5.44 - Reactions at the moving support in the case of the façade without openings subjected to short (a), (b), medium (c), (d) and long (e), (f) settlement: 40x25 block size (a), (c), (e) and 25x12 block size (b), (d), (f) (Landolfo, Gagliardo et al., 2020).

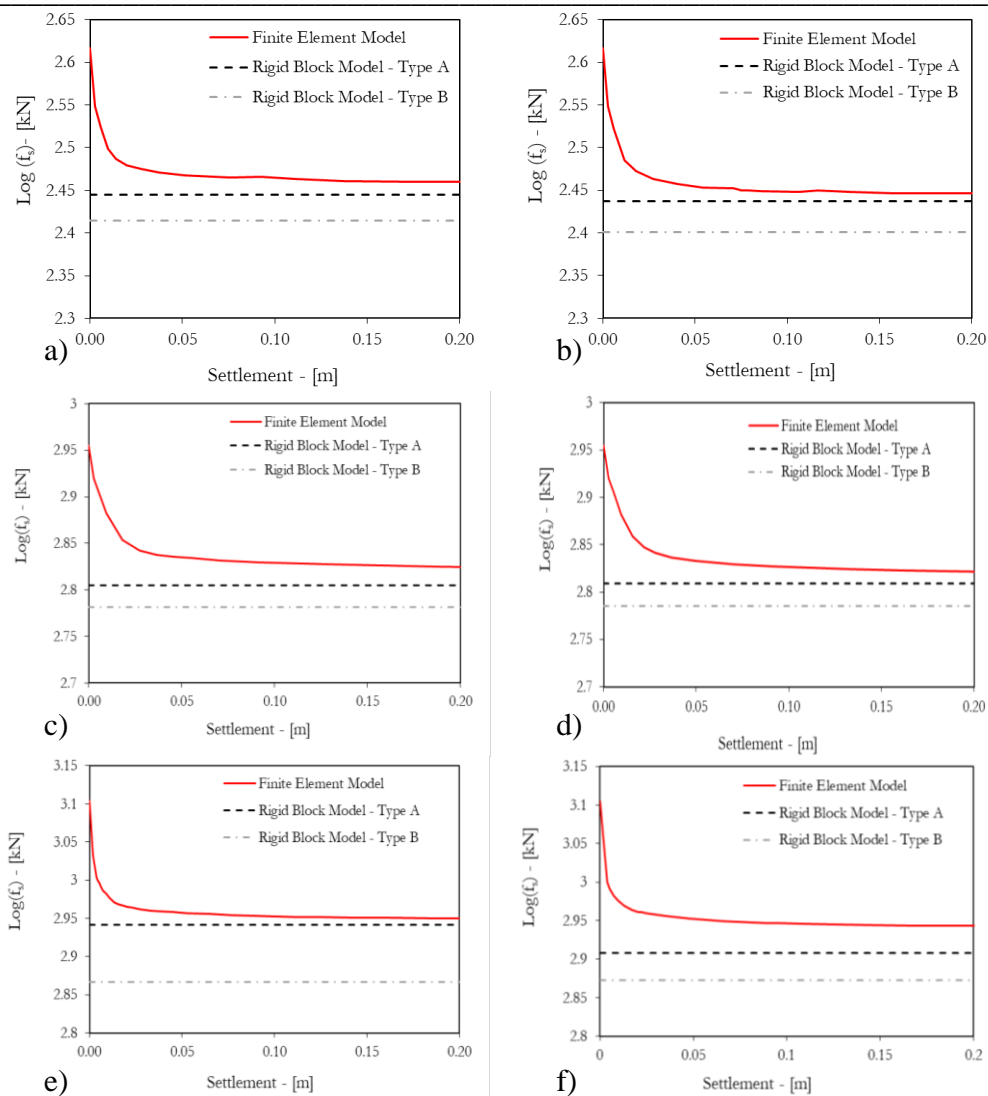


Figure 5.45 - Reactions at the moving support in the case of the façade with openings subjected to short (a), (b), medium (c), (d) and long (e), (f) settlement: 40x25 block size (a), (c), (e) and 25x12 block size (b), (d), (f) (Landolfo, Gagliardo et al., 2020).

5.2.3 Applications to case studies subjected to both lateral loads and settlement

In this section, the described case studies are represented by applications where both lateral loads and settlement were considered. A two-story masonry building investigated in (Cascini, Gagliardo and Portioli, 2020) and a huge, monumental building located in Italy will be showed and analysed using the limit analysis model. The monumental building, namely Palazzo d'Avalos (Procida Island, Italy), is one of the main case studies within the PERICLES project.

5.2.3.1 Two-story masonry building

The case study considered in this section is a two-story masonry building comprising two front walls and two side walls with door and window openings at ground and first levels (Cascini, Gagliardo and Portioli, 2020). The geometric configuration (Figure 5.46a and Figure 5.46b) was defined in order to be representative of an historic masonry building and to evaluate the ability of the developed software in predicting different failure mechanisms varying loading conditions, connection configurations, and mechanical parameters. The length of the front and side walls are 8000 mm and 5000 mm. The wall thickness at ground and first levels are 500 mm and 300 mm, respectively. A barrel vault with 4000 mm span and 250 mm thick is modelled at the first level. The dimensions of the blocks used for discretization are $400 \times 200 \times 500$ mm. The unit weight of masonry was taken as 18.0 kN/m^3 and the friction coefficient as 0.60. Floor loads at the second level were represented by vertical forces applied at each support block along the corresponding courses in the front walls and were calculated assuming a distributed load of 3.75 kN/m^2 . The building is subject to horizontal loads expressed as a factor of dead loads and directed along the side walls. In order to investigate the accuracy of the implemented software when different failure mechanisms are activated, different assumptions were considered for connections between the front and side walls, namely no connection and interlocked connection. In addition, the effects of tie rods were also investigated using additional rectangular blocks with dimensions 400×400 mm to represent the anchor plates, where constant horizontal forces are applied.

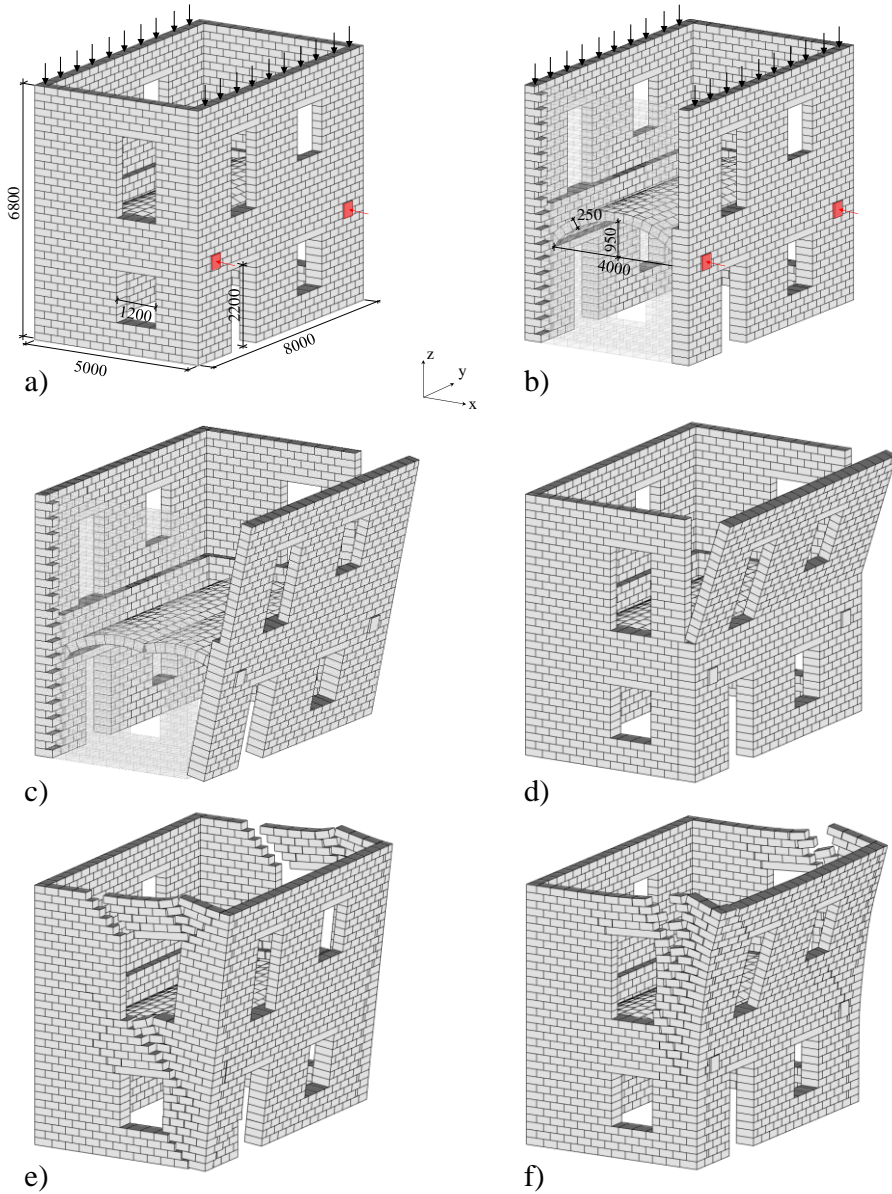


Figure 5.46 - (a) Size of two-story masonry building; (b) interior view with barrel vault dimensions. Failure modes under the assumption of: (c) no interlocking and tie forces equal to 3.0 kN; (d) no interlocking and tie forces equal to 25.0 kN; (e) with interlocking and without ties; and (f) with interlocking and tie forces equal to 25.0 kN (Cascini, Gagliardo and Portioli, 2020).

As such, four configurations were analysed: (i) no interlocking between front and side walls and tie-forces equal to 3.0 kN; (ii) no interlocking between front and side walls and tie-forces equal to 25.0 kN; (iii) front and side walls interlocked with no ties; and (iv) front and side walls interlocked and tie-forces equal to 25.0 kN.

Model	Model size (b × c)	Associative solution		Non-associative solution	
		α_{ass}	CPU Time (sec)	$\alpha_{\text{non ass}}$	CPU Time (sec)
Simple overturning	2114 x 23548	0.008	2.3	0.008	11.9
Simple overturning with ties	2116 x 23580	0.067	2.5	0.067	10.4
Complex overturning	2130 x 24148	0.103	6.3	0.095	49.9
Complex overturning with ties	2132 x 24180	0.143	4.5	0.130	63.5

Table 5.14 - Two-story masonry building subjected to horizontal live loads along x-axis. Numerical results for the investigated configurations.

The predicted failure mechanisms and collapse load factors are shown in Figure 5.46c, Figure 5.46f and Table 5.14. For the case studies (i) and (ii), the failure mechanisms involve simple overturning of the façade at floor and first level, as expected, considering that no interlocking between front and side walls is considered in these configurations and that increasing values of tie-forces are assumed (Figure 5.46c and Figure 5.46d). For the case (iii) the overturning failure mechanism of the façade at floor level also involves portions of the sidewall due to interlocking effects (Figure 5.46e). In the case of the front walls interlocked with tie forces (iv), the predicted failure mode involves overturning of the façade with sidewalls, being the collapse mechanism mainly restricted to the first level due to the effect of tie actions (Figure 5.46f). The collapse load factors for the associative and non-associative behaviour corresponding to the predicted failure mechanism show that the influence of dilatancy is negligible, with the exception of the case (iv), where the difference between the load multiplier is about 9%. It was worth noting that the load factors computed for the configuration types (i) and (ii) closely match the analytical values obtained from the application of the virtual work principle to the macro-elements (i.e., the whole façade or the wall panel at the first level). Also, the comparison of case studies (ii) and (iv) shows the influence of interlocking on the collapse load factor when the same values of horizontal forces are applied to the blocks representing the anchor plates.

A sensitivity analysis to friction coefficient was also carried out in the case of the building subject to horizontal loads along the longitudinal (y axis) direction to evaluate the effects on the failure mechanism and collapse load multipliers.

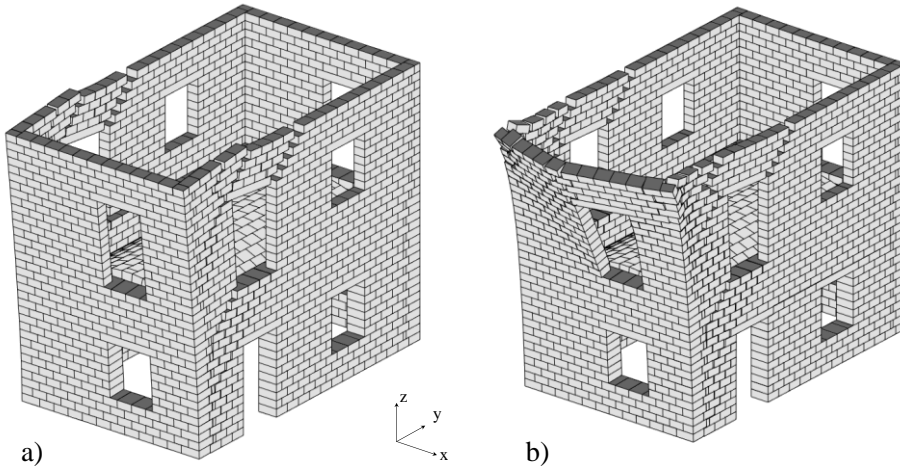


Figure 5.47 - Failure mechanisms predicted for horizontal live loads along y-axis: (a) $\mu = 0.6$ and (b) $\mu = 0.3$ (Cascini, Gagliardo and Portioli, 2020).

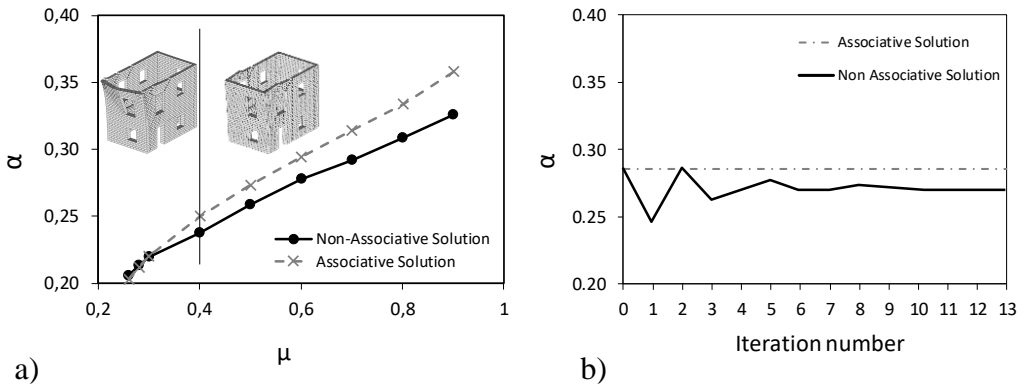


Figure 5.48 - (a) Sensitivity analysis to friction coefficient μ ; and (b) collapse load factor vs. iteration for $\mu = 0.6$ (Cascini, Gagliardo and Portioli, 2020).

Three failure mechanisms were observed from the numerical solution varying the friction coefficient. For values of the friction coefficient greater than 0.40, a simple overturning mechanism occurs. When the friction coefficient is comprised

in the range 0.3–0.4 the façade is subjected to bending failure at the first level (Figure 5.47). For lower values of μ , a pure sliding failure mechanism of the building at the first level is obtained. Figure 5.48 shows the difference of associative and non-associative solutions varying the friction coefficient. The results show that the formulation adopted is stable and robust even when unfeasible values of the friction coefficient are assumed.

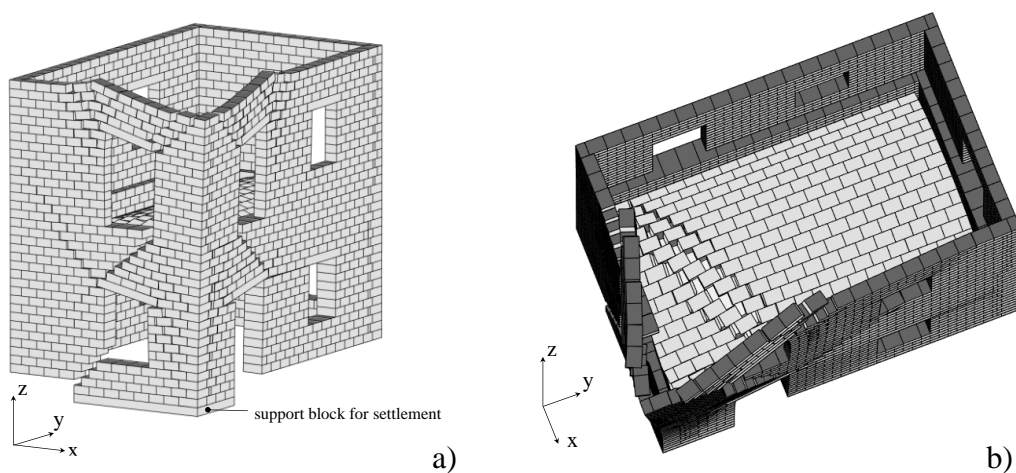


Figure 5.49 - Two-storey masonry building: Predicted failure mechanism under support vertical movement (Cascini, Gagliardo and Portioli, 2020).

The same case study of a two-masonry building with barrel vault above presented in the section of seismic-induced lateral loads is now investigated against foundation movements. In Figure 5.49 the failure mechanism predicted imposing a vertical movement to end piers using an L shaped support block is shown. The reaction f_s calculated at the moving support for the non-associative solution is equal to 101.4 kN. Figure 5.49b also shows the distribution of cracks predicted on the barrel vault and the out-of-plane behaviour of the corner at the top of the building. The solutions of the limit analysis problems took up to about 60 sec, which is a quite short CPU time considering that in this case the numerical models generated comprise up to 2132 blocks and 24,180 contact points.

5.2.3.2 *Palazzo d’Avalos*

In this section, a very huge masonry case study is investigated using the limit analysis proposed approach. The object is represented by a historical monumental building, named Palazzo d’Avalos, located in Terra Murata historic village, in the Procida Island, Italy. It is worth noting that this case study is developed within the activities of PERICLES project and was deeply studied and investigated in the Mastery thesis titled “Edifici monumentali a rischio idrogeologico: il caso di Palazzo d’Avalos, Procida” defended by Giovanni De Simone in 2019 at the Department of Architecture of the University of Naples “Federico II”.



Figure 5.50 – Palazzo d’Avalos in Procida, Italy. Picture by Giovanni De Simone, 2018.

Procida is an island located in the Gulf of Naples, being the littlest among the islands belonged to the so-called “campano archipelago”, with about 3.7 km² total surface. The geological history of Procida is strictly connected with that of the eruptive centres of the Campi Flegrei and Ischia island. The three of them (Procida, Ischia and Campi Flegrei) represent a complex vulcanological system. As already said, the case study is in Terra Murata, the ancient heart of the island, located in the highest point of Procida (about 92 metres a.s.l.). The historic masonry building appears completely similar to a defensive fortress, built with

the aim to defend against the enemy attacks. On one side, the palace is protected by walls sink from the sea while on the other side the protection is assured by the presence of fortified walls, which gave the title of “Terra Murata” to the historical village. In this framework, the defensive nature of the village has date back even before the Palazzo d’Avalos walls built, to protect the inhabitants of the island from the invasions of the barbarian first (in the early Middle Ages) and of the Saracens later. To this scope, in that time (before the palace had built) the type of construction method used to build the houses in Terra Murata already reflected this defensive spirit, being very close each other in order to not leave any free spaces and with very few or even zero openings outwards.



Figure 5.51 – The position of the Palazzo d’Avalos on Procida island, located in Terra Murata village (source: Google Earth).

Palazzo d’Avalos dominates all the island, especially Terra Murata. It was built in the XVI century by D’Avalos family which governed the island until the XVIII century. After the requisition of the island during the reign of Carlo V d’Asburgo, Procida went to Alfonso d’Avalos d’Aragona. With the aim to furthermore protect the island from invasion, the cardinal Innico d’Avalos d’Aragona,

Alfonso's son, asked to build his fortress-home on the east side of Terra Murata, creating a connection web with the other constructions via a long and heavy city walls. The building was designed by the roman architect Giovanni Battista Cavagna, who was working a lot in Naples area. Giovanni Battista Cavagna arrived in Procida to substitute Benvenuto Tortelli, another architect who had a high-level expertise in fortresses design.

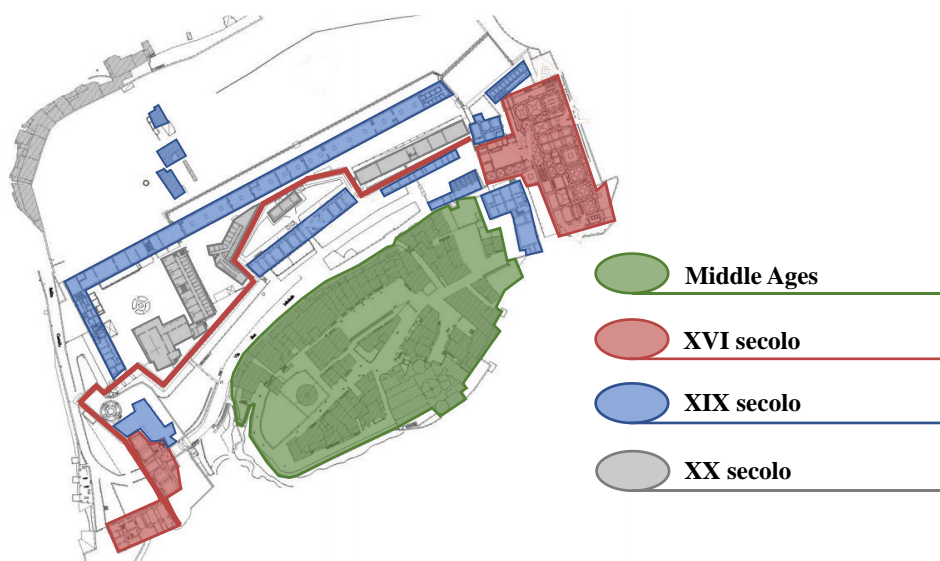


Figure 5.52 – Palazzo d'Avalos historic evolution from the construction until the current days.

The construction of Palazzo d'Avalos, which is currently the domain monumental building in the island, defined new typical spaces, changing the inner paths, the entries system, somehow drawing the lines for the future development of the urban village. It is a combination between a residential and a defensive project, being at the same time a fortress towards the sea and an elegant home in the opposite side. With the construction of the new and huge city wall, the ancient "Terra Casata" became "Terra Murata" and the main entry was represented by "iron door", located at the end of new road (namely Via Nuova) in the west part of the village. The road was the main link with the new port of Marina di Sancio Cattolico. The architectural and structural interventions demanded by the cardinal Innico d'Avalos in the XVI century included the design

and the construction of Santa Margherita Nuova architectural complex, the rebuilding of San Michele Arcangelo abbey church (originally built in 1026) and the construction of Veterani complex, a structure located in continuity with city walls with the scope to end the southern buttress, where another entry was positioned, the so-called “porta del Carmine”.

Later, Procida feud was confiscated again, moving from the hands of Giovanbattista d’Avalos to those of Carlo di Borbone. At that time, the palace started a new age of its history, being subjected to the first operation specifically devoted to the change of the original architectural system. This important restoration design was made by the engineer Agostino Caputo in 1738 involving an overall rearrangement of internal spaces as a consequence of the changed conditions which produced the transformation of the palace in a royal residence. In the same project the trapezoidal shape Italian garden was also involved, whit the access directly provided at the ground storey in connection with royal flat.

Other successive interventions were designed in 1769 by the architect Ferdinando Fuga and in 1802 by Carlo Vanvitelli. The latter was aimed to rebuild the track connecting the sea with the Palace via a monumental stone-made stair (la Cordonata), which is unfortunately quasi-completely destroyed today. It seems to be sure that already in the XVIII century the static condition of the structures was affected by settlement due to the very particular soil and geological features. With this in mind, a series of huge buttresses were built on the sea front, which also had an aesthetic and architectural function beyond the structural one.

During the French domination (1806-1816), the entire Procida island was subjected to military interventions aiming at strengthening the fortresses walls especially along the sea front in order to defend the capital of the Kingdom. In that time, Palazzo d’Avalos was converted in flats for the troops employed on the island and the area close to the porta del Carmine was designated as military hospital. Santa Margherita complex was also transformed and added to the hospital. During the Bourbon restoration, the king Ferdinando I created a military school on the island inside the Royal Palace, but it lasted very few times. In the decade 1830-1840 the number of jail structures highly improved in the Bourbon Kingdom. With the scope to save money, abandoned castles and cloisters were

usually used to host the prison function. In this framework, Palazzo d’Avalos was transformed in a jail in 1830, named “Bagno Penale”.

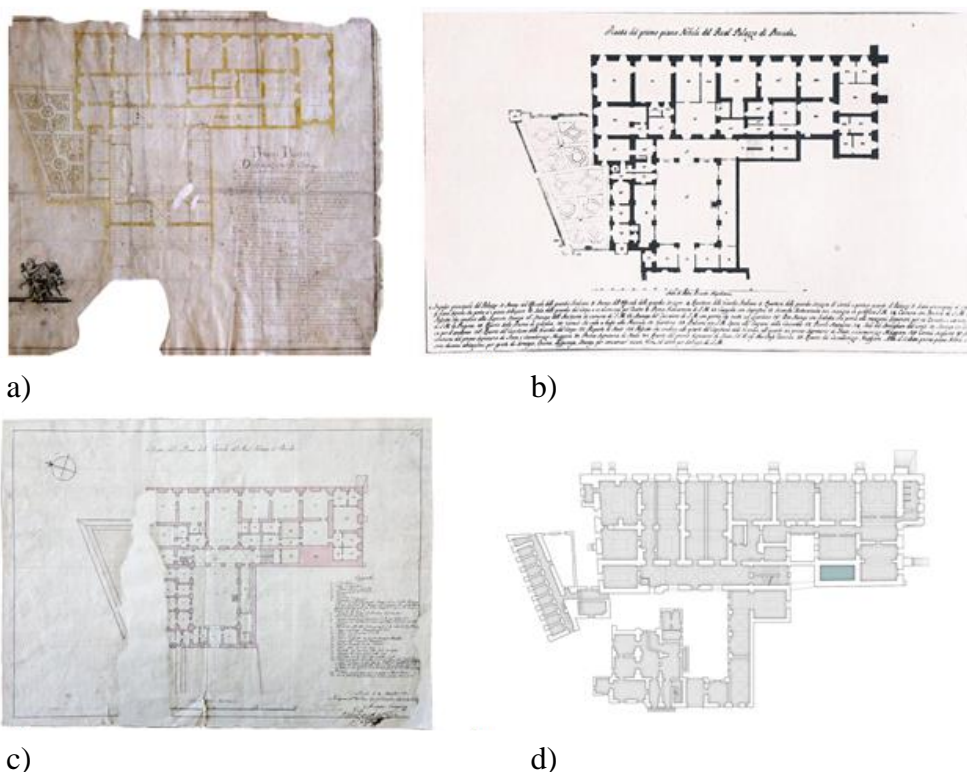


Figure 5.53 – Palazzo d’Avalos historic evolution maps: (a) design by Eng. Agostino Caputo, 1738; (b) actual intervention realized in 1738; (c) design by Eng. Giovanni Campana; (d) current state of the building.

The building suffered severe changes and extensions to allow the conversation into a big prison, completely altering its early system. The inside spaces were changed to realize the jail cells, isolation rooms, kitchens, common areas. It was in this time that a two-levels moat was excavated, probably inducing structural problem especially at the foundation system. Floors, frescoes and decorations were removed little by little. Finally, the palace was completely locked in 1978. Although the various tampering suffered by the building during the years,

Palazzo d’Avalos still shows the quality of the architectural and structural system (Assante, 2015; Di Liello and Rossi, 2017; Iodice, 2017).

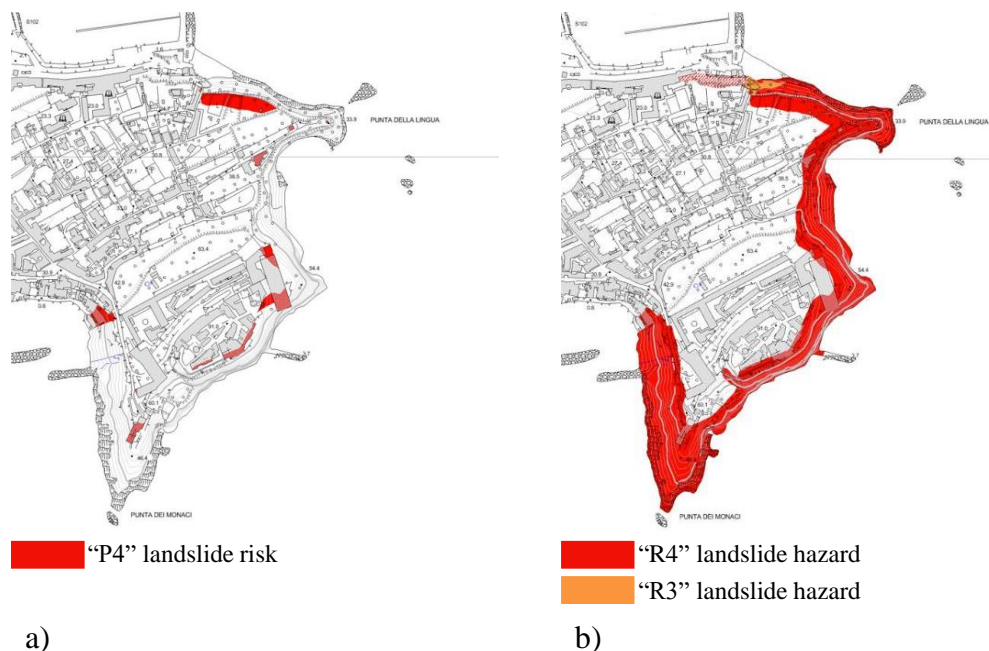


Figure 5.54 – Maps developed in (Regione Campania, 2017): (a) landslide risk and (b) landslide hazard.

The specific structure of Terra Murata and the specific sub-soil type make the building highly sensitive to ground movement and landslide hazard. According to the maps produced in (Regione Campania, 2017), the palace is located very close to area affected by landslide hazard level R3 and R4 and landslide risk P4, as showed in Figure 5.54. R3 landslide hazard stands for “high level”, meaning the possibility of problems for life safety, functional damages to structures and infrastructures which are not more practicable, interruption of socio-economic activities and damages to the Cultural Heritage. R4 landslide hazard stands for “very high level”, meaning the possibility to loss of human lives, sever damages to people, buildings and infrastructures, destruction of the socio-economic activities, damages to the Cultural Heritage. P4 landslide risk stands for “very high level”.

With regard to the structure, Palazzo d'Avalos is part of a more complex and huge structure, where it is possible to read the various changes and transformations suffered during about four centuries of life, especially in the XIX century after the conversion into a royal jail. Apart from this, the palace managed to save the integrity of the original structural system. The two main façades of the buildings well tell the double nature of the building, at the same time strong to defend against the enemies and comfortable to host at the best the King and the royal family. The façade on the sea appears to be highly strict and marked only by the regular rhythm of the openings but without any type of decoration. On the other side, the inner façade on the entry courtyard is characterized by a high level of decorations, with pillars and arches to give a harmonious picture to the whole façade.

The huge structure is based on a very simple rectangular plan, which is the same for the four storeys, among them only two are elevated with regard to the entry level. The first level is positioned at the same height of the doorway; a stair allows to move upward to the two higher floors. The same stair also was the path to arrive to the two lower storeys. The floors most affected by the transformations during the times were the two lower levels. The structural scheme is low and linear. The system is made by a frame of tuff-masonry bearing walls: it is possible to identify four main bearing walls and eight secondary bearing walls, differently arranged in order to host the stair and the functional spaces. The horizontal system is mainly represented by vaulted elements, with different architectural solutions (mainly barrel vaults, cross vaults and pavilion vaults). With regard to the roof, it was severely transformed. Most of the roof system was fully rebuilt in last ages, with horizontal floor made by steel beams, metal sheet and infill materials. The static capacity of the building is highly supported by the presence of a system of huge masonry buttresses along all the perimeter. The buttresses extend until the ground floor and even to the two underground floors in some points. As for the foundation system, a very important survey operation was performed in 1989 by the collaboration between Prof. Eng. Mario Rosario Migliore and Prof. Giovanbattista de Medici, where 24 drillings in various points of the soil were designed. The outcomes of such a survey revealed the high irregular type of the support soil under the numerous bearing walls, especially in

a comparison between the longitudinal wall panel of the façade above the sea and the transversal walls. The foundation level of the longitudinal sea-side façade goes down even beyond the level of the two underground floors, while the other bearing walls (both transversal and perimetral) are characterized by a foundation level is not so deep, being even stopped to the planking level in some cases.



Figure 5.55 – Foundation drilling surveys designed by Prof Eng. Mario Rosario Migliore and Prof. Giovanbattista de Medici, 1989.

With regard to the current crack pattern, a very detailed survey operation was performed by Giovanni De Simone in its Master thesis investigation step, using classical and advanced survey techniques (such as the use of a DJI Phantom 4 Pro drone). The outcome of this huge survey operation showed that the structure of Palazzo d'Avalos is characterized by several crack pattern scenarios. With the scope to clearly depict them, it is possible to separate local cracks and global failure mode related cracks. In this framework, the following ongoing collapse mechanism can be recognized in the structure:

- the main failure pattern is due to the out-of-plane mechanism of the main façade on the seaside, whit a separation between the latter and the transversal bearing walls, highlighted by vertical and sub-vertical cracks.

-
- signals of a foundation settlements located on the southern bearing masonry walls of the palace.
 - a severe crack pattern involving the angular walls at the corner of the longitudinal façade towards the sea.
 - a widespread crack pattern observed in the vaults (both lunette and pavilion vaults) due to the compression stress produced by truss loss related to the settlement of masonry bearing walls.

The first describe crack pattern is the dominant one because it is associated with a collapse mechanism which involves every masonry wall at different heights. It appears with vertical and 45° slope of sub-vertical cracks, where the inclination is towards the inner side of the building. In this case, it should be concluded that the huge operation of construction of the buttresses along the main façade was suggested as a solution to stop the out-of-plane rotation of the façade towards the sea. Nevertheless, recent study on the foundation analysis developed by Mario Rosario Migliore and Giovanbattista de Medici leads to a possible refusal of the previous analysis of the failure pattern. According to their investigation, the observed cracks could be triggered by an opening phenomenon towards the inside part of the long façade, corresponding to the natural slope of the soil, probably caused by the settlement of the transversal bearing walls. The surveys worked by them the results showed that the longitudinal part towards the sea is not affected by any foundation displacement whit a major crack pattern propagation at the lower floors where the cracks grow up in an upwards direction. According to these new results, it seems to be excluded the hypothesis of an out-of-plane rotation of the main façade, which should cause a more severe crack width at the higher levels. The trigonometric leveling also showed that all the building is involved in a critical situation due to the widespread foundation settlement mechanism. As already said, this mechanism became stronger in South direction during the times. Figure 5.56 shows the crack pattern surveyed by Giovanni de Simone in his Master thesis work. Furthermore, the presence of the huge buttresses gave a very high stiffness to the longitudinal main façade, creating a dangerous heterogeneity of the structural stiffness in the building, which is a triggering cause of high sensitivity to settlements.

All the previous described structural vulnerability is even exacerbated by the very complex subsoil configuration, which is characterized by several layers with highly different mechanical properties. It seems to be clear that this subsoil mechanical heterogeneity does not allow for a uniform bearing capacity. To this scope, it should be known that the monumental building lies on a tuff-made base in North-West direction, located on a further pyroclastic layer characterized by an incoherent and not uniform thickness. The pyroclastic layer presents greater widths in the North-West area and very lower widths in the other parts. In the case this heterogeneity in the soil configuration was associated to some water infiltrations during the years, the hypothesis for foundation settlements seems to be much more validated.

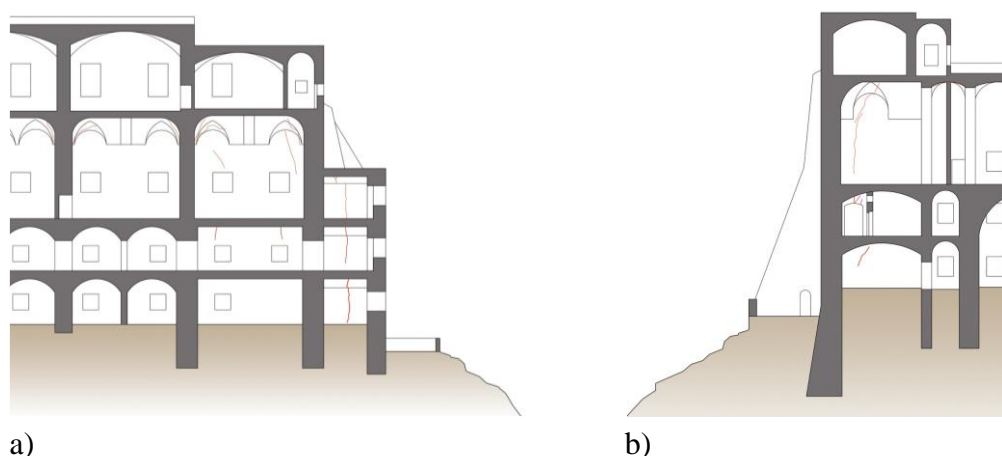


Figure 5.56 – Crack pattern representation in order to describe the settlement-induced collapse mechanism exhibited by Palazzo d'Avalos. (Source: Master Thesis by Giovanni de Simone, 2019).

Apart from this, it is worth nothing that all the palace is characterized by a terrible maintenance condition, which lasts from the time the building left the jail function. Extraordinary maintenance interventions were designed in the last 1990s by the Soprintendenza per i Beni Architettonici di Napoli, mainly aiming at the structural static safety rehabilitation. The works mainly involved the piano nobile of the palace, with the substitution of the roof (also contemplating the substitution of the parts affected by water infiltrations with innovative structural system using steel material). The interventions also contemplated the

improvement of the mechanical properties of the masonry walls through mortar injections and ties application.

The detailed reported description of the case study of Palazzo d’Avalos allowed to understand to which extent the demand for an appropriate modelling and analysis step represents a crucial point. The first reason is the investigation of the main crack pattern causes, i.e. the collapse mechanism observed in the main façade towards the sea. With this in mind, the numerical and modelling application has the goal to study the most coherent cause of that failure mode among a lateral-load induced out-of-plane mechanism and a settlement-induced ground movement due to the very specific subsoil structure and to the foundation system heterogeneity. The proposed limit analysis based rigid block numerical procedure was applied to the case study in order to face this topic. It is worth noting a modelling difference between the two investigated scenarios. In the case of lateral load induced collapse mechanisms analysis, a 3D model of an entire part of the building was produced using the CAD geometrical procedure already described in the dissertation. On the other hand, the settlement-induced failure mode investigation consists in a planar analysis involving only a 2D model of a façade (included in the same building part analysed in the lateral load case) subjected to a uniform settlement displacement.

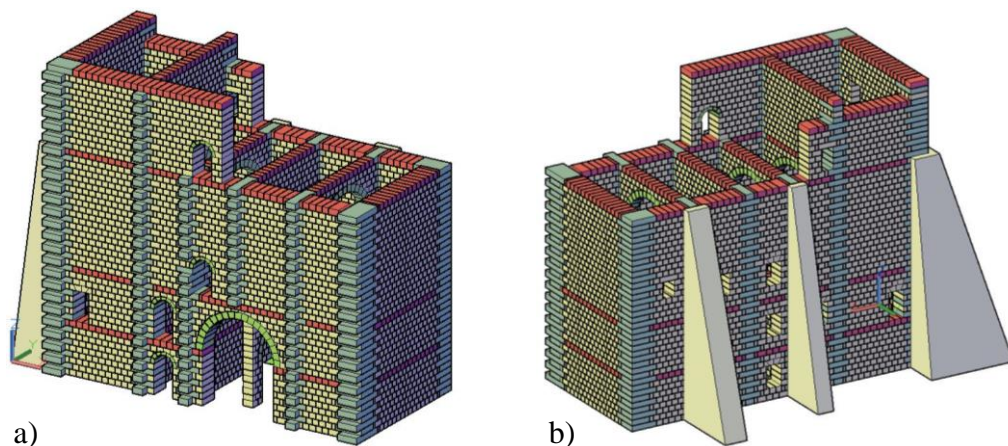


Figure 5.57 – Rigid block model (generated in CAD environment) of the investigated portion of Palazzo d’Avalos.

The building area selected for the numerical investigation corresponds to the most damage affected according to the previously described survey operation. The selected portion corresponds to a rectangular structural cell located in the South-East corner of the building. The rigid block model generated in AutoCAD is represented in Figure 5.57. The model is composed by 6349 rigid blocks and 76776 contact points. Arched openings are accounted for and the huge buttresses are modelled as well. According to the mechanical properties, the weight for unit volume is equal to 18 kN/m³ and the friction coefficient is equal to 0.6.

In the case of lateral-load collapse mechanisms analysis, the model structural response was investigated against four possible directions of the lateral loads. The obtained failure modes and crack patterns are showed in Figure 5.58. For sake of clarity, Figure 5.58a and Figure 5.58b deals with the collapse mechanisms predicted in the case of longitudinal lateral loads for both directions; Figure 5.58a and Figure 5.58b deals with the collapse mechanisms in the case of transversal lateral loads for both directions. In the first case (Figure 5.58a), the collapse mechanism is represented by a local crack pattern with only the rotation of the upper part of a wall panel also influenced by the presence of an arch window. The second failure mode in the case of longitudinal actions (Figure 5.58b) is characterized by an out-of-plane mechanisms of the perimetral transversal façade also involving the two side walls in the from the bottom to the top with a sub-vertical crack whose paths is influenced by the presence of the arch window in the low level. Both the failure modes predicted by the limit analysis tool in the case of transversal lateral forces show an out-of-plane mechanism of the perimetral façade involved with a crack pattern characterized by a sub-vertical crack moving from the bottom to the top of the side façades with increasing widths upwards.

The numerical outcomes related to the previous describe collapse mechanisms were summarized in Table 5.15 in terms of load factor (or collapse multiplier) and value of the collapse load. As a matter of facts, the values of the load factor are very high, meaning a good capacity of the investigated model against settlement-induced lateral loads.

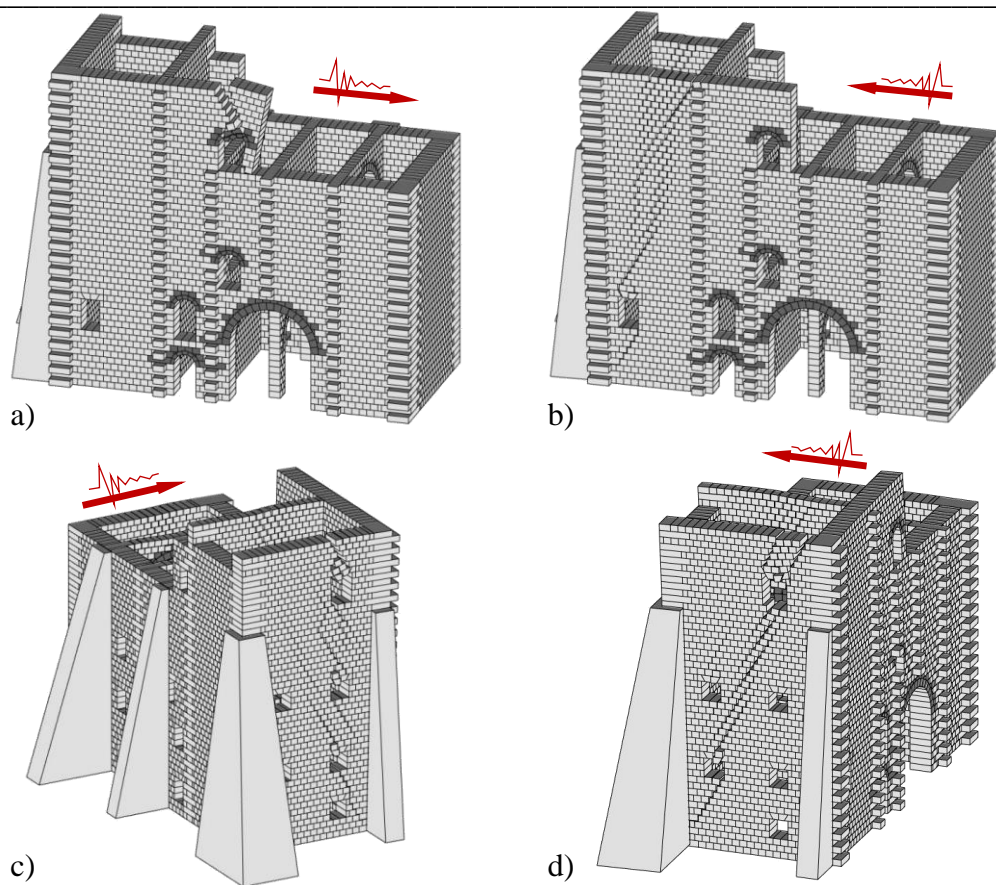


Figure 5.58 – Collapse mechanisms predicted by the limit analysis rigid block proposed formulation in the case of lateral live loads applied in both (a)(b) longitudinal and (c)(d) transversal directions.

Model size (b x c)	ρ [kN/m ³]	μ [-]	Loading case	Numerical solution	
				α [-]	αf_L [kN]
6349 x 76776	18	0.6	Figure 5.58a	0.23	11408.89
			Figure 5.58b	0.28	13537.03
			Figure 5.58c	0.15	7515.99
			Figure 5.58d	0.28	13648.07

Table 5.15 – Numerical outcomes of the collapse mechanisms analysis in the case of lateral live loads applied in both longitudinal and transversal directions.

The second investigation is related to the capacity of the model against the settlement movements. In this case a 2D analysis was performed by using the same modelling technique based on limit analysis and rigid block assumptions. The selected façade is part of the 3D system analysed in the case of seismic actions and highlighted in Figure 5.59a (red zone). In this case the planar model consists of 1916 blocks and 21892 contact points. The same mechanical properties applied to the previous described analysis were used as well. The settlement was simulated by an additional rigid block located in the foundation layer. The length of the movable support block was selected as the full wall length in order to study the case of a uniform settlement of the overall façade, as showed in Figure 5.59.

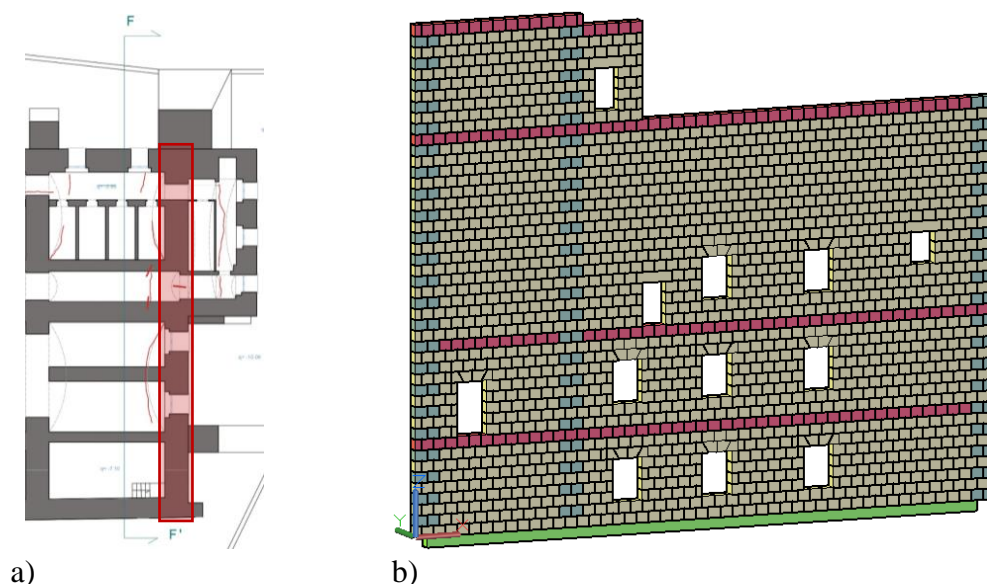


Figure 5.59 – Settlement-induced collapse mechanism capacity investigation: (a) identification of the selected masonry wall used for the 2D settlement analysis and (b) rigid block model (generated in Cad environment) of the selected bearing wall.

The outcome in terms of failure mode is represented in Figure 5.60b. The crack pattern is characterized by a typical settlement failure configuration, with diagonal cracks creating a central triangular wedge. The value of the loss of base reaction at collapse is equal to 2531.31 kN. In Figure 5.60 the predicted failure

mode is also compared with the cracks observed in the piano nobile level of the analysed masonry walls. The comparison showed a good agreement between actual survey and numerical model in terms of position and direction of the crack.

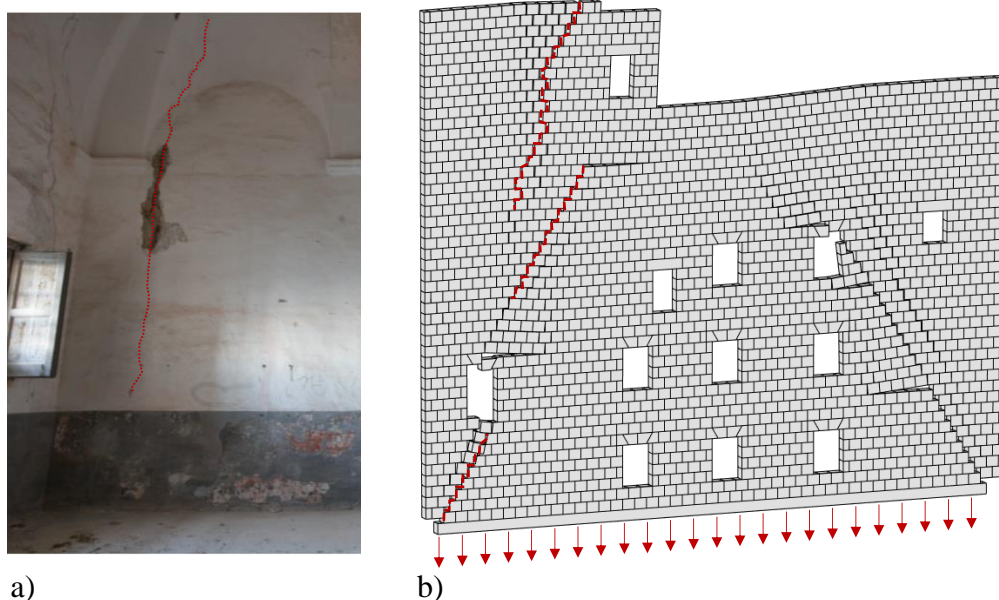


Figure 5.60 – Comparison between (a) the current crack pattern observed in the investigated façade and (b) the crack pattern predicted by the limit analysis rigid block proposed formulation in the case of uniform settlement applied to the entire bearing walls.

Conclusions

The present Chapter showed a large number of applications for the linear kinematic analysis proposed model. Several numerical case studies were presented and discussed, testing the abilities of the computational strategy in the masonry structures capacity and response investigation. The described applications move from the field of seismic induced lateral loads to that of spreading supports and settlement-induced ground displacements, as in the spirit of the dissertation thesis.

As for the amount of the case studies analysed, it is worth noting that in the case of LiABlock_3D (which is the name of the software tool implemented for the limit analysis model) 3D models can be analysed for both lateral live loads and support base movements. On the other hand, in the case of the non-linear kinematic model (applied in the next Chapter), the field of application is currently limited to the case of 2D rigid block assemblages subjected to settlement-induced base support movement.

As for the outcomes, the performed analysis showed that the proposed limit analysis-based model has high capabilities in the prediction of the structural response of masonry structures. Most of the applications and comparisons revealed an adequate agreement between numerical and experimental results in terms of collapse mechanisms and load factors.

The next Chapter 6 will complete the section on the numerical applications by describing the results obtained by using the second proposed formulation, i.e. the numerical procedure based on rigid block non-linear kinematic analysis. In this case a limited experimental campaign will be described with the main scope to validate the proposed rigid block model.

References

- Assante, F. (2015) *La regina delle galere. Storia e storie del carcere di Procida*. Edited by Giannini editore.
- Casapulla, C. and Maione, A. (2018) ‘Modelling the dry-contact interface of rigid blocks under torsion and combined loadings: Concavity vs. convexity formulation’, *International Journal of Non-Linear Mechanics*, 99, pp. 86–96. doi: 10.1016/j.ijnonlinmec.2017.11.002.
- Cascini, L., Gagliardo, R. and Portioli, F. (2020) ‘LiABlock_3D: A Software Tool for Collapse Mechanism Analysis of Historic Masonry Structures’, *International Journal of Architectural Heritage*, 14(1), pp. 75–94. doi: 10.1080/15583058.2018.1509155.
- Coccia, S., Di Carlo, F. and Rinaldi, Z. (2015) ‘Collapse displacements for a mechanism of spreading-induced supports in a masonry arch’, *International Journal of Advanced Structural Engineering*, 7(3), pp. 307–320. doi: 10.1007/s40091-015-0101-x.
- Forgács, T., Sarhosis, V. and Bagi, K. (2018) ‘Influence of construction method on the load bearing capacity of skew masonry arches’, *Engineering Structures*, 168, pp. 612–627. doi: 10.1016/j.engstruct.2018.05.005.
- Gagliardo, R., Terracciano, G., *et al.* (2019) ‘Application of Liablock_3D to the analysis of failure modes in masonry structures subjected to seismic action’, in *COMPDYN Proceedings*, pp. 742–749. doi: 10.7712/120119.6953.19741.
- Gagliardo, R., Cascini, L., *et al.* (2019) ‘Blind-test numerical simulation of shake-table tests on three-leaf masonry walls: An application of LIA block_3D’, in *COMPDYN Proceedings*, pp. 4699–4706. doi: 10.7712/120119.7261.19695.
- Gagliardo, R. *et al.* (2021) ‘A rigid block model with no-tension elastic contacts for displacement-based assessment of historic masonry structures subjected to settlements’, *Engineering Structures*, 229. doi: 10.1016/j.engstruct.2020.111609.
- Gilbert, M., Casapulla, C. and Ahmed, H. M. (2006) ‘Limit analysis of masonry block structures with non-associative frictional joints using linear programming’, *Computers and Structures*, 84(13–14), pp. 873–887. doi: 10.1016/j.compstruc.2006.02.005.

Iannuzzo, A. *et al.* (2018) ‘Modelling the cracks produced by settlements in masonry structures’, *Meccanica*, 53(7), pp. 1857–1873. doi: 10.1007/s11012-017-0721-2.

Iodice, R. (2017) *Palazzo d’Avalos e l’ex carcere di Procida. Il complesso monumentale rinascimentale tra passato, presente e futuro*. Edited by Nutrimenti.

Landolfo, R. *et al.* (2020) ‘Rigid block and finite element analysis of settlement-induced failure mechanisms in historic masonry walls’, *Frattura ed Integrità Strutturale*, 14(51), pp. 517–533. doi: 10.3221/IGF-ESIS.51.39.

Di Liello, S. and Rossi, P. (2017) *Procida architettura e paesaggio. Documenti e immagini per la storia dell’isola*. Edited by Nutrimenti.

Livesley, R. K. (1992) ‘A computational model for the limit analysis of three-dimensional masonry structures’, *Meccanica*, 27(3), pp. 161–172. doi: 10.1007/BF00430042.

Malena, M. *et al.* (2019) ‘Collapse mechanism analysis of historic masonry structures subjected to lateral loads: A comparison between continuous and discrete models’, *Computers and Structures*, 220, pp. 14–31. doi: 10.1016/j.compstruc.2019.04.005.

Mastrodicasa, S. (1943) *Dissesti statici delle strutture edilizie. Diagnosi e Consolidamento*. Edited by Ulrico Hoepli Editore. Milano.

Ministero delle infrastrutture e dei trasporti. (2018) *Decreto ministeriale 17 gennaio 2018 - Aggiornamento delle «Norme tecniche per le costruzioni»*.

Ochsendorf, J. A. (2006) ‘The masonry arch on spreading supports’, *Structural Engineer*, pp. 29–35.

Portioli, F. *et al.* (2014) ‘Limit analysis of 3D masonry block structures with non-associative frictional joints using cone programming’, *Computers and Structures*, 143, pp. 108–121. doi: 10.1016/j.compstruc.2014.07.010.

Quinonez, A. *et al.* (2010) *Small-scale models for testing masonry structures, Advanced Materials Research*. doi: 10.4028/www.scientific.net/AMR.133-134.497.

Regione Campania (2017) *Piano Stralcio per l’Assetto Idrogeologico*

dell’Autorità di Bacino della Campania Centrale - Tavole “Rischio da frane” e “Pericolosità da frane” 465013.

Restrepo Vélez, L. F., Magenes, G. and Griffith, M. C. (2014) ‘Dry stone masonry walls in bending-Part I: Static tests’, *International Journal of Architectural Heritage*, 8(1), pp. 1–28. doi: 10.1080/15583058.2012.663059.

Rossi, M., Calderini, C. and Lagomarsino, S. (2016) ‘Experimental testing of the seismic in-plane displacement capacity of masonry cross vaults through a scale model’, *Bulletin of Earthquake Engineering*, 14(1), pp. 261–281. doi: 10.1007/s10518-015-9815-1.

Sab, K. (2003) ‘Yield design of thin periodic plates by a homogenization technique and an application to masonry walls’, *Comptes Rendus - Mecanique*, 331(9), pp. 641–646. doi: 10.1016/S1631-0721(03)00144-X.

Sab, K., Dallot, J. and Cecchi, A. (2007) ‘Determination of the overall yield strength domain of out-of-plane loaded brick masonry’, *International Journal for Multiscale Computational Engineering*, 5(2), pp. 83–92. doi: 10.1615/IntJMultCompEng.v5.i2.20.

Simulia, D. S. (2014) ‘Abaqus 6.14’, *Abaqus 6.14 Analysis User’s Guide*.

Tran-Cao, T. (2009) *COLLAPSE ANALYSIS OF BLOCK STRUCTURES IN FRICTIONAL CONTACT*. The University of New South Wales, Sydney, Australia.

UNESCO World Heritage List (1997) *18th-Century Royal Palace at Caserta with the Park, the Aqueduct of Vanvitelli, and the San Leucio Complex*. Available at: <https://whc.unesco.org/en/list/549>.

Wang, J. (2004) *The three dimensional behaviour of masonry arches*. University of Salford.

Zessin, J. (2012) *Collapse analysis of unreinforced masonry domes and curving walls*. Harvard University.

Zessin, J., Lau, W. and Ochsendorf, J. (2010) ‘Equilibrium of cracked masonry domes’, *Proceedings of the Institution of Civil Engineers: Engineering and Computational Mechanics*, 163(3), pp. 135–145. doi: 10.1680/eacm.2010.163.3.135.

Chapter 6

Comparisons with experimental tests using non-linear kinematic analysis

The contents of Chapter 6 are published in (Gagliardo et al., 2021).

6.1 Introduction

The contents of Chapter 6 are mainly devoted to the application of the rigid block model for non-linear kinematic analysis proposed in Chapter 4. Various comparison with experimental and numerical case studies will be also showed in order to validate the computational procedure in terms of reliability of the predicted outcomes. In this case, the main goal is represented by the experimental calibration of the push-down capacity curves for the purposes of the next Chapter where a displacement-based approach is proposed for the damage assessment of masonry panels subjected to foundation movements. To this end, an experimental campaign on small-scale masonry panels was performed for sake of validation.

In this spirit, the current version of the on-going numerical project is mainly devoted to the masonry structures performance in the case of foundation movements induced by support settlements. The model has been showing high potentialities in the analysis of settlement vulnerability, which is a field mainly focused on the damage state investigation in terms of initiation and propagation of crack patterns rather than to the incipient collapse state. The reason of this

observation lies in the high resilience capacity of masonry structures to accommodate large amount of settlement displacement before the reach the maximum capacity. On the other hand, the possibility to study the crack pattern evolution in terms of crack location and widths step-by-step represents a very useful and powerful tool especially for historic and monumental masonry buildings, where specific strengthening interventions are highly demanded to save their historic and artistic priceless values.

6.2 Comparisons of rigid block model for non-linear kinematic analysis with experimental tests

In this section, the novel non-linear kinematic analysis model is validated against experimental tests on small-scale masonry panels. As deeply reported in Chapter 4, the present computational formulation is able to analyse 2D rigid block assemblages against several types of ground displacement at the foundation level. This numerical model represents an extension of the limit analysis model in the large displacement regime, but it is still an on-going numerical project. With this in mind, the applications here proposed aim to validate the non-linear kinematic strategy via a series of comparisons with experimental tests performed both at the University of Naples “Federico II” and in literature papers.

The rigid block model with elastic contact interfaces was compared with the results from experimental tests on various small-scale, dry jointed masonry models subjected to support movement. The comparison mainly aims to evaluate to which extent the proposed model is able to capture the response of the investigated specimens in terms of failure mechanisms, reaction and displacement at moving support, as well as in terms of crack width. Two case studies are represented by a single-leaf small scale wall panel and a small-scale portal frame already tested at University of Naples “Federico II” and analysed in (Portioli and Cascini, 2016). Then, the proposed non-linear kinematic formulation was validated against the experimental tests on a set of tuff masonry T-connection panels subjected to vertical support movement, which was specifically developed for the present study and already investigated in (Gagliardo *et al.*, 2021). The second case study is a 1/20 scaled model of the

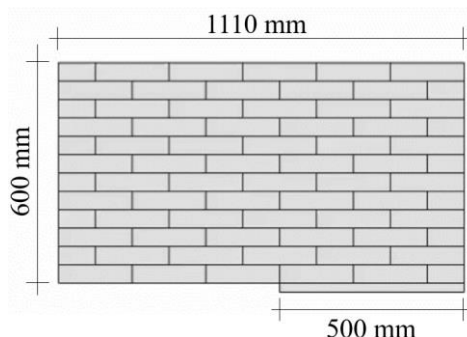
arched façade of the Loggia Palace in Brescia (Italy), experimentally tested and analysed in (Giardina *et al.*, 2020).

6.2.1 Small scale single-leaf wall panel

In this section the case study is represented by one of the experimental test investigated in (Portioli and Cascini, 2016) to validate the numerical model against experimental outcomes, designing and realizing ad-hoc test set-up to reproduce the foundation settlements. A single-leaf wall panel made of dry jointed tuff masonry blocks with dimensions of 200 x 100 x 50 mm was tested in (Portioli and Cascini, 2017). The bearing support system is designed to allow part of the panel to move along the vertical axis. Further information about the experimental set-up are available in (Portioli and Cascini, 2017).



a)



b)

Figure 6.1 - Wall sample 12C: experimental set-up (a) and geometrical properties (b).

With regard to displacement protocol, in the experimental test a set of 1.0 mm incremental displacements was applied to the test apparatus and corresponding weight variation was registered at each step of the test. The test was carried out until collapse. The investigated specimen is the 12C model according to (Portioli and Cascini, 2017). The wall specimen is five-and-half bricks width (1100 mm), half-brick thick (100 mm) and twelve courses high (600 mm) as showed in Figure 6.1. The brickwork is arranged in a stretchers bond pattern with all bricks laid as stretchers and half-bats at the beginning or at the end of alternate courses. The

value of friction coefficient and weight for unit volume experimentally measured was equal to 0.72 and 12.50 kN/m³.

The collapse of the masonry panels is induced by the progressive settlement of the movable bearing and the collapse load multiplier is evaluated through the base reaction at failure. According to the adopted assumptions, wall panel failure is attained as soon as the decreasing support reaction becomes stable (until a steady state load is reached) so that increments in displacements do not produce weight losses at the support.

The deformed shapes observed from testing for support vertical movements of 20.0 mm and 50.0 mm are shown in Figure 6.2a and Figure 6.2b. In the experimental test, just two macroblocks separated through a ‘stair-stepped’ crack can be observed at collapse: the first macro-block, which is supported by the fixed base, and the second one, translating downwards on the movable support. The reaction for the wall panel 12C measured at the movable support in the starting configuration (i.e. prior to the application of the imposed settlement) is equal to 375 N. The base reaction at failure is equal to 87 N.

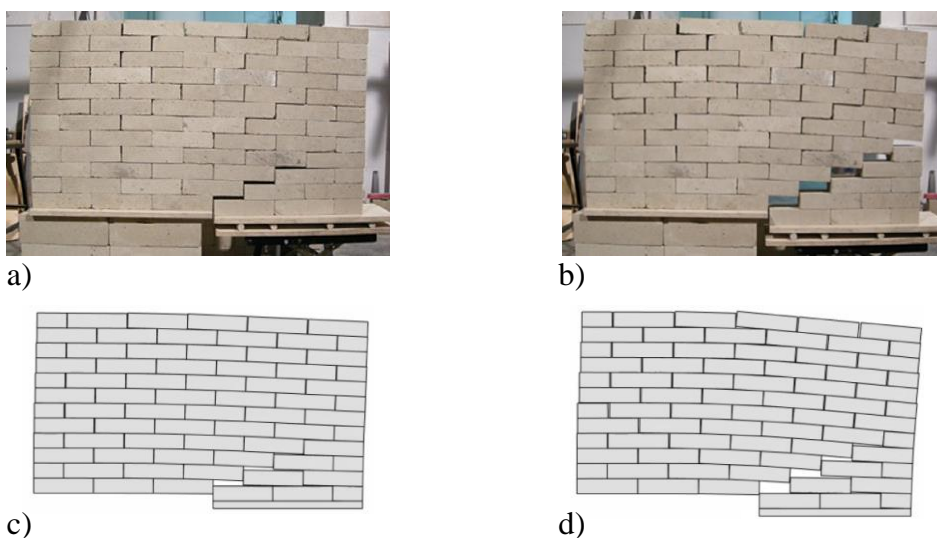


Figure 6.2 - Wall sample 12C (Portioli and Cascini, 2016) comparison between experimental (a)(b) and non-linear kinematic numerical (c)(d) outcomes: deformed shape of the specimen and plot of the failure mode at vertical displacement equal to (a)(c) 20 mm and (b)(d) 50 mm.

In the numerical simulation, the value of friction coefficient was set in the range between 0.6-0.7 for the horizontal bed joints and in the range between 0.2-0.5 for the vertical head joints, and the unit weight was set equal to 12.0 kN/m³. The normal stiffness at contact point was set equal to 1e2 kN/m³. The failure modes computed for the non-linear kinematic solution are shown in Figure 6.2c and Figure 6.2d in the case of vertical displacement equal to 20 mm and 50 mm respectively. The failure mechanism predicted for the wall panel 12C involves the middle part of the wall panel, which is subjected to sliding and rocking failure, and the macro-block over the movable support, which translates downwards and in horizontal direction, according to experimental tests. It is worth noting that these numerical results represents an improvement compared to the rigid model result presented in (Portioli and Cascini, 2016), where failure mechanism predicted involved the vertical movement of the masonry macro-block which was separated through a stepped diagonal crack propagating from the left end side of the support block with a large difference in the comparison with the experimental model. A good agreement in terms of collapse mechanism can be noticed in the experimental versus numerical comparison.

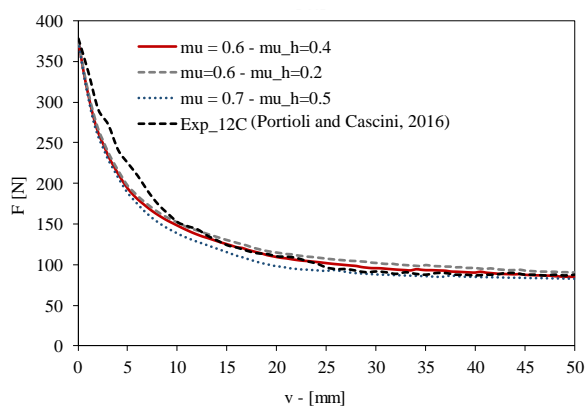


Figure 6.3 - Wall sample 12C (Portioli and Cascini, 2016) comparison between experimental and non-linear kinematic numerical outcomes in terms of loss of base reaction against vertical imposed settlement.

Figure 6.3 shows the comparison between experimental and numerical outcomes for wall sample 12C in terms of loss of base reaction against vertical imposed

settlement. Different combinations of vertical and horizontal friction behaviour were considered in a sensitive sense. The results show a very good agreement between numerical and experimental curves. The starting value of the base reaction of the numerical simulation is equal to 375 N, exactly the value of the reaction experimentally measured in the starting configuration. Then, the experimental and numerical curves are almost overlapped until 50 mm, that is the last step considered in the experimental test.

6.2.2 Small scale portal frame

The case study analysed in this section is represented by a small scale portal frame already investigated in (Portioli and Cascini, 2017), where ad-hoc experiments were carried out to investigate failure modes and maximum allowable displacements at moving supports just before the collapse. In the previous work the portal frame, namely δB_FH was numerically analysed by using a large displacement formulation where the elastic behaviour is not taken into account and the model is fully rigid. In this framework, the work developed for the present dissertation thesis also aims at the extension of the previous set of analysis and at the comparison between the two models, one accounting for the elastic behaviour and one neglecting it.

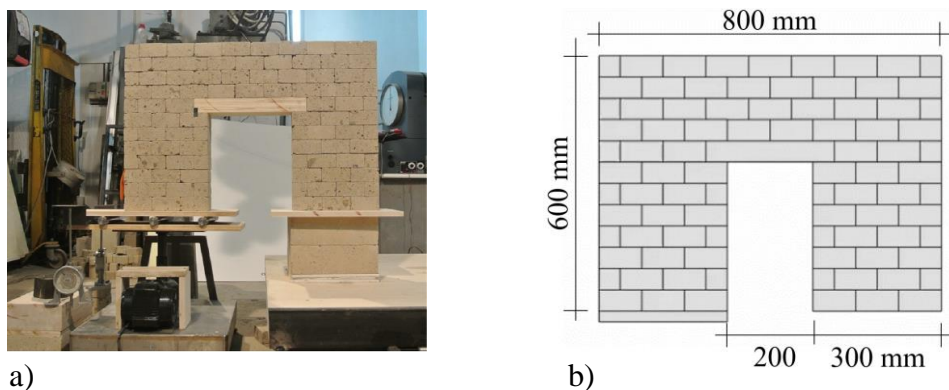


Figure 6.4 - Portal frame δB_FH : experimental set-up (Portioli and Cascini, 2017) (a) and geometrical properties (b).

The panel was made of tuff blocks with dimensions of 100 x 100 x 50 mm. The wall specimen investigated is eight bricks width (800 mm), one brick thick (100 mm) and twelve courses high (600 mm). The dimension of the opening was two bricks width (200 mm) and seven courses high (350 mm). In the adopted configuration, the horizontal displacement at the movable support (the timber table supporting the left pier) was free. The experimental set-up and the geometrical properties are also reported in Figure 6.4.

Also in this case, the brickwork was arranged in a stretcher bond pattern with all bricks laid as stretchers and half-bats at the beginning or at the end of alternate courses. A timber lintel was used to span the openings. The test set-up adopted for foundation settlements on the investigated wall panels was arranged according to (Portioli and Cascini, 2017). A displacement rate of 0.1 mm per second was applied to the test apparatus and corresponding weight variation were registered during the test. The failure mode observed from testing just before the collapse for the small-scale portal frame is shown in Figure 6.5a. The vertical movement imposed to the left pier involves the rotation of the timber lintel and of a part of the supported spandrel around the right end support the timber lintel. This rotation is associated to the formation of stepped diagonal cracks at the top of the right pier and to vertical cracks in the middle part of the left pier due to sliding failure. The above-mentioned rotation is also associated to a horizontal rigid body movement of the left pier, which is free to slide. The collapse of the wall panels is attained when the relative sliding displacement between the left bottom corner of the lintel and the upper right corner of the supporting tuff block below is greater than the staggering length (i.e. half a block length in this case, given the running bond pattern).

For the numerical simulations, unit weights of tuff masonry blocks and timber lintel were taken as 12.3 and 4.3 kN/m³. The friction coefficients at tuff-to-tuff and tuff-to-timber joints were taken as 0.72 and for horizontal bed joints and in the range between 0.40 and 0.72 for the vertical head joints, respectively. The sensitivity analysis was also performed against the value of the normal contact stiffness, where both 1e5 kN/m³ and 5e5 kN/m³ stiffness were adopted. The results of the numerical analysis are reported in Figure 6.5b. The comparison of

failure mode with testing outcomes shows that the collapse mechanism predicted by the numerical model for the small-scale portal frame are in good agreement with the experimental tests. The predicted failure mode involves the rotation of the spandrel over the right pier and the vertical and horizontal movement of the left support. According to experimental tests, the maximum displacement capacity is attained when the relative sliding displacement of the left bottom corner of the timber lintel overcomes half the length of the supporting tuff block.

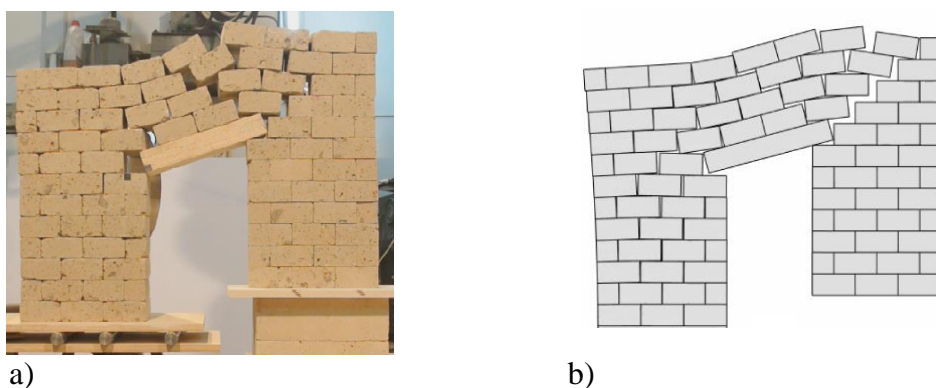


Figure 6.5 - Portal frame 8B_FH_2: comparison between experimental (a) and non-linear kinematic numerical (b) outcomes: deformed shape of the specimen and plot of the failure mode at vertical displacement equal to 100 mm.

The experimental and numerical capacity push-down curves are compared and plotted in Figure 6.6 in terms of loss of base reaction against foundation vertical displacement. The experimental curve can be schematized in three phases. In the first phase, the response is characterized by high-rate decreasing values of the reaction-displacement curve. In this phase, the failure mechanism starts to develop progressively within the wall panel, with random activation of failure (i.e. toppling and sliding) at dry joints due to the variability of mechanical properties and geometric imperfections. In the second phase, the failure mechanism is completely developed in the whole wall panel and the magnitude of the base reaction is approximately constant with increasing displacements at the movable support. During the third phase, the base reaction increases slightly with increasing movements at base support due to the effects of large displacements.

The starting values of base reaction at the movable support are also reported for comparison in Figure 6.6. It can be noted that the experimental and numerical values are in good agreement, equal to about 249 N. Slight differences between the predicted and experimental value of the base reactions can be observed for small values of support displacement, in the first part of the capacity curve. This can be ascribed to the high sensitivity of the results to the parameter of the normal contact stiffness of the proposed sequential numerical procedure. Conversely, the results of experimental tests show that large displacements are necessary for the mobilization of the complete failure mechanism.

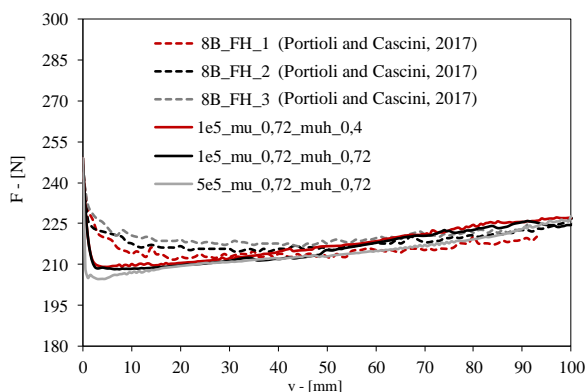


Figure 6.6 - Portal frame 8B_FH (Portioli and Cascini, 2017) comparison between experimental and non-linear kinematic numerical outcomes in terms of loss of base reaction against vertical imposed settlement.

6.2.3 T-panels with and without interlocking

The test specimens consist of a set of T-panels, similar to (Mastrodicasa, 1943), arranged in two different configurations, namely without and with interlocking (indicated with S1 and S2 in the following). Three tests were carried out per each configuration. Figure 6.7 reports a front and an axonometric view of the specimens as well as sketches of the set-up. Each panel was made of tuff blocks with dimensions of 100×100×50 mm and with a volumetric weight equal to 12.5 kN/m³. The specimens are eight bricks long (800 mm), one brick thick (100 mm) and seven courses high (350 mm). The orthogonal panel (i.e. the flange of the T) was three bricks wide (300 mm). The brickwork was arranged in a stretcher bond

pattern with all bricks laid as stretchers and half-bats at the beginning or at the end of alternate courses.

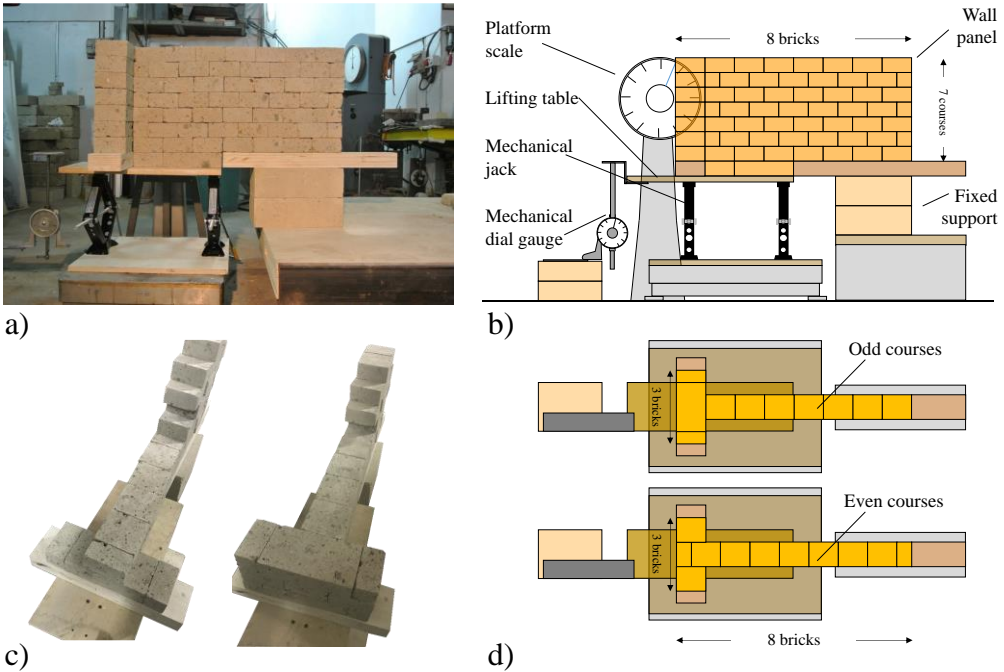


Figure 6.7 - T-panel: views (a)(c) and sketches (b)(d) of the experimental test set-up (Gagliardo et al., 2021).

The support system was designed to impose vertical movements only to the base of the wall panel. The set-up was arranged so that the right side of the panel is fixed while the left side is placed on a lifting table for a length of 4 bricks. In such a way both the T-flange and half of the front wall can settle down. The lifting table was made of a timber table directly bolted on two mechanical scissor jacks. The jacks were also bolted on another timber table to the bottom side in order to prevent horizontal displacements. The scissor jacks were actioned applying a simultaneous screwing to impose a uniform vertical displacement. The jack system was positioned on a platform scale with a maximum capacity of 600 N, in order to directly measure variations of dead load distribution when the settlement is imposed. A mechanical dial gauge, fixed to the floor and connected

to the lifting table with a S-shape steel plate, was used to measure the vertical displacements of the lifting table itself. The dial gauge reads 0.1 mm over a range of 200 mm. Displacements of the lifting table and weight variations were registered at each screwing of the jacks. Two cameras, positioned in front of the specimens and on the left-hand side, captured pictures at each screwing.

The first tests investigated the behaviour of the S1 specimen: at incipient collapse (Figure 6.8a) the flange of the T-panel exhibited an overturning around a rotational hinge, between the first and second course. The overturning is induced by the failure of a portion of the front wall, corresponding to the part separated by the two opposite stepped openings originated from the right side of the moving support. A similar collapse mechanism was observed in the case of S2 specimen (Figure 6.9a) but, in this second case, the orthogonal wall overturned around a rotational hinge located in a different position.

The failure mechanisms predicted with the numerical models are reported in Figure 6.8b and Figure 6.9b. For numerical analyses, the friction coefficient was set equal to 0.72, according to (Portioli and Cascini, 2017). The normal stiffness per unit contact surface was calibrated on the basis of the response observed from S1 specimen and is equal to $5e4 \text{ kN/m}^3$. Although this stiffness seems to be quite low, it is interesting to note that similar values were found in (Gaetani *et al.*, 2017) in the case of shaking table test on a scaled dry-joint arch.

In order to account for the weight of the orthogonal wall in the developed planar rigid block model, the dead loads applied at the full blocks along the left end side of the model were assigned accordingly. Displacement increments equal to 0.50 mm were applied at the two blocks used to model the moving support. Two increments with zero displacements were imposed before the application of vertical displacement increments to stabilize the numerical response under the effects of dead loads in the elastic regime.

The comparison with experimental tests shows that, in both configurations, the numerical simulations are in good agreement with the observed collapse mechanisms. Differences in the position of the rotational hinges at the orthogonal walls can be noted. In the case of specimen S2, those can be also ascribed to three dimensional effects of interlocking.

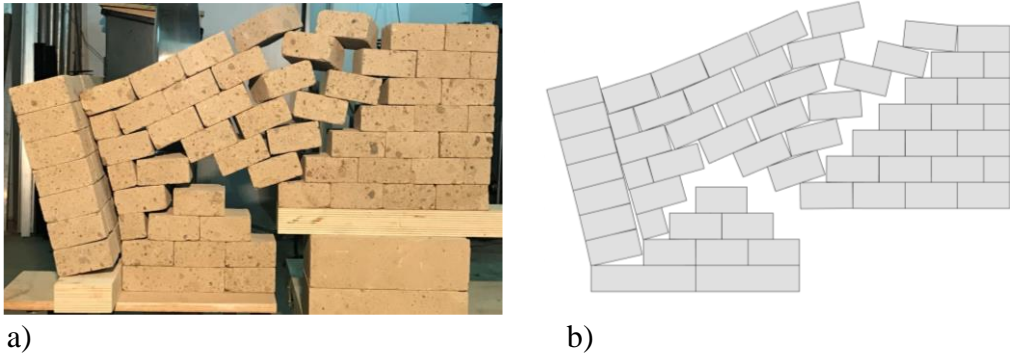


Figure 6.8 - Failure mechanism at incipient collapse ($\delta = 110$ mm) of the T-panel without interlocking (S1 specimen): experimental (a) versus numerical (b) comparison (Gagliardo et al., 2021).

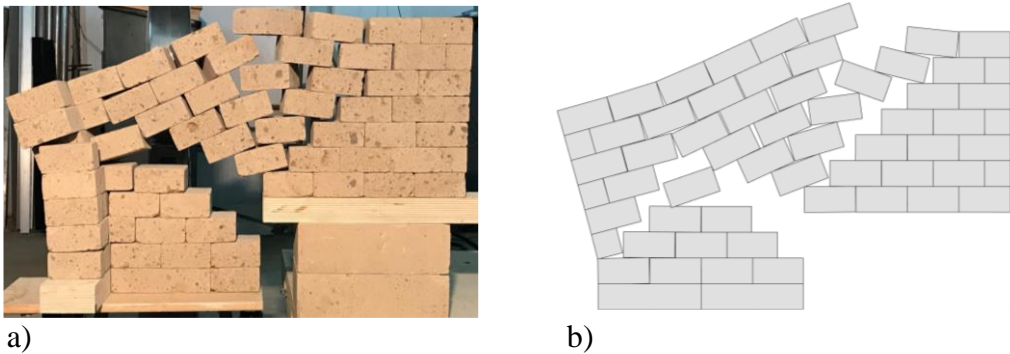


Figure 6.9 - Failure mechanism at incipient collapse ($\delta = 140$ mm) of the T-panel with interlocking (S2 specimen): experimental (a) versus numerical (b) comparison (Gagliardo et al., 2021).

The experimental and numerical results were also compared in terms of push-down/capacity curves, which represent the variation of the reaction at the moving support as a function of the imposed vertical displacement (Figure 6.10). In general, the following response was observed. The support reaction progressively decreases attaining a minimum value at the complete formation of the failure mechanism. Then the support reaction slightly increases, as a consequence of large displacement effects, until the collapse displacement is attained. The capacity curves obtained from the previously developed rigid model with rigid

contacts are also plotted for comparison (Portioli and Cascini, 2017). The latter, of course, does not catch the evolution of the support reaction in the first part of the analysis, when the elastic behaviour prevails, but after that, the two curves are in perfect agreement.

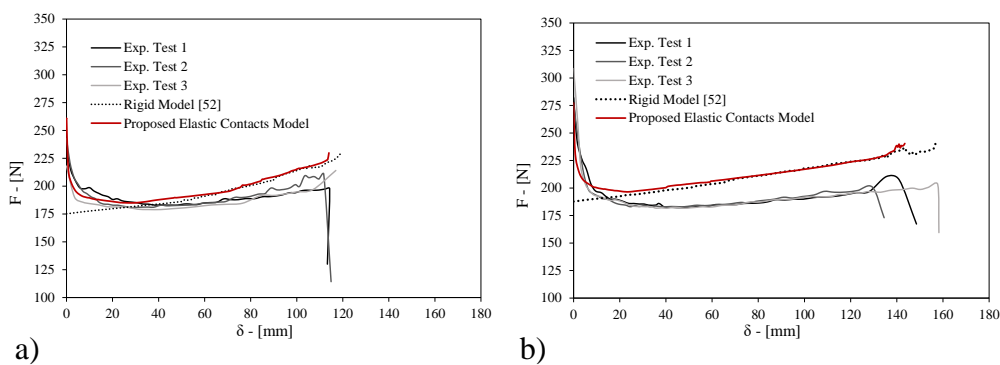


Figure 6.10 - Base reaction against vertical settlement displacements for three test repetitions: S1 (a) and S2 (b) specimens (Gagliardo *et al.*, 2021).

The comparison of numerical and experimental curves shows also a quite good agreement. The ultimate displacements obtained from the numerical model closely match the average experimental values, indicating the adequacy of the model to calculate the ultimate displacement capacity. As for the trend of support reactions, for a settlement up to 10 mm the maximum difference between numerical and experimental results is equal to about 5% and 7% in the case of S1 and S2 model respectively (Table 6.1). Besides, for larger values of the displacement the experimental and numerical curves show an increasing deviation between support reactions in tests and simulations up to about 15%. The discrepancies can be mainly ascribed to the fact that the rigid blocks located in the upper part of the front panel assume different position at collapse (e.g. see the position of rigid blocks in the upper courses of the front panels). As a consequence, a higher weight rests on the platform for the experimental specimens, compared to the one measured in the numerical analysis. The reasons for this shall be found in the simplification that a planar model may introduce respect to a 3D analysis and, most of all, in the geometric and mechanic imperfections that the numerical models disregard. A further investigation on

these aspects is of course worth of interest but beyond the scope of the present study. It is worth to note that the difference in the value of the starting reaction in the case of S1 model (see Table 6.1) reflects a small misalignment of the moving support respect to the fixed base at the beginning of the test, which could be confirmed with the numerical model by using a lower stiffness at the base joint.

Specimen	Model size (b × c)*	$f_s(\delta = 0 \text{ mm})$ [N]		$f_s(\delta = 10 \text{ mm})$ [N]		δ_u [mm]		CPU Time [s]
		Num.	Exp.	Num.	Exp.	Num.	Exp.	
S1	61 × 161	260.8	231.3	189.5	192.5	116.5	115.1	115.0
S2	61 × 159	277.4	271.8	200.3	194.8	145.0	148.2	160.0

Table 6.1 - Small scale wall panels: comparison of numerical and experimental (average of three tests is given) results.

6.2.4 Small-scale masonry façade

The case study of a small-scale masonry façade analysed in (Giardina *et al.*, 2020) was also investigated to evaluate the ability of the proposed model to predict the evolution of crack widths. The tested specimen is a 1/20th scaled model of the arched façade of the Loggia Palace in Brescia (Italy). The façade was assembled in the laboratory of the University of Brescia using 705 blocks of Botticino Classic marble, the same material of the Loggia Palace (Giardina *et al.*, 2020). The case study represents an example of historic masonry structure on isolate wooden-pile foundation on soft-soil, which are severely affected by differential settlements. In this dissertation the tests on dry-jointed models were analysed, namely Test 1 and Test 2 in (Giardina *et al.*, 2020).

In Test 1, the specimen was subjected to its self-weight only, and no additional loads were applied. As for the displacement protocol, two left columns were involved in differential settlements according to the following displacement history: 1) a 7.5 mm settlement was applied to the left end column by lowering the supporting plate in 18 steps of 0.42 mm, which corresponds to a settlement of 150 mm on the full-scale structure; 2) the same vertical displacement was gradually imposed to the second column from the left. In Test 2, additional loads were applied to the façade as reported in Figure 6.11b. The value of the additional loads was derived according to the test described in (Giardina *et al.*, 2020),

corresponding to a distributed load equal to 0.85 kN/m, 0.42 kN/m, 1.27 kN/m, 0.87 kN/m and 0.39 kN/m in the case of f_1 , f_2 , f_3 , f_4 and f_5 respectively. In this case, only the first left column was subjected to settlement, after applying the load. The settlement was applied to the column in 21 steps of 0.42 mm, reaching a final displacement of 8.8 mm, in order to simulate the effects of an equivalent total settlement of 176 mm on the full-scale structure. The monitored parameters in Test 1 were the crack widths. In Test 2 the horizontal displacements were measured at points a, b and c as indicated in Figure 6.11a.

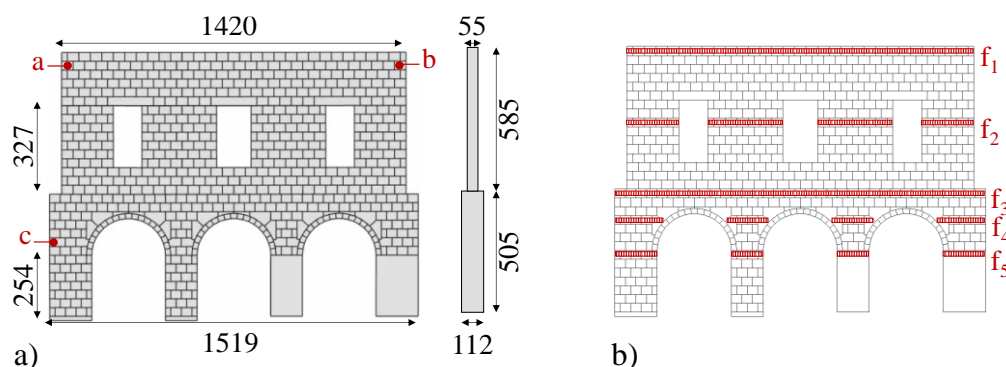


Figure 6.11 - Small-scale model of the Loggia Palace in Brescia (Italy): (a) dimensions in mm and location of dial gauges at points a, b and c; (b) location of the additional loads (Gagliardo *et al.*, 2021).

As for numerical analysis, the mechanical properties were set in accordance to (Giardina *et al.*, 2020): the volumetric weight ρ is equal to 27.0 kN/m³ and the friction coefficient μ was set equal to 0.45 (corresponding to a friction angle of 24°) for both bed and head joints. The value of the normal stiffness per unit contact surface at block interfaces was calibrated on basis of the experimental results and was set equal to 2e5 KN/m³. The comparison between the numerical failure mechanism and the experimental crack patterns are reported in Figure 6.12 and Figure 6.13 for Test 1 and 2 when the vertical settlement is applied to the left end column. In the case of Test 1, the numerical failure pattern is represented by three main cracks around the opening on the left at the first floor and is in a good agreement with the experimental test (Figure 6.12). Compared

to the experimental crack pattern, the numerical one clearly shows multiple cracks in the case of both crack 1 and crack 3.

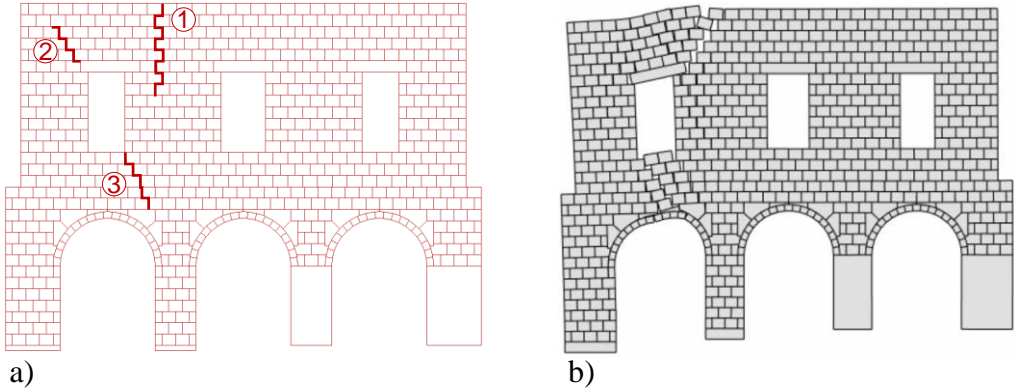


Figure 6.12 - Test 1: crack pattern for both experimental (a) and numerical (b) case (Gagliardo et al., 2021).

As for test 2, the experimental crack pattern is localized in the left portion of the façade, where three diagonal cracks developed: crack 1 is located at the top of the left side, over the window; crack 2 appeared in the area between the window and the first arch from the left; crack 3 appeared in the upper side of the left end column. The numerical model predicts crack 1 to some extent and crack 2 but fails in the opening of the crack 3 (Figure 6.13).

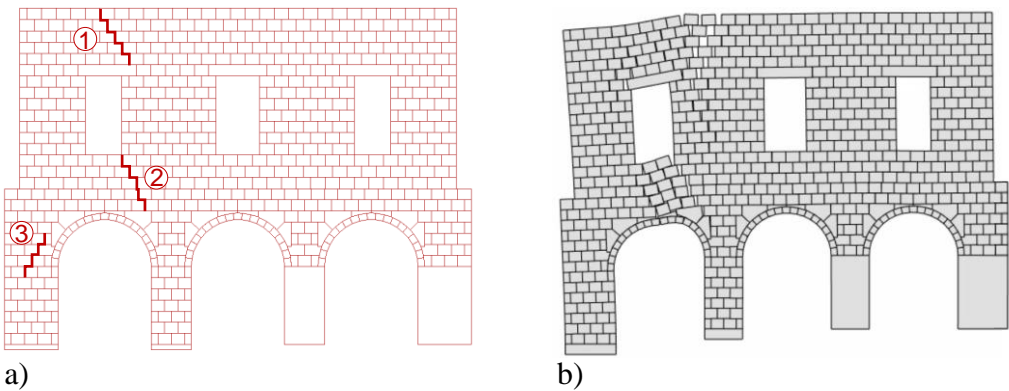


Figure 6.13 - Test 2: crack pattern for both experimental (a) and numerical (b) case (Gagliardo et al., 2021).

Figure 6.14a shows the comparison of in terms of crack widths for the crack 1 and crack 3 of Test 1 (see Figure 6.12a). The numerical values of the crack width were calculated as the sum of openings associated to the multiple cracks obtained in the rigid block model. In the case of crack 1, numerical results are in good agreement with the experimental one, being the last measured value equal to 2.5 mm and 2.9 mm for the numerical and experimental respectively. Major differences are in the comparison on crack 3. The two curves are close until 2 mm settlement. Then the numerical curve continues almost linear to the end reaching a final value of 4.9 mm against 3.1 mm of the experimental test. Also in this case, differences between numerical and experimental results should be ascribed to simple assumptions which govern the formulation proposed and to the effect of geometric imperfections.

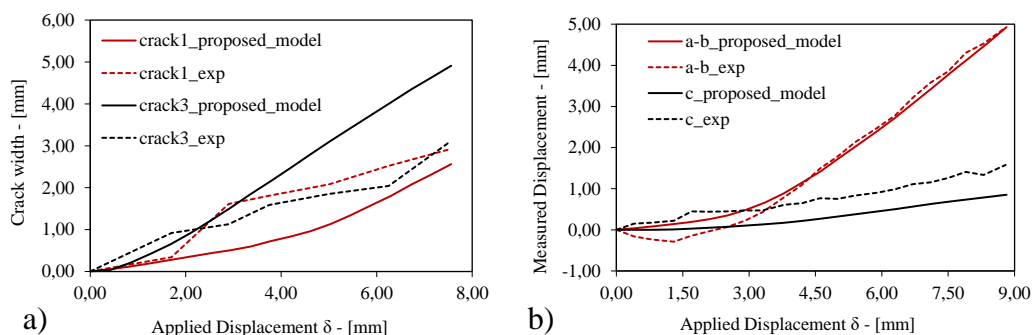


Figure 6.14 - Experimental measured values versus numerical results, in terms of crack width and horizontal displacement against vertical settlement: (a) Test 1; (b) Test 2 (Gagliardo *et al.*, 2021).

Figure 6.14b shows the comparison between Test 2 and numerical results in terms of horizontal relative displacement between points a and b (curve a-b in Figure 6.14b) and displacements at point c. The a-b experimental curve exhibits a negative slope in the first three steps, due to some compaction of the blocks in the horizontal direction caused by the vertical settlement, as described in (Giardina *et al.*, 2020). The slope becomes positive and almost constant from the fourth step, due to the increasing crack opening. The agreement between the numerical curves and the experimental one is satisfactory. As for the curve c the

numerical response slightly underestimates the value of the measured displacement.

Conclusions

Chapter 6 aimed to validate the proposed model based on non-linear kinematic analysis. A series of comparisons with experimental tests performed on small-scale masonry panels were presented and discussed, testing the abilities of this numerical formulation in the masonry structures capacity and response investigation under settlement. Contrary to the applications of the limit analysis-based rigid block models described in the previous Chapter 5, in the case of the non-linear kinematic model, the field of application is currently limited to the case of 2D rigid block assemblages subjected to settlement-induced base support movement. In this spirit, the main scope in the case of the non-linear kinematic model is represented by the validation of the novel formulation against experimental tests on small-scale panels subjected to moving supports.

The outcomes of numerical versus experimental comparison showed high potentialities of the non-linear rigid block model in the prediction of the structural behaviour of masonry structures subjected to foundation displacements. A good agreement between numerical and experimental results was revealed especially in terms of crack pattern propagation and force-displacement response.

In the next Chapter 7, the validated numerical procedure based on rigid block non-linear kinematic analysis will be applied as computational support for the definition of a performance-based damage assessment approach of masonry panels subjected to foundation movements. A proposal for settlement-related damage classification will be introduced within the framework of a comprehensive overview of the classical and empirical damage assessment methods developed in literature in the last decades.

References

- Cascini, L., Gagliardo, R. and Portioli, F. (2020) ‘LiABlock_3D: A Software Tool for Collapse Mechanism Analysis of Historic Masonry Structures’, *International Journal of Architectural Heritage*, 14(1), pp. 75–94. doi: 10.1080/15583058.2018.1509155.
- Gaetani, A. *et al.* (2017) ‘Shaking table tests and numerical analyses on a scaled dry-joint arch undergoing windowed sine pulses’, *Bulletin of Earthquake Engineering*, 15(11), pp. 4939–4961. doi: 10.1007/s10518-017-0156-0.
- Gagliardo, R., Terracciano, G., *et al.* (2019) ‘Application of Liablock_3D to the analysis of failure modes in masonry structures subjected to seismic action’, in *COMPdyn Proceedings*, pp. 742–749. doi: 10.7712/120119.6953.19741.
- Gagliardo, R., Cascini, L., *et al.* (2019) ‘Blind-test numerical simulation of shake-table tests on three-leaf masonry walls: An application of LIA block_3D’, in *COMPdyn Proceedings*, pp. 4699–4706. doi: 10.7712/120119.7261.19695.
- Gagliardo, R. *et al.* (2021) ‘A rigid block model with no-tension elastic contacts for displacement-based assessment of historic masonry structures subjected to settlements’, *Engineering Structures*, 229. doi: 10.1016/j.engstruct.2020.111609.
- Giardina, G. *et al.* (2020) ‘Analysis of a scaled stone masonry facade subjected to differential settlements’, *International Journal of Architectural Heritage*, 14(10), pp. 1502–1516. doi: 10.1080/15583058.2019.1617911.
- Landolfo, R. *et al.* (2020) ‘Rigid block and finite element analysis of settlement-induced failure mechanisms in historic masonry walls’, *Frattura ed Integrità Strutturale*, 14(51), pp. 517–533. doi: 10.3221/IGF-ESIS.51.39.
- Malena, M. *et al.* (2019) ‘Collapse mechanism analysis of historic masonry structures subjected to lateral loads: A comparison between continuous and discrete models’, *Computers and Structures*, 220, pp. 14–31. doi: 10.1016/j.compstruc.2019.04.005.
- Mastrodicasa, S. (1943) *Dissesti statici delle strutture edilizie. Diagnosi e Consolidamento*. Edited by Ulrico Hoepli Editore. Milano.
- Portioli, F. and Cascini, L. (2016) ‘Assessment of masonry structures subjected to foundation settlements using rigid block limit analysis’, *Engineering*

Structures, 113, pp. 347–361. doi: 10.1016/j.engstruct.2016.02.002.

Portioli, F. and Cascini, L. (2017) ‘Large displacement analysis of dry-jointed masonry structures subjected to settlements using rigid block modelling’, *Engineering Structures*, 148, pp. 485–496. doi: 10.1016/j.engstruct.2017.06.073.

Chapter 7

Damage assessment by a performance-based approach

The contents of Chapter 7 are published in (Gagliardo et al., 2020, Gagliardo et al., 2021).

7.1 Introduction

The present chapter aims at developing a performance-based approach for the assessment of full-scale historic masonry buildings affected by the threats of the ground movements at the foundation layer mainly due to the hydrogeological risk. In the spirit of an on-going project, the focused subject is currently represented by masonry panels, such as walls and façades. The ambition of such a performance-based assessment approach lies in investigation of the possibility to use the proposed rigid block model with no-tension elastic contacts together with the definition of a damage classification with the purpose to use the capacity push-down curves as a tool for the identification of various performance (and damage) levels a structure can exhibit when subjected to settlement-induced foundation movements.

In this framework, the dissertation thesis introduces an assessment procedure where the damage level that a structure can accommodate when is settlement-involved is based on the value of the vertical displacement applied to the movable foundation, introducing a control point at the foundation movable block to detect

the amount of the settlement displacement per each step. It is worth noting that this kind of approach needs the preliminary organization of a damage assessment and classification method to define specific damage peculiarities which can identify a performance levels out from the others. To achieve this scope, an overview of the empirical damage assessment by literature is studied and describe in the following sections.

As a matter of fact, the proposal of a procedure developed within the theory of the performance-based assessment philosophy is supposed to be in the field of the limit states approaches. The idea of limit states is based on the consideration that a structure is able to exhibit various performance levels (PLs) which represent the attainment of specific damage states (DSs) and produce specific damage levels (DLs). It is worth noting that the limit states approach was widely used for the assessment of the seismic capacity of structures, as showed by the high attention the international codes addressed to this point (*EN 1998-2005. Eurocode 8: Design of structures for earthquake resistance*, 2005; Consiglio superiore dei lavori pubblici, 2010; American Society of Civil Engineers, 2017; Ministero delle infrastrutture e dei trasporti., 2018, 2019). With reference to the hydrogeological risk and settlement analysis, it is clear that the limit state of interest is represented by the serviceability limit state being the ultimate state so far to be achieved in the case of monumental historic masonry structures which can accommodate significant foundation movements before to collapse under settlement. Following the philosophy and the consolidated background of the performance-based assessment approach developed in the field of the structural seismic capacity, the introduction of a set of parameters is a basic assumption to propose a classification of the damage levels that a structural type can exhibit. According to classical and empirical damage classification methods proposed in literature, several parameters in the case of a simple panel subjected to a movement of the foundation layer, assuming that the structural behaviour of the masonry type is the same of the equivalent beam. It is worth to note that most of the identified parameters are related to the value of the critical tensile strain, which is highly dependent on the amount of the applied settlement displacement. As well, another classical parameter for the damage assessment of settled masonry types is represented by the severity of the crack width. Such a parameter

is for sure highly significant but is not able to provide a damage quantification in terms of safety level for an overall structure.

In the seismic contest, the research has been producing much more results in the damage assessment and risk mitigation (Lagomarsino, 2012) because the last seismic events proved the high earthquake vulnerability of the historical masonry Cultural Heritage (Oliveira, 2003; Lagomarsino, 2012; Cattari *et al.*, 2014; Hofer *et al.*, 2018). Lagomarsino (Lagomarsino and Cattari, 2015) proposed a method based on the seismic performance-based assessment (PBA) of the Cultural Heritage, based on three steps: the first considers the classification, safety and conservation requirements, seismic hazard definition and knowledge of the structure; the second refers to modelling and verification procedure; the third deals with the rehabilitation decisions. The limit states identification occurs on the global pushover curve, where each limit state corresponds to a specific displacement rate. The displacement promoting the attainment of a limit damage is computed as the minimum value between the values corresponding to the limit conditions attainment by single element. In this study, Lagomarsino also discussed about the complexity of the seismic assessment existing building, mainly due to two motivations. First of all, it's a complex task to interpretate and model the seismic response of such a structure, because any provisions for earthquake still existed at the time those structures were built. Most of the case, these ancient masonry buildings were built following empirical rules handed down from one generation to another. The second reason is the impossibility to perform invasive investigation on the structure, resulting in a very high complexity of obtaining as-built information useful for the knowledge of material parameters and structural details which can be considerably different point to point in the buildings. These observations can be properly applied also to the field of ancient masonry structures subjected to settlement.

7.2 Damage classification: state of art on empirical methods

The ambitious attempt carried out in this thesis, i.e. the proposal for a performance-based assessment approach for settled masonry panels, demands for

a preliminary introduction dealing with the existing solutions suggested in literature with regard to the classification of damage for masonry panels subjected to foundation settlement.

Several damage classification criteria were proposed in the last decades considering different parameters. The main challenge is to introduce a correlation between the ground movement and the consequent damage. Damage classification could derive by subjective and perception features. Codified guidelines do not exist at all, and the experience and observation of building damage played a fundamental role in the damage classification. The settlement-produced damage could affect essentially the aesthetic, the serviceability and the stability of the building: increasing the foundation movements, the buildings damage progresses from the first to the third category. It appears clear that one of the parameters involved in the damage classification is the amount of the crack openings and the consequent ease of repair of the visible damage. All the methods proposed in literature aim at developing a damage classification, introducing some parameters in order to identify several classes of damage. Most of them are based on the so-called Limiting Tensile Strain Method (LTSM), where the investigated parameter is the critical tensile strain ε_{crit} , which represents the value of the deformation that corresponds to the development of the first crack. Several authors (Polshin, D.E., 1957; Burland and Wroth, 1974; Boscardin and Cording, 1989) proposed methods and approaches to identify values of the ε_{crit} that represents the attainment of a specific performance level for the structure, involving aesthetic, functionality, and stability problems for the stone buildings. Another involved parameter (Skempton and Mac Donald, 1956) is represented by the angular distortion, that is the ratio between the differential settlement among two columns and the linear distance between the two columns. The limitation of these proposed approaches in literature is that most of them were based on the observation of the crack patterns. The masonry assemblage, the quality of involved materials and the geometrical features can highly influence the crack opening, also affecting the capacity analysis of the masonry type or building. The above-mentioned empirical methods for the damage classification of masonry structures are now described in detail.

The approach proposed by (Skempton and Mac Donald, 1956) is based on the assumption that the damage can be assessed on the value of the performed angular distortion, i.e. the ratio between the differential settlement and the horizontal length. The authors investigated 98 case studies, both reinforced concrete frames and masonry bearing walls. The parameters considered for the damage classification were the maximum settlement, the differential settlement and the angular distortion.

The selected parameters show that the criterion assumes that the damage is produced by shear deflection rather than flexural bending deflection. The examined case studies showed mainly aesthetic damage rather than operational or structural. They also proposed critical values of the angular distortion: 1/300 corresponds to the first crack opening; 1/150 to the structural damage; 1/500 to the design value.

The criterion proposed by (Polshin, D.E., 1957) introduced the concept of critical tensile strain ε_{crit} . This method was based on the analysis of several settled buildings in URSS in the XX century. They divided the structures in two classes: frame buildings and bearing wall buildings. In the case of frame structures, the main parameter for the damage assessment is the differential settlement between two close columns. In the second case, i.e. bearing wall structures, the parameter considered is the critical value of the tensile strain in the wall. The authors suggested a threshold for the critical value of the tensile strain equal to 0.05%. In such a proposal, they formulated a correlation between the differential settlement and the cracks opening based on the length-to-height ratio of the panel.

The assessment procedure introduced by (Burland and Wroth, 1974) expanded upon the investigation of the critical tensile strains, assuming an equivalent elastic beam behaviour. The authors referred to the model of a simple rectangular beam with a length L and a height H . These are essentially: the settlement ρ ; the absolute differential settlement δ_ρ ; the grade θ ; the angular strain α (sagging or hogging); the relative differential settlement Δ ; the distortion Δ/L ; the rigid rotation ω ; the relative rotation β ; the average horizontal strain ε_h . Burland and Wroth also agreed with Polshin and Tokar, assuming that the settlement-induced damage is mainly represented by the cracks due to the critical value of the

horizontal tensile strain ε_h , resulting in a lower value of admissible settlement. Burland and Wroth observed that previous criteria, based on the amount of settlement, confined the damage to the cladding and finishes, neglecting the structural members. Starting from this point, they investigated the role of the horizontal tensile strain on the onset of the cracks. They introduced two approaches in order to study the building response to the ground movements induced by tunneling excavation, that allow to evaluate the behaviour of bearing walls both parallel and perpendicular to the excavation axis. They fixed particular values of this parameters, considering different structural types. According to (Burland and Wroth, 1974), the critical value of the tensile strain is in the range between 0.05% and 0.10% for masonry structures and in the range between 0.03% and 0.075% for reinforce concrete structures. These values do not correspond to the values activating collapse in tension. The authors also stated that cracks opening does not correspond to damage limit state attainment since the structure can exhibits further deformations before collapse.

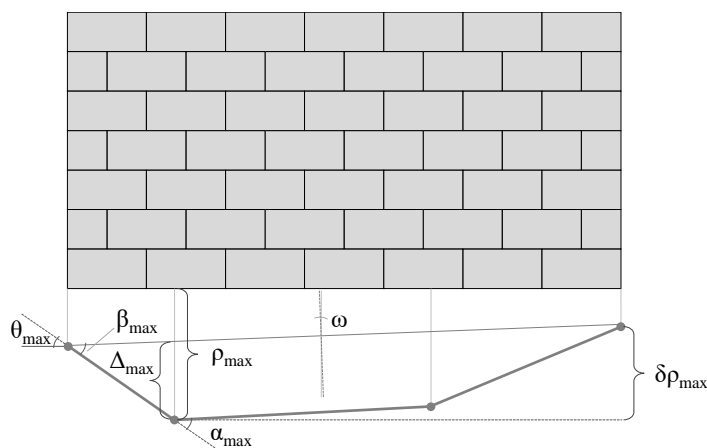


Figure 7.1 - Parameters involved in the damage classification proposed in (Burland and Wroth, 1974).

(Burland, Broms and de Mello, 1978) introduced the concept of limiting tensile strain in place of the critical strain, meaning a parameter useful for the serviceability limit state. The damage assessment procedure proposed by (Boscardin and Cording, 1989) developed this concept, introducing a damage

classification with different damage category (from negligible to very severe) related to specific tensile strain ranges.

7.3 Assessment by push-down curves

In this section the displacement-based assessment approach to damage classification is proposed with the scope to evaluate the possibility to extend consolidated procedures for the assessment of global behaviour in the field of seismic assessment to the case of settlements.

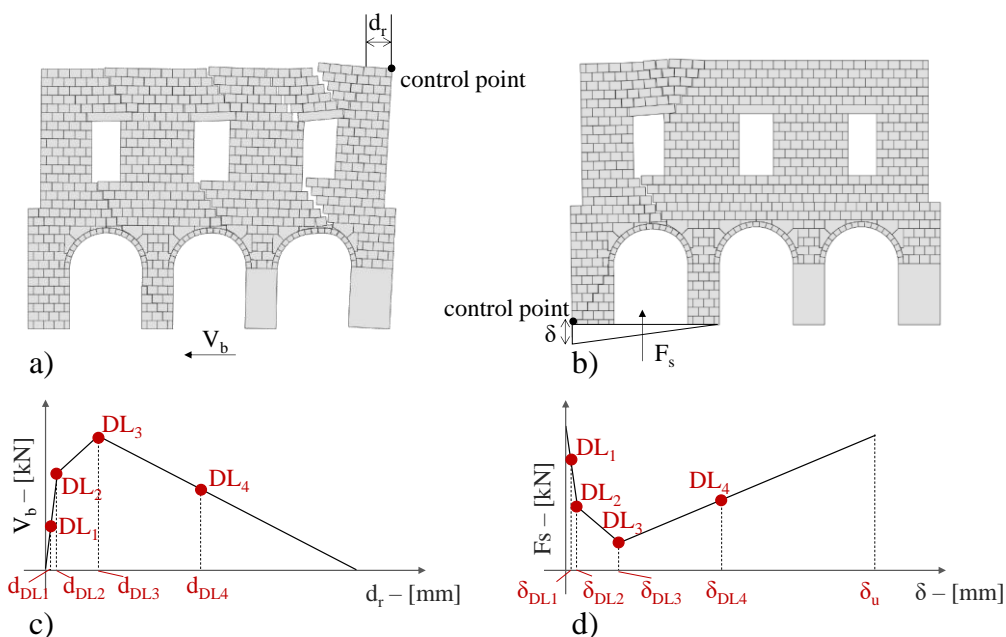


Figure 7.2 - Damage levels definition in the case of (seismic) push-over analysis (a), (b) and (settlements) push-down analysis (c), (d) (Gagliardo et al., 2021).

According to the current state of the art and codes on seismic assessment of masonry structures, the use of capacity curves obtained from push-over analyses is a common procedure to quantify performance levels when a nonlinear static (or kinematic) analysis is carried out. In this case, capacity curves generally express the relation between the base shear force and the horizontal roof

displacement (or another relevant point that controls the structural global response) as given in Figure 7.2a and Figure 7.2b. Here, V_b is the reaction at the base of the wall and d_r is the horizontal displacement on the top right of the building where a mechanism is formed. Damage levels and corresponding displacements, related to the attainment of various limit states, are then obtained on the basis of the capacity curves.

The use of static push-down analysis and capacity curves for the assessment of damage states and performance levels in the case of settlements is here proposed. Thus, non-linear kinematic analysis is used to evaluate the capacity of a structure to withstand an external demand related to an imposed settlement profile. Capacity curves are obtained plotting the variation of the base reaction at the moving supports versus the displacement of a control point (i.e. the progressive ground vertical displacement). The limit states identification is carried out on the global push-down curve, where each limit state corresponds to a specific displacement rate.

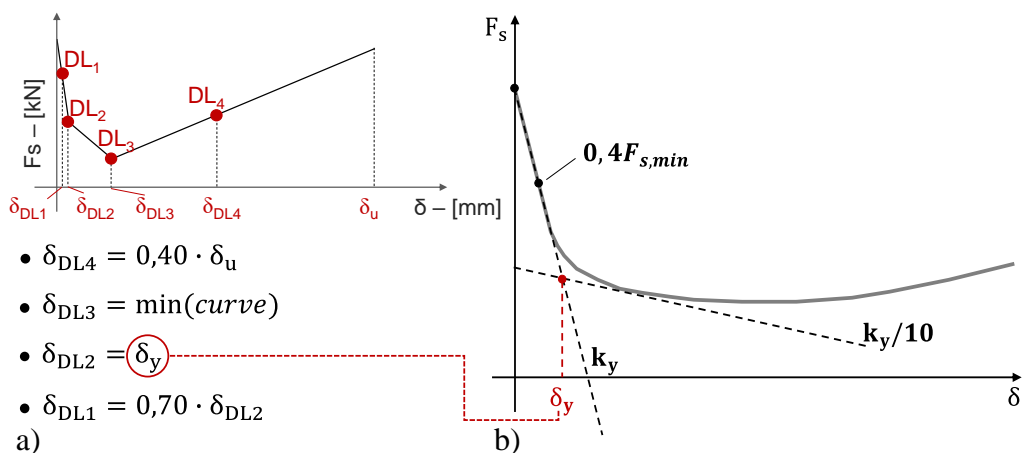


Figure 7.3 - Damage levels identification by using push-down capacity curve: (a) proposed criteria; (b) yielding displacement definition.

Similarly to (Lagomarsino, 2015; Lagomarsino and Cattari, 2015), four damage levels (DL) are identified on the push-down curve, ranging from damage limitation (DL1) to near collapse state (DL4) (Figure 7.2b). Those are

representative of the response in the linear range as well as of the value of the displacement at incipient collapse (δ_u). Following the classification approach presented in (Lagomarsino, 2015) for lateral loads, the value of the settlement displacement δ_{DL4} corresponding to the attainment of DL4 is set equal to the 40% of the ultimate displacement δ_u . The third damage level is characterized by a vertical displacement δ_{DL3} which corresponds to the minimum reaction in the capacity curve. It is worth to note that this criterion can be assumed only for push-down curves with a minimum point followed by an increase of the support reaction. The case where the stiffness keeps decreasing is out of the scope of the proposed approach. The attainment of the second damage level corresponds to the end point of the linear field of the capacity curve. The proportional limit was defined at the intersection between the secant stiffness from the origin of the push-down curve to 40% of the minimum base reaction and the tangent with the slope of 10% of the secant stiffness, as showed in Figure 7.3b. Finally, the value of the settlement displacement for the DL1 is assumed to be equal to the 70% of the displacement corresponding to DL2.

In the spirit of the dissertation thesis, the capacity curves for the application of the proposed performance-based assessment method are plotted by using the numerical procedure described in the previous sections based on non-linear kinematic rigid block model with elastic contacts. It is worth to note that the procedure hereby introduced is not intended to provide general definitions and/or universal damage thresholds for the investigated typology of buildings. Conversely, it is intended as a working example to discuss the potential application of the developed model towards a future definition of limit states and performance levels for masonry structures subjected to settlements.

In the next sections, the proposed displacement-based approach will be tested against two full-scale masonry façades, essentially a monumental building and an historic church, both located in Italy. The scope is to investigate the potentialities of the proposals in the analysis of macro-elements masonry structures subjected to foundation vertical displacements.

7.3.1 Application to a full-scale monumental building façade

The application of the proposed rigid block modelling approach to a full-scale monumental building façade aims to evaluate the sensitivity to model parameters when real-scale macro-elements or entire buildings are analysed. The results are also used for the comparison of different damage assessment methods presented in the following section.

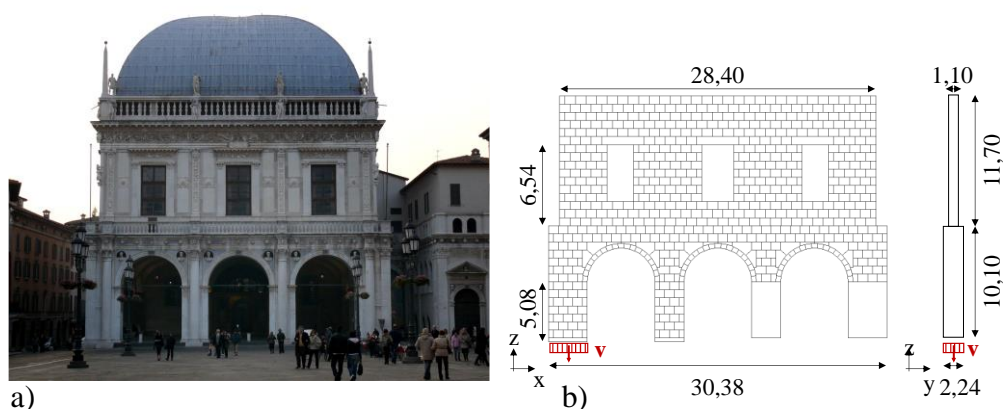


Figure 7.4 - Loggia Palace in Brescia (Italy) (a); geometrical properties (measures in m) and loading condition of the full-scale façade model (b).

To this end, the façade already analysed in the section 3.2, is now modelled at full-scale (Figure 7.4). The numerical analysis considers an imposed vertical movement of the left end column with the façade subjected to its self-weight on, which corresponds to the first part of Test 1 in Section 3. The values of the volumetric weight ρ and the friction coefficient μ are the same adopted in the small-scale model, assuming that these parameters are not affected by any scale effect. Conversely, a different value of the normal stiffness is adopted, according to typical full scale masonry results. Considering that the current formulation introduces the elastic behaviour at the contacts only, the adopted value of normal stiffness is calculated as the ratio between the Young modulus E – set equal to 1500 MPa for regular stone masonry according to (Ministero delle infrastrutture e dei trasporti., 2019) – and the block height, h_b . The settlement protocol is

characterized by a displacement rate for each step equal to 5.0 mm, except for the first two steps, characterized by a zero displacement.

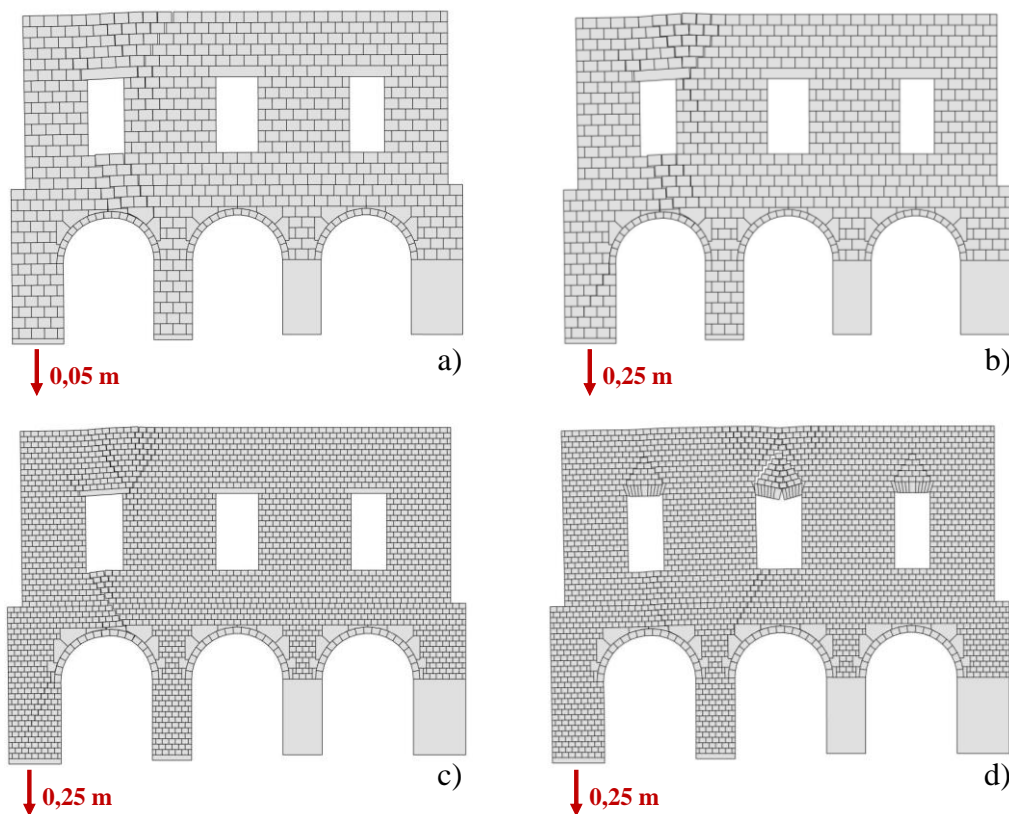


Figure 7.5 – Full-scale monumental building façade. Sensitivity analysis to the block size: large mesh (a)(b); reduced mesh with one-block-lintels (c); reduced mesh with flat arch lintels (d) (Gagliardo *et al.*, 2021).

A sensitivity analysis is performed to assess the influence of block size and lintel geometry of the structural response (Figure 7.5). Two block sizes were analysed to this scope: a coarse one with average block size equal to 946.70x731.20x1100.00 mm for the first floor and 868.00x721.40x2240.00 mm for the ground floor; a refined one with average block size equal to 473.30x365.60x1100.00 mm for the first floor and 434.00x360.70x2240.00 mm

for the ground floor. The corresponding values of normal stiffness per unit contact surface are equal to $2.05e6 \text{ kN/m}^3$ and $4.10e6 \text{ kN/m}^3$ for the coarse and refined mesh respectively, so that the correct elastic stiffness of the continuum is replicated. Different configurations of the lintels above the windows are also modelled. One-block lintels and multiple-blocks lintels are considered. The latter is discretized in several voussoir blocks to simulate a typical masonry flat arch.

With respect to the crack pattern development, it is interesting to note that the crack pattern obtained for the coarse full scale model are similar to the small scale one. The comparisons among the full-scale models show that the effect of refinement in the block size mainly affect the form of cracks, which are more concentrated. As for the effect of lintel geometry, a larger sensitivity is observed, considering that, when a flat arch is modelled, additional cracks develop above all the openings and local failure is observed similar to the one reported in Figure 2.1a-b.

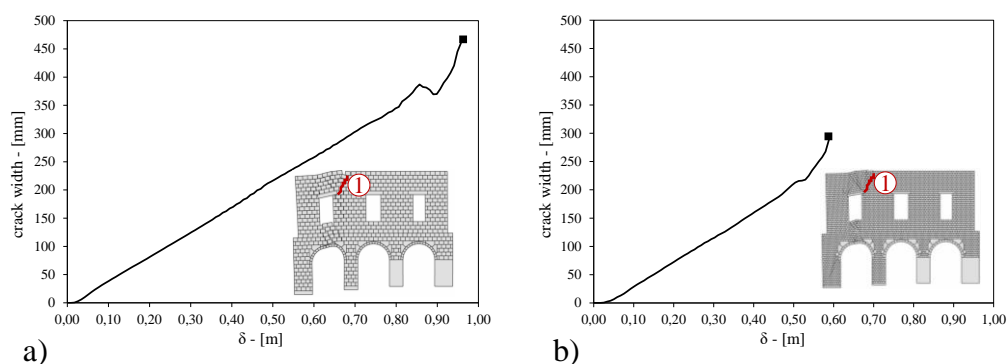


Figure 7.6 - Full-scale monumental building façade. Crack 1 openings development in terms of measure of the crack width against settlement: large mesh (a) and reduced mesh (b) (Gagliardo et al., 2021).

A comparison of different damage assessment methods was carried out using the numerical results obtained on the full-scale masonry façade. In particular, support movements and crack widths are compared for different damage levels with the approaches proposed by (Skempton and Mac Donald, 1956; Polshin, D.E., 1957; Burland and Wroth, 1974; Boscardin and Cording, 1989). The proposed

displacement-based approach towards classification of damage levels is also considered which relies on the numerical push-down curve relating the base reaction and the support movement.

The comparison is summarized in Table 7.1, where monitored parameters, damage levels and corresponding support movements are reported for the different damage classifications. In the case of (Skempton and Mac Donald, 1956), three damage thresholds are considered which correspond to structural damage, crack opening and design. The limit values of the support movement corresponding to the critical value of the tensile strain proposed by (Polshin, D.E., 1957; Burland and Wroth, 1974) were estimated assuming the critical tensile strain as the sum of two contributions, which are the average horizontal strain ε_h and the flexural strain ε_b . The strain ε_h is obtained from the ratio between the length variation induced by settlement and the initial distance between two foundation points. The flexural strain ε_b is calculated according to (Burland and Wroth, 1974) and depends on the geometrical features of the equivalent beam and on the allowable vertical displacement. For the support movements corresponding to the damage thresholds indicated by (Boscardin and Cording, 1989), the same procedure is applied, under the simplified assumption of the equivalence between the critical and limiting tensile strain parameters.

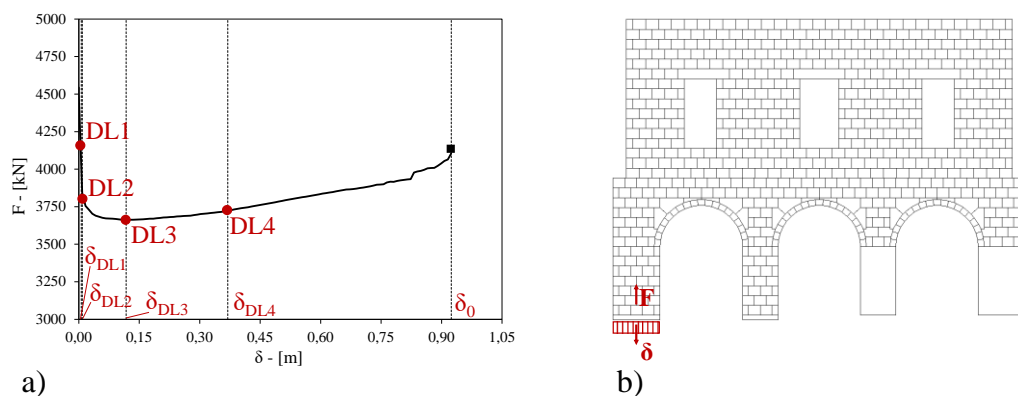


Figure 7.7 - Criteria proposed for the definition of the damage limits in the case of a push-down curve obtained with the non-linear kinematic rigid block model with elastic contacts applied to a full-scale monumental building façade (Gagliardo et al., 2021).

The support movements corresponding to the four damage levels for the proposed classification approach applied to the case study of the full-scale façade above described are indicated on the capacity curve in Figure 7.7 and are reported in Table 7.1. Adopting the damage assessment criterion proposed in the last section, the ultimate displacement δ_u calculated in the numerical model is equal to 0.924 meters. Once the value of δ_u is known, the settlement threshold for each damage level can be calculated as above described. The DL1 is reached after 2 steps, where the value of the vertical displacement δ_{DL1} applied to the left end column is equal to 0.006 meters. The attainment of the second damage level takes place after 3 steps, when the amount of the vertical settlement is equal to 0.009 meters. The 16th step represents the threshold for the DL3, corresponding to a settlement δ_{DL3} equal to 0.118 meters. Finally, the DL4 occurs after 45 steps that is equivalent to a total settlement δ_{DL4} equal to 0.369 meters.

Damage classification approach	Monitored parameters	Damage levels	Support movement – δ [m]	Crack width – [mm]
(Skempton and Mac Donald, 1956)	Angular distortion - δ_p/L	1/150 (damage)	0.200	/
		1/300 (crack)	0.100	/
		1/500 (design)	0.060	/
(Polshin, D.E., 1957)	Critical tensile strain - ϵ_{crit}	0.05%	0.006	/
(Burland and Wroth, 1974)	Critical tensile strain - ϵ_{crit}	0.05-0.10% (masonry)	0.006 – 0.011	/
(Boscardin and Cording, 1989)	Limiting tensile strain - ϵ_{lim}	0.000-0.050% (DL1)	0.000 – 0.006	0.000 – 0.100
		0.050-0.075% (DL2)	0.006 – 0.008	0.100 – 1.000
		0.075-0.150% (DL3)	0.008 – 0.016	1.000 – 5.000
		0.150-0.300% (DL4)	0.016 – 0.032	5.000 – 15.00
		> 0.300% (DL5)		15.00 – 25.00
		> 0.300% (DL6)	> 0.032	> 25.0
Proposed	Force-displacement response at the moving support	DL1	0.000 – 0.006	0.000 – 0.001
		DL2	0.006 – 0.009	0.001 – 0.002
		DL3	0.009 – 0.118	0.002 – 46.08
		DL4	> 0.118	> 46.08

Table 7.1 - Comparison of settlement-induced damage classifications proposed in literature and in the present paper applied to a full-scale monumental building façade.

The comparison shows that the proposed damage classification approach is in a good agreement with the empirical methods by (Polshin, D.E., 1957; Burland and Wroth, 1974; Boscardin and Cording, 1989) in terms of support movement when

a negligible or moderate damage is considered. A remarkable difference can be noted in the case of (Skempton and Mac Donald, 1956) where different damage levels are taken into account and a different parameter is monitored for the classification. The comparison with the crack widths estimated by (Boscardin and Cording, 1989) for the different damage levels also shows the consistency of the values obtained with the proposed approach.

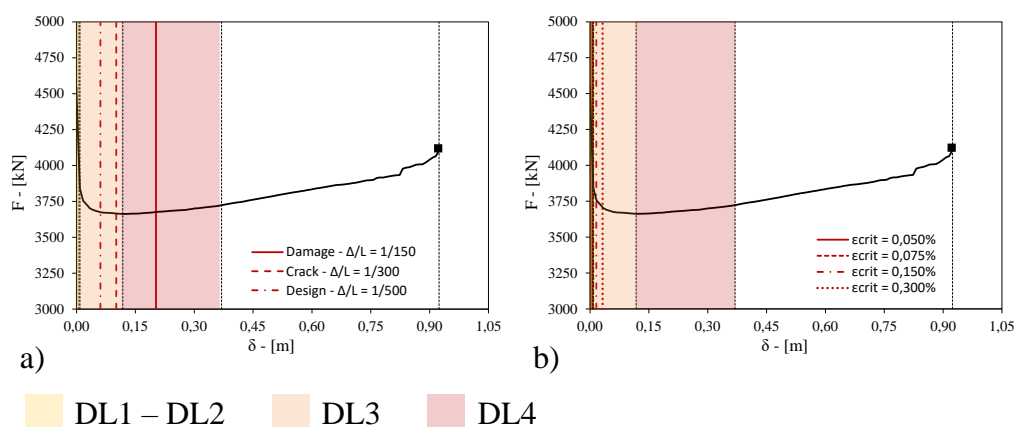


Figure 7.8 - Full-scale monumental building façade. Comparison of the proposed approach with empirical methods: (Skempton and Mac Donald, 1956) (a); (Boscardin and Cording, 1989) (b).

With the scope to deeply investigate the damage assessment method comparison, Figure 7.8 develop the comparison of the proposed approach with the empirical methods proposed in literature by (Skempton and Mac Donald, 1956) and (Boscardin and Cording, 1989) on the capacity curve. The main feeling is that the empirical methods underestimated the PLs thresholds introduced in the proposed approach, probably due to the assumption of the equivalent beam model in the calculation of the parameters which define the attainment of the limit states. It is worth noting that most of the limit adopted in the methods in literature are in the range between the DL1 and DL3 of the proposed formulation. This is due to the idea that empirical methods were mainly based on the crack patterns analysis. These assumptions neglect the contribution due to the geometrical features of the building affecting the capacity assessment. In the case of the method proposed by Skempton & Mac Donald (Figure 7.8a), the selected

parameter is the angular distortion, and the identified damage limit state corresponds to a settlement in the range field of the DL4 of the proposed approach (red zone in the plot), while the crack and design limit state are both behind the DL3 threshold displacement. The other empirical methods above described are not plotted in Figure 7.8 but the analysis showed that also in those cases, the critical values identified are very low, each one of them by in the range DL1-DL2 of the proposed approach.

7.3.2 Application to a full-scale historic masonry church façade

In this section the case study of the façade of the church of the Natività della Beata Vergine Maria in Bondeno, Italy (Figure 7.9a), already investigated in (Chiozzi *et al.*, 2018; Tralli *et al.*, 2020), is presented. The case study of this historic masonry church façade is first of all used for sake of comparison between the linear and non-linear kinematic model proposed in the previous chapter. After this preliminary computational comparison, the case study is adopted to test the performance-based approach proposed in the present chapter.

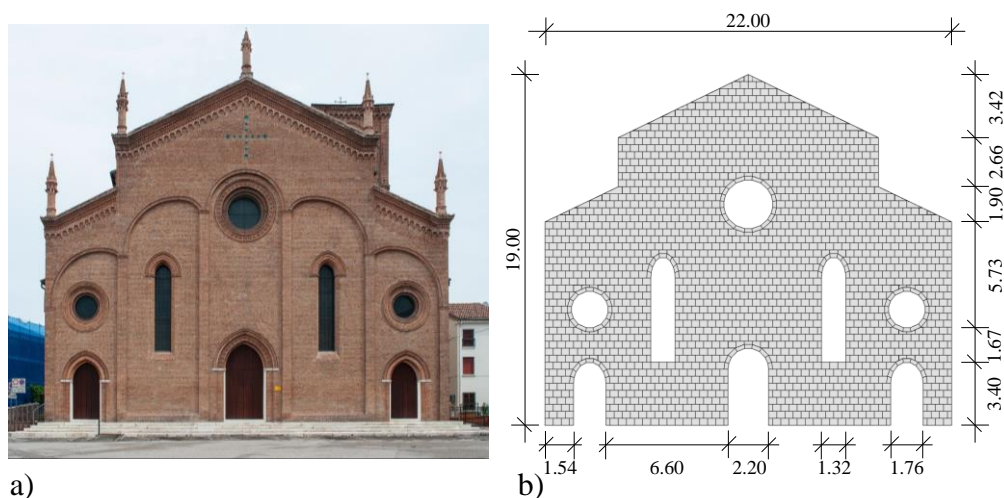


Figure 7.9 – (a) Façade of the church of the Natività della Beata Vergine Maria in Bondeno; (b) numerical model and geometry.

The façade is part of a single nave church with lateral chapels. The architectural style is typical of the Romanesque church with rose windows and pointed arch doors and windows. The present church was built in the second half of the XV century in place of the original medieval church dated back to 1114. The floor was completely rebuilt during the XVI century. The roof was restored two times during the XVII century and a curved steel truss structure was finally installed in the XX century to sustain the low load-bearing capacity wooden roof. The present neogothic appearance was a result of expansion works of the church in 1855-56. The façade as it is today was designed by Achille Bonora in 1939. The church was temporarily locked because of damages suffered by the earthquake in 2012. The façade is 22.00 meters long and 19.00 meters high. The numerical model consists of 1873 polyhedral rigid blocks and 20176 contact points (Figure 7.9b). The average block size is equal to 44x50x38 cm.

As for the numerical comparison among the proposed computational approaches, In the case of the limit analysis-based linear kinematic formulation (LiABlock_3D), the rigid block model of the church façade above described was submitted to a uniform foundation settlement of half of the base to analyse the structural performance at collapse in terms of both global failure mode and base reaction at incipient collapse (Gagliardo *et al.*, 2020). According to the collapse mechanisms predicted by the linear analysis simulation, the façade under settlement exhibits a global failure mode with several cracks, involving both translations and rotations of the rigid blocks. The foundation movement caused a diagonal crack moving from the right end side of the façade at the bottom and involving the first pointed arch door and rose window from the right, as showed in Figure 7.10a. Two main cracks appear in the central zone of the façade: a diagonal crack develops from the arch of the main door to the right side of the façade; a less severe vertical crack also moves in the zone between the main door and the monumental rose window, keeping on over the rose window. Two symmetrical diagonal cracks move upward from left and right side of the centred rose window, creating a rotational wedge on the top. Both associative and non-associative flow rules were considered in that case. The value of the base reaction at collapse is equal to 881.75 kN and 898.85 kN in the case of associative and non-associative solutions, respectively. The numerical results showed the

computational ability of the procedure to find the solution of the numerical problem in few iterations as well as the high speed of calculation (CPU Time).

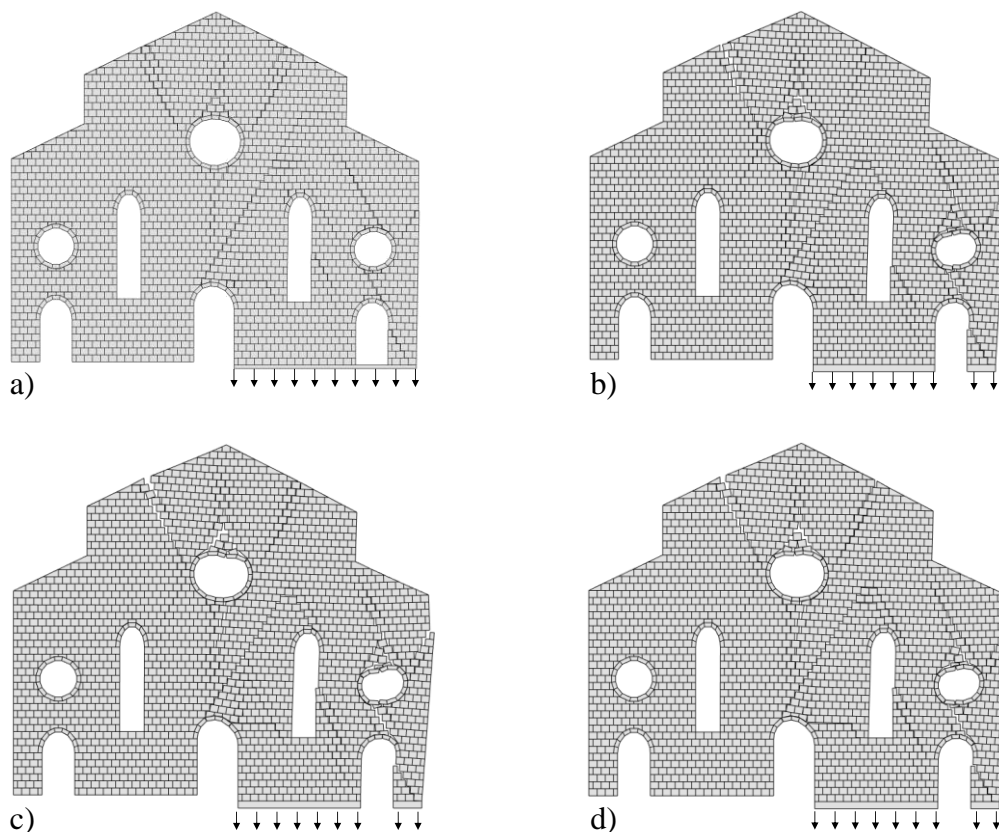


Figure 7.10 – Predicted failure modes and crack patterns for the church façade. Comparison between (a) linear kinematic model outcomes, and non-linear kinematic model outcomes in the case of (b) $2e6 \text{ kN/m}^3$, (c) $4e6 \text{ kN/m}^3$ and (d) $8e6 \text{ kN/m}^3$ normal contact stiffness k_n .

Similarly to limit analysis, the non-linear kinematic analysis was carried out imposing a vertical movement to one half of the façade, assuming a settlement vector characterized by 5.0 mm displacement per each step up to the collapse, with two zero-displacement steps at the beginning to stabilize the model response when subjected to its self-weight only. The values of the volumetric weight ρ and the friction coefficient μ are the same adopted in the limit analysis case. A

sensitivity analysis to the value of the contact stiffness was performed in order to investigate to what extent such a parameter can computationally affect the structural response of the masonry church façade. According to typical full-scale masonry results, the contact normal stiffness in compression is selected in the range between $2e6$ and $8e6$ kN/m^3 .

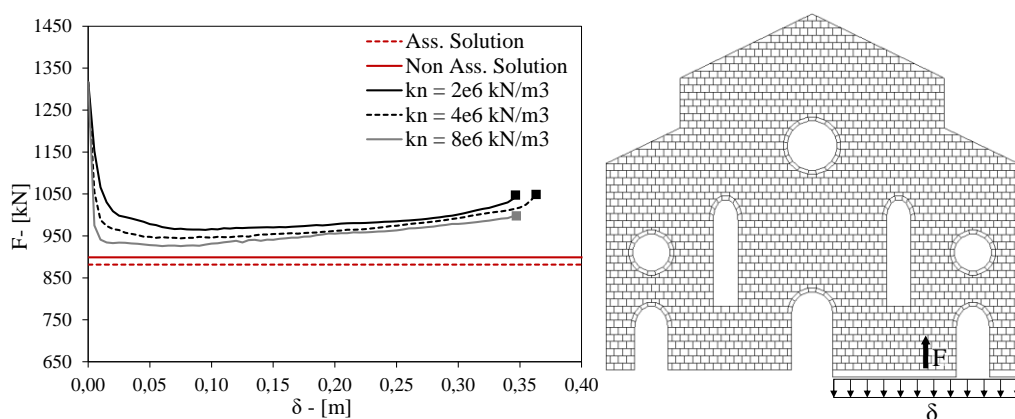


Figure 7.11 - Comparison between linear and non-linear kinematic outcomes in terms of loss of base reaction against applied settlement displacement at foundation of a masonry church façade.

The comparison between the two proposed numerical models results is showed in Figure 7.10 and Figure 7.11, in terms of failure mode and push-down capacity curves respectively. As for the crack pattern at collapse, the comparison showed a very good agreement between the two computational codes, without any relevant influence of the normal contact stiffness in the case of the large displacement-based formulation.

On the other hand, the sensitivity analysis to the value of the contact stiffness showed much more interesting results in the case of the push-down curves Figure 7.11. First, the comparison between the two numerical models in terms of base reactions is quite good. The results show that the reaction for the onset of failure obtained from the rigid block limit analysis represents a lower bound value of the base reaction computed by the non-linear kinematic model. The push-down curves obtained for the three values of the imposed normal contact stiffness showed that higher values of this parameter return a lower path of the capacity

curve, closer to the limit analysis solutions, corresponding to a rigid contact behaviour. Finally, Table 7.2 summarizes the main numerical outcomes obtained in the comparison between the two proposed computational models.

μ [-]	ρ [kN/m ³]	Numerical model	Flow rule	Contact stiffness [kN/m ³]	Base Reaction [kN]	Maximum settlement [m]
0.60	18.00	Linear	Associative	/	881.75	/
			Non-Associative	/	898.85	/
		Non-Linear	Associative	2e6	964.58	0.35
				4e6	944.26	0.36
			Non-Associative	2e6	925.83	0.35
				4e6	925.83	0.35

Table 7.2 – The façade of the church of Natività della Beata Vergine Maria in Bondeno: comparison between linear and non-linear kinematic: numerical outcomes.

The damage propagation analysis is also performed in the case of the church façade in terms of crack width evolution. The study of the behaviour in the early step of the capacity curve still represents a highly debated issue in the field of masonry structures subjected to foundation movements. Contrary to the seismic case, where the collapse state is to be very well investigated, masonry structures commonly showed a high resilience against settlement, most of the case exhibiting a relevant capacity to accommodate severe foundation displacement up to the structural collapse. In such a case, the analysis of the propagation of the cracks in the masonry panels becomes a crucial topic to be faced in order to in time identify the on-going failure mechanisms and design appropriate strategies to manage them. It is well known by the literature that the crack shape and forms can be strongly affected by the mesh properties, i.e. the block sizes in the case of discrete masonry models. To this scope, a second coarse mesh was added to the previous one with an average block size of 88x50x76 cm. It is worth noting that for sake of simplicity the size of voussoir blocks in the arch windows, doors and rose windows was not changed in the case of coarse mesh, being the same already used for the refined mesh.

The numerical investigation of the damage propagation in the façade of the church is showed in Figure 7.12 and Figure 7.13. As for the contact stiffness properties, the sensitivity analysis was performed assuming a value of the compressive contact stiffness equal to 2e6 and 4e6 kN/m³ in the case of the coarse and refined mesh, respectively.

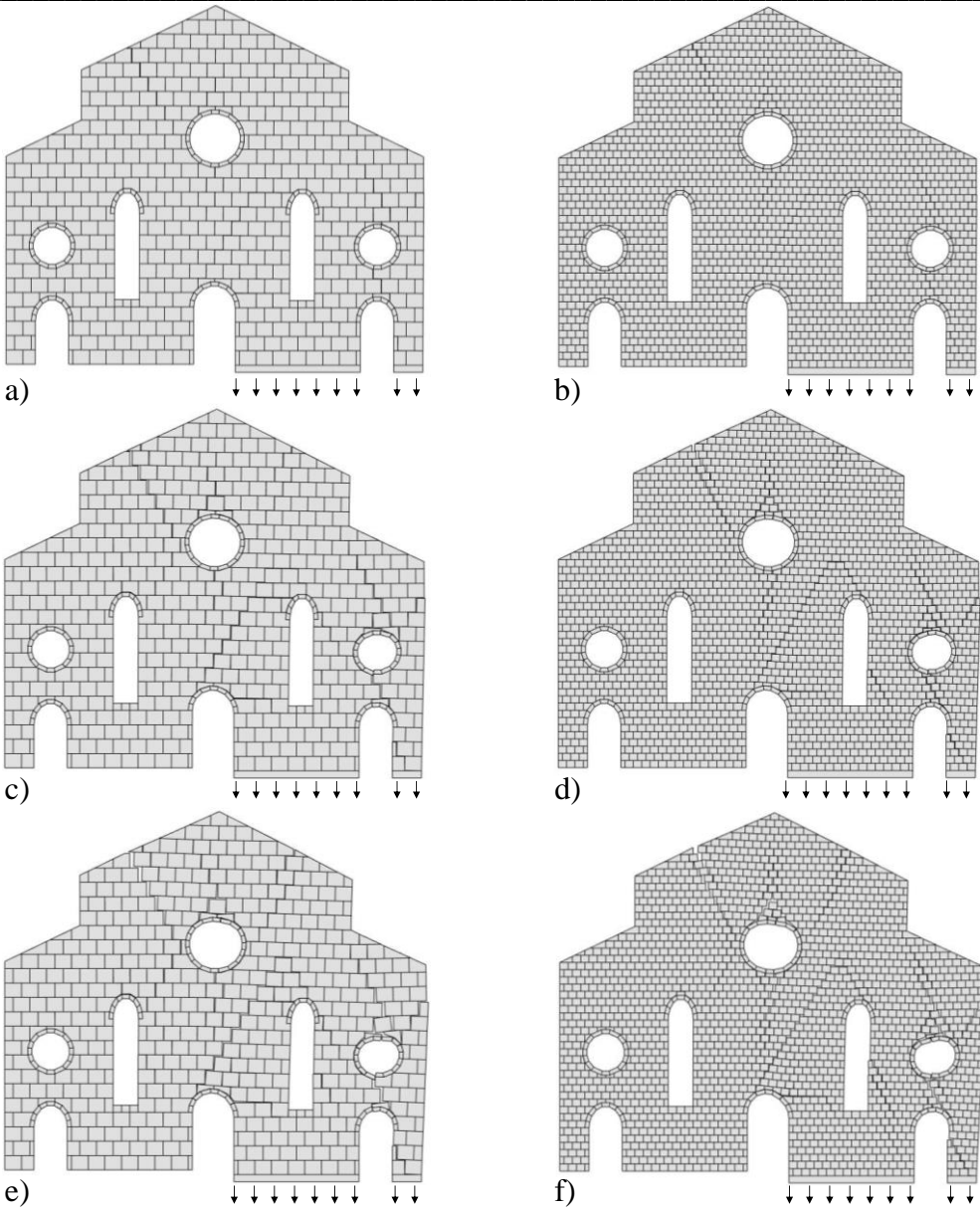


Figure 7.12 - Damage propagation analysis of the full-scale masonry church façade. Predicted crack patterns at (a)(b) 0.05 m. (c)(d) 0.15 m and (e)(f) 0.25 m according to the (a)(c)(e) coarse and (b)(d)(f) refined mesh.

Figure 7.12 shows the shape and size of cracks at 0.05 m, 0.15 m and 0.25 m foundation displacement, according to the two meshes. The comparison demonstrated that the block size mainly affects the form of cracks, which are more concentrated in the refined mesh case, even if the crack position is quite similar. Both mesh cases present a first diagonal crack in the left side of the upper part of the façade moving from the roof gable to the central rose window, opening even for low value of the imposed settlement. The crack pattern starts to increase for higher value of the applied ground displacement, exhibiting a diagonal crack in the centre zone of the façade between the main arch door and the rose window and several smaller cracks concentrated in the right side of the façade, where the base displacement is mainly located. Figure 7.13 focuses on the comparison between the two adopted mesh size in terms of crack widths against base vertical movement. Two main cracks were selected in order to perform the comparison, namely crack A and crack B, as showed in Figure 7.13.

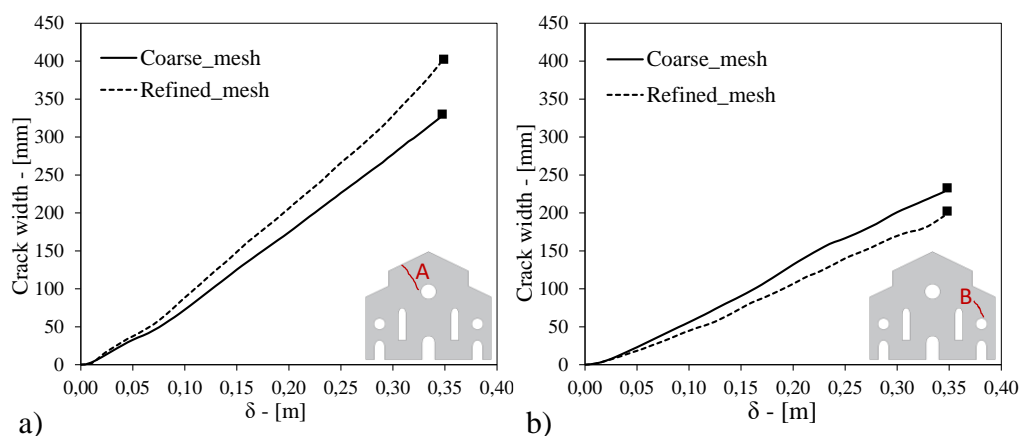


Figure 7.13 - Full-scale masonry church façade. Sensitivity analysis to the mesh size in terms of crack widths against foundation settlement: (a) crack A and (b) crack B.

The comparison in terms of crack widths revealed that the unit size does not effectively influence the crack propagation. In the case of crack A (Figure 7.13a) the refined mesh returned larger widths of the crack with a maximum difference of 20% respect to the coarse mesh. The case of crack B (Figure 7.13b) showed a better agreement between the results obtained with the two different mesh types.

The two curves are very close, where the coarse mesh curve is slightly higher with a maximum difference of about 7% with the refined mesh curve.

The case study of the historical masonry church façade is mainly investigated to test the proposed displacement-based approach for the analysis of masonry structures subjected to foundation settlements. As for the previous case study, a comparison of different damage assessment methods was performed in terms of support movements and crack widths for various damage levels. The proposed approach is compared with the empirical methods described in (Skempton and Mac Donald, 1956; Polshin, D.E., 1957; Burland and Wroth, 1974; Boscardin and Cording, 1989).

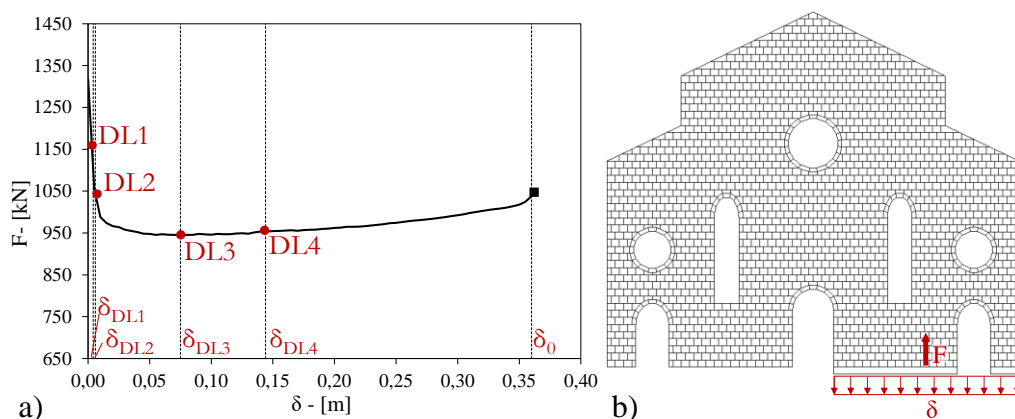


Figure 7.14 - Criteria proposed for the definition of the damage limits in the case of a push-down curve obtained with the non-linear kinematic rigid block model with elastic contacts applied to a full-scale historic masonry church façade.

Table 7.3 shows the monitored parameters, damage levels and corresponding support movements according to the different damage classifications for sake of comparison with the proposed approach. As for the adopted empirical classification methods, the same observations already described for the case study of the monumental building façade continue to be true. With regard to the proposed approach, the vertical foundation settlements corresponding to the onset of the various damage levels can identify by using once again the push-down capacity curve, as showed in Figure 7.7. The damage limits in terms of

both vertical displacement and maximum crack width are also reported in Table 7.3. In the case study of the historical masonry church façade, the proposed damage assessment criterion returns a value of the ultimate displacement δ_u calculated in the numerical model equal to 0.360 meters. The value of δ_u allows for the calculation of the settlement threshold corresponding to each damage level thanks to the procedure above detailed. In this framework, the attainment of the first damage level takes place after 2 steps, when the amount of the vertical settlement is equal to 0.004 meters. The DL2 is reached after 3 steps, where the value of the vertical displacement δ_{DL2} applied to the base of the façade is equal to 0.006 meters. The push-down curve shows that the 17th step represents the limit for the DL3, corresponding to a settlement δ_{DL3} equal to 0.075 meters. Finally, the last damage limit (DL4) corresponds to a total settlement δ_{DL4} equal to 0.144 meters, when the numerical analysis comes to the step 30.

Damage classification approach	Monitored parameters	Damage levels	Support movement – δ [m]	Crack width – [mm]
(Skempton and Mac Donald, 1956)	Angular distorsion - δ_p/L	1/150 (damage)	0.150	/
		1/300 (crack)	0.070	/
		1/500 (design)	0.040	/
(Polshin, D.E., 1957)	Critical tensile strain - ϵ_{crit}	0.05%	0.003	/
(Burland and Wroth, 1974)	Critical tensile strain - ϵ_{crit}	0.05-0.10% (masonry)	0.003 – 0.006	/
(Boscardin and Cording, 1989)	Limiting tensile strain - ϵ_{lim}	0.000-0.050% (DL1)	0.000 – 0.003	0.000 – 0.100
		0.050-0.075% (DL2)	0.003 – 0.005	0.100 – 1.000
		0.075-0.150% (DL3)	0.005 – 0.010	1.000 – 5.000
		0.150-0.300% (DL4)	0.010 – 0.019	5.000 – 15.00
		> 0.300% (DL5)		15.00 – 25.00
		> 0.300% (DL6)	> 0.019	> 25.0
Proposed	Force-displacement response at the moving support	DL1	0.000 – 0.004	0.000 – 0.059
		DL2	0.004 – 0.006	0.059 – 0.668
		DL3	0.006 – 0.075	0.668 – 58.21
		DL4	> 0.075	> 58.21

Table 7.3 - Comparison of settlement-induced damage classifications proposed in literature and in the present paper applied to a full-scale historic masonry church façade.

Conclusions

This Chapter faced the main scope of the present dissertation thesis, i.e. the proposal for a performance-based damage assessment approach of masonry structures subjected to movable foundation and settlements. The topic is a very big challenge in the specific literature, which has been investigating for various decades. The proposed approach commits to the idea of the performance-based limit states definition, which is a highly powerful method well-established in the literature and even adopted in most of the international codes and standards. It is worth noting that such a performance strategy is much more used and tested in the field of earthquake engineering than in other fields, such as the one related to the ground settlement induced by natural or man-made hazards.

In this framework, the chapter described the adoption of a system for the classification of the settlement-induced damage, where various performance levels were identified on the base of the exhibited foundation displacement. The capacity curve, named push-down curve in the spirit of this dissertation, was assumed as the numerical support for the clear identification of the different performance levels. To this scope, the numerical procedure based on the rigid block non-linear kinematic analysis (described in the previous Chapter 6) was assumed as the computational strategy in the overall performance-based method. In such a case, the application of that numerical formulation allowed for the development of the numerical capacity push-down curves, which can be used as a tool for the identification of the performance levels in terms of allowable foundation displacements. To this end, criteria for the damage thresholds definition were proposed in the text, by using consolidated procedures adopted in the earthquake engineering.

The proposed method was applied to two real full-scale case study located in Italy: a monumental building masonry façade, with arch windows and doors and a historic masonry church façade. The first selected case study has the same geometrical features of one of the numerical applications already presented in Chapter 6 for the validation of the proposed numerical procedure. The obtained damage levels thresholds were also compared with those calculated according to

the empirical damage classification methods available in literature, showing an adequate agreement in terms of foundation vertical settlement and crack width at the onset of the various performance levels, as discussed in the text.

References

- American Society of Civil Engineers (2017) *Minimum Design Loads and Associated Criteria for Buildings and Other Structures (7-16)*.
- Boscardin, M. D. and Cording, E. J. (1989) ‘Building Response To Excavation-Induced Settlement’, *Journal of Geotechnical Engineering*, 115(1), pp. 1–21. doi: 10.1061/(ASCE)0733-9410(1989)115:1(1).
- Burland, J. B., Broms, B. B. and de Mello, V. F. B. (1978) ‘Behaviour of foundations and structures. State-of-the-art report’, *International Journal of Rock Mechanics and Mining Sciences & Geomechanics Abstracts*, 2, pp. 495–546. doi: 10.1016/0148-9062(78)91791-6.
- Burland, J. B. and Wroth, C. P. (1974) ‘Settlement of buildings and associated damage’, in *Settlement of Structures, Proceedings of the Conference of the British Geotechnical Society*, pp. 611–654.
- Cattari, S. *et al.* (2014) ‘Damage assessment of fortresses after the 2012 Emilia earthquake (Italy)’, *Bulletin of Earthquake Engineering*, 12(5), pp. 2333–2365. doi: 10.1007/s10518-013-9520-x.
- Chiozzi, A. *et al.* (2018) ‘UB-ALMANAC: An adaptive limit analysis NURBS-based program for the automatic assessment of partial failure mechanisms in masonry churches’, *Engineering Failure Analysis*, 85, pp. 201–220. doi: 10.1016/j.engfailanal.2017.11.013.
- Consiglio superiore dei lavori pubblici (2010) *Circolare n. 26/2010 - «Linee guida per la valutazione e la riduzione del rischio sismico del patrimonio culturale con riferimento alle Norme tecniche per le costruzioni di cui al decreto del Ministero delle Infrastrutture e dei trasporti del 14 gennaio 2008»*.
- EN 1998-2005. *Eurocode 8: Design of structures for earthquake resistance (2005)*.
- Gagliardo, R. *et al.* (2020) ‘The prediction of collapse mechanisms for masonry structures affected by ground movements using Rigid Block Limit Analysis’, *Procedia Structural Integrity*. Elsevier B.V., 29, pp. 48–54. doi: 10.1016/j.prostr.2020.11.138.

Gagliardo, R. *et al.* (2021) ‘A rigid block model with no-tension elastic contacts for displacement-based assessment of historic masonry structures subjected to settlements’, *Engineering Structures*, 229. doi: 10.1016/j.engstruct.2020.111609.

Hofer, L. *et al.* (2018) ‘Seismic damage survey and empirical fragility curves for churches after the August 24, 2016 Central Italy earthquake’, *Soil Dynamics and Earthquake Engineering*, 111, pp. 98–109. doi: 10.1016/j.soildyn.2018.02.013.

Lagomarsino, S. (2012) ‘Damage assessment of churches after L’Aquila earthquake (2009)’, *Bulletin of Earthquake Engineering*, 10(1), pp. 73–92. doi: 10.1007/s10518-011-9307-x.

Lagomarsino, S. (2015) ‘Seismic assessment of rocking masonry structures’, *Bulletin of Earthquake Engineering*, 13(1), pp. 97–128. doi: 10.1007/s10518-014-9609-x.

Lagomarsino, S. and Cattari, S. (2015) ‘PERPETUATE guidelines for seismic performance-based assessment of cultural heritage masonry structures’, *Bulletin of Earthquake Engineering*, 13(1), pp. 13–47. doi: 10.1007/s10518-014-9674-1.

Ministero delle infrastrutture e dei trasporti. (2018) *Decreto ministeriale 17 gennaio 2018 - Aggiornamento delle «Norme tecniche per le costruzioni»*.

Ministero delle infrastrutture e dei trasporti. (2019) *CIRCOLARE 21 gennaio 2019, n. 7 C.S.LL.PP - Istruzioni per l’applicazione dell’«Aggiornamento delle «Norme tecniche per le costruzioni»*».

Oliveira, C. S. (2003) ‘Seismic vulnerability of historical constructions: A contribution’, *Bulletin of Earthquake Engineering*, 1(1), pp. 37–82. doi: 10.1023/A:1024805410454.

Polshin, D.E., and R. A. T. (1957) ‘Maximum Allowable Non-uniform Settlement of Structures’, *4th Int. Conf. Soil Mechanics and Foundation Engineering*, 1, pp. 402–406.

Skempton, A. W. and Mac Donald, D. H. (1956) ‘Allowable Settlement of Structures’, in *Proc. Institute of Civil Engineers, Part III*, pp. 727–768.

Tralli, A. *et al.* (2020) ‘Masonry structures in the presence of foundation settlements and unilateral contact problems’, *International Journal of Solids and*

Structures, 191–192, pp. 187–201. doi: 10.1016/j.ijstr.2019.12.005.

Chapter 8

Conclusions

8.1 Conclusive remarks

The research carried out in this dissertation thesis deals with the investigation of the structural performance of masonry structures subjected to the support movements or foundation settlements. The main scope is the proposal for a displacement-based damage assessment approach for masonry panels under settlement through the identification of performance levels (or limit states) by using push-down capacity curves implemented in an in-house rigid block model for non-linear kinematic analysis.

The work is developed within the activities of the research project PERICLES “Protecting the Cultural Heritage from water-soil interaction related threats”, funded by the Italian Ministry of Education, Universities and Research (MIUR). The project has the goal to develop sustainable management strategy for Cultural Heritage exposed to landslides and subsidence, with a special focus on vulnerability assessment models for masonry structures. Another important scope of the project PERICLES is the development of a sustainable management strategy for Cultural Heritage at water-soil interaction risk in order to better

identify priorities and innovative methodologies for risk assessment, monitoring and mitigation together with conservation and valorisation measures for CH sites and structures.

The first part of the thesis is devoted to a comprehensive and critical review of the relevant state of art in the field of settlement-induced damage (Chapter II), masonry-like material structural behaviour (Chapter III) and numerical models and formulations proposed in literature for the investigation of masonry structures performance (Chapter IV). The description of the state of art showed a very complex and highly debated research field with a huge number of still open issues.

The crucial point of the dissertation is represented by the proposal of two rigid block numerical approaches devoted to the structural investigation of masonry structures discretized as collections of rigid blocks interacting via frictional contact surfaces. The first proposed approach is represented by a rigid block model with rigid contacts for the linear kinematic analysis model based on the formulation of a limit equilibrium problem according to the lower bound theorem of limit analysis. The computational formulation is condensed in an in-house MATLAB® implemented code (named LiABlock_3D) for analysis of 3D blocks assemblages against both lateral loads and foundation settlements. The second proposed computational approach represent the actual novelty of this thesis, dealing with a rigid block model with no-tension elastic contacts for the non-linear kinematic analysis for the investigation of 2D masonry structures subjected to various types of foundation vertical displacements (uniform, linear etc.). The non-linear model can account for unilateral elastic contacts with finite normal stiffness in compression. The main output consists of special capacity curves, named push-down curves, plotting the loss of base reaction against the displacements of a control point located at the movable foundation block.

As for the computational proposal of the linear kinematic model, a huge number of numerical applications was performed, and the following remarks can be pointed out:

- The comparison with numerical case studies from the literature showed that failure modes and load factors predicted with the developed tool

exactly match in the simplest cases, such as simple circular arches subjected to point live loads or spreading supports. Maximum difference of 15% were obtained in the case of more complex case studies, such as the two ring arches and barrel vaults subjected to live point loads.

- The validation against experimental case studies also showed that predicted results are similar to those obtained from testing outcomes, with differences less than 17% in the case of non-associative solutions. In the interests of safety, it is also worth noting that the non-associative load factors computed for the experimental case studies are up to 12% lower than those obtained for the associative behaviour.
- The application to real-scale numerical case study of masonry buildings and churches with several geometrical complexities (vaults, arched windows and doors etc.) confirmed that the developed tool can be used to model complex assemblages involving different structural elements, with a valuable computational efficiency in terms of speed of calculation (i.e. CPU Time).
- Numerical comparisons with finite element model solutions were also performed, showing an overall good agreement of failure mechanisms observed, indicating the ability of the discrete and the continuous models to capture similar local behaviour and damages in the case of in-plane and out-of-plane collapse as well as to predict failure mode and the reduction of the reaction at the foundation that activates the failure mechanism, when varying the shape of the masonry units, the wall openings and the width of the settled area. Discrepancies in the predicted failure mechanism from the two models were observed only when the continuum model was not able to capture the masonry bond patterns considered in the rigid block model. In the case of settlement, the failure mode is only slightly affected by the loads provided by the floors, while is strongly affected by the presence and disposition of openings and by the width of the settled area. As a matter of fact, width of the moving support can affect the failure mechanism, turning from local (i.e. affecting a limited part of the wall) to global (i.e. interesting all the wall).

The non-linear kinematic formulation was validated against numerical and experimental case studies as well. The push-down capacity curves obtained by using this proposed computational model were then applied to develop a damage-based assessment approach for masonry panels subjected to foundation settlements and spreading supports. After a full review of the existent empirical method for the classification of masonry structures under settlements, a novel definition of performance and damage levels for settled masonry panels was presented. A series of conclusive remarks can be pointed out as for this second numerical formulation:

- The non-linear numerical tool was tested against experimental test on small-scale masonry panels and façade. The results showed that the numerical model is able to well predict the ultimate displacement at collapse, with a maximum difference of about 2.0% with the experimental values. The comparison in terms of total base reactions at collapse showed that the numerical model overestimates the experimental values with differences in the range of 12-19%. In the case of the small-scale façade, the comparison with experimental outcomes showed some difference in terms of crack positions because the numerical model failed in the opening of some cracks. The crack width analysis and comparison exhibited good results especially in the first steps of the analysis when very small displacements were applied to the model base. Then, differences between numerical and experimental values of the crack width started becoming larger. These differences can be ascribed to the simplification adopted in the numerical model, to geometric imperfections and to the uncertainties related to the experimental measures, for example the crack width. Nevertheless, the analysis of the experimental case studies showed the stability and the computational efficiency of the proposed model.
- The second proposed numerical model was also applied to the case study of two full-scale monumental masonry façades aiming to show the abilities of this approach in the assessment of failure mechanisms induced by foundation settlements on entire buildings, involving a sensitivity analysis to block size and to lintel bond pattern. The outcomes showed

that scale-effect does not affect the crack pattern and failure mode in case of full-scale masonry façades. Conversely, block size and lintel bond pattern play a major role.

- The outcomes of the two full-scale models analysis were then used to develop a comparison between various settlement-induced damage assessment methods. The adopted displacement-based approach allows to define different damage levels on the capacity curve and was so compared with four empirical classification approaches available in literature (Skempton and Mac Donald, 1956; Polshin, D.E., 1957; Burland and Wroth, 1974; Boscardin and Cording, 1989). The comparison was carried out in terms of support displacement, crack width and on the basis of reaction-displacement response at the settling foundation. The results showed a substantial agreement between the compared classification methods from the literature and the adopted displacement-based approach. Differences in the value of the support displacements and crack widths corresponding to damage levels can be ascribed to the different monitored parameters and to the different assumptions adopted for the material and structural model.
- The proposed linear and non-linear kinematic rigid block computational models proposed in this dissertation were also compared among them in order to highlight the differences of the two tools in the performance investigation of masonry structures subjected to movable supports. The analysis demonstrated that the limit analysis based linear model represents a conservative computational method, returning an upper bound value of the base reaction promoted collapse compared to that obtained by the non-linear model. In this framework, it is possible to state that the limit analysis formulation can be used to obtain a fast and preliminary results dealing with the collapse behaviour of the investigated structures. When more in-depth outcomes are demanded, the non-linear kinematic model can be eventually applied, in order to study not only the performance at collapse but the damage initiation and propagation as well.

8.2 Further developments

The work developed within the present dissertation thesis is part of an on-going research project on computational methods for the study of masonry structures subjected to settlement of the foundation system. Therefore, the study is intended to be further developed. The next topic to be faced deals with the investigation of the capacity of masonry structures subjected to a combination of lateral loads and foundation movements. The scope is mainly represented by the possibility to study to what extent the settlement-induced foundation movements can affect the seismic fragility of masonry structures. The latter can be regarded as a crucial and challenging task in literature, being involved two typical and widespread natural hazards, such as seismic and hydrogeological. The settlement-to-earthquake interaction is a dangerous condition which represents a severe risk for the integrity and safety of historical masonry structures as well as any other type of structures and infrastructure.

The possibility to investigate the structural capacity of masonry structures subjected to such a combination of natural hazards is strictly related to another crucial topic (highly debated in literature), i.e. the use of fragility and vulnerability functions for the analysis of structural performance of masonry structures. Various studies have been developing in literature on this interesting topic (Couto, Bento and Gomes, 2020). These probabilistic tools showed to be very powerful in the performance assessment of engineering structures against any type of natural hazards. It is important to make a difference between the idea of “vulnerability” and “fragility”: the vulnerability functions deal with the probability of losses given a specific level of the selected intensity measure (e.g. peak ground acceleration in the case of ground motion); the fragility functions deals with the probability of exceeding a specific limit states or performance level (damage, collapse etc.) given a specific level of the selected intensity measure (e.g. peak ground acceleration in the case of ground motion). These two different probabilistic functions present a typical shape which allows to immediately identify them, as showed in Figure 8.1. The Figure shows that the vulnerability function shape reports the level of intensity measure against the mean damage ration whereas the fragility function shape reports the level of the intensity

measure against the probability of exceeding the specific performance level. It can be ascribed that vulnerability functions are somehow dependent on fragility functions, being the first derived from the second through specific consequence functions.

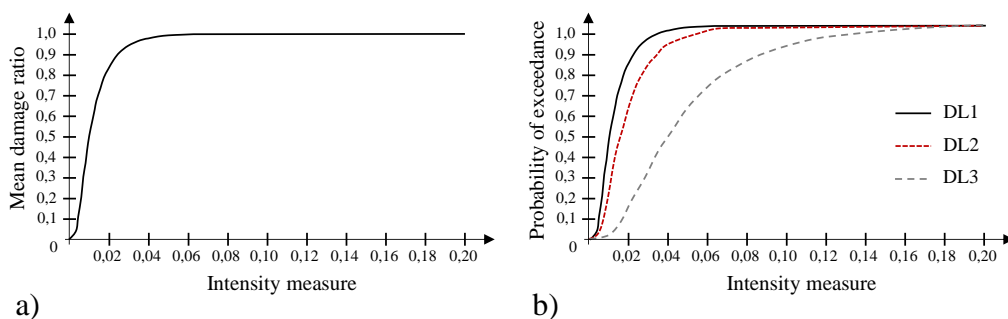


Figure 8.1 – Qualitative examples of (a) vulnerability curve and (b) fragility curves.

Fragility functions are graphically described by the so-called fragility curves Figure 8.1b, which has been developing in the last decades as a powerful tool for the natural hazards risk assessment. As a matter of fact, such a curve relates the generic hazard intensity to the probability of reaching or even exceeding a specific level of damage (e.g., minor, moderate, extensive, collapse) for each element at risk. The first issue is to quantify the current level of the considered hazard by introducing different hazard intensity parameters. In the earthquake case, the most common intensity parameters are represented by peak ground acceleration (or velocity or displacement), the spectral acceleration, the spectral velocity or the spectral displacement. In the case of settlement hazard, the most common intensity parameters consist of maximum settlement, differential settlement, angular distortion, limit tensile strength and average tensile strength. The intensity parameters are commonly described by a typical lognormal probability distribution function, as described in the following equation (8.1).

$$P_f(d_s \geq d_{s,i} | IM) = \Phi \left[\frac{1}{\beta_{tot}} \cdot \ln \left(\frac{IM}{IM_{mi}} \right) \right] \quad (8.1)$$

where:

-
- P_f is the probability of reaching or exceeding a level of damage.
 - d_s is the investigated damage corresponding to a given hazard intensity level.
 - $d_{s,i}$ is the damage level corresponding to a damage state threshold.
 - IM is the selected hazard intensity measure (e.g. PGA or maximum settlement).
 - Φ is the standard cumulative probability function.
 - IM_{mi} is the median threshold value of the hazard intensity measure IM demanded to reach the i_{th} damage state.
 - β_{tot} is the total standard deviation.

As for the numerical approach for the fragility curves development, the literature provided with several solutions, especially with regard to the seismic vulnerability assessment. All the various numerical proposals can be grouped in four classes, namely empirical, judgmental, analytical and hybrid methods. Empirical methods are based on past events surveys. In this case, the curves are devoted to describe a specific site since they are based on specific hazard conditions and properties of the damaged structures (Spence *et al.*, 1992; Sabetta, Goretti and Lucantoni, 1998; Rossetto and Elnashai, 2003). As for judgment methods, fragility curves derived from expert opinion and experience. This approach has the advantage to be quite versatile and time-saving. It is worth noting that judgment curves reliability is strictly depended on the available expertise level. Analytical methods have been highly spreading in the last years as a powerful tool to assess the natural hazard vulnerability of structures. These functions adopt damage distributions simulated by structural analysis with increased intensity measure values in a statistical sense. It is globally admitted that such an approach produces high reliable results in terms of vulnerability assessment (Rossetto and Elnashai, 2003). Fragility curves can be also derived by a combination of the previously described methods, thus developing hybrid approaches. Procedures based on such methodological interaction has the advantage to compensate the lack of data ascribable to the single approaches (Calvi *et al.*, 2006; Kappos *et al.*, 2006).

An important issue to be faced in the fragility and vulnerability assessment of any type of buildings is represented by the possibility to group structures with similar structural features and responses and located on similar soil conditions, because these structures are expected to exhibit the same performance for a specific seismic motion or settlement displacement regime. Within this framework, it is possible to assume that damage level is a function of the structural typology of the exposed buildings. The term structural typology deals with a large field of descriptors, among them essentially geometry, material properties, morphological features, age, soil and foundation conditions etc. The possibility to create well-organized inventories for each typology and for various region represents a very powerful tool in order to best implement the study of the fragility and vulnerability of structural types. Many efforts were developed in the last decades especially in the case of buildings and bridges subjected to seismic-induced ground motion, but the same is demanded to be performed for other structural types and natural hazard phenomena.

Performance levels definition represents a second crucial point in the evaluation of the risk level for structural elements and buildings. As already described in the previous chapter, the possibility to introduce performance levels is related to the definition of specific limit states, i.e. specific damage thresholds. This means that a generic limit state can be regarded as the threshold between two damage severity levels. Such a damage intensity classification is possible to be performed in terms of both qualitative and quantitative criteria. Qualitative approach is the most applied, where the damage state is classified in terms of occurred consequences due to the natural event. This aspect is a main passage to develop fragility curves generally based on a discrete damage scale. In this framework, the selection of the most appropriate intensity measure (IM) is the actual challenge to assess the fragility of buildings and structures. This choice should be moved from the possibility to select an IM which can represent the analysed phenomena and correlate with the structural response. In earthquake field, many intensity measures have been proposed, each one of them dealing with a specific characteristic of the ground motion (Cornell *et al.*, 2002; Mehanny, 2009).

The potentialities to apply the fragility and vulnerability functions in the field of masonry structures belonged to the built Cultural Heritage were widely tested within the activities of PERPETUATE project, with regard to the seismic actions (Lagomarsino, 2015; Lagomarsino and Cattari, 2015). PERPETUATE project has intended to develop a methodology for the assessment of seismic risk to cultural heritage assets and design of interventions. The main goal was to develop European Guidelines for evaluation and mitigation of seismic risk to cultural heritage assets, applicable in the European and other Mediterranean countries. As for the definition of the performance limit states, PERPETUATE project starts from the shared opinion that it is not possible to define strict safety levels for cultural assets, since the "case by case" approach is always preferable. The definition of "acceptable" safety levels may be intended as a compromise: on the one side, they must prevent the damage deriving from environmental actions (earthquake, flood, aging); on the other side, they must prevent from invasive interventions, designed in order to avoid future damage from environmental actions but unwillingly producing immediate and significant loss in terms of conservation. To conciliate these issues is of fundamental relevance. "Acceptable" safety levels for cultural heritage assets aimed to be based on the concept of performance limit states. Both serviceability limit states and ultimate limit states are accounted for, the first dealing with occurrence of reparable damages limiting temporary the use and the second usually corresponding to near collapse conditions.

References

- Boscardin, M. D. and Cording, E. J. (1989) ‘Building Response To Excavation-Induced Settlement’, *Journal of Geotechnical Engineering*, 115(1), pp. 1–21. doi: 10.1061/(ASCE)0733-9410(1989)115:1(1).
- Burland, J. B. and Wroth, C. P. (1974) ‘Settlement of buildings and associated damage’, in *Settlement of Structures, Proceedings of the Conference of the British Geotechnical Society*, pp. 611–654.
- Calvi, G. M. *et al.* (2006) ‘Development of seismic vulnerability assessment methodologies over the past 30 years’, *ISET Journal of Earthquake Technology*, 43(3), pp. 75–104.
- Cornell, C. A. *et al.* (2002) ‘The probabilistic basis for the 2000 SAC/FEMA steel moment frame guidelines’, *Journal of Structural Engineering, ASCE*, 1284, pp. 526–533.
- Couto, R., Bento, R. and Gomes, R. C. (2020) ‘Seismic performance and fragility curves of historical residential buildings in Lisbon downtown affected by settlements’, *Bulletin of Earthquake Engineering*, 18(11), pp. 5281–5307. doi: 10.1007/s10518-020-00906-z.
- Kappos, A. J. *et al.* (2006) ‘A hybrid method for the vulnerability assessment of R/C and URM buildings’, *Bulletin of Earthquake Engineering*, 4, pp. 391–413. doi: 10.1007/s10518-006-9023-0.
- Lagamarsino, S. (2015) ‘Seismic assessment of rocking masonry structures’, pp. 97–128. doi: 10.1007/s10518-014-9609-x.
- Lagamarsino, S. and Cattari, S. (2015) ‘PERPETUATE guidelines for seismic performance-based assessment of cultural heritage masonry structures’, *Bulletin of Earthquake Engineering*, 13(1), pp. 13–47. doi: 10.1007/s10518-014-9674-1.
- Mehanny, S. S. F. (2009) ‘A broad-range power-law form scalar-based seismic intensity measure’, *Engineering Structures*, 31(7), pp. 1354–1368. doi: 10.1016/j.engstruct.2009.02.003.
- Polshin, D.E., and R. A. T. (1957) ‘Maximum Allowable Non-uniform Settlement of Structures’, *4th Int. Conf. Soil Mechanics and Foundation Engineering*, 1, pp. 402–406.

Rossetto, T. and Elnashai, A. (2003) ‘Derivation of vulnerability functions for European-type RC structures based on observational data’, *Engineering Structures*, 25, pp. 1241–1263. doi: 10.1016/S0141-0296(03)00060-9.

Sabetta, F., Goretti, A. and Lucantoni, A. (1998) ‘Empirical Fragility Curves from Damage Surveys and Estimated Strong Ground Motion’, in *11th European Conference on Earthquake Engineering*.

Skempton, A. W. and Mac Donald, D. H. (1956) ‘Allowable Settlement of Structures’, in *Proc. Institute of Civil Engineers, Part III*, pp. 727–768.

Spence, R. J. S. *et al.* (1992) ‘Correlation of ground motion with building damage: The definition of a new damage-based seismic intensity scale’, *10th World Conference on Earthquake Engineering, Madrid, Spain*, pp. 551–556.